ALMA MATER STUDIORUM A.D. 1088
UNIVERSITÀ DI BOLOGNA

SCUOLA DI SCIENZE

Corso di Laurea Magistrale in Geologia e Territorio
Dipartimento di Scienze Biologiche, Geologiche ed Ambientali

Tesi di Laurea Magistrale
in idrologia e rischio idraulico - costruzioni idrauliche e protezione idraulica del territorio

A probabilistic approach to classify the levee reliability

Candidato:
Andrea Franco

Relatore:
Prof. Mario V. L. Martina

Correlatore:
Dott. Ing. Alessio Domeneghetti

Sessione Marzo 2016
Anno Accademico 2014-2015

Dedicato ad Arturo ed Augusto

i nonni che avrei tanto voluto conoscere.

Summary

INTRODUCTION AND PREMISE

MATERIALS AND METHODS

DATA PROCESSING

CLASSIFICATION PROPOSAL

HAZARD ANALYSIS

FINAL CONSIDERATION

ATTACHMENTS

1. Topographic input data
2. Classifications and indexes
3. Indexes maps
4. Classification maps
5. Residual Hazard maps
6. Summary sheet of flooding water volumes

C'era la gente del mio paese sull'argine, ferma,

con le facce trepide, infantili anche quelle senili.

E da lontano veniva un rombo:

l'onda di piena arrivava

e avrebbe rotto in qualche parte....

Cesare Zavattini da *E l'uomo creo la terra:*

il Po tra Casalmaggiore, Colorno, Sabbioneta, Viadana

Ci sono cose che i geologi non sanno fare e gli ingegneri si,

ci sono cose che gli ingegneri non vedono ma i geologi si…

la soluzione è una stretta collaborazione,

per proteggere insieme questo mondo e renderlo un posto migliore.

1. Scopo della tesi

Al giorno d'oggi è ormai noto, anche per chi di questa materia non se ne intende, che l'Italia è un paese ad alto rischio idrogeologico, dove le frane e le alluvioni non vengono più percepite come un evento eccezionale o "catastrofico" ma sono parte della nostra vita quotidiana, senza sapere esattamente dove e con quanta imprevedibilità queste possano avvenire.

Sin dall'antichità le popolazioni si sono insediate nelle vaste piane fluviali e sempre più vicino ai corpi idrici e ai grandi fiumi per poterne sfruttare al meglio le risorse, finché la natura non ha avuto il sopravento e "si è ripresa gli spazi a lei rubati", ieri come oggi, ed è in queste occasioni che l'uomo si rende conto di essersi *esposto troppo a rischio*.

Da quando se ne ha consapevolezza, per proteggersi da questi fenomeni noti come alluvioni oppure "onde di piena", opere note come costruzioni idrauliche vengono poste in sito allo scopo di impedire l'allagamento delle aree limitrofe ai corsi d'acqua.

Tra le costruzioni idrauliche più note e usate, ci sono i *sistemi arginali*, lunghe dighe in terra di svariate forme e dimensioni che si estendono per chilometri nelle aree golenali e anche a ridosso del corpo idrico.

Ma queste opere non sono destinate a durare e a proteggere per un tempo illimitato e, come tante altre cose create dall'uomo, anche gli argini possono aver dei difetti e dunque possono "fallire".

Il lavoro in questione ha lo scopo di andare a valutare l'affidabilità degli argini fluviali, andando a calcolare la probabilità di "fallimento" per determinati tratti arginali condizionati da diversi livelli di carico, utilizzando metodi probabilistici che fanno uso delle *Curve di fragilità* ottenute attraverso il Metodo Monte Carlo. Come meccanismi di rottura sono stati considerati il sormonto arginale e il sifonamento (dal momento che questi risultano essere i più frequenti) e si prende in analisi il sistema arginale maestro del fiume Po nel tratto compreso tra Piacenza e Cremona, nel settore medio basso della Pianura Padana.

La novità di questo approccio sta nel verificare l'affidabilità di interi tratti arginali, e non solo delle singole sezioni, tenendo conto della variabilità della geometria del sistema arginale tra un tratto e l'altro.

Inoltre si va a considerare, per ogni tratto arginale analizzato, una distribuzione di probabilità delle variabili di carico in gioco per la definizione delle curve di fragilità, dove questa viene influenzata della diversità della topografia e della morfologia dell'alveo fluviale, lungo l'asta analizzata, associata all'andamento del sistema arginale nello spazio.

Viene in oltre proposta una classificazione, per entrambi i meccanismi di rottura, volta a definire un'indicazione del grado di affidabilità del tratto arginale analizzato su base delle informazioni ricavate dalle curve di fragilità.

A completamento del lavoro si è ricorso ad un modello idraulico, dove viene simulata una piena cinquecentennale utile per determinare il valore di pericolosità di allagamento, attraverso le curve di fragilità utilizzate nelle analisi, per ogni tratto arginale in corrispondenza dei relativi tiranti idrici, e dunque confrontare i risultati con le classi ottenute.

Questo lavoro ha inoltre lo scopo di porsi come interfaccia tra il mondo della geologia applicata e l'idraulica fluviale, dove al giorno d'oggi un stretta collaborazione tra le due figure professionali è necessaria per risolvere e migliorare la stima del rischio idraulico.

ABSTRACT

Since antiquity, people have settled down in vast fluvial plains near water bodies and major river systems to make the most of the available resources. Inevitably, nature maintains the upper hand and "takes back what is taken from her". Today, as in times past, mankind has realized *he is too exposed to risk*. It is currently well known, even for people that are not experts on the subject, that Italy is a country with a high hydro-geological risk. So much so that landslides and floods are often not perceived as exceptional or "catastrophic" events. Instead, they are part of daily life without knowing exactly where and how they will occur. With mankind's knowledge and ability to provide protection from these phenomena, works known as hydraulic constructions are put in place in order to prevent the flooding of areas near waterways.

The most well-known and often-used hydraulic constructions to protect areas from flooding are levee systems. These systems are comprised of long, earthen embankments, also called dikes, of various shapes and sizes; they are placed throughout the floodplain and also near the main river. However, levees are not meant to last or protect indefinitely and like so many other things created by the mankind, they can eventually fail.

This work aims to evaluate the reliability of these levee systems, calculating the probability of "failure" of determined levee stretches under different loads, using probabilistic methods that take into account the *fragility curves* obtained through the Monte Carlo Method.

For this study overtopping and piping are considered as failure mechanisms (since these are the most frequent) and the major levee system of the Po River with a primary focus on the section between Piacenza and Cremona, in the lower-middle area of the Padana Plain, is analysed.

The novelty of this approach is to check the reliability of individual embankment stretches, not just a single section, while taking into account the variability of the levee system geometry from one stretch to another.

This work takes also into consideration, for each levee stretch analysed, a probability distribution of the load variables involved in the definition of the fragility curves, where it is influenced by the differences in the topography and morphology of the riverbed along the sectional depth analysed as it pertains to the levee system in its entirety.

A type of classification is proposed, for both failure mechanisms, to give an indication of the reliability of the levee system based of the information obtained by the fragility curve analysis. To accomplish this work, an hydraulic model has been developed where a 500-year flood is modelled to determinate the residual hazard value of failure for each stretch of levee near the corresponding water depth, then comparing the results with the obtained classifications.

This work has the additional the aim of acting as an interface between the world of Applied Geology and Environmental Hydraulic Engineering where a strong collaboration is needed between the two professions to resolve and improve the estimation of hydraulic risk.

2. Introduction to the work

Flood plains have always represented an attractive environment for societies to settle and develop. Modern societies seem to have inherited the tendency to settle near waterways (Di Baldassarre et al., 2010a), exposing themselves to the potentially negative consequences of water-related hazards. It is a sort of trade-off between benefits and damages.

Several researchers over the past decade (Ohl and Tapsell, 2000; Milly et al., 2002; Opperman et al., 2009; Di Baldassarre et al., 2010a) have shown that the urbanization ratio of deltas and flood plains, increasing population growth, and changes in land use and climate have contributed to an increasing number of fatalities and economic losses attributable to water-related hazards.

Traditionally, levees are a structural measure widely adopted for flood control (Heine and Pinter, 2012; CIRIA, 2013), accepted and trusted by populations living in flood plain areas. The presence of levees may even induce a false sense of safety in the population, influencing their decision to develop further in floodplains because they feel safer (Mazzoleni et al., 2014). Nevertheless, besides reducing the frequency of flooding in the stretches they are supposed to protect, building a levee system along a river might induce the so-called “levee paradox” (White, 1945) which is related to the change in the hazard perception related to levee strengthening.

The lower the hazard perception, the higher the urbanization in the flood prone areas and exposure to the flooding hazard (Mazzoleni et al., 2014) whereby some societies are paradoxically incentivized to develop in the floodplains and thus expose themselves to high-consequence and low-probability events. As a result, the reduced frequency of flooding attributable to the structural measure modifies the perception of risk (Burton and Cutter 2008; Di Baldassarre et al., 2009; Ludy and Kondolf, 2012; Di Baldassarre et al., 2013). Therefore, the negative consequences associated with failure of a levee system vary dramatically with the extent of the inundation area; the size of the population; the economic activities exposed to risk; and the amount of the available warning time (Masoero et al., 2013). While providing an efficient protection against low magnitude flood events, levees may fail under the load of extreme water levels and long flood durations.

Losses arising from subsequent inundation may be dramatic not only because of the high value concentration in undeveloped backcountry, but additionally due to fast water level rise and

high flow velocities caused by rapid breach outflow (Alkema and Middelkoop, 2005).

Implicitly accounting for the effects of the levee paradox and widespread anthropization of most of the territories of the European countries, European Union (EU) directive 2007/60/EC (European Parliament Council 2007; Mostert and Junier, 2009) stresses the importance of non-structural methods to mitigate flooding risk. A key aspect of this approach is the drawing, by member states, of flooding hazard and risk maps for potential flooding areas. Maps should be drawn to show three different flood events with (1) low, (2) medium, (i.e., likely return period ≥100 years), and (3) high probability of occurrence (de Moel et al., 2009). A little flexibility is given to each member state in the definition of the return period. According to Italian law, for instance, D.L. 49/2010 defines high-probability events as those with return period between 20 and 50 years; medium probability as those occurring once every 100 or 200 years, on average; and low probability as those with a return period up to 500 years. The current legislative framework motivated the development of several studies aimed at proposing new methodologies to address the evaluation of flooding-hazard maps. Assessing the flooding hazard is in fact affected by various sources of uncertainties (Ranzi et al., 2012), which are related to a cascade of hydrological, hydraulic, and geotechnical uncertainties.

This study focuses on the development and application of a new modelling approach for a comprehensive flood hazard assessment along protected river stretches with a focus on levee failures due to overtopping and piping. The primary levee system, specifically the stretch between Piacenza and Cremona, of the Po River in northern Italy has been analysed yielding sufficient data to create a model showing high variability with regards to both morphology and topography. In addition, the results change as a function of this variability that is concurrent with previous flooding events in this area that were caused by a series of levee breaches.

Hydraulic structures and other secondary levee systems inside the floodplains are not considered in the analysis. Although their effects are neglected, the results from the final modelling are discussed taking their presence into account.

In the part one of this work, an introduction to the case study is presented describing the levee system of the Po River and summarizing the historical flood and levee breaches in these last two hundred years.

Then, a short description of the section between Piacenza and Cremona is given briefly explaining all the characteristics of the area in terms of geology, hydrography, and hydrology.

Part two will further describe the applied usage of probabilistic methodology to evaluate levee

reliability. In analysing the levees, two approaches were used to obtain the necessary fragility curve with the Monte Carlo Method (using MatLab), where topographic sections from the *Agenzia Interregionale per il Fiume Po (*AIPO) are set as a centred point (first approach) or limits as boundary conditions (second approach). Lastly, all physical knowledge about the failure mechanisms considered in this work are described where *overtopping* is taken from the formula used in the previous works of Vorogushyn and *piping* from the gradient model elaborated by M. Mazzoleni. A provision will also be given to the in-depth analysis of all the sections of the input data analysing all uncertainty and errors. These include data from literary research related to geotechnical and surface cover factors. Additionally, topographic information is incorporated from the moment that the levee geometry has a strong weight for the results from the data processing followed by a proposed implementation.

Part three details the data processing and analysis of the fragility curves for each mechanism of failure in correlation to the different approaches. An implementation on the fragility curve is done by taking into account a hypothesized probabilistic distribution of the hydraulic variables and the morphological variability of the riverbed associated to the levee system.

Part four presents a classification for overtopping and piping to identify a class of unreliability for levee stretches. The classes are discretized on indexes based on the characteristics of the fragility curves. A performance classification for overtopping is proposed to understand levee reactions to different hydraulic stress.

Lastly, in the part five, a hazard analysis using the fragility curves is completed. This achieved by simulating a flood, for the section from Piacenza to Cremona, with a return period of 500 years. This is done to determine where a hydraulic load could cause dangerous conditions to locate possible flooding area(s).

An estimation of the flooding water for overtopping is also proposed. This is done with a probabilistic discharge water volume terms, instead of a probabilistic flooding map, as a function of overtopping flow time and determined return time. Concluding this work will be a summary of the results with considerations and correlations between the unreliability classes and hazard value found within the fragility curve. This will be followed by a summary of the work, as well as all the observations about the methodologies.

2.1 The hydraulic risk

2.1.1 The risk formula

Defined in the *Piano stralcio per l'Assetto Idrogeologico* (PAI), and consistent with what is defined in the national and international headquarters, the various factors that connect risk to the hydraulic inundation scenarios of floodplains are summarized in the following expression (AdbPO, 2005):

$$\boldsymbol{R = E \times H \times V}$$

Where:

R = relative risk to a particular element, defined as the expected value of the damage which on average can undergo the same element in a predetermined time period;

E = amount of elements at risk, such as people and goods that may be damaged when an event occurs, measured in different ways depending on their nature;

H = hazard, corresponding to the probability of the event occurring in one specific time interval (*T*) and in an area such as to affect the risk item. The value of *H* is a function of the return time *T* event; it expresses the interval time in which the event occurs on average once. That is in fact the relationship $H = 1 - \left(1 - \frac{1}{T}\right)^t$;
where *t* is the time interval in which the hazard is estimated, expressed in years.

V = vulnerability, defined as the attitude of the element at-risk to suffer damage due to the event itself (rate of the element at risk that is damaged); is between 0 and 1.

It is evident that different values of *E* and *V* can compete against one another depending on the event's characteristics. Moreover, with equal conditions, equivalent *E* and *V* may vary depending on purely random factors such as the time of year, day of week, and time when the event occurs. Therefore, *E* and *V* can be considered random variables (AdbPO, 2005). For this reason, in order to properly define the risk, one must be as accurate as possible to try to obtain a hazard value (*H*).

2.1.2 The Residual Hazard

From the moment that an area protected by levee system is studied, it is correct to speak about *Residual Hazard.* The residual hydraulic hazard is related to the occurrence of flood events that are higher than those of flood design (ex: A full PAI project of the Po River with a return of 200 years). Residual hazard is more representative of higher flood scenarios than the project scenarios such as those that exceed the safety margins of defense works. Therefore, the necessary risk remains following the implementation of the proposed measures for arrangement of the watercourse project achievement. The necessary risk also assumes different significances in relation to the different vulnerabilities of the surrounding areas (Comune Monticelli, 2012).

Consistent with the definition of flood risk previously explained, is possible to define (AdbPO, 2005):

- *Residual hydraulic hazard of flooding by overtopping:* probability that events of greater magnitude than the flood design occur; this is assumed for the dimensioning of levee systems, both in terms of event intensity and for characteristics not taken into account in the analysis of the levee system itself.

- *Residual hydraulic hazard of flooding by levee breaches*: joint probability of a flood event that determines both high water levels and structural failure of the embankment;

- *Residual risk of flooding:* product hazard for residual social damage and economic potential, represented by the value of the elements at-risk and their vulnerability.

Using the main levee system of the Po River as an example, the set design of the stretch of the watercourse, defined in the PAI, is the reference planning tool for which the levees have to be adjusted (with the franc equal to one meter). This is adjustment is done according to the reference flood profile in terms of hydraulic restraint and structural characteristics with respect to the phenomena of filtration and piping along the embankment. With respect to the holding function, the presence of the franc close to zero, compared to the 200-year flood, allows one to consider that the flow capacity of the flood section, without overflow, is above a flood with a return period of 500 years (Comune Monticelli, 2012).

2.2 The Po Basin

The catchment area of the Po River has a total area of about 70,700 km^2 (Cati, 1981). This includes most of northern Italy, along with some small areas in Switzerland and France, (5.2% and 0.2%, respectively) determined using GIS dosing techniques (G. Nigrelli, 2013). Under geographical and geomorphological aspects, the basin is composed of three main sectors:

1. Alpine (45% of the total area);
2. Apennine (15%);
3. The Po Valley (40%), defined as the strip of territory situated between the Alpine and Apennine sectors with a total length of approximately 490 km and a variable width from 20 to 120 km.

Figure 1: Po Basin, image obtained by Terra Modis Satellite 19/09/2003 (http://rapidfire.sci.gsfc.nasa.gov/)

In general, the basin is presented as rectangular in form having an east-west orientation with respect to surface drainage. The Po River network has a dendritic drainage pattern type. It begins at an altitude of 2,022 m on the northwest slope of Mount Viso (3,841 m above sea level) and winding along the 45th parallel. The Po River first travels north then east flowing into the Adriatic Sea with a strong projection delta (G. Nigrelli, 2013).

It is, in many ways, the most important river in Italy. Its approximate 652 km in length make it the longest river within Italy's borders. Its maximum discharge, approximately 10,300 m^3/s, was measured in Polesine during the flood on November 14, 1951. It is this area, located between the lower reaches of the rivers Po and Adige near Adriatic Sea, that has the largest basin defined by Italian law 183/89: *"…the territory from which rainwater or melting snow and glaciers, flowing out to the surface, are harvested in a given watercourse directly or through tributaries, as well as the area that can be flooded by the waters of the same river, including its terminal branches with the mouths into the sea and the closest maritime coast* (art. 1)."

The Po Basin contains rivers and tributaries with very different hydrological flood characteristics depending on the exposure to meteoric disturbances, morphology, as well as the type of soil and ground cover present.

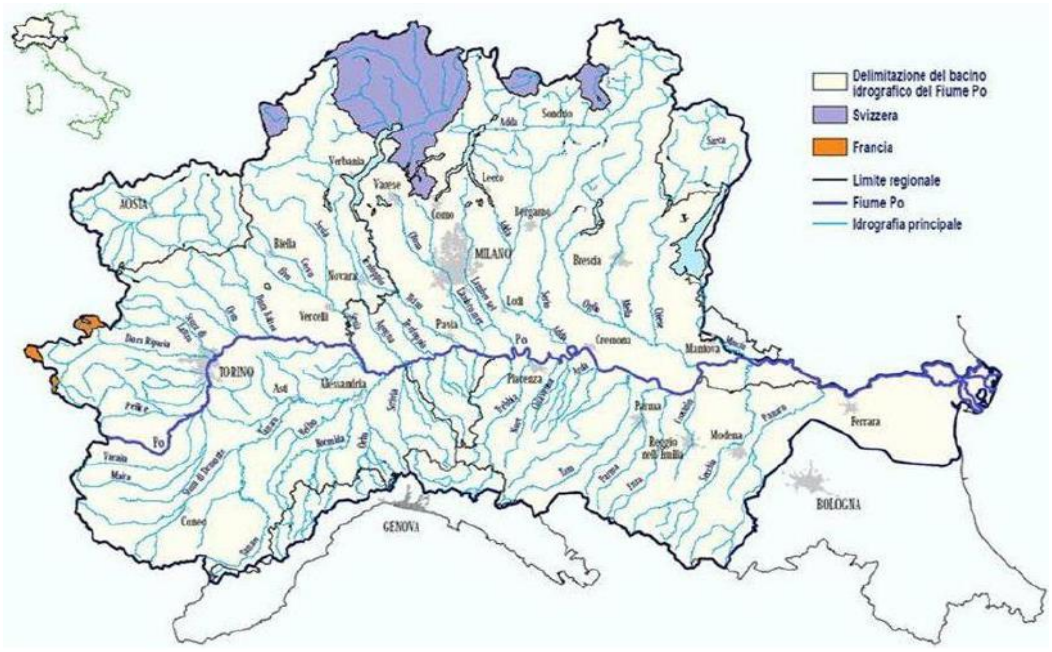

Figure 2: The Po River and its tributaries (F. Carisi, 2011)

It is possible to recognize five different areas with a homogeneous behaviour (F. Carisi, 2011):

- Alpine interior basins;
- Alpine foothill basins;
- Piedmont/Apennine basins;
- Alpine/Lombard basins;
- Emilia-Romagna Apennines basins.

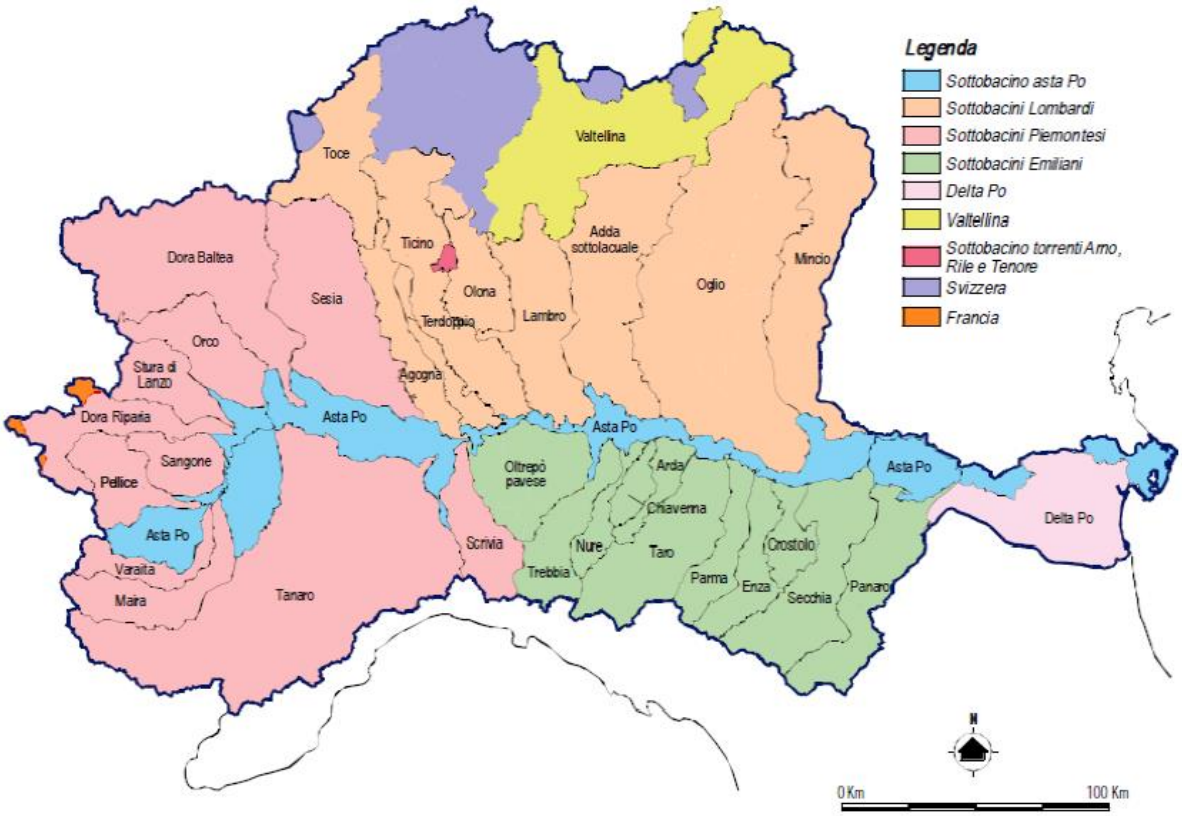

Figure 3: Borderline of the main hydrographic under basin (F. Carisi, 2011)

The climate of the basin is complex and varied in correlation to the geographical position that it occupies along with the composition of each sectors' morphology. Under the meteorological aspect, the basin is located in an area of confrontation between polar masses and tropical air. In particular, there is a situation that is interposed between the cold, sub-polar air of the north; the warm one from the Mediterranean; the humid maritime climate of the west; and the dry climate from the mainland; or the peri-desertic from Eastern Europe. This situation causes very diverse climatic conditions during the year manifesting in various forms in different geographical sectors (G. Nigrelli, 2013).

The mean annual precipitation in the basin is 1,100 mm, while the Alps and Apennines receive around 2,000 mm. The river plain receives approximately 750 mm of precipitation (Turitto et al., 2010).

In the Alpine catchments, the intensity of torrential floods carrying a large amount of sediment is increasing at an alarming rate; the geo-hydrological risk, often accentuated by inadequate spatial planning, manifests itself through forms and processes that, more and more often, involve the plain sector and the stem of the main basin.

2.3 The Po River levee system

2.3.1 Characteristics

The Po River has been historically characterized by a continuous system of embankments. Over time, and especially following the events of most relevant floods, they progressively extended upstream, becoming a real soil dike system. These embankments have been raised and enlarged in the middle and lower part of the plain with a maximum height of up to about 10 meters. Today, these embankments are no longer significantly adaptable in height due to the structural boundary conditions they have reached (AdbPO, 2014). This portion of the Po Valley is defined as ARS - Area at Risk Significant. This is due to the importance of this defensive system, the extension and intensity of processes of flooding resulting from scenarios of residual risk, and the extent of potentially floodable, exposed structures.

The levee system consists of about 1,100 km of embankments defending 8,500 km^2 of potentially floodable area in the Po Valley from levee rupture.

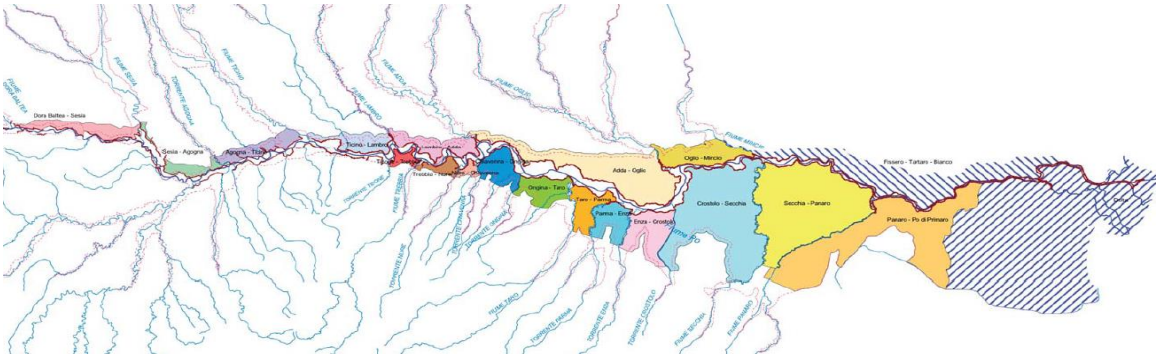

Figure 4. : The Po River levee system and its compartments (AdbPO, 2009)

In the upstream stretch, near Turin, lies the Orco confluence and, further south, the Tanaro confluence (93 km). Here, the main levee system has been better implemented and more recently completed than downstream stretches due, in part, to floods in both 1994 and 2000. These levees are usually located in the floodplain, with only a few short stretches close to the river.

From the Tanaro confluence to the Adda (138 km), the levees are nearly continuous along both sides with some interruptions related to the presence of regurgitation embankments along the main tributaries. Along the edge of the high terrace or where the embankments need to be completed, the towns of Pieve del Cairo, Sannazzaro de Burgondi, San Cipriano Po, Port'Albera and Arena Po are currently in the flooding hazard zone with a medium flooding

probability.

Down from the Adda confluence to the Mincio (133 km), the levees are continuous along both banks and define a wide—typically 2-3 km, but up to 5 km—river region where there are numerous internal levee systems whose importance is fundamental for the flood lamination.

Embankments begin getting closer to one another from the Mincio confluence to the sea (154 km). Further downstream this trend is also present in the Panaro confluence where a series of dams, corresponding to the Po's riverbanks, are relatively--500m to 1km—close together.

2.3.2 Evolution in time

The major or main levee is the most important passive hydraulic passive work in defence of the territory behind it compared to the river. The main levee is designed so that it is never exceeded by floodwaters and consists of a tall, substantial embankment able to withstand even the most violent flood. Therefore, when calculating appropriate project sections, it is important to consider the types of materials used and the hip's inclination or vestments. Additionally, the share of the embankment top, compared to the height reached by the highest known historical floods, should ensure a franc of at least one meter (V. Ferrari et al. 2008).

The entire section of the fluvial embankments are then analysed on both sides of the riverbed, which have been built at different times, but with good continuity since the early 1800s. Over time, in order to enhance the efficiency of the original defence system, the embankments have been developed in length, height and width. Each time, new material is overlayed on ancient containment works of which the geometry, composition, and the nature of the support deposits are not well known (G. Nigrelli, 2013).

In the twentieth century, this system has had significant phases of rising, slub and extension upstream at the main tributaries. These phases were particularly intensified during the floods of 1929, 1951, 1994 and 2000 (Figure 5). One outcome of the flood in November 1994 was functional testing for the interventions made after the flood in 1951 since many levees had been repaired although untested by flood until 1994. Also as a result, in accordance with *Piano Stralcio PS45*, many measures were implemented to change the height and shape of levees (AdbPO, 2005).

Installations of these interventions were further intensified after the flood in October 2000; the embankments have been mostly adequate with upper sections following the directives from project SIMPO 82 project while in other stretches, mainly in correlation to population

centers, the adjustment was commensurate with the flood profile defined in the Transitional Plan PAI (TR = 200 years) (AdbPO, 2005).

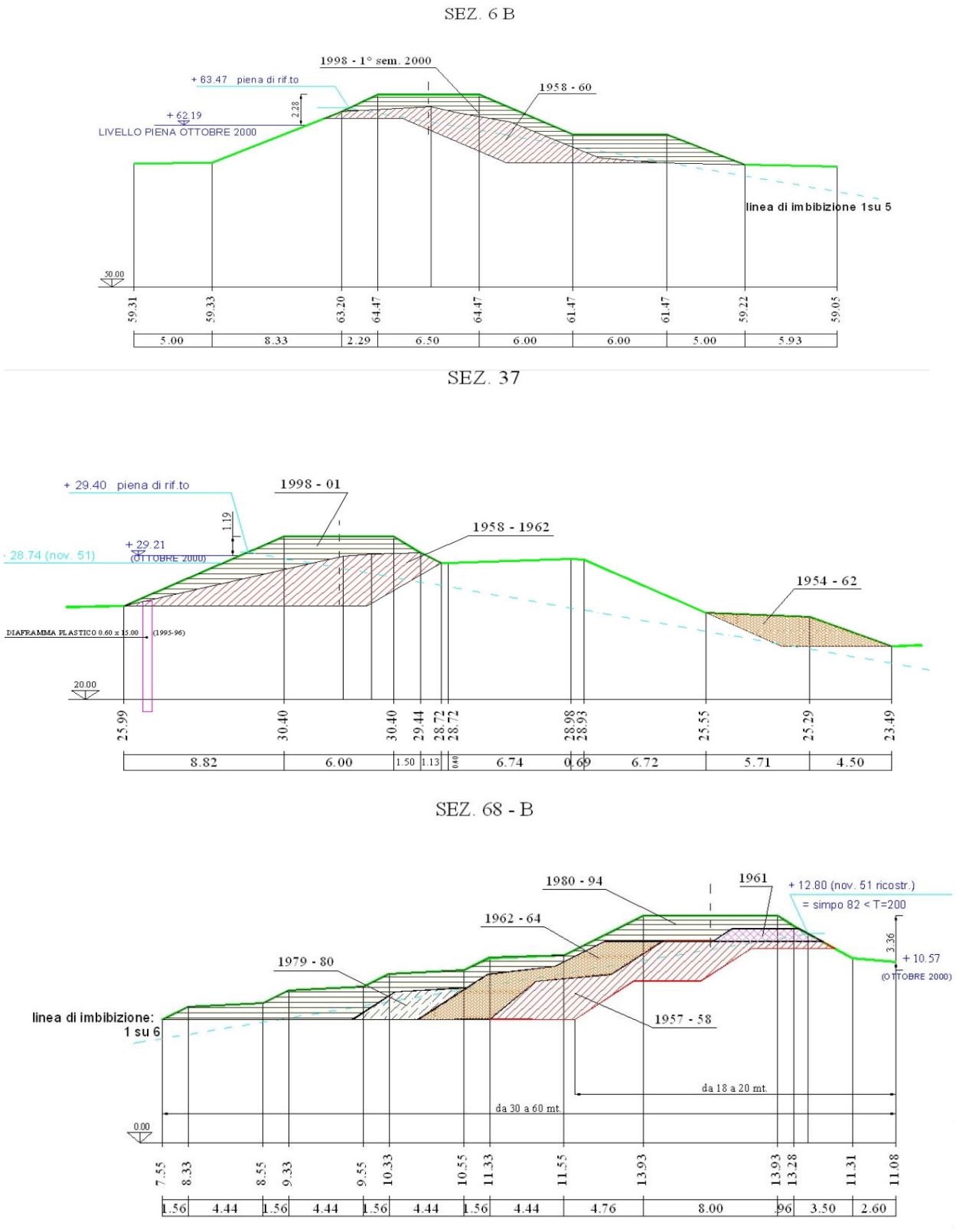

Figure 5: Levee evolution in the upper-middle (sec. 6-B), middle (sec. 37), and lower section (68-B) of the Po River (AdbPO, 2005)

2.4 The historical flood events and levee breaches of the Po River

2.4.1 The historical floods of the 19th and 21th centuries

The extensive historical documentation available allows an analysis of floods that affected the Po from the beginning of the eighteenth century to the present. Figure (6), based on data taken from a section between Mantova to the sea, shows a clear trend towards increased peak water in direct relation to progressive development of the levees' length and height that were almost constant on both sides early as the sixteenth century (AdbPO, 2005).

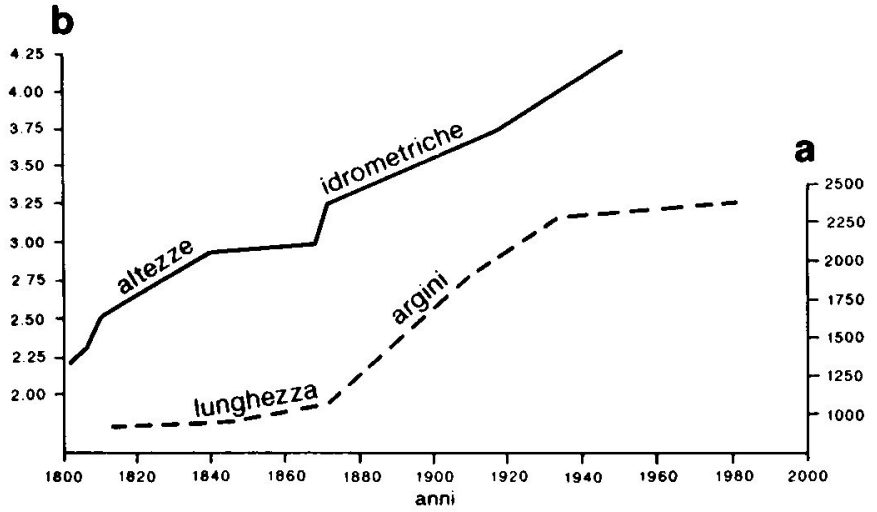

Figure 6: Trend of water load in relation to main levee length; (a) levee development in time along the Po River and (b) the increase of the water height measured at Pontelagoscuro (AdbPO, 2005)

Subsequently, the containment works were primarily extended upstream in the Lombardy and Emilia-Romagna regions' main tributaries resulting in a progressive increase in flooding containment volume, reduced lamination in the plain areas of the basin, and increased values of flood peak in the main stem. This process has gradually reduced the amount of lowland areas that are naturally unprotected and subject to flooding as well as flooding caused by levee failure, caused by overtopping, by erosion foot or by piping (F. Carisi, 2011).

In the nineteenth century, a quick succession of floods in the stretch from the Ticino confluence to the Delta upset the levee system of the Po River. The century opened with a flood in November 1801, (Gallizia, 1878) second only to the flood in 1705. After six years, in December 1807, another flood occurred and, in some places, exceeded the maximum water load that occurred in 1801 causing numerous breaches in the left levee in Mantova area (Govi & Turitto, 2000).

Three decades of relative tranquility passed—significant floods occurred, just not on a catastrophic level—until October 1839 when another great flood upset the riverbed causing several levee ruptures and extensive flooding. Other floods, all of great significance, followed in 1846, 1857, 1868, as well as the spring and autumn of 1872. The last great flood of the nineteenth century happened in 1879. Among other things, this flood caused the failure of the levee downstream of Revere, resulting in flooding for the third time in a forty-year period (Gallizia, 1878).

Thirty years passed with relative calm until October 1907 with flooding near Lodi, Pavia, and Piacenza. Further flooding occurred in Lodi a decade later in 1917. Approximately a decade after the flood in Lodi, Piacenza experienced a flood in May of 1926 (Govi & Turitto, 2000). Twenty-five years, in November 1951, there was the disastrous flood that caused levee failures in Paviole and Occhiobello along with a consequential flood of about 1,000 km^2 in the province of Rovigo.

The last great floods of the century happened in 1994 and 2000. Although they proved catastrophic for several major tributaries of the Po, such as the Tanaro, Dora, Baltea, etc., they have not caused appreciable levee failures along the main stem.

Data	Becca	Piacenza	Cremona	Casalmaggiore	Borgoforte	Pontelagoscuro
Novembre-dicembre 2002	496 (6840)	718 (7094)	438 (8275)	663	864 (9634)	261 (8120)
Ottobre 2000	781 (11600)	**1050**	**615 (11800)**	**801**	**993 (11800)**	366 (9750)
Novembre 1951^	785 (11250)	1025 (12800)	594	764 (12100)	976 (11800)	**428 (10300)**
Ottobre-novembre 1928	634	826 (9340)	447	657 (10070)	860 (9540)	367 (8780)
Ottobre-novembre 1926	613	800 (8620)	450	621	845 (9530)	347 (8550)
Maggio 1926^	**788 (11700)**	963 (11630)	462	637 (9695)	823 (9200)	370 (8850)
Maggio-giugno 1917^	756 (10100)	900 (12000)	541	552 (10220)	889 (10270)	372 (8900)
Ottobre-novembre 1907^	756 (10100)	857 (9205)	539	654 (10220)	852 (9536)	330 (7880)
Maggio-giugno 1879^	681	770	495	595	823	321
Ottobre 1872^	701	795	517	602	851	332
Maggio 1872^	591	nd	nd	nd	nd	225
Ottobre 1868^	702	760	539	607	823	305
Ottobre 1857^	784	731	541	596	795	296
Novembre 1839^	560	581	463	552	762	295
Ottobre 1839^	660	682	475	554	711	269
Ottobre 1812^	nd	nd	nd	492	725	255
Dicembre 1807^	nd	nd	nd	524	725	232
Novembre 1801^	631	635	504	561	750	219
Ottobre 1755^	nd	nd	nd	520	723	182
Novembre 1705^	745	nd	nd	556	nd	132

Table 1: Maximum values shown comparing high stages (cm) and flow (m^3/s) in brackets, detected by the principal gauges of the Po River, from 1705 to 2002 (G. Nigrelli, 2013)

From November 5-24, 2014 three consecutive floods occurred along the Po. The first, occurring between November 5-10, offered of minimum relief. The second, of greater importance, with peak flow in Pontelagoscuro of 7,900 m^3/s affected the main stem of the Po from November 13-16 with stages above the L2 threshold levels (critical moderate). Finally, a third flood occurred between November 16-23 while the previous flood was still draining with peak flow in Pontelagoscuro of 8,400 m^3/s and stages at critically high L3 levels (G. Zannichelli & S. Pavan, 2015).

		Sezioni idrometriche 1/2 (monte)											
		Becca			Spessa			Piacenza			Cremona		
Evento		h	Q	T	h	Q	T	h	Q	T	h	Q	T
1994		7.60	11500	-	" "	11500	32.3	9.98	11600	71.3	5.94	11300	39.7
2000		7.81	11600	-	8.94	11600	33.7	10.50	" "		6.15	12100	61.0
2002		4.96	7200	-	6.19	7000	4.5	7.18	7400	7.6	4.38	8100	7.2
2009		5.51	7800	-	6.47	7600	5.8	7.60	7500	8.1	4.00	8200	7.6
2014 (13- 16 novembre)		4.60	-	-	5.80	6800	4.1	6.94	6600	5.0	3.65	7500	5.3
2014 (16 -23 Novembre)	Oss	5.22	-	-	6.37	7700	6.1	7.55	7500	8.5	4.35	8650	9.2
	Data	16/11			17/11			17/11			17/11		
	Ora	21:00			01:00			12:00			17:20		

Table 2: Hydrometric mountain section. (h) Height [m zero hydrometric], (Q) flow [m^3/s], and (T) return times [years] to the peak flow along the main stem during floods events from 1994 to 2014 (G. Zannichelli & S. Pavan, 2015)

		Sezioni idrometriche 2/2 (valle)											
		Casalmaggiore			Boretto			Borgoforte			Pontelagoscuro		
Evento		h	Q	T	h	Q	T	h	Q	T	h	Q	T
1994		7.64	11300	-	8.42	10300	31.8	9.35	10800	42.2	3.04	8700	15.1
2000		8.01	12000	-	9.06	11800	76.4	9.92	11800	78.0	3.66	9600	27.6
2002		6.63	8300	-	7.75	8600	11.9	8.64	9200	16.0	2.61	8100	10.1
2009		6.47	8200	-	7.41	8100	9.0	8.07	8200	8.8	2.46	7700	7.8
2014 (13- 16 novembre)		6.34	-	-	7.54	8200	9.5	8.12	8300	9.4	2.70	7850	8.6
2014 (16 -23 Novembre)	Oss	7.01	-	-	8.18	9100	15.7	8.83	9300	16.7	3.00	8350	11.7
	Data	18/11			18/11			19/11			19/11		
	Ora	7:30			20:30			04:00			09:30		

Table 3: Hydrometric valley section. (h) Height [m zero hydrometric], (Q) flow [m^3/s], and (T) return times [years] to the peak flow along the main stem during floods events from 1994 to 2014 (G. Zannichelli & S. Pavan, 2015).

In terms of ground effects, these events resulted in flooding in the most remote riverside floodplains. These low-populated areas in the countryside experienced the widespread effects of filtration along with the triggering of sand-boils, especially in the areas near Ferrara and the Po Delta. Among the reasons for the failure of the levees in the riverside floodplains, as well as the overtopping of the smaller ones, culpability is given to piping based on the presence of holes that have proliferated the embankment net in recent years.

The analysis of historical events consents to define four reference scenarios, which define the types of most frequent association of under basin, associated to one or more regional areas, which is attributable to a significant contribution in the formation of flood along the Po River (F. Carisi, 2011):

-*1st (Piedmont)*: the events are characterized, almost exclusively, by inflow of the rivers Sesia, Tanaro and Ticino. The Po Basin sector involved is the western or central-west; historical events involved are those of 1705, 1755, 1857, 1907, 1994 and 2000 all occurred in Autumn;

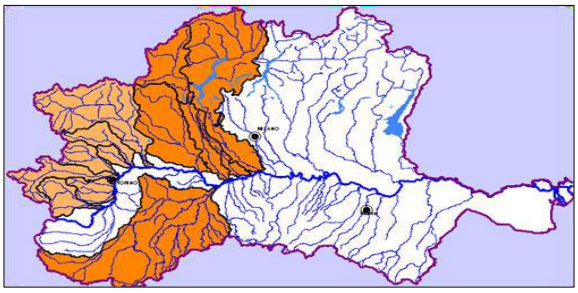

Figure 7: Piedmont scenario (F. Carisi, 2011)

- *2nd (Lombardy):* is characterized by the simultaneous participation of the Ticino, Lambro, Adda and Oglio rivers; the primary Po River Basin area involved in the central sector. The floods assignable to this type are those from 1807, 1812 and 1968.

- *3rd (Piedmont-Lombardy)*: the waterways that provide more decisive contribution to the Po are the Sesia and the Tanaro; also notable are the contributions of Adda and Oglio rivers. The basins of central and western side of the Alps are also involved; floods in this scenario occurred in 1801, 1917 and 1926.

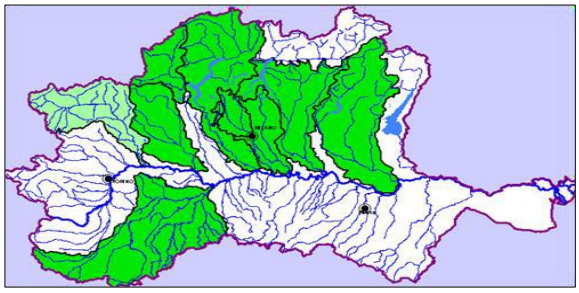

Figure 8: Piedmont-Lombard scenario (F. Carisi 2011)

- *4th* (Entire Po Basin): there is an obvious spatial dimension of this event along with the large number of rivers that, in the different sectors of the Po River system, participate in the formation of floods. The events represented in this type happened in 1839, 1872, 1879 and 1951.

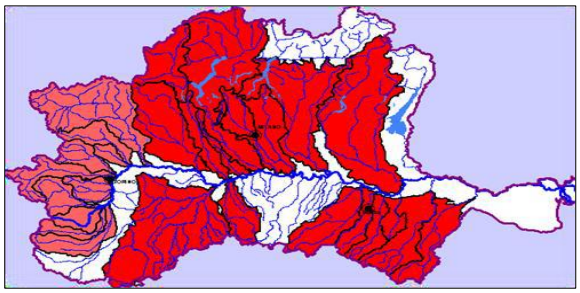

Figure 9: Whole Po basin scenario (F. Carisi 2011)

2.4.2 Levee breaches of the Po River

Over the past two centuries, more than 200 flood events have caused the breakup of the embankments, including the flood in 1951. It was during this flood when the failure of the left levee in the Veneto region caused the flooding of 1,000 km^2 of territory that remained submerged for several months with maximum values of water load, in some areas, equal to 4 - 6 meters in height; the main causes of failure can be traced to overtopping of the levee, to filtration in the body of the dike or in foundation soils and erosion phenomena erosion caused by the current (AdbPo, 2014).

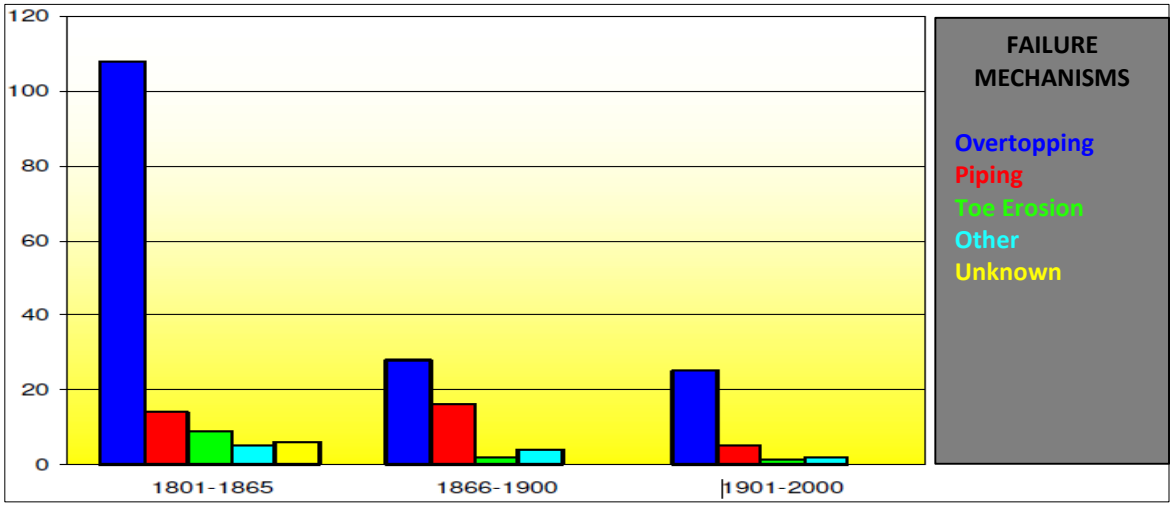

Figure 10: Levee breaches in function of the failure mechanism; distribution in time (AdbPO, 2005)

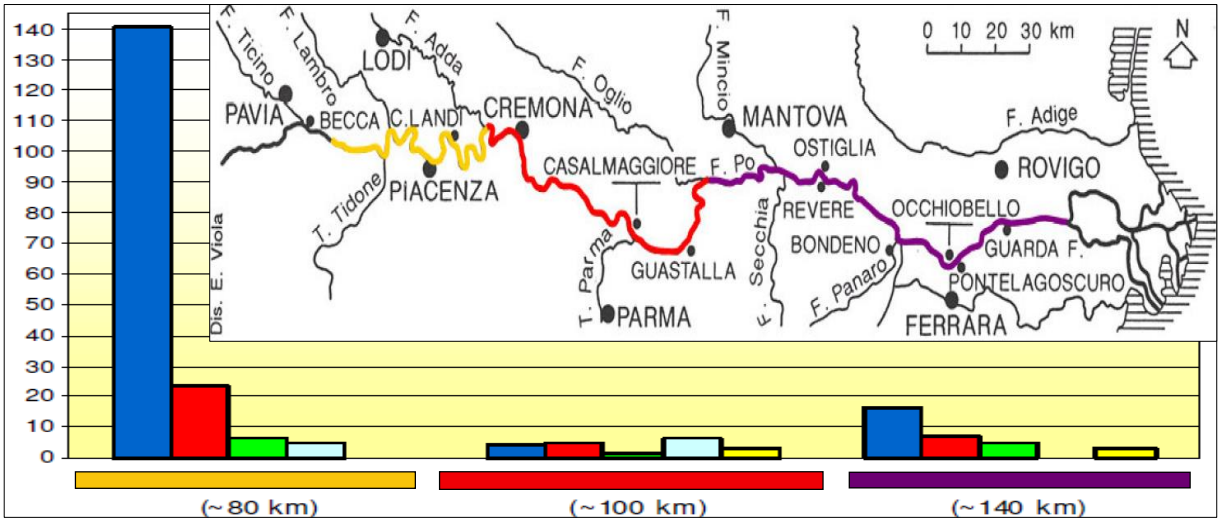

Figure 11: Levee breaches as function of the failure mechanism; distribution in space (down, related to different fluvial model) (AdbPO, 2005)

Considering only events for which information is available, there have been seven floods since 1700 that have caused the most widespread and serious flooding: November 1705, November 1801, October-November 1839, May 1872, October 1872, May-June 1879, November 1951.

In the upper-middle stretch near Piacenza there have been at least seventeen events caused by flooding in the same areas.

Seventeen of the eighteen floods that occurred between 1705 and 1951—excluding the flood 1951—were more prevalent in the Lodi and Piacenza sectors as areas of expansion.

In 2004, the Basin Authority, in collaboration with CNR-IRPI of Turin, conducted a detailed, complete gathering and organizing of activities of the information available on historical ruptures that have occurred in the lower-middle part of the Po's main stem.

In total, 225 breaches have been counted beginning with the very serious floods in 1801.

204 of these cases occurred in the main levee system while the remaining 21 occurred in the final stretches of Po River's main tributaries. Each of these breaches has archival material available that has been collected and organized detailing the place and date of course; the failure mechanism; the size of the gap; the hydrometric data of the nearest measure station; information in relation to the dynamics; and the flooded surface area.

These activities allow highlighting of how the type of failure that occurred more frequently is associated with the phenomena of overtopping as well as piping.

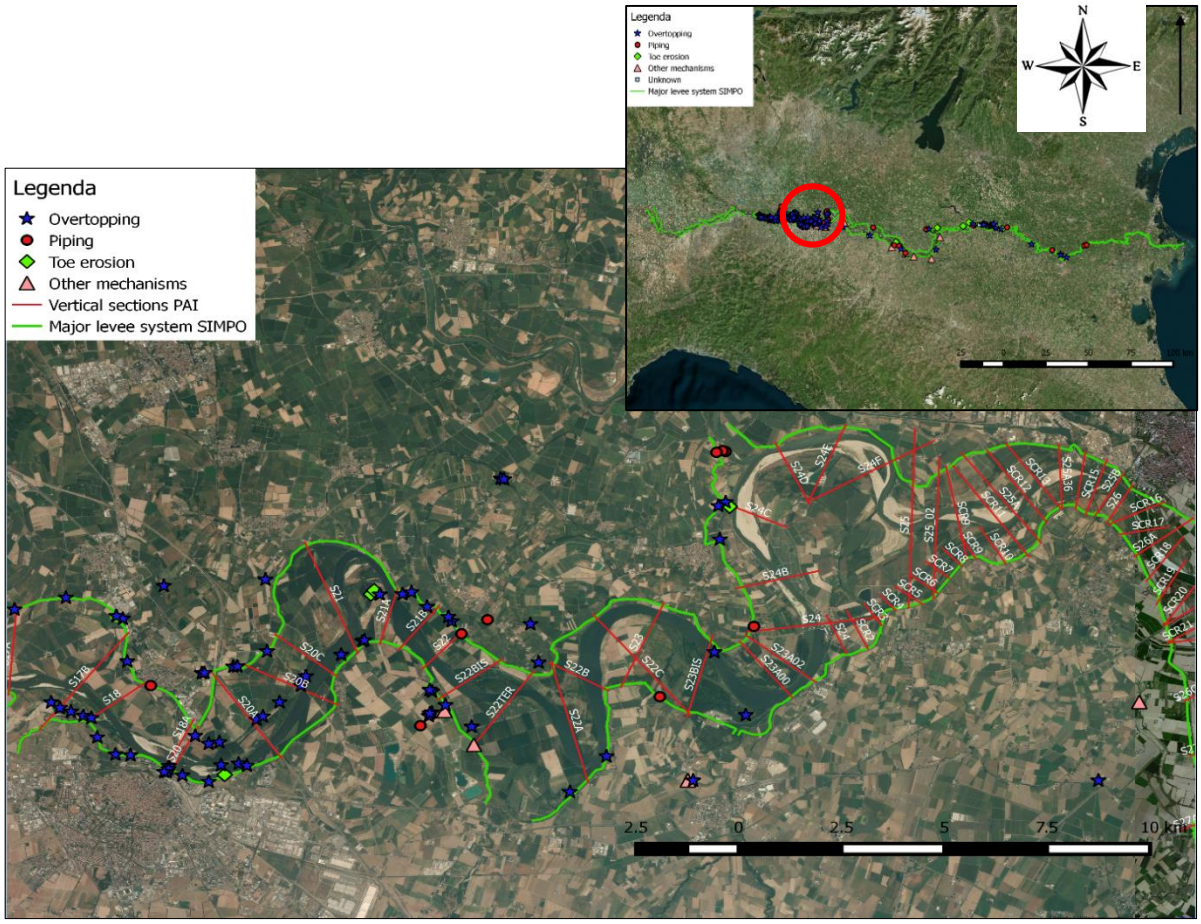

Figure 12: Localization of the historical breaches along the Po levee system (top) and in detail the area of the work

3. Case study: the levee system from Piacenza to Cremona

There are many reasons why this area has been chosen. Literary research has shown this area to been heavily affected by flooding in prior centuries where many of the failure mechanisms of this stretch's levee breaches were caused by overtopping and piping. A large amount of useful data is also available to obtain fragility curves utilizing the work of Alessio Domeneghetti, Ph.D., who previously studied this area. The variation in topography and the morphology of the levee system yield an interesting analysis where the results change as a function of this variability. It was also possible, in collaboration with Dr. Domeneghetti, to generate a 1D hydraulic model for a flood in this stretch of the main stem with a return period of 500 years for a hazard estimation.

3.1 Geographical location

This study has analyzed, as previously mentioned, the *main levee system* of the Po River focusing on a specific stretch in the lower-middle section of the main stem. The 45 km stretch, in the middle of the Padania Plain, is bounded by a levee system on both sides of the river from Piacenza in the Emilia-Romagna region to Cremona in the Lombardy region.

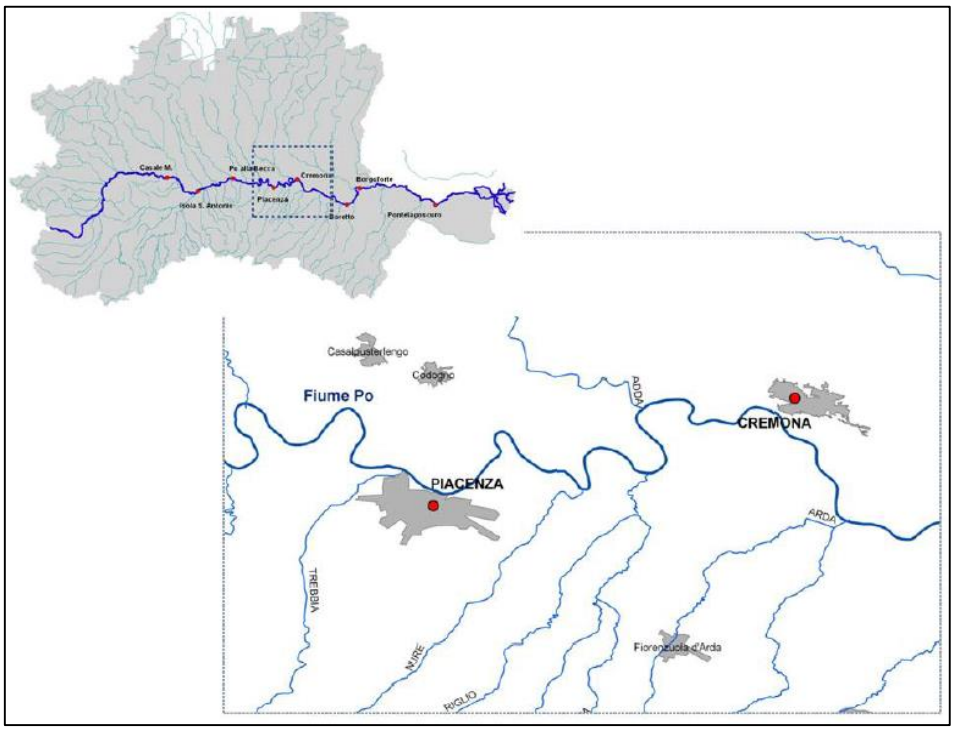

Figure 13: Area of analysis: Po River between Piacenza e Cremona (45 km) (A. Domeneghetti, 2011)

In recent times (Cadaster map of the Po River's main levee system - AdbPo) no levee breaches due to overtopping have been occurred in this section, even for piping. However, a series of sand-boils occurred upstream from Castelnuovo d'Adda during floods in 1994 and 2000. Along the embankments of the meandering floodplain, during the 2000 flood, these sand-boils occurred with a modest solid transports along the toe of the embankment of Serafini Island (*Isola Serafini*) floodplain as shown in figure (17) below. In the same year, small sand-boils were also reported on the rear right side of the main levee during the flood near San Nazzaro, with mediocre solid transports from the toe of the levee associated with filtration. Sand-boils were also reported near the right levee of the Serafini Island valley floodplain.

During the October 2000 flood, all stations between Piacenza and Boretto, a city downstream of Cremona, registered water levels higher than the previous historical record set in 1954. This event was characterized by a broad period, approximately 6 hours, of hydrometric ridging and a considerable drainage volume. The record water levels caused regurgitation in confluence areas that contributed to the lamination of the flood wave due to the invasion of the nearby floodplain of the Emilia and Lombardy tributaries. Downstream from Piacenza, the presence of the nearby floodplains also had a significant contribution to the wave lamination.

In the following table, a comparison of the historical maximum level registered in the stations of Piacenza and Cremona is shown:

Station	**Basin**	**Maximum water level (m^3/s)**			
		Historical flood (year)			
	km^2	**1951**	**1968**	**1994**	**2000**
Piacenza	*42,030*	*12,800*	*9,500*	*11,055*	*12,240**
Cremona	*50,726*	*13,750*	*10,600*	*11,300*	*11,850*

(*This value has been deduced by the stage-discharge available from the offices of the Enel Serrafini Island dam)

Table 4: Comparison between the historical floods and their registered values

3.2 Hydrographic characteristics

This stretch of the Po River has an approximate length of 45 km and is supplied by a series of secondary affluences, particularly from the Apennine side. The first of these, the Trebbia River, discharges just before Piacenza on the southern bank of the Po. Further downstream, the Adda River crosses the main stem of the Po on the northern bank before the city of Cremona and in front of Seraffini Island. Additional affluences, such as the Nure Torrent, join the Po on the southern bank at Roncarolo. The Chiavenna Torrent, also joining the Po on the southern bank discharges into the main stem further down river near San Nazzaro.

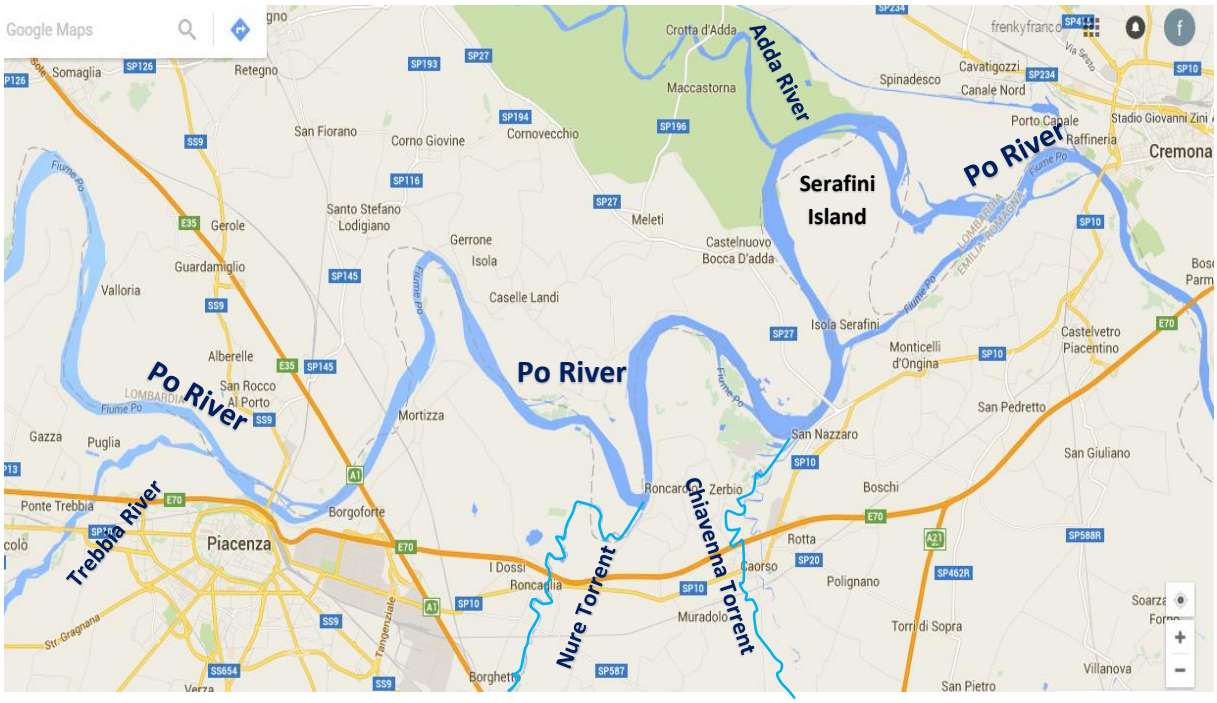

Figure 14: Map of Po River in the area analyzed (Google Maps)

Downstream, near Monticelli Pavese, the Po develops a classic meander model that, over time, has remained nearly unchanged and is not affected by significant bank erosion phenomena (AdbPO, 2005).

In the stretch between the Trebbiaand the Adda confluences, the riverbed generally has a sinuous trend close to the embankments in all the curved stretches. In general, it can be classified as single-twist with a meander (A. Domeneghetti, 2012). The width between the banks is continuously variable with islands of appropriate and stable size in the process of reconnection with one of the two banks.

The watercourse in this section is characterized by a secondary riverbed of variable width between 200 and 500 meters. The flood plains in this area, extending up to 2km in a few significant cases, are not protected by secondary levee systems.

There is also a near universal absence of significant erosion of the banks. With a slight, widespread tendency of deposits resulting in a modest rise in the riverbed bottom over the last decade, this trend manifests itself presumably due to the regurgitation of Serafini Island's hydroelectric dam. Confirming this hypothesis, between 1954-88 there was a lack of significant movement of the lean riverbed—excluding the area of Serafini Island—with substantial stability of the meandering axis (AdbPo, 2005).

The embankments in this stretch are continuous and contain large floodplains that alternate from the left bank to the right. One closed flood bed of significant signs is located near Piacenza. In two particular situations, the curves of Mezzano Passone and Roncarolo posses highly irregular flow conditions that are disturbed during significant flood patterns (AdbPo, 2005).

The main geometric characteristics of the river stem are mentioned below:

- Axis length—28.45km;
- Average distance between embankments—1,450 m;
- Average height of embankments of the floodplain—6.0 to 6.5 m;
- Average width of lean riverbed—200 to 300 m;
- Average depth of the engraved riverbed—7.5 to 8.0 m;
- Etched riverbed surface per km of river channel—0.41 km^2/ km;
- Open floodplain surface for km of river channel—0.89 km^2/km;
- Closed surface floodplain for km of river channel—0.15 km^2/km;
- Overall development of protection banks—31.91 km;
- Development defenses (left bank) of stretch length—55.2%;
- Development defenses (right bank) of stretch length—56.9%;
- Sinuous index—2.10.

The annual hydrological regime of the Po is generally characterized by two soft periods (spring and autumn) and two dry periods (summer and winter).

The runoffs observed at hydrometric stations positioned along the main stem, vary significantly in relation to the hydrological regimes of its 141 main tributaries showing different hydrological characteristics depending on the geographical area of membership (G. Nigrelli, 2013):

- Snowfields and glaciers feed the northern tributaries from the Alpine region (ex. The Adda). These are mostly affected by temperature, rainfall, and winter. They provide a considerable amount of water during the summer as a result of snowmelt and ice;
- The southern bank tributaries (ex. Trebbia, Nure, and other torrents) drain rainwater from the Apennine region. These are tributaries are characterized by shorter lengths (average heights are less than northern tributaries), providing scarce water contributions in the summer, but high volumes during spring and autumn seasons.

3.2.1 The Serafini Island Dam

The construction of the Serafini Island Dam, which began operating in 1963, together with the cutting of the meandering island of Mezzadra during the flood in 1951, resulted in two additional effects (AdbPo, 2005):

- It has prevented the development of the meander cutting, the natural tendency of erosion upstream and of deposit downstream. Downstream, main river dam has consequently developed a strong erosion of the bottom and a high instability of the riverbed morphology;
- It reduced the recurring transfer of downstream sediment transport in relation to both the structural changes of the riverbed and the management of the dam's regulation.

The overall effect is represented by a greater deepening of river bottoms intersecting the main stem immediately downstream of the dam (with particularly relevant values in correlation to Cremona) accompanied by overall morphological instability phenomena.

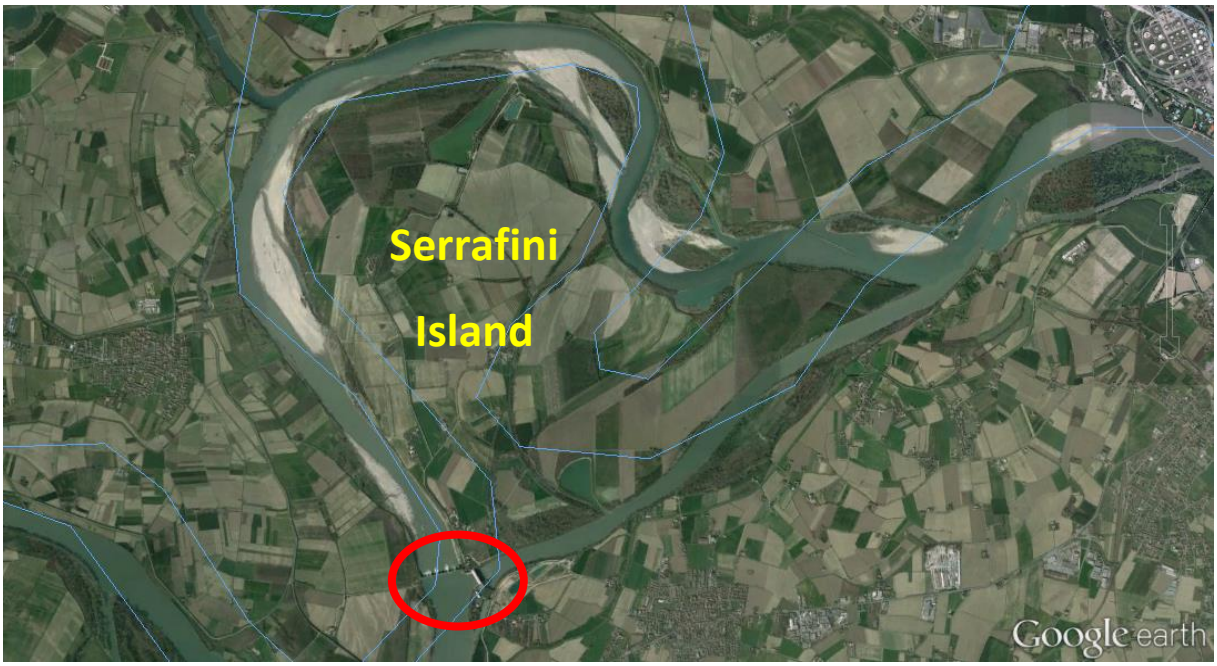

Figure 15: Localization of the dam of Isola Serrafini (Google earth)

After the historical flood in 1951, where the meander around Serafini Island was cutting at the beginning of 1960, the construction of the hydroelectric dam and its connected works stabilized the planimetric track along with the profile of the riverbed bottom throughout the stretch of riverbed upstream of the dam.

Figure 16: The Isola Serrafini dam (AdbPO, 2005)

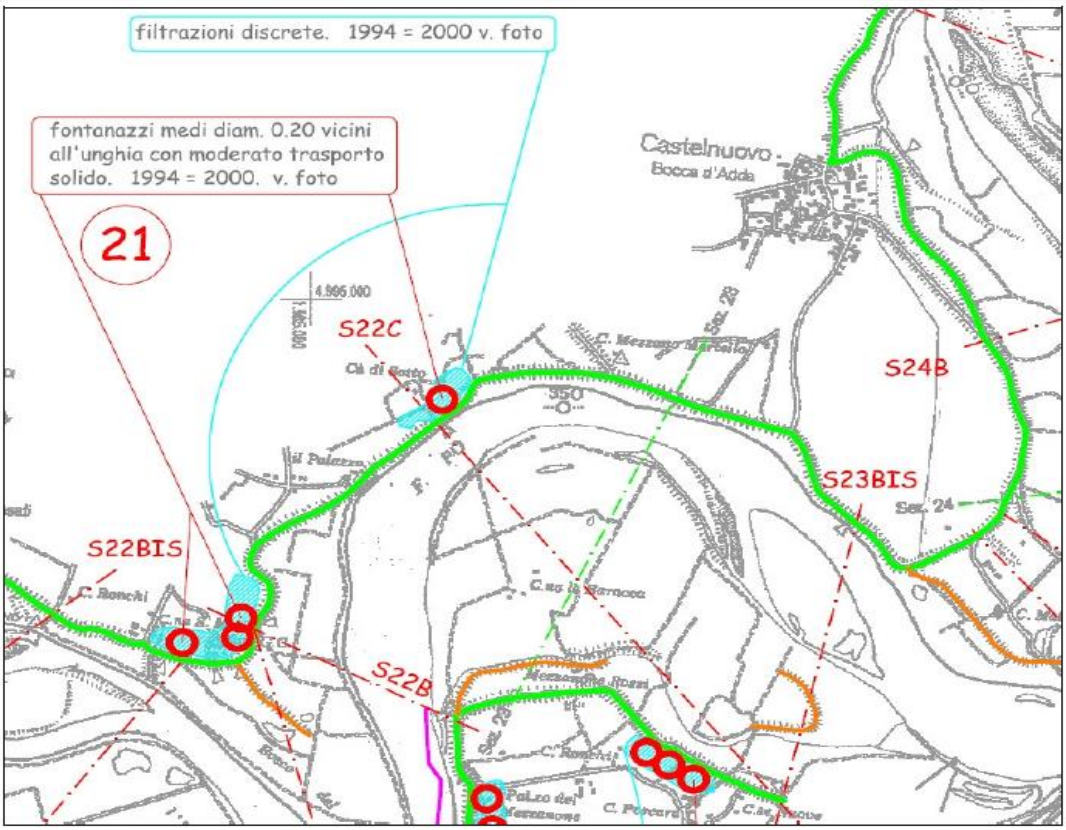

Figure 17: Piping phenomena observed during the flood events in 1994 and 2000 inside and in front the island (AdbPO, 2005)

3.2.2 The levee system between Piacenza and Cremona

Upstream, the embankments are initially discontinuous and spaced 1.7 km to 4 km apart. Downstream from the Trebbia confluence they become more continuous and closer together—1.4 km apart on average. In the second part, downstream from the Adda confluence, the embankments become continuous and spaced about 2.6 km apart creating a large area for flood lamination.

Floods in this stretch usually have their peak flow between Piacenza and Cremona and then modulated. Due to longitudinal works favoring navigability, the channel becomes single-twist all the way to the river mouth (C. Carisi, 2011).

The levee system continues along Po until interruptions corresponding to the confluence of a secondary river (or progression along them), as in the case of Nure Torrent, leaving some area unprotected by floods.

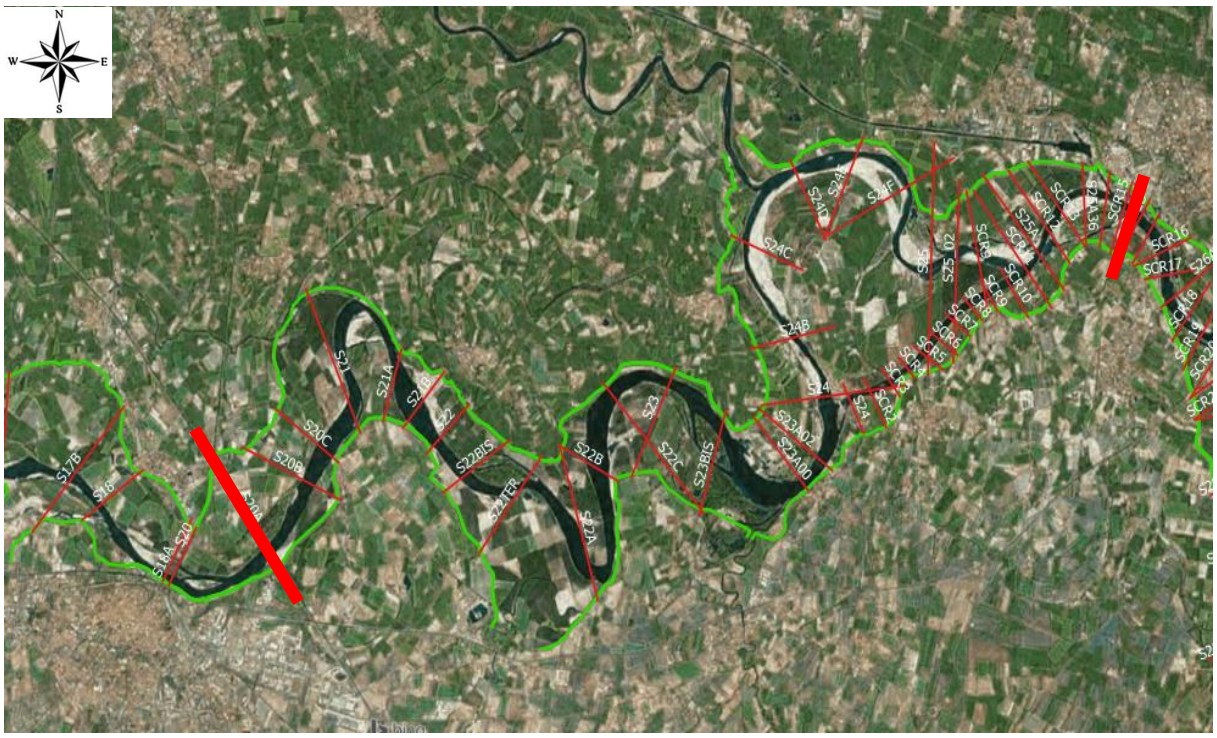

Figure 18: The levee system (light green) from section S20A (Piacenza) to section SCR 15 (Cremona) (AdbPO, 2005)

The vertical sections (red lines on the map above) available from AdbPO, allow a suitable analysis of the topography and the geometry of the embankments (green lines on the map), especially on the right side, where the sections are much closer to each other's (1 km) in the area near San Nazzaro and Monticelli d'Ongina, in front of Serrafini Island (Figure 18). The left banks show a greater distance between the sections with a maximum distance of almost 3 km measured. This aspect will be discussed in greater detail in the chapter (4).

Figure 189: View of the main levee system in Cremona Province (V. Ferrari, F. Leandri, and C. Milesi, 2008)

3.3 Geological framework and land use

3.3.1 Geology and land cover

With regards to the geological aspect, the catchment area of the Po River is characterized by high complexity that is composed of sectors that, for their origin and morphology, are very different from each other.

The Alpine field began to develop about 130 million years ago during the Cretaceous period (Gradstein et al., 2004) as a result of the subduction of the Mesozoic ocean and the subsequent collision between the European and Adriatic continental margins. The Apennine sector and western hills are the result of a series of sedimentary processes that have developed in the marine platform—escarpment and bathyal zones—united and interspersed with tectonic movements occurring around 38 million years ago in the late-Eocene to 10 million years ago during the middle-Miocene after the gradual compression of the Tethys Ocean. The Po Valley is the result of massive erosive-depositional activity that began 500,000 years ago during the Pleistocene ice age and its three interglacial phases (Gunz, Mindel, Riss and Wurm). The material is composed of fluvial-continental and fluvial-glacial deposits from the Pleistocene as well as the Holocene located above a base of marine origin. The Plio-Pleistocene sediments vary in thickness from 0.3 to 8.0 km and are highly asymmetric with the deepest part located under the foot of the Apennines (AIPO, 2006).

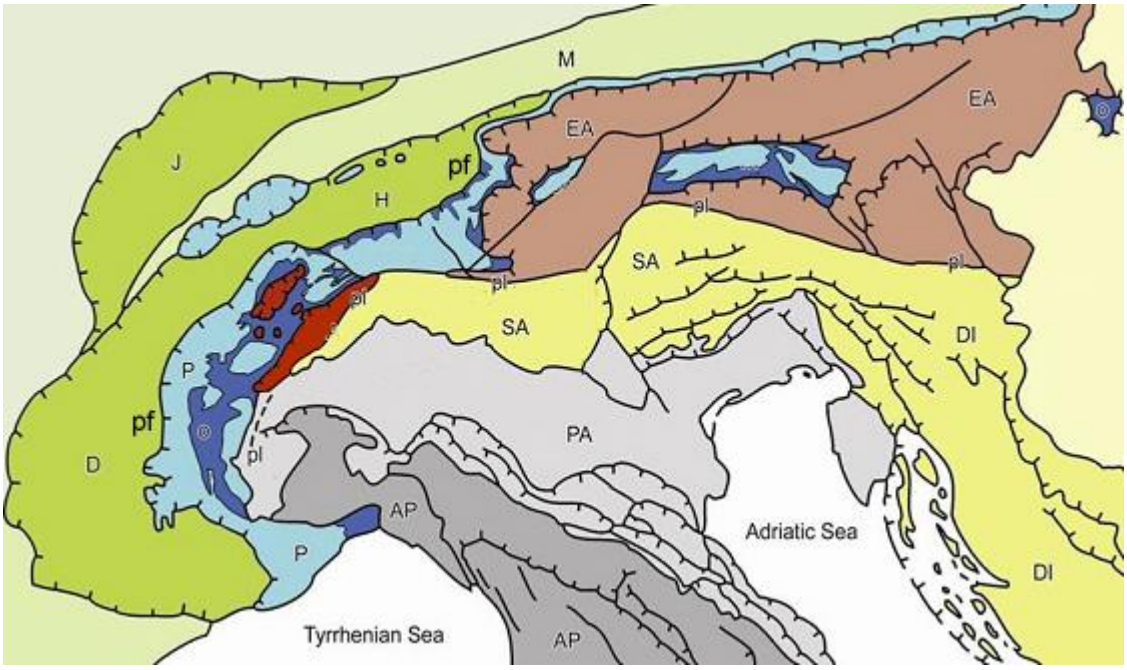

Figure 20: Structural-geology map in the occidental Alps (Dal Piaz G.V., Bistacchi A., Massironi M. (2003))

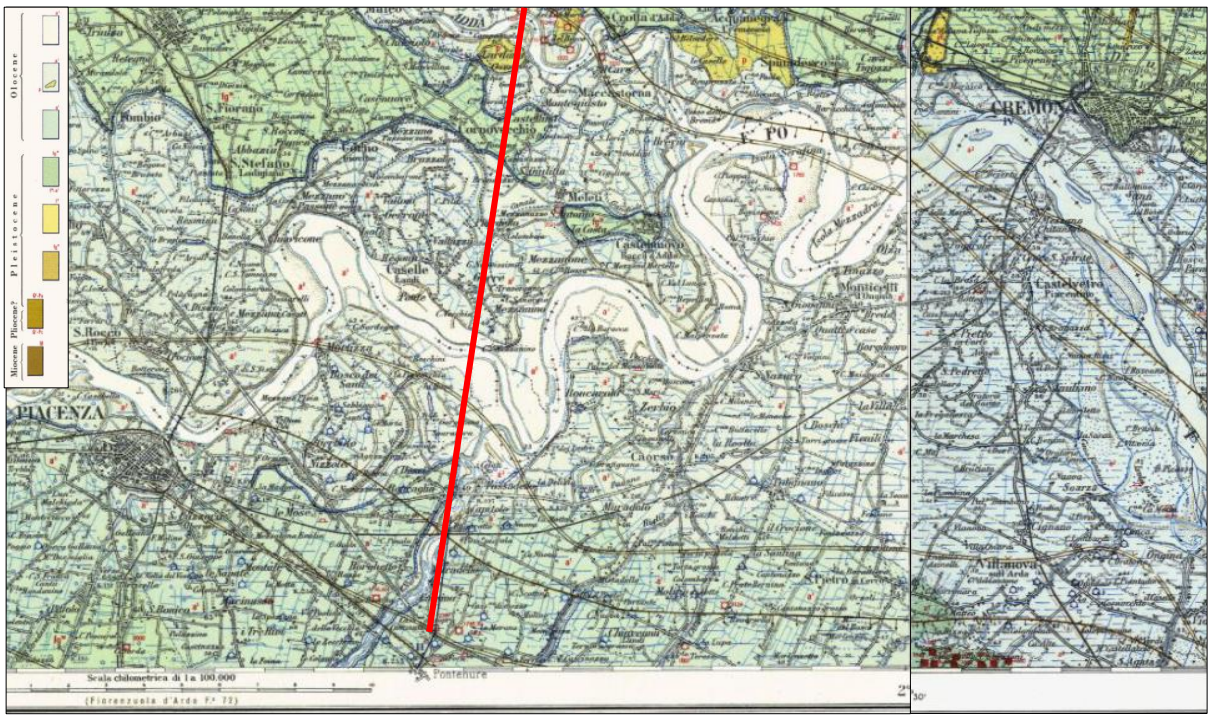

Figure 21: Excerpt from Foglio 60 (Piacenza) and Foglio 61 (Cremona) of the geological map. Scale 1:25000 (ISPRA)

Looking at the geological map of the area available from ISPRA web site is possible to recognize the main geological formation and recent deposit that interest the part close to the Po River and where the levee system lies. (Foglio 60, Piacenza; Foglio 61, Cremona).

Moving away from the river, it is possible to identify the following flood formations and deposits:

- White—Gravel and sand;
- Very light-blue: Silt or sandy silt (locally); Lake basin deposits and clay primarily (*Olocene*);
- Light-blue: Sandy gravel and silty clay; ancient, post-glacial era (*Olocene*);
- Green: fluvial-glacial and fluvial-continental; silty and thin gravel lenses with brown-surface coloration (*Olocene-WURM*);
- Yellow: fluvial-glacial and fluvial-continental, sandy-silts with gravel lenses and yellow-red clay surface coloration (*RISS*);
- Light-brown: Fluvial-glacial and fluvial-continental with natural terraces; sandy-gravel, with a well hardened alteration layer up to 4 m of thickness; often partially eroded (*MINDEL*)

From the map's legend, it is possible to recognize what other underground formations are present in the Padania Plain as well as tectonic structure. The subsurface formations are:

- Yellow-brown: sand with clay intercalations, limestone and conglomerates with fossils (S. Colombo Form. Calabriano- superior Pleistocene);
- Dark brown: marl and clay with sandy and gravely intercalations with few fossils (S. Agata Marl, Tortoniano)

In Figure (22) below, under the analyzed area, some submerged faults are presented: one, on the left, is an indirect type that cut the last two formation described above; the right side shows tow faults, where an indirect fault is cut by a direct fault, in the formation.
The result is a typical anticline and syncline shape, submerged by the recent quaternary deposit that generated the Padania Plain.

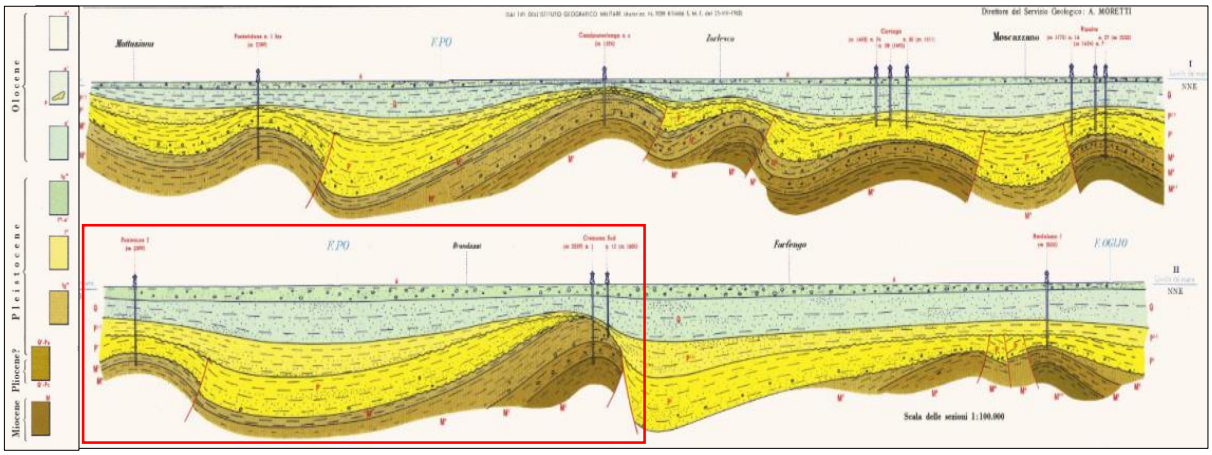

Figure 22: Quaternary Coverages on the plain in the section between Piacenza and Cremona

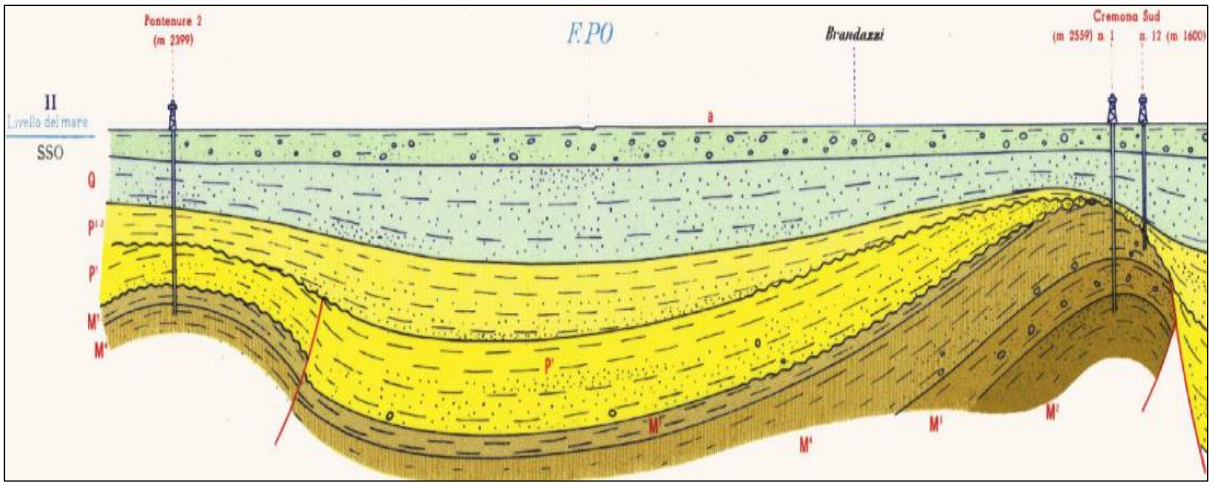

Figure 23: Vertical sections of the area analyzed (ISPRA)

With the data available from the service of Emilia-Romagna Region, it is possible to see, in figure (24), the Quaternary coverages on the plain and recognize what type(s) of soils are present under the levees. Observing the soils' distribution, it seems that a large portion of the levee system lies on silty-sand soil (SL, green on Figure 24), prevalent material near the great river. It is plausible think that the same distribution of these soils, more or less, is the same on the left side of the river.

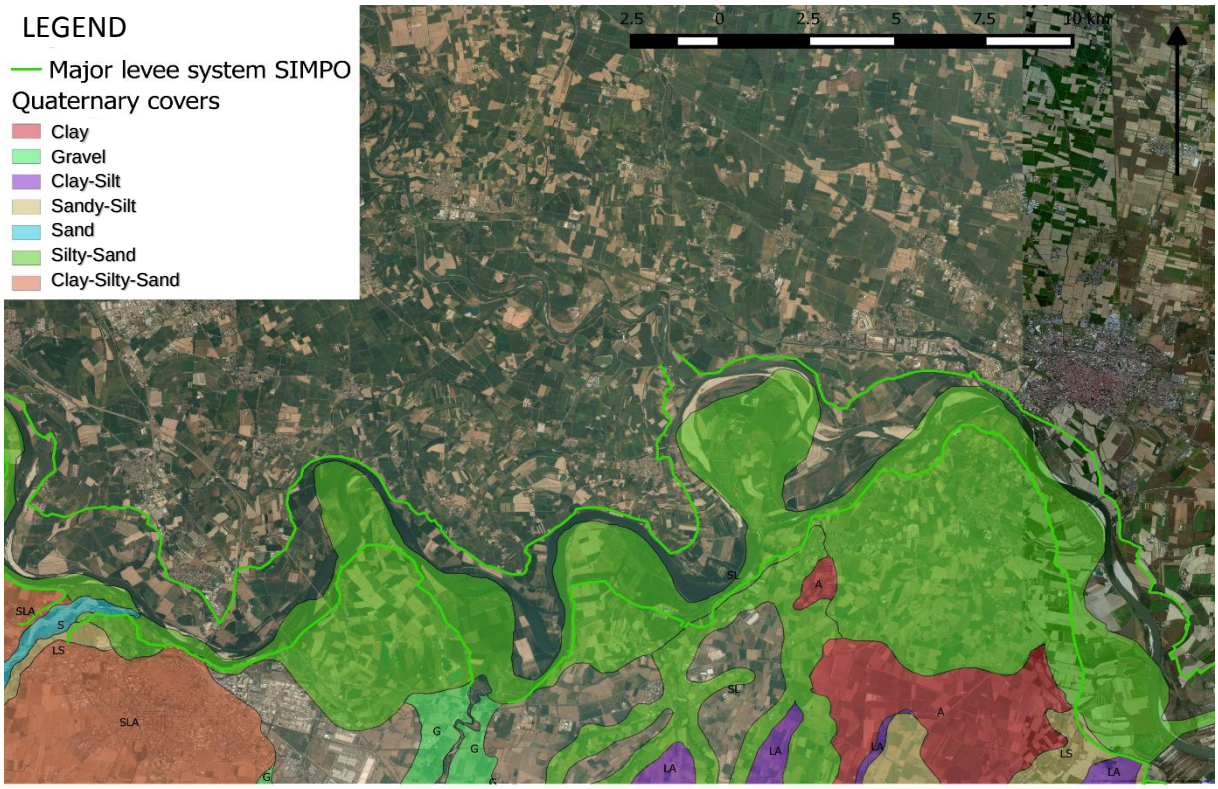

Figure 24: Quaternary Coverages on the plain in the section between Piacenza and Cremona

3.3.2 Land use

The human impact on the entire basin of the Po River, and in particular on the main stem was, and is still today, considerable. It is home to 16 million inhabitants, 27% of the population; one-third, 37%, of the nation's industry; 35% of the Italian agricultural production); and over half, 55%, of the country's livestock. The Po River and its basin are a great source for the entire Italian economy accounting for about 40% Italy's GDP. It is also one of the areas in Europe's with highest concentration of population, industry and business (G. Nigrelli, 2013). The average density of the basin is approximately 225 inhabitants/km^2, considerably higher than the Italian average of 188 inhabitants/km^2 (C. Carisi, 2011).

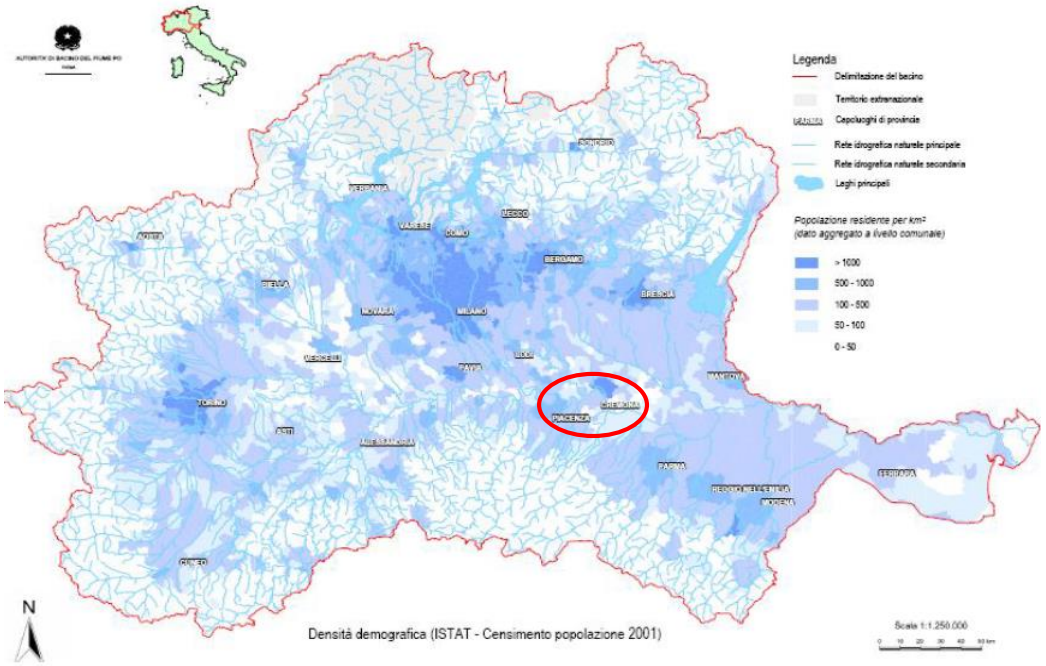

Figure 25: Distribution map of population density with area of study circled (ISTAT 2011)

The Corine Land Cover project yielded a classification, on a Europe-wide level, to distinguish and classify different cover and use of the surface.

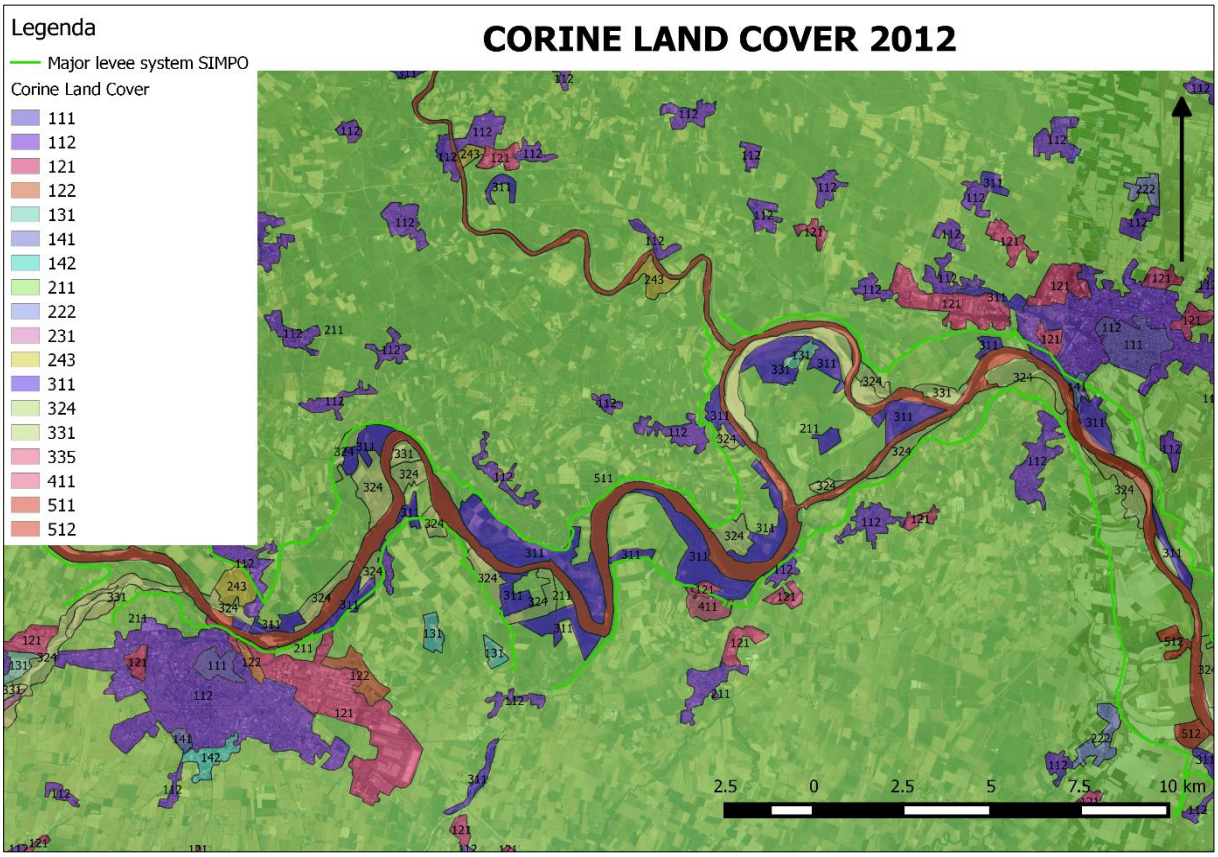

Figure 26: Land Use from the project Corine land cover 2012

The classification system of use and land cover (CLC) is hierarchical and divided into 3 levels. The first level consists of five classes that represent the broad categories of land cover; the second level includes 15 classes that are further divided until reaching 44 classes at the third level. In the area of the work the following categories are recognized:

1.1.1. Residential continuous fabric zone;
1.1.2. Residential more spread out and sparse zone
1.2.1. Industrial, commercial and public services and private area
1.2.2. Road, rail and infrastructure techniques
1.3.1. Mining Area
1.4.1. Urban green Area
1.4.2. Recreational and sports Area
2.1.1. Arable in non-irrigated areas
2.2.2. Fruits tree and soft fruit
2.3.1. Permanent meadows (permanent forage)
2.4.3. Area predominantly occupied by crops with the presence of important natural areas
3.1.1. Broad-leaved
3.2.4. Areas of wooded vegetation and changing shrubs
3.3.1. Beach, dunes and sands
4.1.1. Inner marshes
5.1.1. Course, canals and waterways
5.1.2. Water Basins

4. The Probabilistic Dike Failure Assessment

In this chapter, all the methodology and input data of the *reliability model* will be explained. A detailed description of the probabilistic approaches to obtain the fragility curves will then be presented with consideration given to all sources of uncertainty found during the analysis.

The failure probability assessment of flood protection structures based on fragility functions was introduced by the United States Army Corps of Engineers (USACE) in 1996 and 1999. A *fragility curve* or *fragility function* indicates the probability of structure failure conditional upon loading. These are traditionally applied in system reliability research and have also been used in earthquake research to describe the failure probability of engineering structures as a function of peak ground acceleration (Shinozuka et al., 2000; Bhargava et al., 2002; Kim and Shinozuka, 2004). Fragility functions of flood protection structures recently gained their relevance in flood hazard and risk assessment studies (Vorogushyn 2009). In 2002, the fragility curve concept for a steady large-scale risk assessment was proposed in order to describe the performance of dikes based on their classification and expert judgements about their failure probability (Sayers et al., 2002). The fragility concept was originally developed for overtopping of levees, breaching without overtopping, and breaching as a consequence of overtopping (Hall et al., 2003). The concept was further extended to wall instability and piping mechanisms for fluvial structures based on simple empirical reliability functions (Dawson et al., 2005).

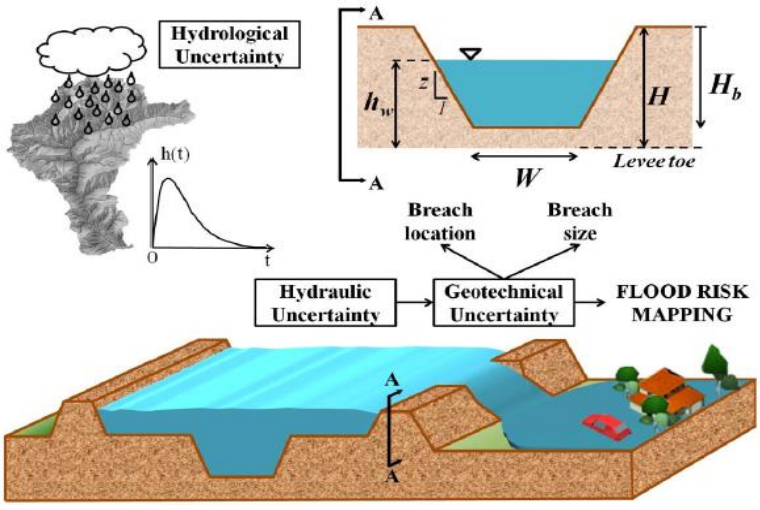

Figure 27: Levee breach geometry and sources of uncertainty in flooding hazard and risk mapping (M. Mazzoleni, 2013)

Dikes may fail as a consequence of various breach mechanisms and combinations thereof; failure mechanisms are generally divided into two groups (Armbruster-Veneti, 1999):

-*Hydraulic failure*: the collapsing of dikes as a result of overtopping and wave scour. Overtopping occurs as a consequence of water level exceeding the crest height or wave swashing. The surface erosion of the landward slope can then be initiated if the shear stress induced by the overtopping flow exceeds the critical shear stress of the dike cover material. The progressive erosion may lead to a breach development and total dike collapse.

-*Geohydraulic failure*: seepage flow through a dike core or dike foundation may initiate erosion processes and transportation of dike foundation material; the erosion processes result in a formation of pipes that lead to a sagging of the dike core with subsequent overtopping, slope failure and collapse. This particular failure mode is referred as *piping* (CUR/TAW, 1990; Vrijling, 2001).

4.1 Monte Carlo Method and the Fragility Function

The probability of collapse of an embankment's section for several failure mechanisms is evaluated by the application to the fragility curves—or function (USACE, 1996; Sayers et al., 2002). This provides an estimate of the failure probability of an embankment when it is subjected to hydraulic stresses (A. Domeneghetti, 2012).
Fragility functions can generally be n-dimensional depending on the number of load variables. They are defined on the interval [0; 1] indicating failure probability upon loading. In developing fragility functions, each load variable can be discretized within a range of feasible values. Each tuple of load variables represents a point in the n-dimensional space, for which the probability of structure failure can be computed in a Monte Carlo Simulation (MCS) with the limit state, or reliability, function. This function should be formulated for each particular failure mode. It represents a relation between the load and resistance variables and can be expressed in a general form as:

$$\boldsymbol{Zi = Ri - Li}$$

where $\boldsymbol{Ri}$ is the resistance and $\boldsymbol{Li}$ is the load (Vorogushyn, 2009).

For a combination of $\boldsymbol{R_i}$ and $\boldsymbol{L_i}$ yielding $\boldsymbol{Z_i > 0}$, no failure occurs. Failure is considered for $\boldsymbol{Z_i < 0}$. Uncertain dike state variables $\boldsymbol{r_1}$, $\boldsymbol{r_2}$, … $\boldsymbol{r_n}$, representing geometrical and geotechnical properties that contribute to dike resistance are randomized in the MCS.

The result of the MCS is a fragility function defined at every discretized point of the load space. Proceeding with the simulations, for every possible stress loading, the probability of failure is defined by the ratio between the number of cases in which the function of resistance limit has not been satisfied and the total number of MCSs performed (A. Domeneghetti, 2012).

$$P_{failure}^{Ln} = \frac{N(Z(r_1, r_2, \dots, r_n) < 0)}{N_{MC}}$$

$$P_f = Prob\{Z\,(X) < 0\} \int_{Z(X)<0} f_X(X)dx$$

Repeating this procedure for every point in n-dimensional space a interpolation surface is obtained; it gives the probability of failure for each possible condition (A. Domeneghetti, 2012). The fragility curve (or surface) is placed within a limit that goes from 0 to 1; this has an increasing trend, expressed as a cumulative density function of probability of failure.

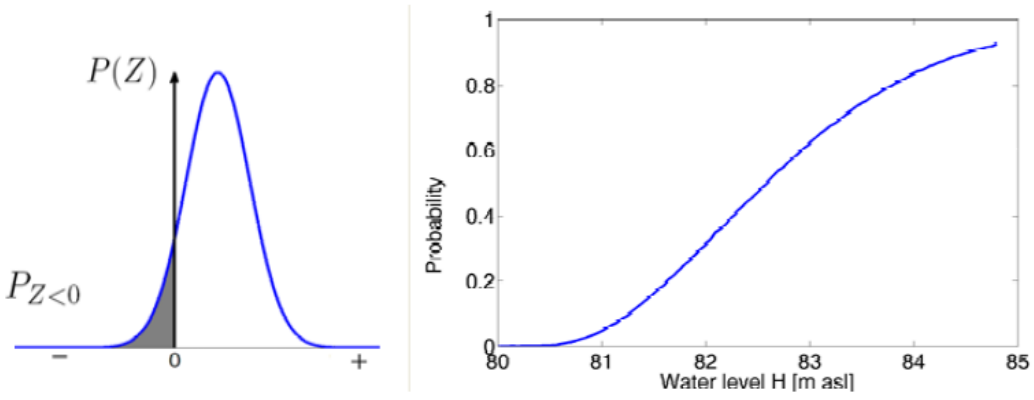

Figure 28: Probability of failure for a specific stress condition (left) obtained by resolution of the fragility function in a MCS; fragility curve (right) provides the probability of failure of the embankment as a function of the water load in the river bed (A. Domeneghetti, 2012).

In summary, the probability of failure, with respect to a specific performance, or limit state, function, $\boldsymbol{Z(X)}$, is defined as the *joint probability distribution function*, $\boldsymbol{f_x(x)}$, over the so-called "failure domain" ($\boldsymbol{Z(X) < 0\ or\ < 1}$):

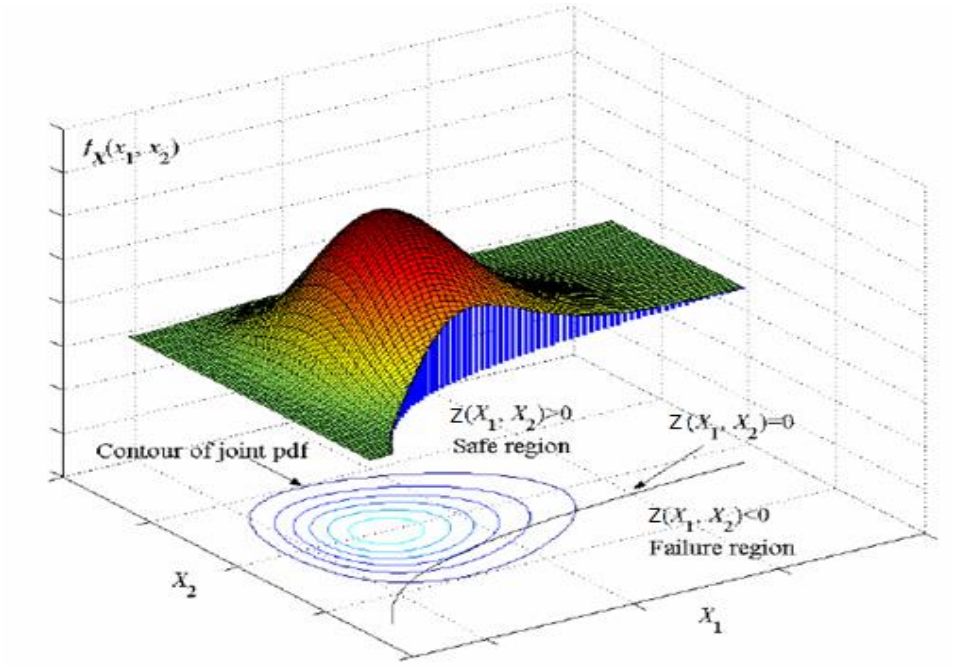

Figure 29: Failure domani obtained by a MCS for a specific fragility function (M. Mazzoleni 2015)

The number of MCSs has a great impact toward defining an accurate result, then to obtain a correct trend of the failure probability distribution. Therefore, as represented in Figure (30) below, the higher the number of simulations—or iterations, the higher the possibility to find a stable value of probability. In order to achieve this value there must be a compromise between the number of simulations performed by the calculation software (MatLab)—which can take several hours to perform a full calculation cycle—and the computational power of the machine.

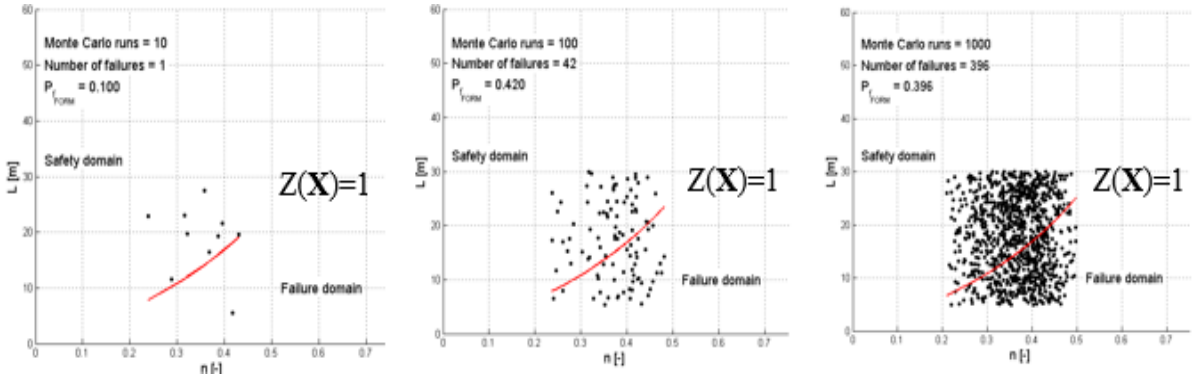

Figure 30: A higher number of MCSs yields more accurate values or probability distribution (M. Mazzoleni, 2015)

4.2 The limit state equation for levee failure

Based on the empirical and physically-based process formalizations reported in the literature, the reliability functions are formulated for selected failure mechanisms. Implementing these functions in a Monte Carlo framework leads to the development of the fragility curves.
The primary considerations adopted for the definition of fragility curves are given in the proceeding sections.

4.2.1 Rupture Due to Overtopping

When overtopping occurs, the water flowing over a dike crest induces shear stresses on the outer slope surface. As the overtopping discharge increases, the critical shear stress is exceeded resulting in progressive slope erosion and breach formation (Vorogushyn 2008).
More sophisticated fragility functions have been developed for dike overtopping conditional upon two load variables: overtopping height and duration (Apel et al., 2004, 2006; Merz, 2006). Hence, the function takes gradually varying load by incorporating the time-dependent component such as load duration.
Depending on the intensity and duration of the overtopping, the erosive effects exerted by the surmounted flow can lead to the removal of material at the levee toe leading to complete collapse. This phenomenon is as fast as higher is the extent of the overtopping and how more yieldable the embankment coating appears, usually consisting of a simple green cover, on the outer side.
For overtopping, the limit state function can be formulated according to the formula proposed by Kortenhaus and Oumeraci in 2002 as:

$$\boldsymbol{Z_o = Q_{crit}(t) - Q_a(t)}$$

where the erosive stress, $\boldsymbol{Q_a(t)}$, is the overtopping discharge [m^3/s] (Apel et al., 2004; Merz, 2006) and the resistance, $\boldsymbol{Q_{crit}(t)}$. This is the critical discharge as a function of time [m^3/s] that is calculated according to the approach that Vrijiling and van Gelder developed in 2000. This defines the flow condition over which initiates erosion of the inner face and subsidence on the outer face of the levee.

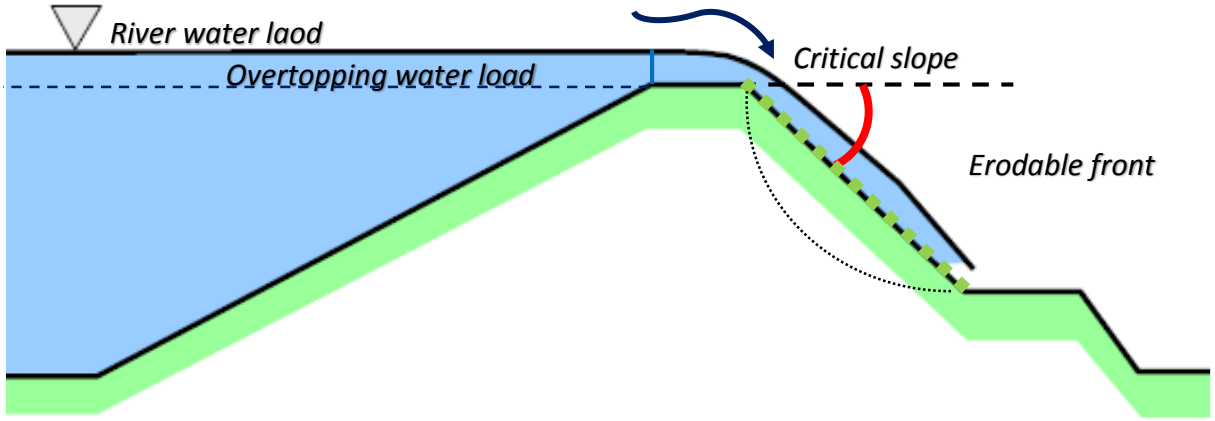

Figure 31: Water load exceeding the height of a levee resulting in overtopping

Discretizing the field of independent variables, represented by the extent of levee overtopping and its temporal duration, the probability of failure associated with a specific stress conditions is defined by using a set of MCSs and evaluating the number of cases in which the limit state equation assumes values less than zero.

4.2.2 Rupture Due to Piping

The collapse of an embankment by piping occurs as a consequence of the phenomena of infiltration and erosion exercised by the fluvial current below the levee. For effect of the water pressure increase in the foundation ground, motions of infiltration of flood waters through layers with a greater permeability can be established, possibly present below the laying surface of the embankment. The difference of pressure between the inner/river side and the outer side may be able to overcome the resistance offered by the weight of the soil layer over the embankment, leading to the rupture of the soil itself and to the ascent to the surface of the water (so-called "sand-boils") (A. Domeneghetti, 2012).

In the next phase, the piping develops further and triggers phenomena of erosion which, extending towards the side of the river, can lead to the formation of real outflow channels that bring the embankment to collapse.

Usually, the triggering moment of the piping mechanism corresponds to the formation of sand boils in the outward side of the levee system. This type of failure mechanism is particularly important in flood management, as its occurrence does not only depend on high flood events (M.Mazzoleni 2012).

Surveys of this phenomenon (Sellemejier, 1989) have highlighted the presence of a critical value, expressed in terms of load difference between the river side and country side, beyond which erosion is activated (A. Domeneghetti 2012).

The *gradient method*, an approach proposed by Maurizio Mazzoleni, is a simplified methodology that describes an ideal condition for the instauration of a piping phenomena through the hydraulic condition with respect to levee geometry and geotechnical proprieties.

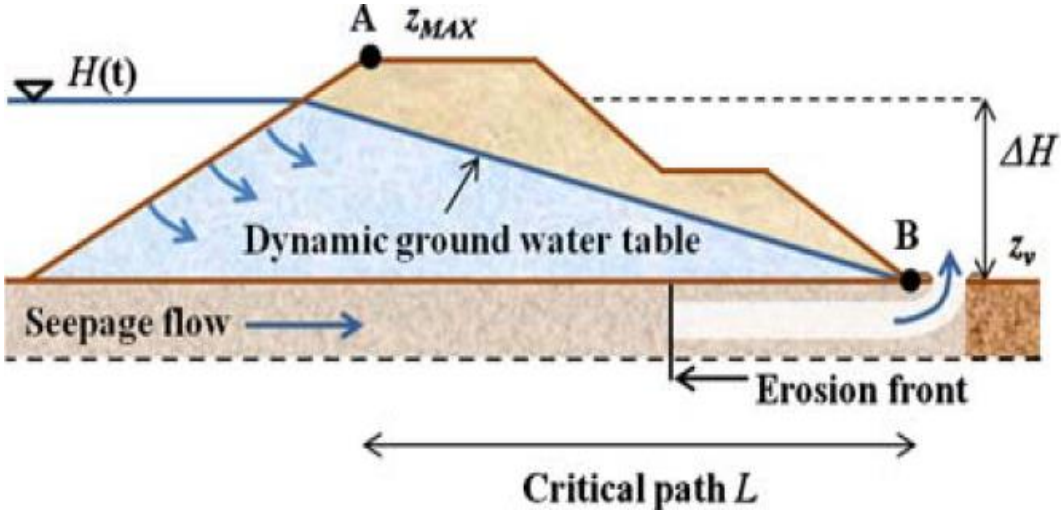

Figure 32: Diagram of the triggering conditions for a piping failure mechanism (Mazzoleni et al., 2014)

In Mazzoleni's study, the loading (or stress) $\boldsymbol{Li}$ is expressed as the hydraulic gradient $\boldsymbol{J}$ using the ratio $J = \Delta H/L$, where $\boldsymbol{\Delta H}$ is the total water head difference between the river and land side of the levee and $\boldsymbol{L}$ is the length of the hydraulic path defined in the technical literature as the critical, or sliding path (Bligh, 1912; Sellmeijer, 1989).

The critical path $\boldsymbol{L}$ is evaluated considering the minimum horizontal distance between points *A* and *B* (as shown in Fig), which leads to the maximum critical value of the hydraulic gradient, $\boldsymbol{J}$. Consideration must be given to the possibility of greater and/or longer infiltration paths due to piping within the embankment and foundation soils; usage of the length $\boldsymbol{L}$ means and making analysis on the safe side.

The resistance of the levee, $\boldsymbol{Ri}$, is expressed by the critical value of hydraulic gradient $\boldsymbol{Jc}$, which is assumed to be an indicator of the piping trigger and related to the geotechnical and geometrical characteristics of the levee itself (Bligh, 1912). Assuming valid the assumptions above, the limit state equation for piping is expressed as (M. Mazzoleni, 2012):

$$\boldsymbol{Z_j = Jc - J}$$

5. Physical Knowledge of Failure Mechanisms

From the literature research, it reveals the recent physical knowledges, for different failure mechanisms, used in the limit state function. These formula are considered using the appropriate boundary conditions and with different, required parameters for the equations.
The incorporation of the available data must then be employed using the most recent formulas applied by other experts. Later, it will be shown that the sources of data are often small and inaccurate.

5.1 The Overtopping Discharge

As previously reported, the limit function overtopping is $Z_o = Q_{crit}(t) - Q_a(t)$ where $\boldsymbol{Q_{crit}}$ is:

$$Q_{crit}(t) = \frac{v_{crit}^{5/2} \cdot k^{1/4}}{125(\tan\alpha)^{3/4}}$$

and $\boldsymbol{v_{crit}}$ is the critical flow velocity in function of the overtopping duration [h], and $\boldsymbol{\alpha}$ is the outer slope angle [°]; $\boldsymbol{k}$ is the *absolute roughness* of the outer slope [m] (Steenbergen and Vrouwenvelder, 2003; Vrijling and van Gelder, 2000), which can be, based on experiments, related to the Manning's $\boldsymbol{n}$ value:

$$n = \frac{k^{1/6}}{c}$$

where the coefficient $\boldsymbol{c = 26}$ according to Bollrich (2000), whereas Steenbergen and Vrouwenvelder (2003) and Vrijling and van Gelder (2000) give a slightly different value of $\boldsymbol{c = 25}$, which is the value used in this work's analysis.
The equation for the critical flow velocity $\boldsymbol{v_{crit}}$ originally proposed by Steenbergen and Vrouwenvelder (2003) and Vrijling and van Gelder (2000), was further refined by Apel et al (in press), based on experiments of for turf covered slopes (Hewlett, 1987):

$$v_{crit} = \frac{3.9177 + 1.5(f_g - 1)}{1 + (0.8575 - 0.45(f_g - 1))\log_{10}(t_e)}$$

where $\boldsymbol{f_g}$ is the turf coefficient [-] comprised in a range between 0.5-1.5.

The overtopping discharge $\boldsymbol{Q_a(t)}$ over the dike crest can be computed as a simplified equation according to the broad-crested weir formula:

$$Q_a = 0.385 \cdot b \cdot \sqrt{2 \cdot g} \cdot H^{3/2} = 1.705 \cdot b \cdot H^{3/2}$$

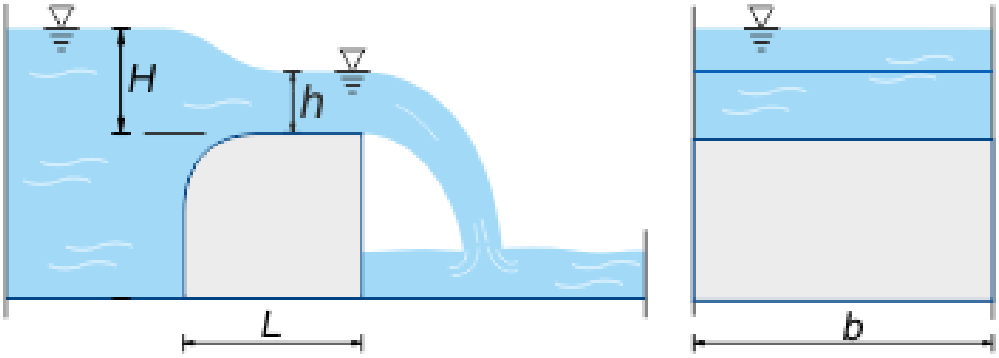

Figure 33: Example scheme of the weir wall with a large base

where $\boldsymbol{b}$ is the width threshold (taken as 1), $\boldsymbol{g}$ is the gravity coefficient and $\boldsymbol{H}$ is the height of the undisturbed fluid upstream of the threshold (load).

5.2 The Gradient Method

This approach takes into account the saturation of the embankment during a flood and does not introduce any limit on the piping inception. In the event the levee systems have sandy foundations, as is the case in many large, lowland area rivers, an evaluation of the critical gradient, adapted to the metric system, is provided by the equation:

$$Jc = \frac{\tau_C}{2.878 \cdot \Upsilon_w} \cdot \left(\frac{n}{\kappa_h}\right)^{0.5}$$

where $\boldsymbol{\kappa_h}$ is the intrinsic permeability (m^2), $\boldsymbol{\Upsilon_w}$ is the water specific weight equal to 9.806 N/m^3, $\boldsymbol{n}$ is the levee foundation porosity and $\boldsymbol{\tau_C}$ is the critical tractive shear stress such that $\tau_C = c \cdot d$ where $\boldsymbol{d}$ is the representative sand particle diameter (m) (Khilar et al., 1985) and $\boldsymbol{c}$ is the coefficient provided by Ojha et al. (2001).

To predict the hydraulic conductivity of soils, the Kozeny-Carman equation, adapted by Carrier (2003) is considered:

$$K_h = \frac{\Upsilon_w}{\mu} \cdot \frac{1}{C_{K-C}} \cdot \frac{1}{S_0^2} \cdot \frac{n^3}{(1-n)^2}$$

where $\boldsymbol{\mu}$ is the dynamic viscosity ($\boldsymbol{N \cdot s/m^2}$). The coefficient $\boldsymbol{C_{K-C}}$ is the Kozeny-Carman empirical coefficient, usually assumed equal to 5, whereas $\boldsymbol{S_0^2}$ is the specific surface area for unit volume of particles, which, for uniform spheres of diameter $\boldsymbol{d}$ in meters, is $^6/_d$ (Chapuis and Aubertin 2003).

By coupling the previous two equations, the critical head gradient can be expressed as a function of the levee foundation porosity $\boldsymbol{n}$*:*

$$Jc = \frac{cd}{2.878_{\Upsilon w}} \cdot \sqrt{\frac{n}{\frac{K_h v}{g}}} = 0.237 \cdot \frac{1-n}{n}$$

where $\boldsymbol{v}$ is the kinematic viscosity of water (m^2/s). Thus, the equation for the limit state equation becomes:

$$g(n, L; \Delta H) = Jc - J = Jc - \Delta H/L = 0.237 \cdot \frac{1-n}{n} - \frac{\Delta H}{L}$$

where $\boldsymbol{g(n, L; \Delta H)}$is the limit state condition, which is a function of the geotechnical and geometrical variables $\boldsymbol{n}$ and $\boldsymbol{L}$ for any given values of the hydraulic load $\boldsymbol{\Delta H}$.

6. Data and Useful Information

Resizing of the old levee system in previous years and the addition of new material on the existing embankment yields a significant problem in developing a real and distributed (in space) value of the geological and geotechnical parameters of the levee and foundation material.

Following the great flood event occurred in October 2000, the Po River Basin Authority (AdbPo) began extensive investigations of the main stem of the Po River and its primary tributaries. In particular, Coratza (2005) began updating the register of the Po River levee system, providing a complete and accurate mapping of key elements, such as: plan position of the main and riverside embankments; location of Brioschi and intermediate sections; and intermediate sections; and highlighting the position of the various tributaries.

These analyses were complemented by the accurate altimetry information (up to 2 meters) provided by the Digital Terrain Model (DTM) used by AdbPo since 2005 for the main stem between the Ticino confluence and the delta (A. Domeneghetti 2012)

6.1 Topographic Information

One of the most important pieces of data for a levee reliability analysis is the embankment geometry. This information provides great insight in defining the levee fragility for a determinate hydraulic condition especially for failure mechanisms such as piping and overtopping.

The topographical information is obtained from the vertical section details available from the Interregional Agency for the Po River (AIPO); this information consists of a series of profiles that start from the beginning of the levee system until the delta in the Adriatic Sea. Every section shows all the elements present in the floodplain between the main levees on each side. Their arrangement is not regular; it seems that the sections are arranged along the progressive distances ranging from 1 km to 3 km maximum, and that lay, more or less, perpendicular to the direction of the river rod. But this could have an explanation.

Thanks to the Brioschi Commission in 1873, an improved initiative against floods was established whereby a series of detailed vertical sections and profiles were produced

(measured) for hydraulic analysis and morphological monitoring of the Po River. Over time, other topographical surveys have been made to update these sections. Additional sections have also been added to fill the gaps previously left by the Brioschi Commission.

Recently, new techniques of surveying, such as Lidar, have made the drafting of a high-resolution DTMs (up to 1 meter) possible.

These DTMs utilize three different types of information: elevations derived from laser scanning survey of the emerged area; the bathymetric relief with sonar to scan the wetlands; and elevation information relative to some traversal sections measured with traditional topographic surveying techniques by AIPO in 2005 (A. Domeneghetti, 2012). The result has yielded an incredible amount of high-altitude precision with no local systematic deviations and very low errors of approximately 0.1m (V. Camorani et al., 2006).

In 2005, AIPO decided to intensify the number of the section (dark blue in Figure 34) in correspondence with the right riverbank in front of Serrafini Island as well as downstream on both sides of the river past Cremona.

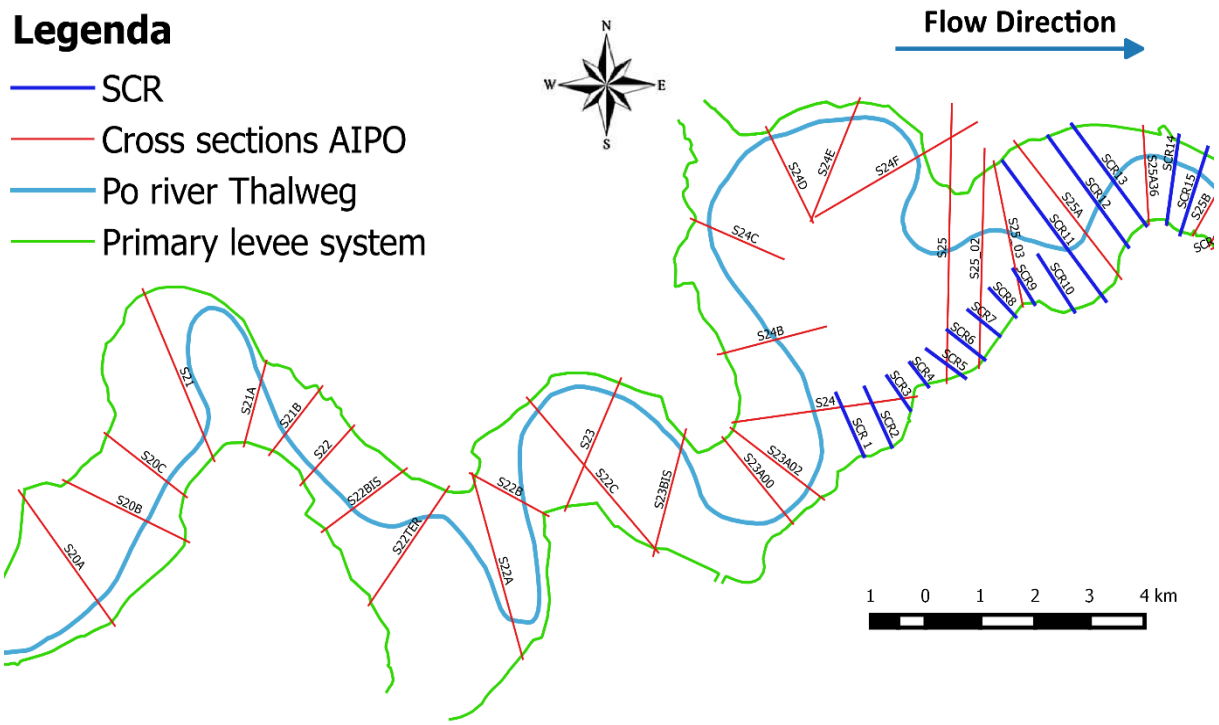

Figure 34: Vertical profile: cross-sections available from AIPO are shown as red, blue lines

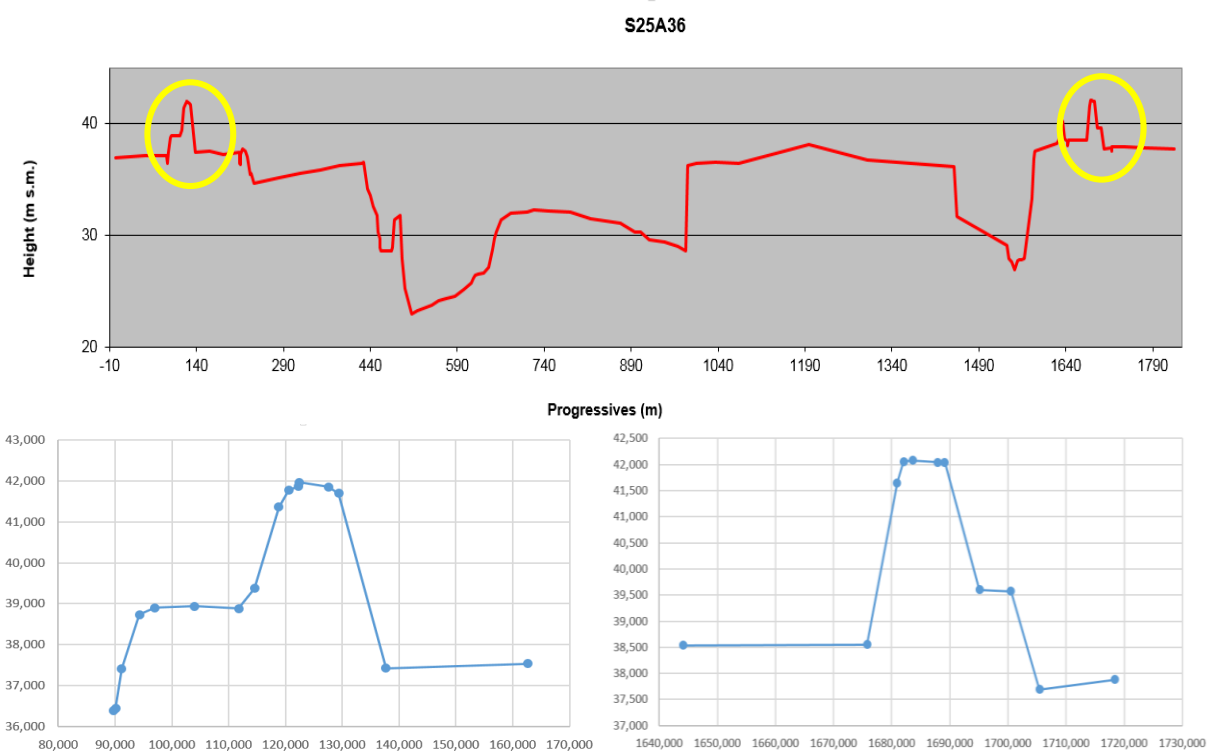

Figure 35: example of vertical section S25S36, with main levee profile details

A total of 42 different sections are used in this work(30 for the left side, 32 for the right side), disregarding the few section in which the levee shape is not well recognized.

The distance between each section plays a great importance in the levee stretches' reliability analysis. Discernibly, a shorter distance between the sections—giving a higher discretization of the levee system—permits a better analysis of the morphology trend as well as a more accurate study of the levee's reliability. Converse, having a higher distance apart would incur loss information in the even of a sudden change in levee shape or the presence of an obstacle not observable by the section. It is for this last reason that the thickened, blue lined sections are used in this study, even if they are present only in a part on the right side of the levee system.

6.2 Dataset from the Literary Research

While the levees' topography along the stretch of study are easily obtainable from the available information, knowledge about the geotechnical parameters of the materials constituting the body of the embankment and the layers of foundations are scarce.

The spatial variability of the foundation soils, the variability of the lithological materials used in various stages of construction, and improvements of the embankment system over the past several of decades, make it questionable, if not impossible, to develope a deterministic approach to defining the geotechnical parameters (A. Domeneghetti, 2012).

Using a stretch of the main levee on the left side of the river near Caselle Landi (Lodi Province, section S22), the AdbPo has performed field surveys in order to study the lithological characteristics of the floodplain and embankments in order to carry out further geoelectric and seismic stratigraphic investigations for the evaluation of soils (AdB-Po-Geovit, ST1_22, 2004; AdB-Po-Department of Structural and Geotechnical Engineering of the Polytechnic of Turin, ST1_12, 2001).

Dr. Alessio Domeneghetti, in his previous work on this site, has adopted a stochastic approach by which the value assigned to a generic parameter is extracted from a probability distribution defined on the basis of information, properly verified and supplemented, if possible, from the information available from field surveys.

His experience has allowed the identification of the average quantities and based physically intervals within which the probability distributions are defined.

In the following table are shown only the parameters used in the analysis, taken from the Ph.d work of A. Domeneghetti:

Description	Variable	Unit	Average	Std. Dev.	Range	P.D.F	Reference
Turf Quality	f_g	[-]	1	0.1	0.5 – 1.5	norm.	Apel et al., 2006
Outer side rougness	k	[m]	0.015	0.025*0.015	0.0003 – 24	log-n	Vrijiling and van Gelder, 2000

Table 5: Summary of random variables used to derive fragility curves: mean, standard deviation, range of variation, probability distribution functions (norm – normal distribution, logn – log-normal distribution) and constant value (const). Selection of the distribution functions and parameter values is based on the provided literature sources or field surveys.

At the suggestion of Dr. Maurizio Mazzoleni, due to a lack of information on the variability of soil porosity along the Po River, a triangular distribution with a minimum porosity value of 0.2 and a maximum value of 0.5, respectively, and mode of 0.4 is assumed (Mozhaev, 2002)

7. Levee Reliability Model

Summarizing all the information explained previously, is possible to define a sort of *"levee reliability model"* as following:

- chosen the failure mechanism;
- wrote the limit state equation with the opportune physical knowledge;
- given the input data taking in account all the source of uncertainty;
- using the M.C. simulation as the probabilistic method for the analysis;
- the result is the probabilistic distribution of failure: the fragility curve.

This model can be shown in the following diagram:

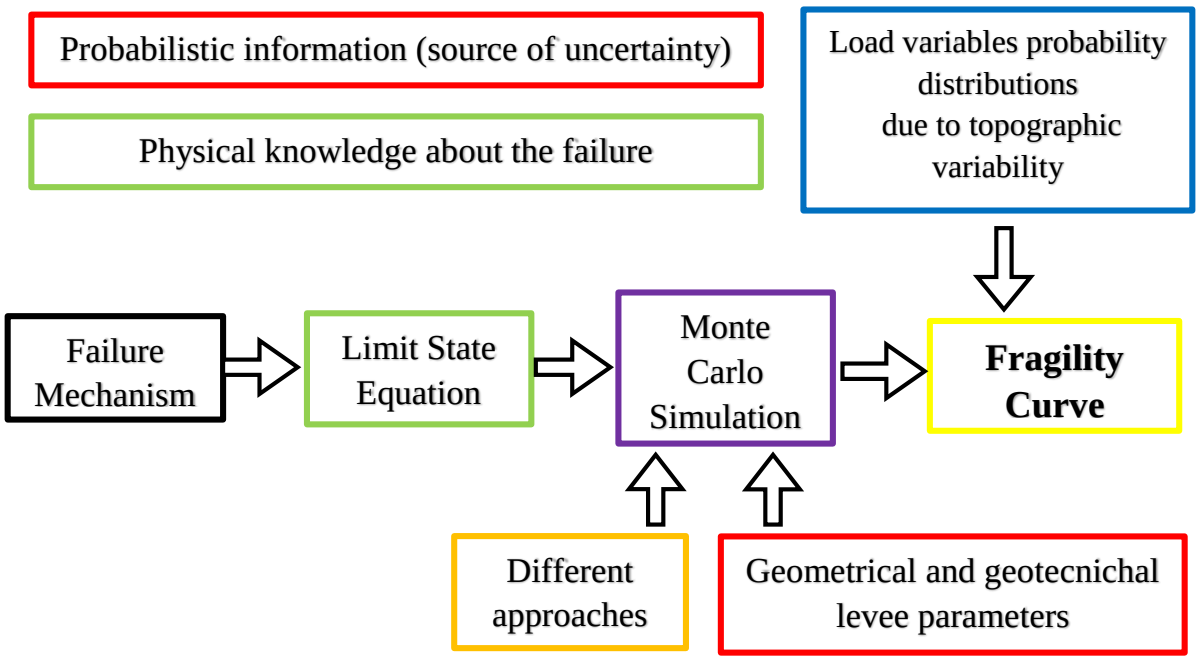

Figure 36: Simplified scheme of the levee reliability model

The contribution of the topographic variability, reflected in the variables probability distribution, is applied once a fragility curves is obtained by the MCSs. This aspect is discussed in chapter (7).

In the past, a reliability analysis for soil embankments worked only for the vertical sections of the levee where the results of failure probability were representative only of a chosen point or a series of points along the levee. Recently, several experts are trying to expand the analysis

to a stretch or a series of stretches always. However, they always begin from information obtained on single sections.

The difficulty of this method is trying to understand how to manage the information obtained by the topographic sections and how to spatially distribute the stretches.

After several considerations, two approaches have been utilized for the reliability analysis as a function of the vertical profiles' positions with respect to the analyzed stretch.

In using these two approaches, the stretches studied will not be the same. Therefore, the results will change with respect to each unique section of the levee.

7.1 Approach 1: Centered Sections

This first approach, suggested by Dr. Mario V.L. Martina, uses a set geometry of a singular section with respect to both sides of where the profile is located for the portion of the levee in the adjacent areas. The geotechnical and the land cover characteristics of the levee are also considered with regard to their spatial variability to yield with a mean value and a standard deviation.

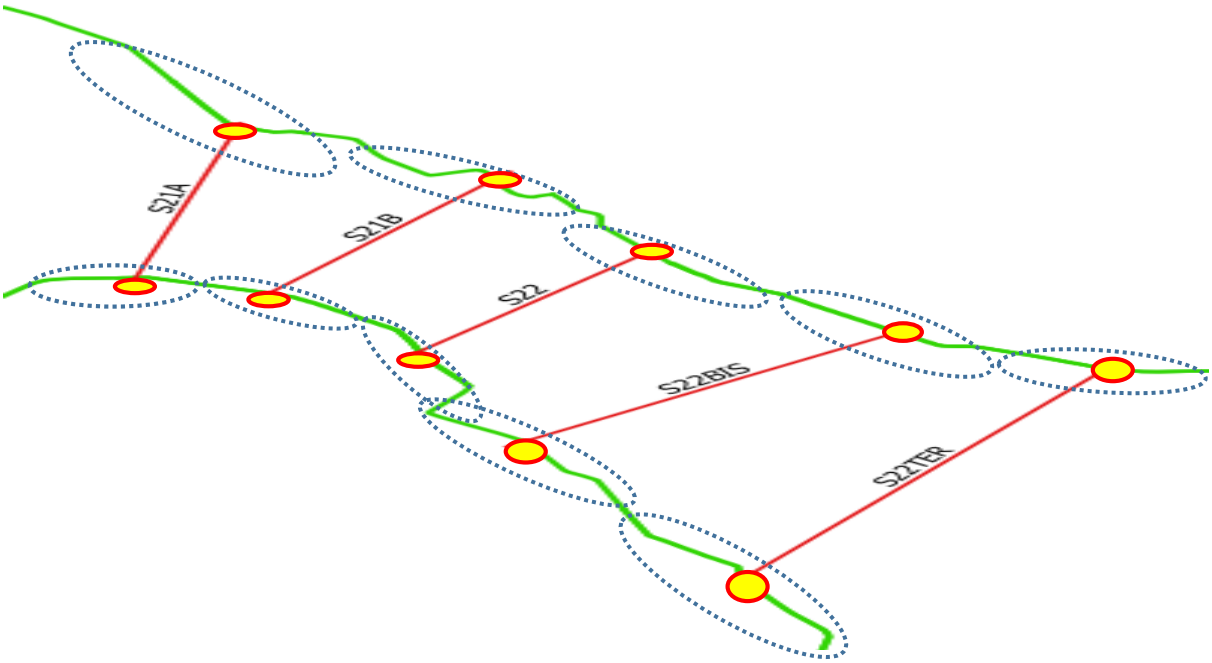

Figure 37: Conceptual scheme of the first approach: singular section (yellow points) as a point of reference for the stretches considered in the analysis (blue circles)

Assuming the levee geometry is the same in the neighboring area to the section, this method's advantage provides very accurate results near the center point of the corresponding point of the section that is considered representative for the portion of levee.

The disadvantage of this approach is that fixing the geometry of the embankments may not be representative of actual spatial trend that could generate overestimated or underestimated results. Moreover, it does not take in account potential obstacles—such as those that could be near to the reference section—that could suddenly change the shape of the levee.

The reference topography (used to reflect the morphological trend in the space) for the reliability analysis is correct at the point where it correlates to the vertical profile and then applied to the neighboring areas in the same manner as the fixed sections. Although it is especially representative of the line corresponding the section, it is not necessarily indicative of the neighboring areas.

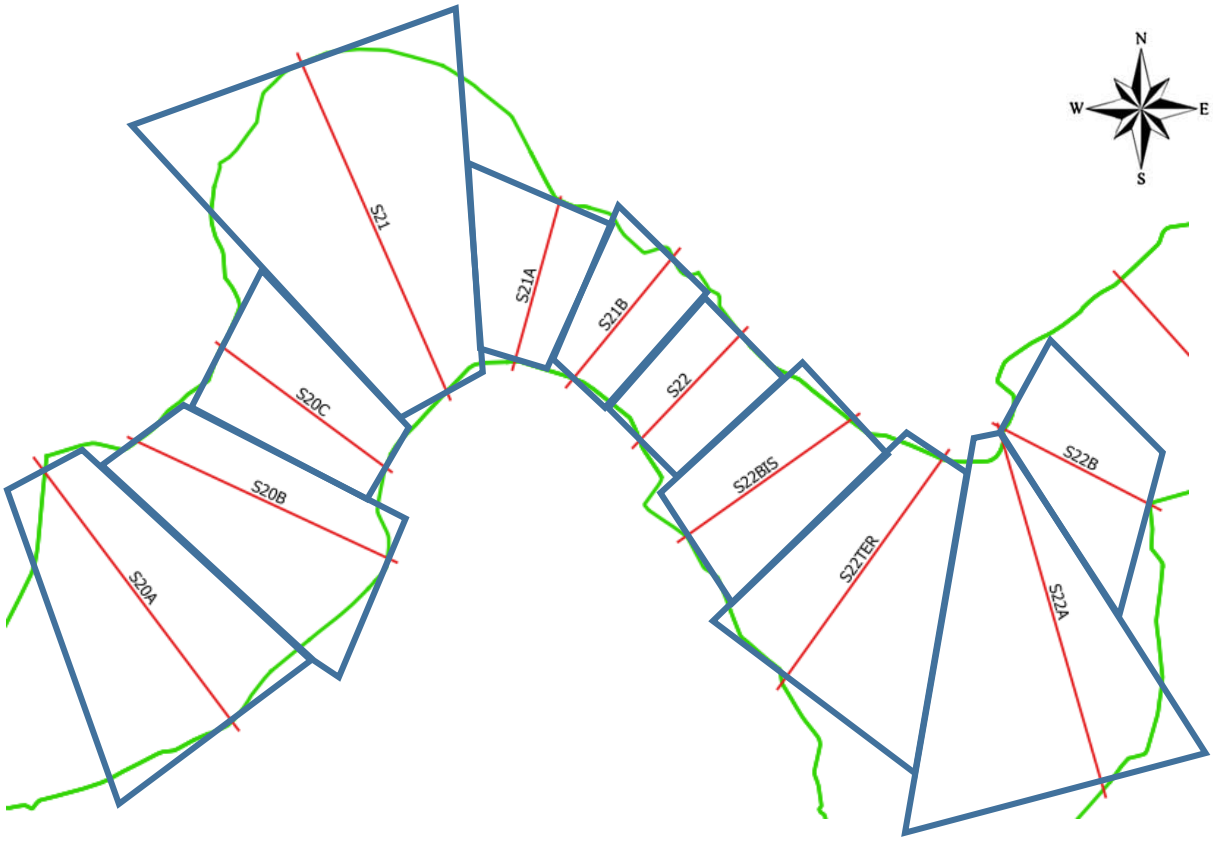

Figure 38: Scheme representing the reference topography for analysis using the first approach.

7.2 Approach 2: Sections Limits

This approach has been previously used by other experts in this field of study, such as Dr. Maurizio Mazzoleni, when considering a stretch of the embankment between two sections. In this approach, the geometry of the levee is not fixed. Instead, the values of the topographic data comprise a range that are then defined by the set limits of the topographic profile, or geometrical boundary conditions, for the levee stretch. Therefore, during an MCSs, the values of the geometrical parameters are randomized for period of time that is a function of the number of simulations required for the analysis. As in the first approach, the geotechnical and the land cover characteristics of the levee are also considered with regard to their spatial variability.

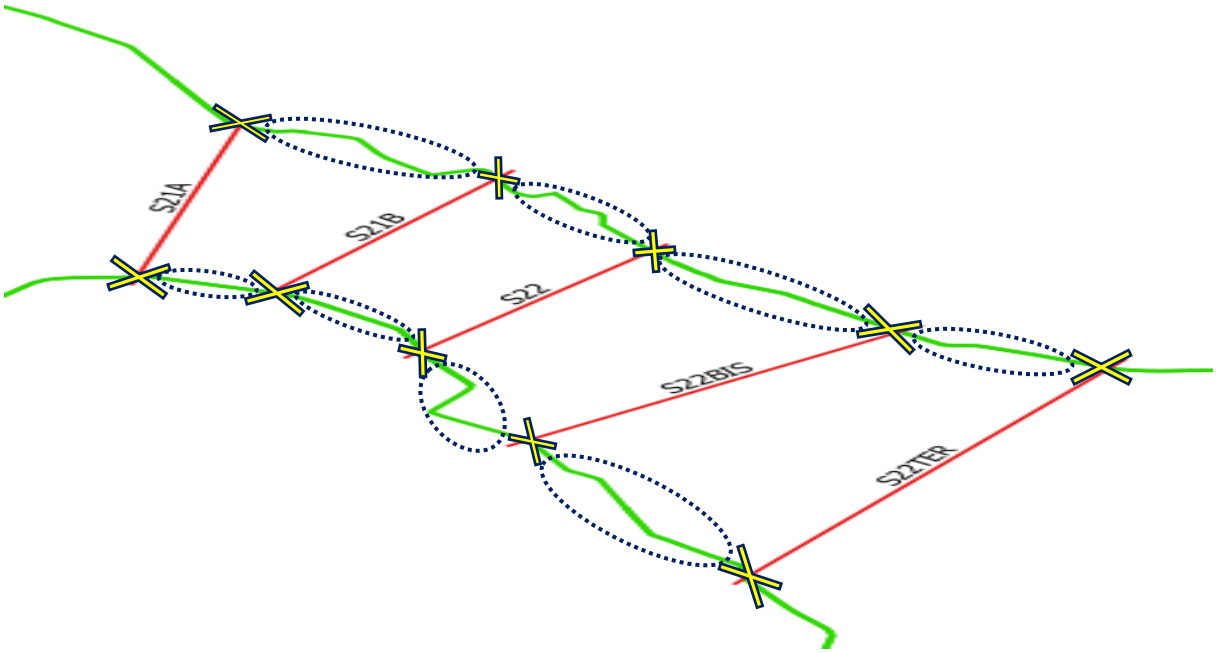

Figure 39: scheme of the second approach: singular section (yellow cross) as boundary condition for the stretches considered in the analysis (blue circles)

The shape of the levee shape corresponding to the last section is taken in account (and the geometry is fixed) only in the cases where the levee system ends due to confluence of the secondary rivers.

The advantage of this approach is that it considers the variability of the levee's shape inside the analyzed stretch. It is then possible to avoid underestimating or overestimating the

reliability of a levee's stretch, even if, like the other approach, it does not take in account the presence of obstacle and sudden change of the levee's geometry.

The reference topography for the reliability analysis is obtained in a different way respect the first approach. At the moment a stretch between two sections is studied, the topography of the riverbed correlated with the levee system is expressed as an average between the two topographic profiles limiting the stretch of the embankment. Using mean values could cause a loss of information. However, it is representative of a defined interval while the first approach it is not.

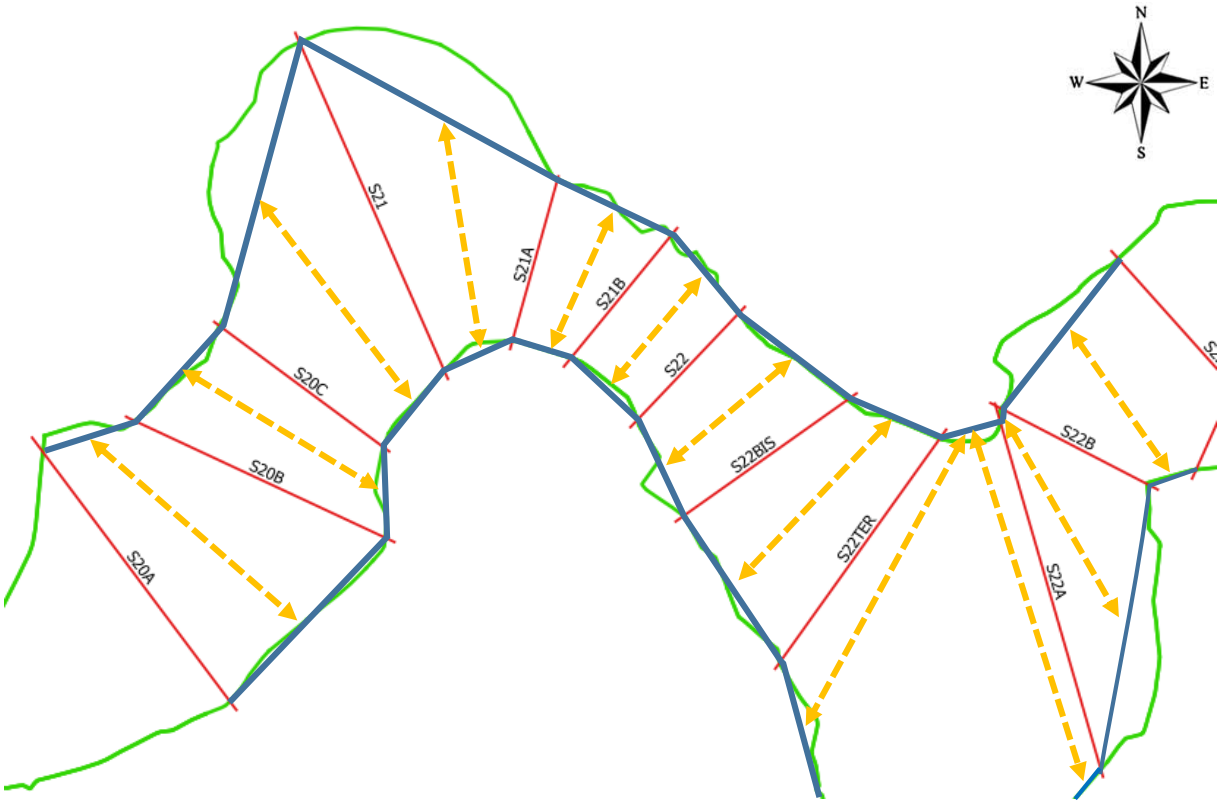

Figure 40: Scheme that represent the reference topography for the analysis using the second approach.

8 Study Approach to Levee Geometry

8.1 Geometrical Analysis

Geometrical data input of the levee's shape is fundamental for a reliability analysis to have a fragility curve with regard to piping or overtopping. Using the vertical sections available by the AdbPo, all useful geometric data is calculated with a calculation matrix written in Excel using the coordinates of each point of the levees' sections (*see table in the Attachments*).

The geometrical parameters calculated are:

- the outer slope (of the upper part of the levee);
- the total width (from the inner to the outer toe);
- the partial width (from the inner top to the outer toe);
- the outer height (from the outer top to the outer toe).

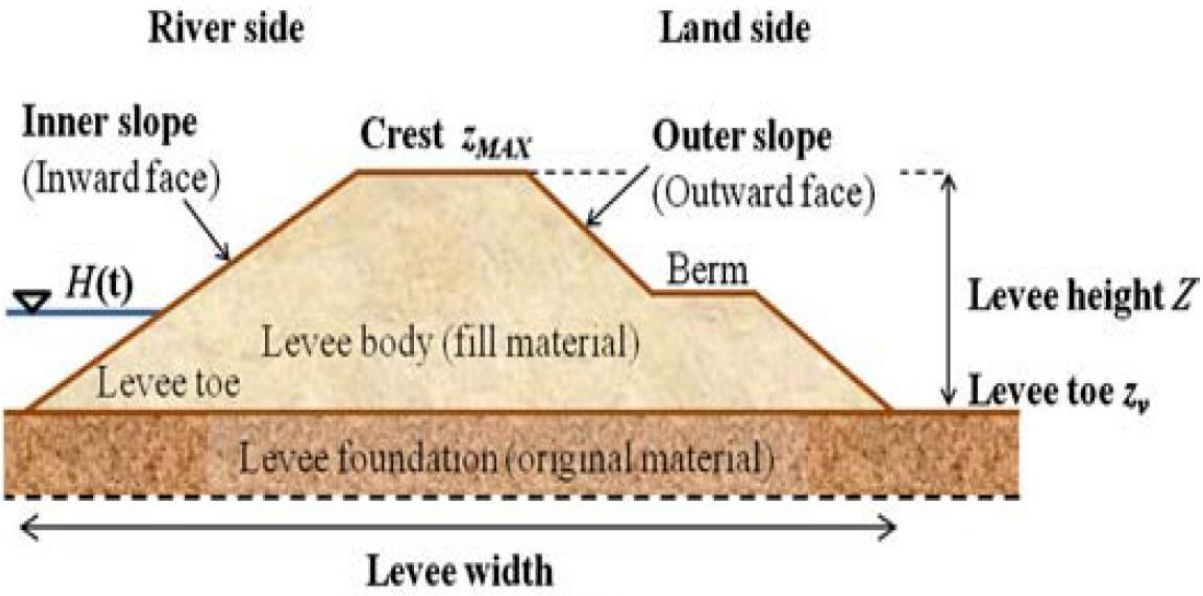

Figure 41: Sketch of the levee system geometry (M. Mazzoleni, 2014)

The base width is the horizontal length from riverside levee's toe to the landside toe, taking in account that the two toes are not at the same topography level. Cause of the variation of the levee shape from the inner to the outer side, also the heights are different for both side.

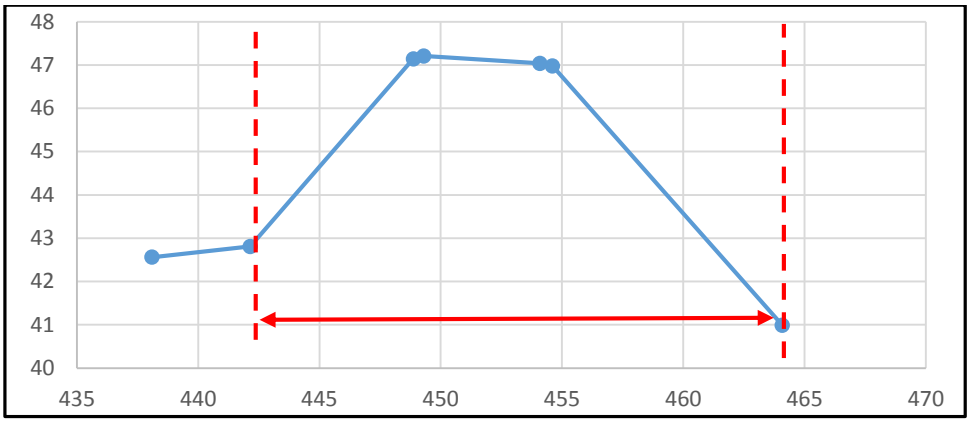

Figure 42: Typical trapezoidal shaped levee

The slope angle calculation is the most difficult to do especially when the levee's shape is not trapezoidal. Occasionally, more than one angle is present when the upper and lower slope of the levee are different due to the presence of a berm; when an overtopping takes place, the upper slope measure for the analysis since it is the most stressed area during and overflow of the levee.When the slope shape is a series of small berms, such an escalator, it is possible to use a mean slope angle. Although this method is can be used, such as when the upper part is less than a half-meter, it can be one type of uncertainty yielding errors in the simulation.

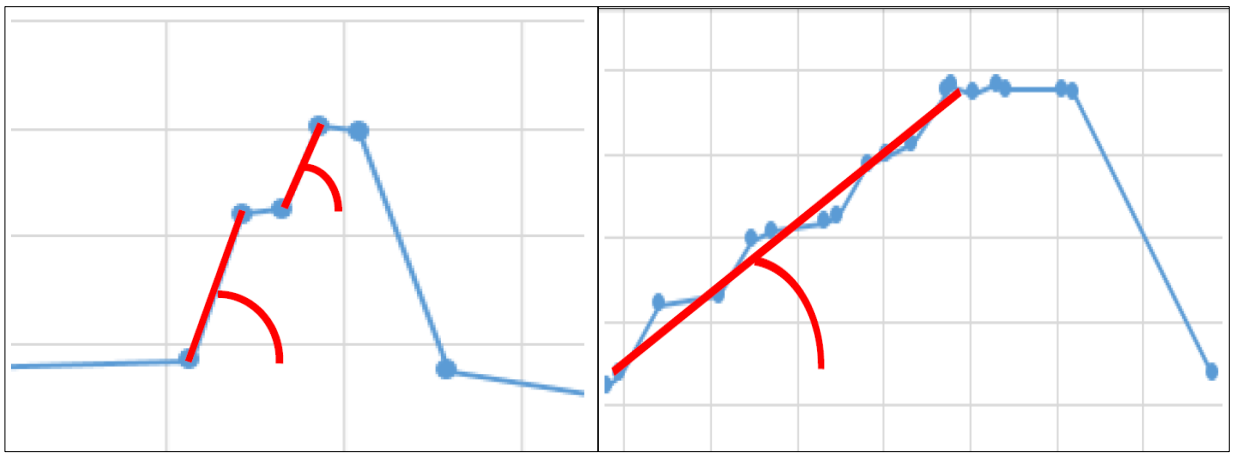

Figure 43: Different levee shape: with one berm (left) and a series of berms (right)

Carta Tecnica Regionale (CTR) and satellite imagery are used to check the topography and morphology of the flood plain thus making analyses easier; Keyhole Markup Language (.kml) files are created using QGIS to load the shape files of the main levee system and all the sections on Google Earth. This allows one to work quickly using satellite imagery, digital elevation models (DEMs), and Google Street View to accurately verify the actual shape of the analyzed levees. The resolution of these resources is enough for this work's purposes.

Figure 44: Images taken from Google Earth, example of berms series of a levee

8.1.1 Sources of Uncertainty and Error Corrections

All the parameters obtained by the calculation are then regrouped and plotted to observe spatial trends. Initially, from Piacenza to Cremona, it would be expected that these parameters would follow a regular trend, but the graphs reveal a random trend, as in Figure 46. Understanding the cause of this trend requires a careful observation of each section using the CTRs, satellite imagery, shape files, and the sections of the main levee system. Consequently, the first source of error is because of the direction of the section in space with respect to the levee's direction. In order to have a correct data series, the section should be perpendicular with respect to the levee's direction, but this not always the case.

Figure 45: Example of reliable [yellow, S22B] section and unreliable [red S22A] section (Google Earth)

Therefore, with the aid of the QGIS software, a *classification of sectional reliability* is created in function of the angle between the two directions.

This classification can be describe as:

- *Reliable* (90°-75°): no, or minute, error of the parameters;
- *Uncertain* (75°-50°): slight level of error;
- *Very Uncertain* (50°-30°): high level of error;
- *Unreliable* (<30°).

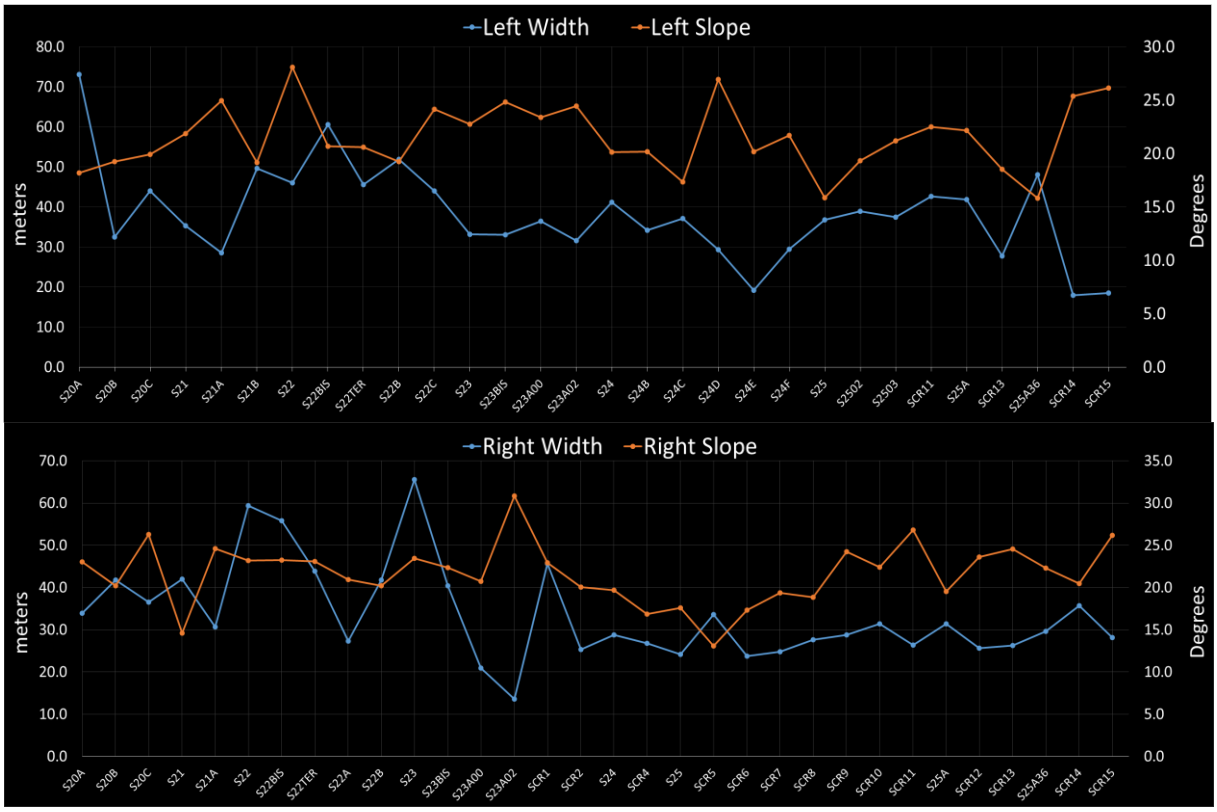

Graphs 1-2: Morphological trend of the levee system for both side

The results indicate 41.9% of the sections are reliable, 51.6% are uncertain, 6.4% are very uncertain, and 1.6% are unreliable.Obtaining the real width is accomplished by calculating the angle (α) between the section direction and the levee direction. After obtaining these values, the real width may be calculated using the the formula:

$$w_{real} = width \times \sin \alpha$$

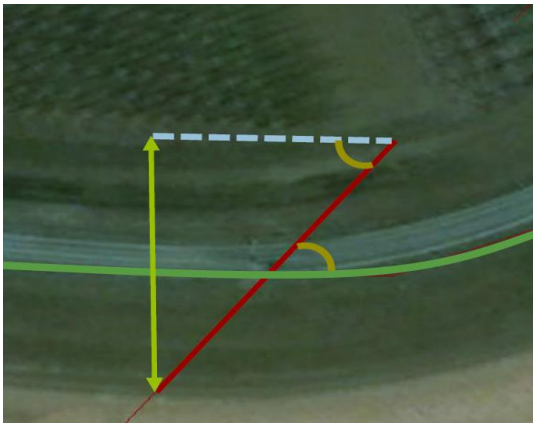

Figure 47: Apparent width (red) and real width (yellow)

The following chart, Figure 48 showing the relationship between the *real* and the *apparent* angle, is needed to obtain the real slope angle. By laying line from the alpha (blue) through the apparent (red) slope, it is possible to extrapolate the real (green) slope angle.

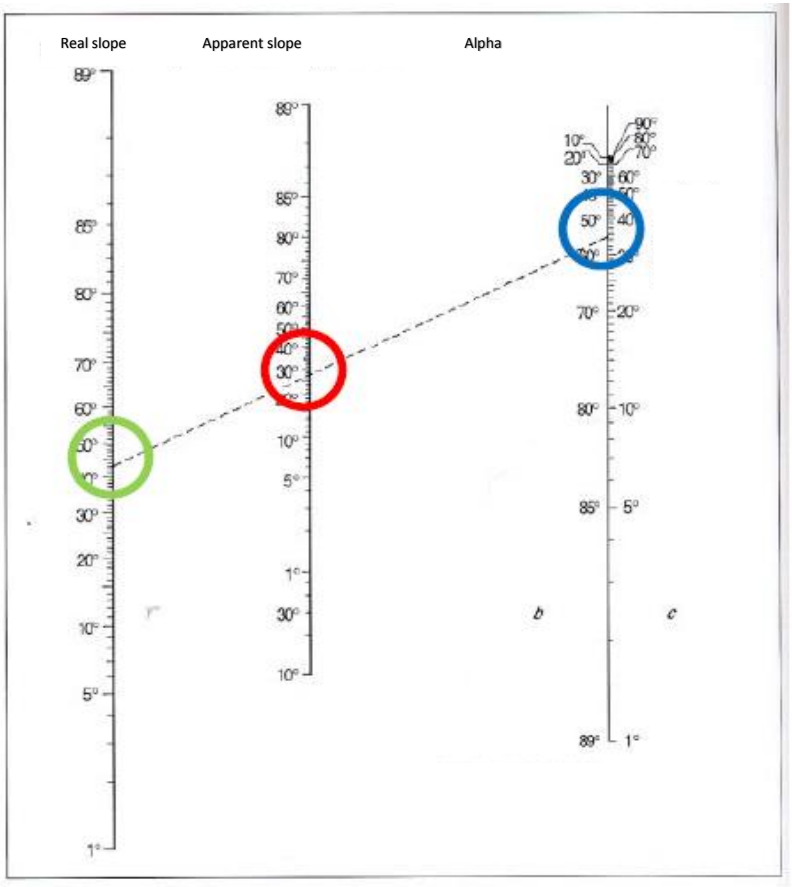

Figure 48: The chart used to obtain the real slope angle.

All geometrical parameters from topographic profiles of the levees have been corrected to permit a complete use of the available information for this work.

Other sources of uncertainty and errors are found by the observation of the satellite images such as:

- road crossings on embankments;
- secondary road next to a levee;
- areas of and subsequent storage areas from bank mitigation efforts in 2005;
- sections on curves;
- mapping errors.

8.2 Morphological Trend

After plotting on graphics all the correct geometrical parameters, it is then possible to see the real spatial trend even though a random trend of the parameters is still present. Three hypotheses are supposed: first, there is the need to adapt the levees' shape to the topography of the flood plain; second, there are construction directives to follow for the rebuilt embankments; third, the informational limits of private property with respect to available details.

In graphs 3 and 4, the trend of the slope angle of the outer upper side of the levee system is presented. Its values range from 18° to 30° degrees on the left side and from 17° to 32° on the right side. The graph makes it possible to visualize the dissimilarity between the calculated and corrected slope as a function of the α angle (white) with difference of over 9°.

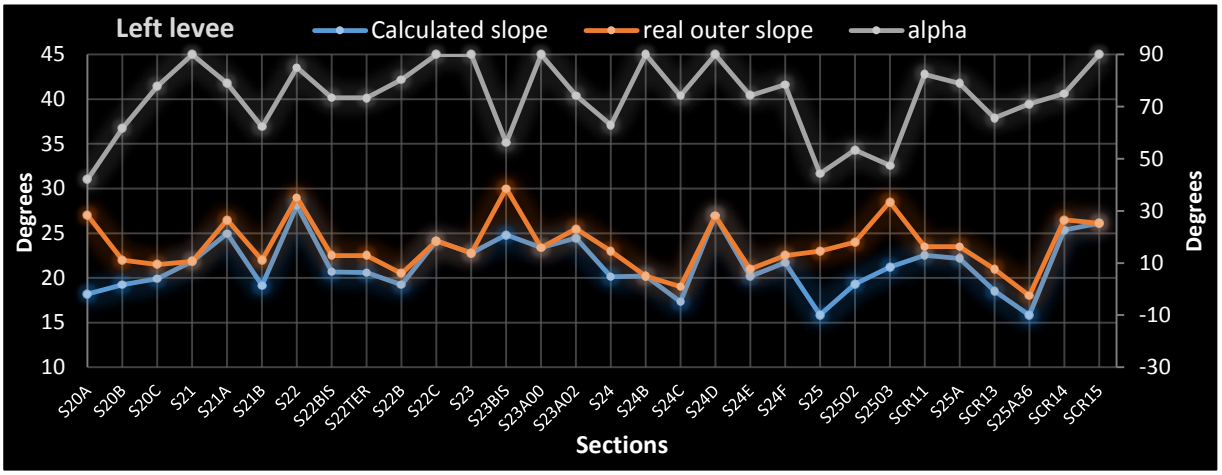

Graph 3: Trend of the slope angle of the upper part of the levee system (left side)

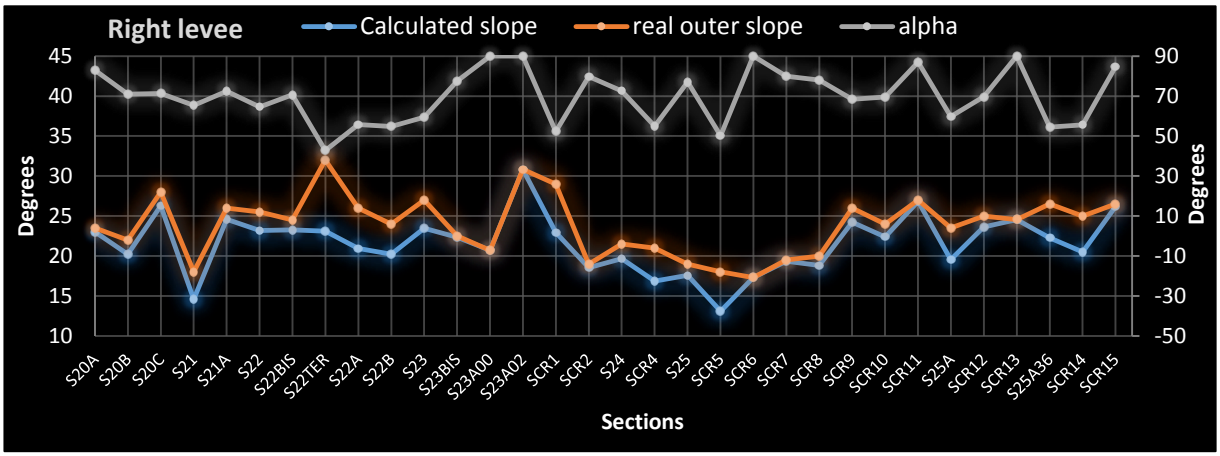

Graph 4: Trend of the slope angle of the upper part of the levee system (right side)

Following, graph 5 and graph 6 shows another distinguishable trend corresponding to the levee system's base width. More variability is present in the downstream section near Piacenza with left side values of 27 to 58 meters and right side values of 13 to 56 meters. After Serafini Island, the real width still shows variability on the left side with values between 18-45 meters, while the right side has more constant values of approximately 26 meters. Observing this trend using satellite imagery, the larger widths match areas of cultivated fields and the smaller widths correspond to urban and industrial zones. With these observations, it is then possible to see a decreasing trend from Piacenza to Cremona using a polyline of interpolation. The difference between the calculated and the corrected base width in relation to the α angle can be up to 23 meters.

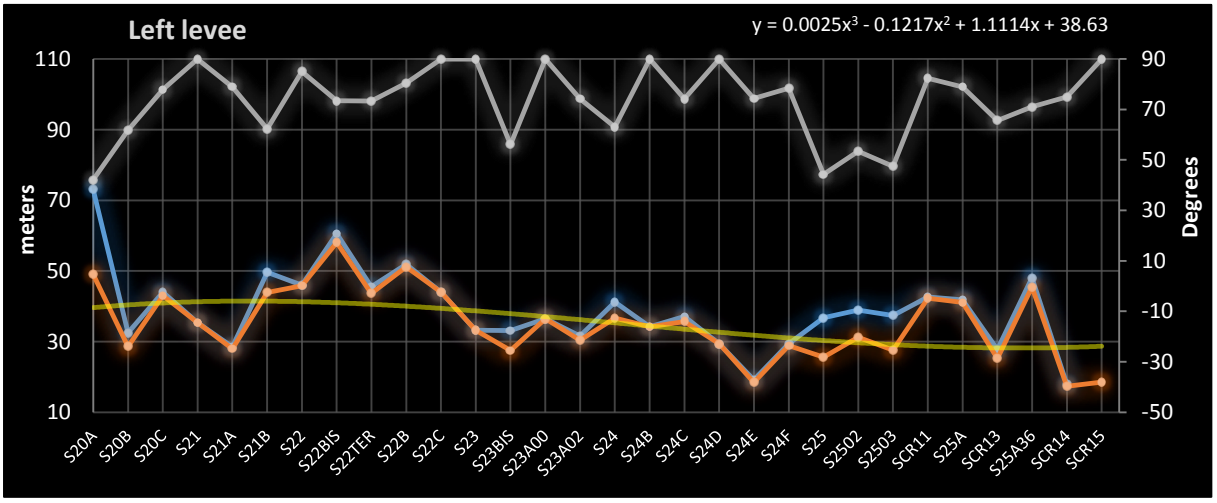

Graph 5: Trend of the base width of the upper part of the levee system (left side)

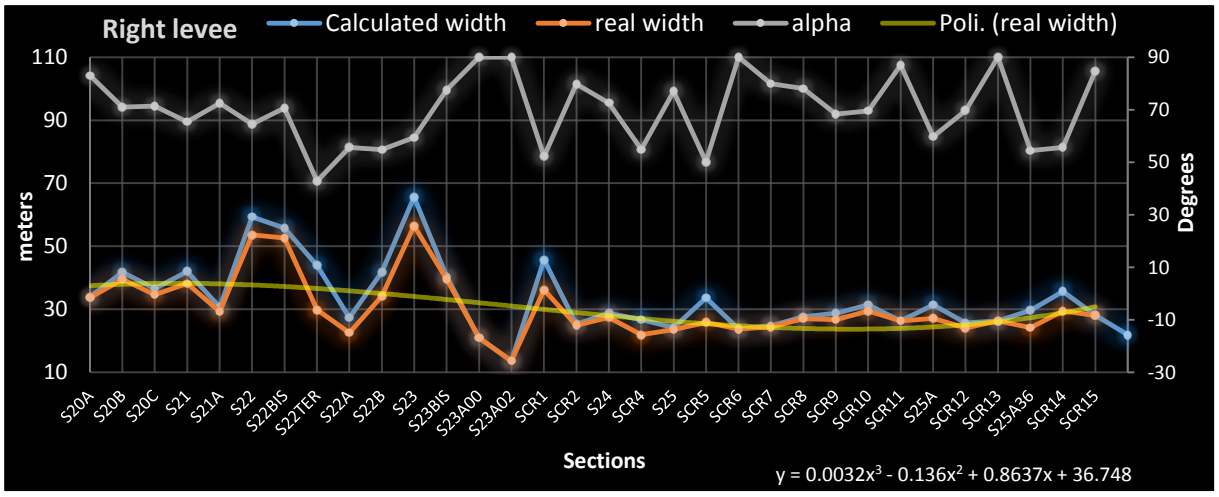

Graph 6: Trend of the base width of the upper part of the levee system (right side)

In graph 7 and graph 8, the landside height of the levee system, where a decreasing trend is also present, has left side values ranging from 2.23 to 6.69 meters and right side values of 1.3 to 7.6 meters.

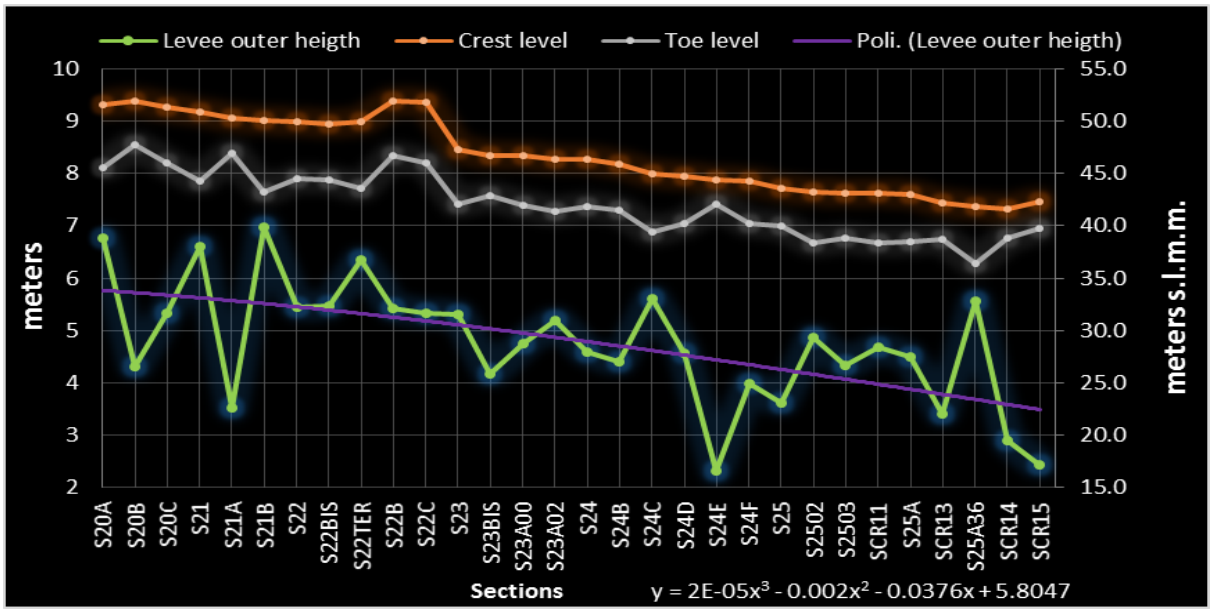

Graph 7: Trend of the outer height of the upper part of the levee system (left side)

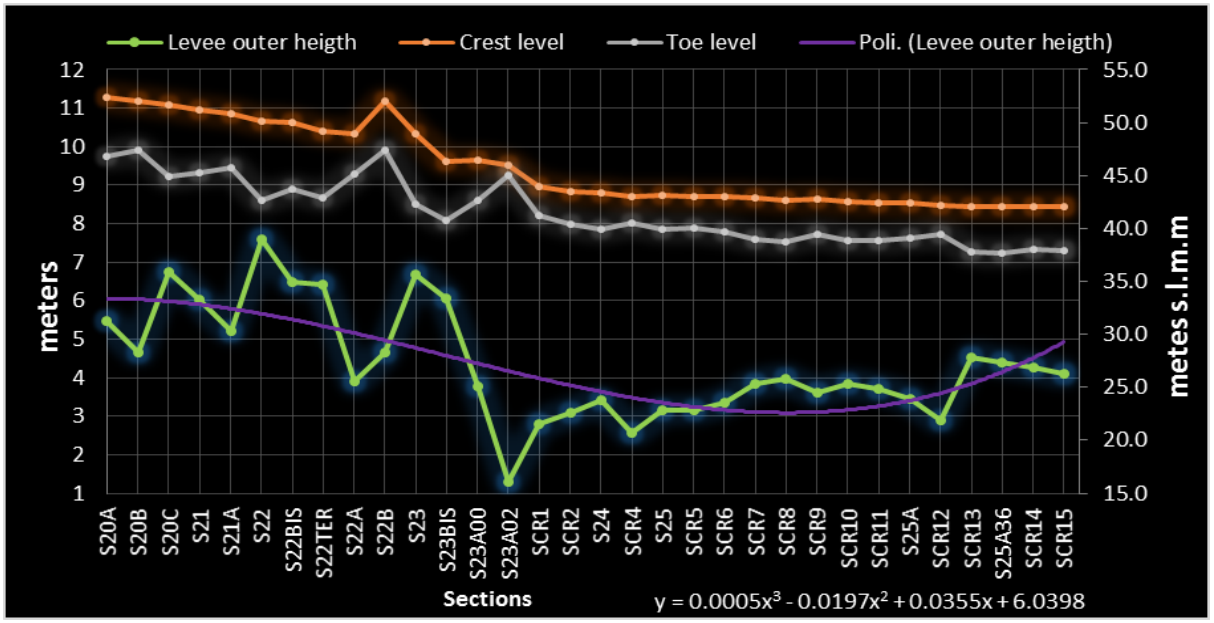

Graphic 8: Trend of the outer height of the upper part of the levee system (right side)

As seen in the graphs above, the difference between toe and levee crest elevations decreases downstream—higher and more variable downstream from Piacenza with more regularity and consistency further down—which constitutes a decreasing value of headwaters along the river along with a decreasing probability of failure due to piping.

The graphs below represent the morphologic trend of the riverbed characteristics associated to the levee system topography:

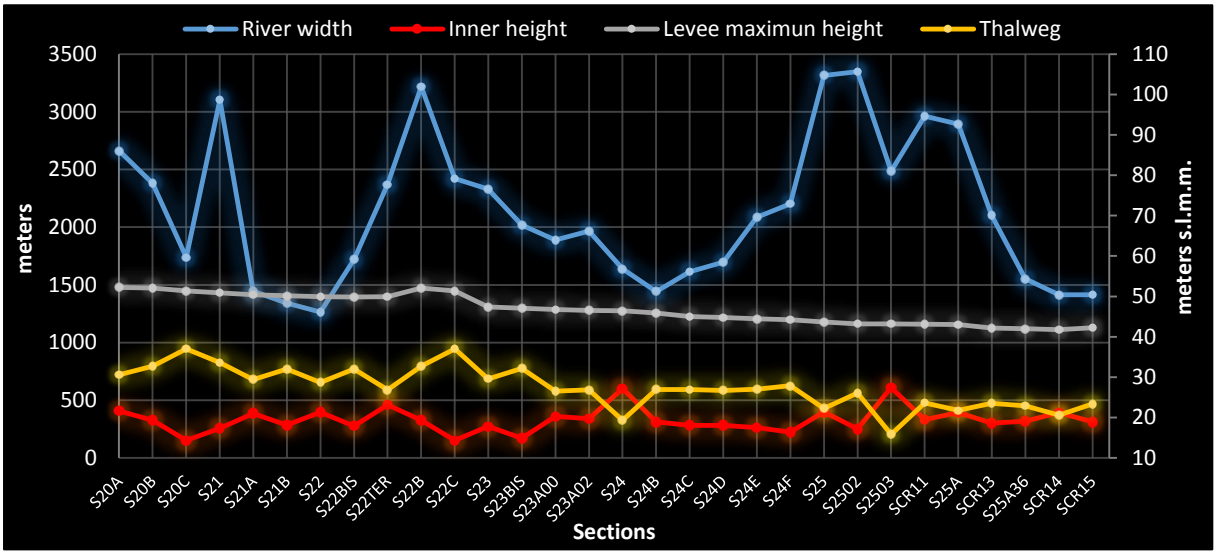

Graphs 10: Riverbed characteristics and their trend associated to the levee system (right sides)

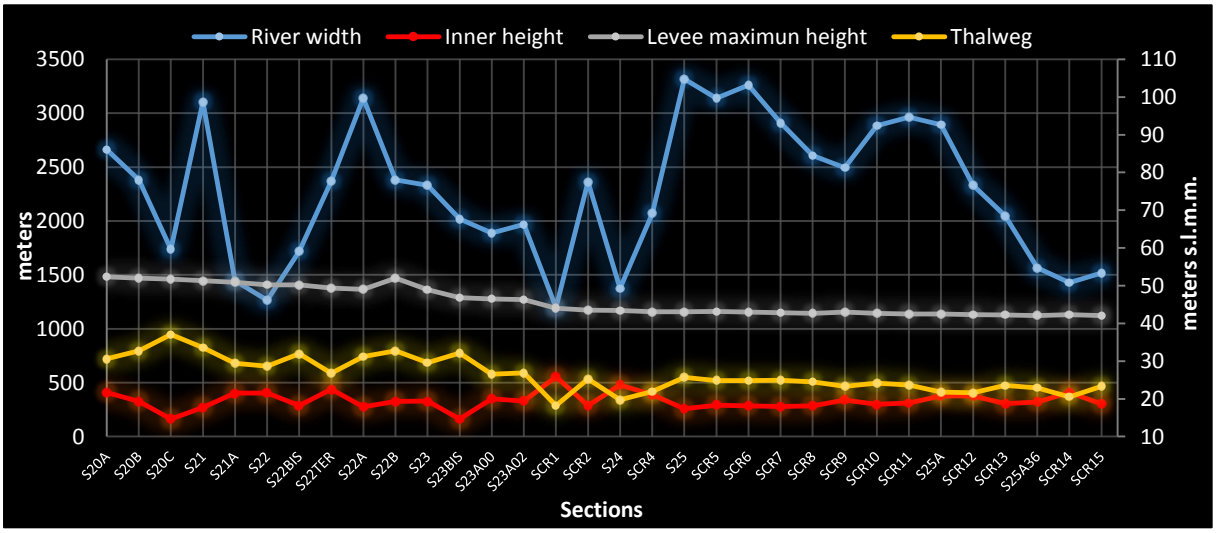

Graphs 10: Riverbed characteristics and their trend associated to the levee system (right sides)

The river width, including the floodplain areas—the distance between the levee inner top on both side is considered—has a random trend due, in part, to new levee system being built on the old one as well as accounting for movement over the years.

The crest level and the Thalweg level have a similar, descending trend from Piacenza to Cremona where their difference (red line), with slight variability, has a maximum value of 27 meters, a minimum of 14 meters, and a mean value of 19 meters.

9 Reliability Analysis

Once settled all the useful parameters (geometrical ones from the topographic sections, surface cover and geotechnical ones from literature) everything is ready for the reliability analysis for levees' stretches. Using the Monte Carlo Method (MCM) it is possible to obtain a distribution of failure probability, resuming the equations previously reported and write a MatLab code for levees' stretches. So a number of simulations are done taking in account the variability of the characteristics along the stretch.

9.1 Probability Distribution of Variables Associated With Topographic Variability

Before to explain the fragility curves obtained, the implementation that take in account the load variables probability distribution is described. Use only singularly the M.C. method is mathematically correct, but it consider a distribution of the variables (as the water load, the overflow water load, the overflow time) as uniform.

To do a correct analysis this distribution should take in account the possibility of the variables to happen, then using a probability distribution of the singular variables considering different flood scenarios, so for various return time, observing different hydrographs for each measuring station and section located along the river.

Not having the possibility to observe a real (or simulated) trend of the variables for different return period, a supposed and reasoned trend is used, where the probability decreases, considering a negative exponential function, while the variable increases. To apply this distribution to the analysis, it is represented as a cumulative density function (CDF) in form of probability of not exceeding $P\ (X\ \leq\ x)$ (Figure 49).

For the overtopping analysis, a probability distribution is applied using the overflow water load (he) and the overflow time (te). Since piping in the gradient method is stationary, only the river water load (Hw) is used. Using MatLab, this curve is expressed as:

$$CDF\ =\ expcdf\ (mu, Hw(x))$$

where $Hw(x)$ is the variable considered and *mu* is a mean value to describe the probability trend; for each variable, such as failure mechanism and approach, a different *mu* is used.

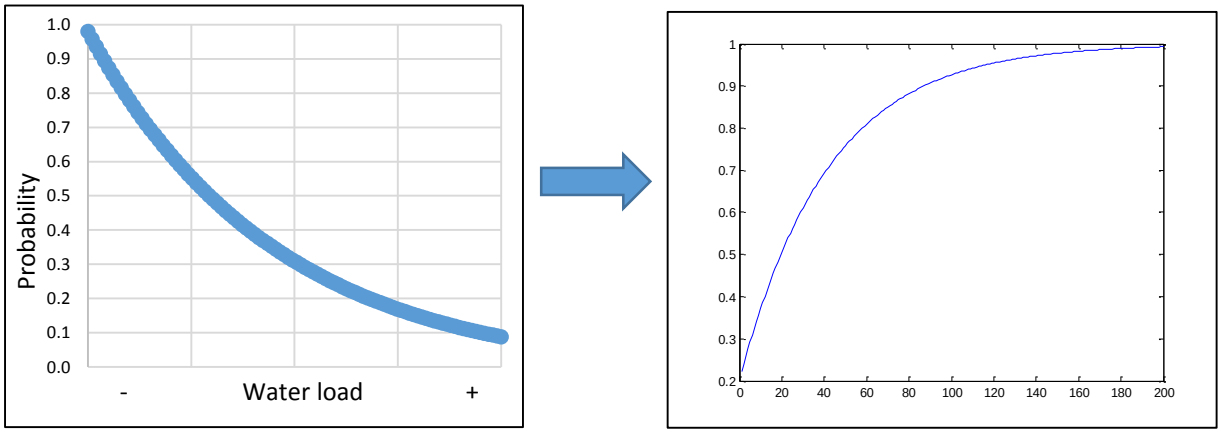

Figure 49: Decreasing trend of probability (left) and its expression as a C.D.F. (right)

Using only one CDF for all analyzed stretches would imply the same probability distribution for the entire stem. In reality, the probability distribution must change because the morphology of the riverbed and the levee system also change along the river. Therefore individual he and Hw CDFs for each levee stretch are generated as a function of the variability of the river width (B) and, with respect to the thalweg, the levees height (Hf), while the distribution for te remains the same.

This means that where B and Hf are higher, the probability of failure is lower and the probability of not exceeding is higher; the converse is the same should B and Hf be lower yielding a higher probability of failure and a lower probability of not exceeding.

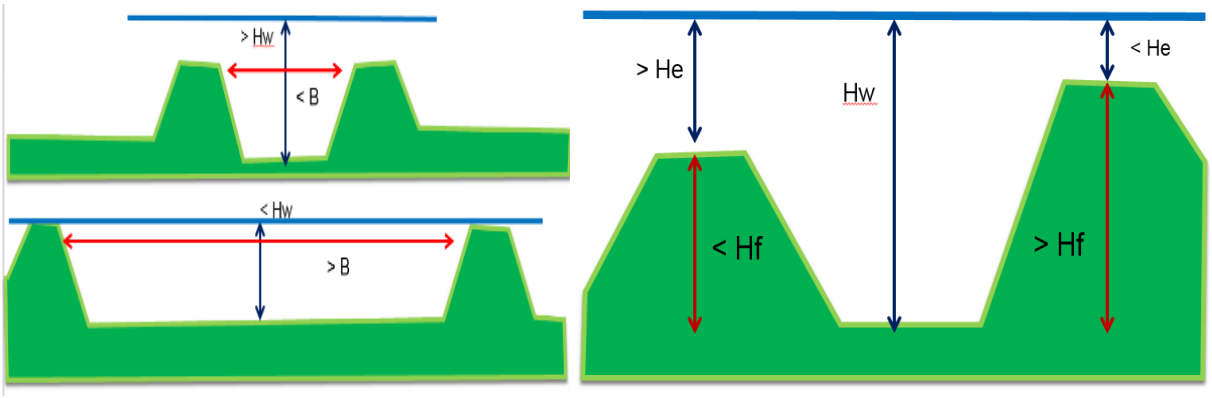

Figure 50: Schematic showing the different topographic situations along a levee system

To do this, two coefficients, in function of *B* and *Hf* are created, as follows:

$$B_{coeff} = (B_i - B_{min})/(B_{max} - B_{min})$$
$$H_{coeff} = (Hf_i - Hf_{min})/(Hf_{max} - Hf_{min})$$

where B_i and Hf_i are the i widths and i heights for each section along the river stem; B_{max} and Hf_{max} are the maximum values and B_{min} and Hf_{min} are the minimum values found in the geometrical analysis.

The product of the two coefficients gives a series of numerical values called "*topographical indexes*". In the first approach, the coefficients are calculated directly from the topographic sections, while in the second approach a mean value of the coefficients for each stretch is considered as previously explained regarding the reference topography.

In order to connect the topographical index with mu to obtain different CDFs, a relation is created where the values of $mu(1)$, previously defined for the first CDF, is correlated to the lower value of the index using the following:

$$mu(i) = mu(1) \times (1 - Top.Index)$$

In this way the higher value of mu, associated to the minimum value of topographical index, corresponds to the CDF that represents a lower probability of not exceeding; while a lower value of mu corresponds to the CDF with a higher probability of not exceeding.

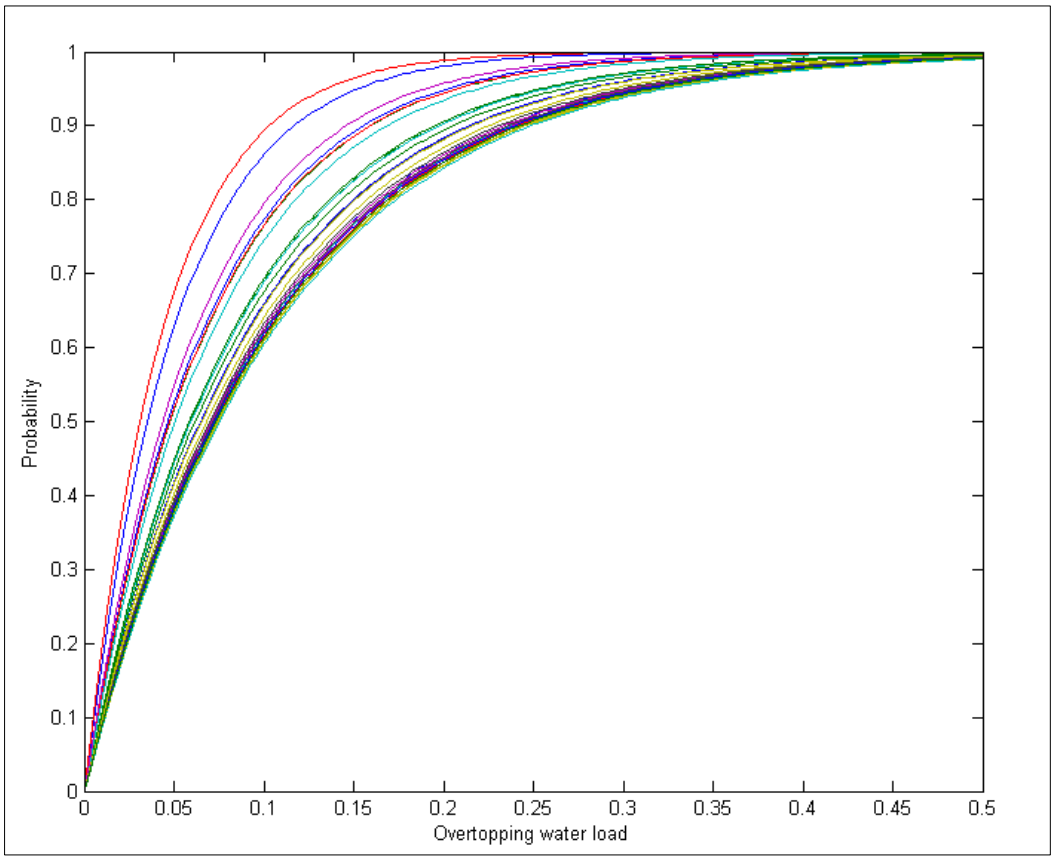

Figure 51: Different CDFs (for he) of the probability distribution as a function of different topographic situations

9.2 Failure probability distribution

9.2.1 Fragility surface for Overtopping

For every stretch identified along the levee system, the probability of failure is obtained spatially discretizing the independent stress variables—the overtopping water load (he) and the overtopping time (te) (200 x 200 steps). Using the MCM, 2×10^3 casual combinations of the variables are evaluated. In this way the failure probability of every point of the discretized space is obtained with the equation of the failure probability (chapter 4.1).

The fragility curve due to overtopping for a levee stretch is presented as a surface, or descent, of probability as a function of hydraulic conditions (he, te), where the probability of failure P ($[0-1]$) is showed.

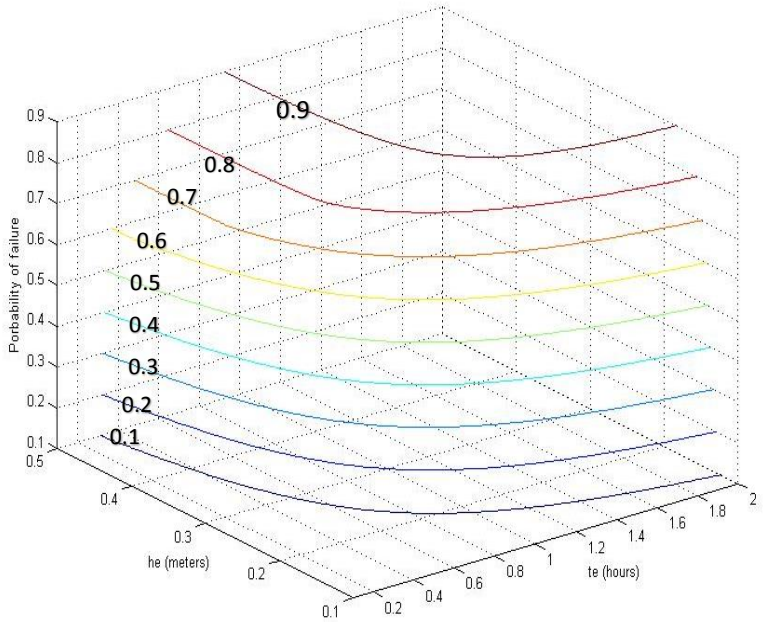

Figure 52: Example of fragility surface for overtopping

The following images represent the fragility surface of different levee stretches.

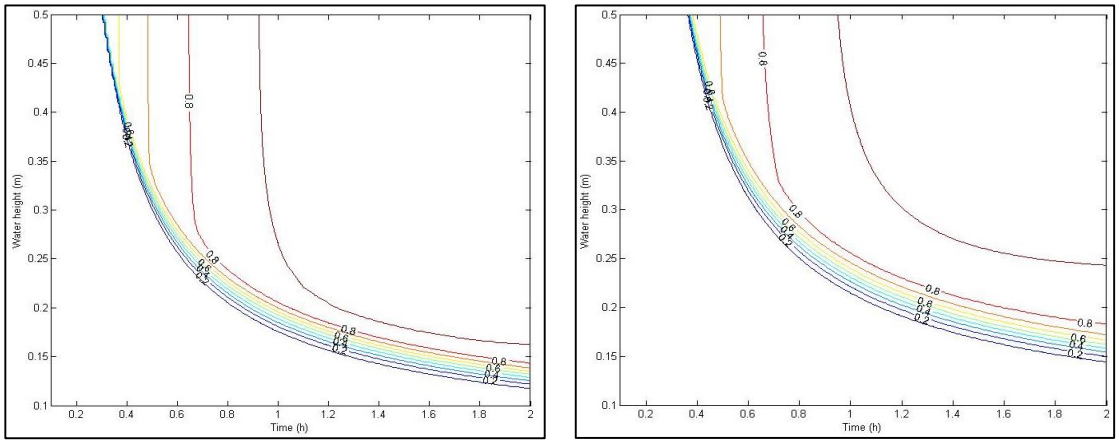

Figure 53: Fragility surface of 1st (S20A) and 18th (S24C) left levee stretch with first approach.

The origin point of the graph begins at 0.1. This is due to values under 0.1 or near 0 creating a numerical error in the MatLab code. Therefore, the fragility surface is neglected for values lower than 0.1 (meters or hours).

It is possible to see in the following graphs how the fragility surface changes with the implementation previously mentioned. Multiplying the probability matrix for the probability distribution of he and te produces in a redistribution and expansion of the failure probability in the discretized space.

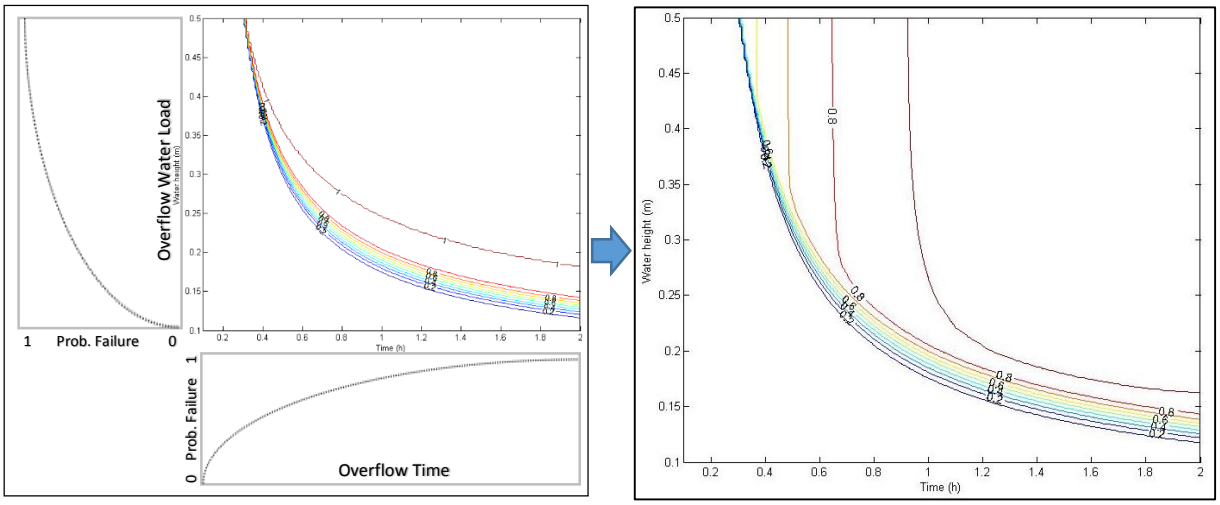

Figure 54: Difference between the fragility surface for overtopping before (left) and after the implementation (right)

9.2.2 Fragility Curves for Piping

The fragility curve for piping is expressed as function of the water load (Hw) with respect to the outer levee toe where its upper limit is higher than the maximum crest level found in the geometrical analysis.

The probability of failure P ($[0-1]$) and the resulting fragility curve are estimated by integrating the joint probability distribution function of the stochastic resistance variables used in the limit state equation with the MCS where 2×10^3 simulations are done considering 200 steps of discretization of the independent Hw variables.

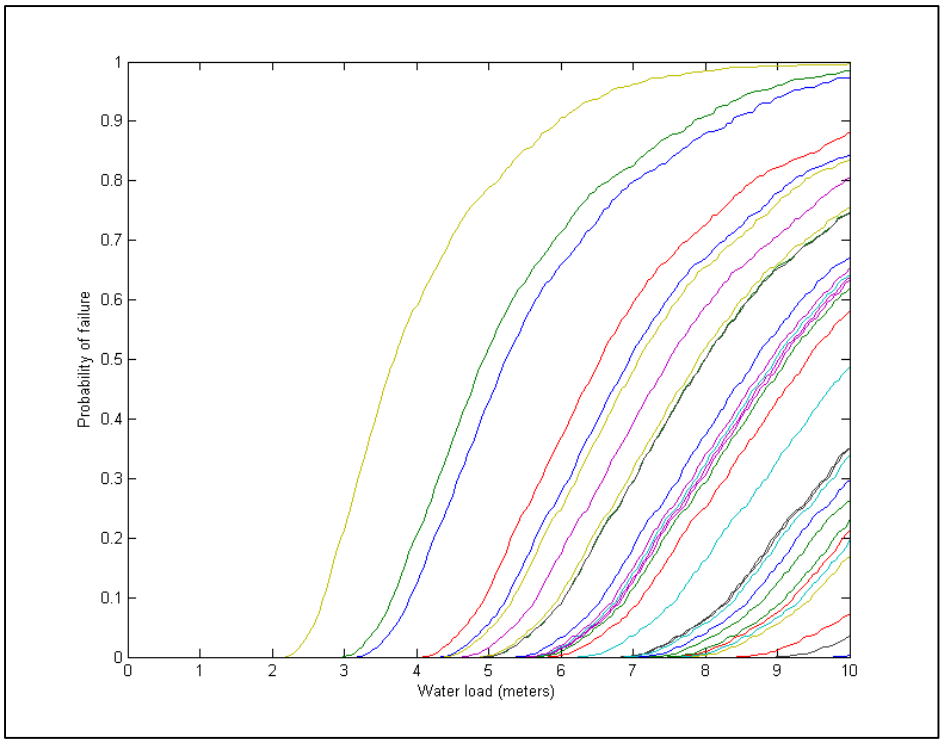

Figure 55: Piping fragility curves for stretches of the left levee system using the first approach.

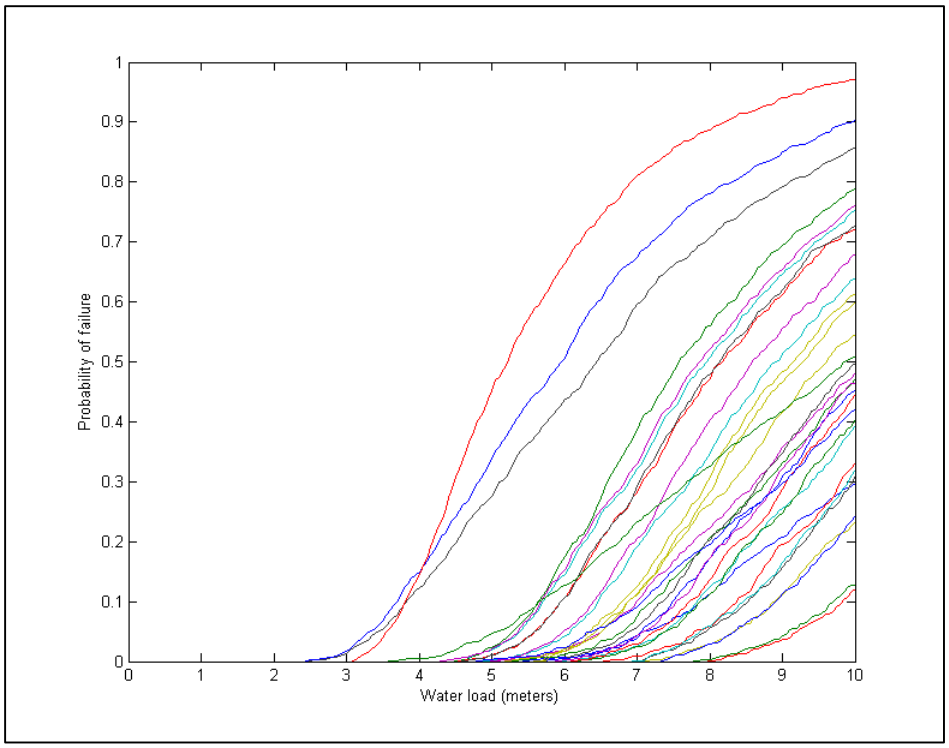

Figure 56: Piping fragility curves for stretches of the left levee system using the second approach.

The effect from applying the implementation on the fragility curves does not have the same impact as the overtopping fragility surface; the values are merely brought down thus giving a more accurate result without drastically altering the shape of the curves.

10 Classifications of Reliability

Once all of the fragility curves are obtained for overtopping and piping, they may then be assigned an applicable *reliability class* to each discreet levee stretch analyzed with consideration given to the two failure mechanisms and the different approaches. Often, the term *fragility* is used to refer to a mechanical process. It is, therefore, better to adopt the term *reliability* to describe the classes since they are the result of a probabilistic method. Defining the classes involves introduces indexes to characterize the fragility. Some indexes are taken from the parameters that are related to the probability distribution (physical indexes) while others are the ones that describe the shape (shape indexes) of the curves. Every index is divided into a subjective range using five different classes for each failure mechanism. The ranges, from *reliable* to *extremely unreliable*, have been defined observing the indexes' trend. Consideration has also been given to the sections of the levee system downstream of Cremona until Borgoforte, analyzed during a stage period, for the opportunity to take into account more indexes' values as well as see their spatial variability.

10.1 Definition of indexes

Since the shape of the fragility curves are different for the two failure mechanisms, different indexes, ranges, and classifications are generated. However, the number of classes remain the same.

10.1.1 Overtopping Classifications

For overtopping, two kinds of classification are proposed. The first associates a reliability class as a function of probability found on the fragility curve using a fixed value of the overtopping water height and the overtopping flow time (standard physical indexes). The indexes are fixed to account for the spatial probability of all the analyzed curves, where he is established at 0.25 meters from the levee crest and the flow time at $8/10$ of one hour (approximately 48 minutes). In this way, five classes are created with a range of 20% of probability. Evaluating different fragility curves for levee stretches, those with lower values of probability of failure are more reliable than those with high values.

The second classification uses indexes that describe the shape of the fragility curves. It can also be considered as a *performance classification* from the moment that it represents the behavior of the discrete levee stretch under a hydraulic stress.

The first index is set as the *minimum loading condition* (in this case, he), which generates a probability of levee failure equal to a threshold value set to 10% (ΔH_{min}); it is the minimum distance (in meters) from the origin on the graph to the curve of 10% of probability (it is not referred to a value on the *he* axis). This index provides the first indication of initial triggering conditions of a levee stretch having the probability to fail. If different fragility curves are considered, the levee that is more likely to fail is the one with smaller ΔH_{min} value.

The second index represents the *surface width* of the steep sections of the fragility curves (10% - 80%). In other words, a transition along the short section from lower values of failure probability to higher ones. Where this index shows lower values, it takes less overtopping water load to reach a higher probability of failure. The opposite is also true for the index's higher values.

The combination of these indexes—divided in subjective range—on a chart, gives five classes of performance, where small values of ΔH_{min} do not necessarily imply an unreliable levee stretch. This can simply be offset by a high surface width value and vice versa.

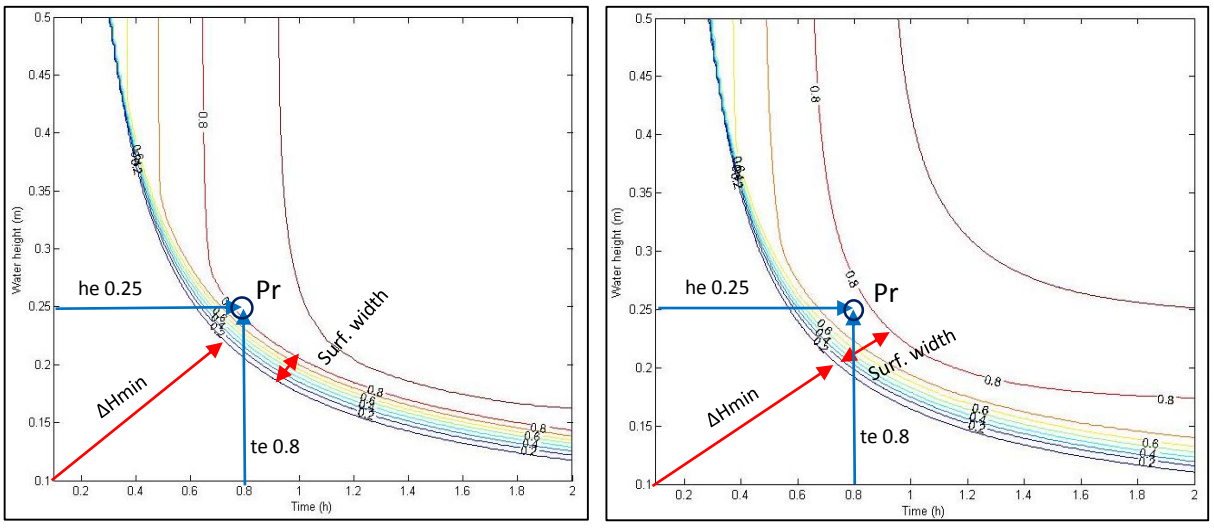

Figure 57: Example of indexes for S20A and S23bis left levee stretch, first approach; in blue the indexes of the first classification, in red the ones of the performance classification.

10.1.2 Piping Classification

Two indexes are used in this classification in order to obtain the reliability classes using, as a model, the previous work of Maurizio Mazzoleni for a piping classification (M. Mazzoleni, 2014).

The first index considers the minimum loading condition (in this case of *water head*), which generates a probability of levee failure equal to a threshold value set to 1%. The ΔH_{min} is thus compared to the levee crest height, Z, which is the maximum water head value in the measured discrete levee stretch (M. Mazzoleni 2014). When ΔH is greater than Z, the levee will incur failure for overtopping rather than piping.

After these considerations, this index is set as the *ratio* between the water load at 1% of probability and the crest height of the levee stretch. Using the second approach (sections limits), a mean value of crest level is used considering the two values of levee height calculated from the boundary topographic sections.

Using the ratio, the limits of the range can be plotted on a graph and be beneficial for every stretch analyzed.

The second index is the *standard deviation of the fragility curve* (in term of probability), (σ) which is used as indicator of the gradient of the fragility curve, so the pace at which the levee system reaches the failure condition: higher is the value of σ, higher is the sensitivity of the fragility curve to the hydraulic load ΔH.

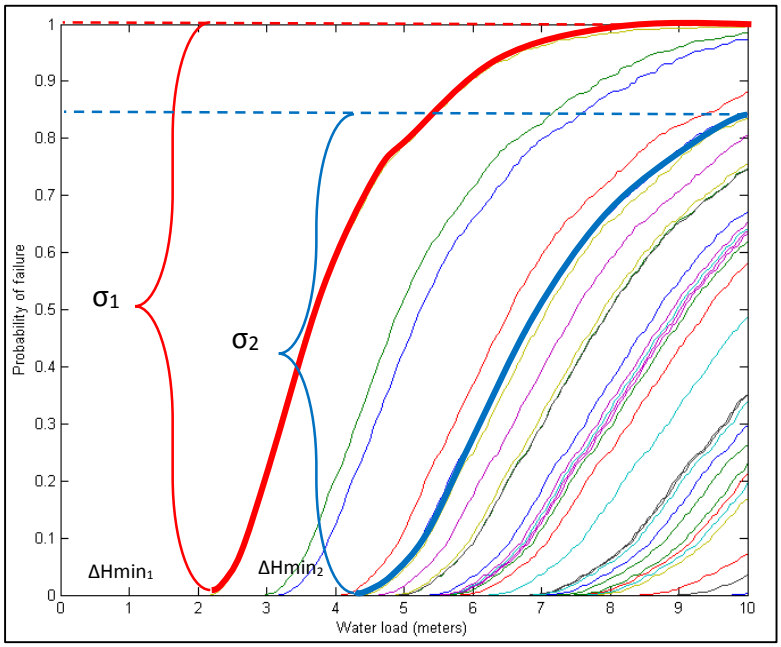

Figure 58: Indexes for piping classification

As the considerations for the overtopping, greater values of σ do not necessarily mean an unreliable levee system. A large value of ΔH_{min} merely implies that the headwater has to be higher than the ΔH_{min} value in order to achieve a first failure condition even with a high value for σ.

10.3 Classes for Discreet Levee Stretches

Indexes are generated for every levee stretch analyzed, with the two approaches, to associate each stretch to a reliability class. All the results are reported on a graph to observe their distribution and then drawn on maps.

The first classification for overtopping, which identifies the *standard probability*, is shown with a trend line associated with the outer slope angle. Graph 11 shows an example of the left levee system for the first approach. The other classifications, and their associated tables with correlating indexes, values, and classes, are reported in the attachment.

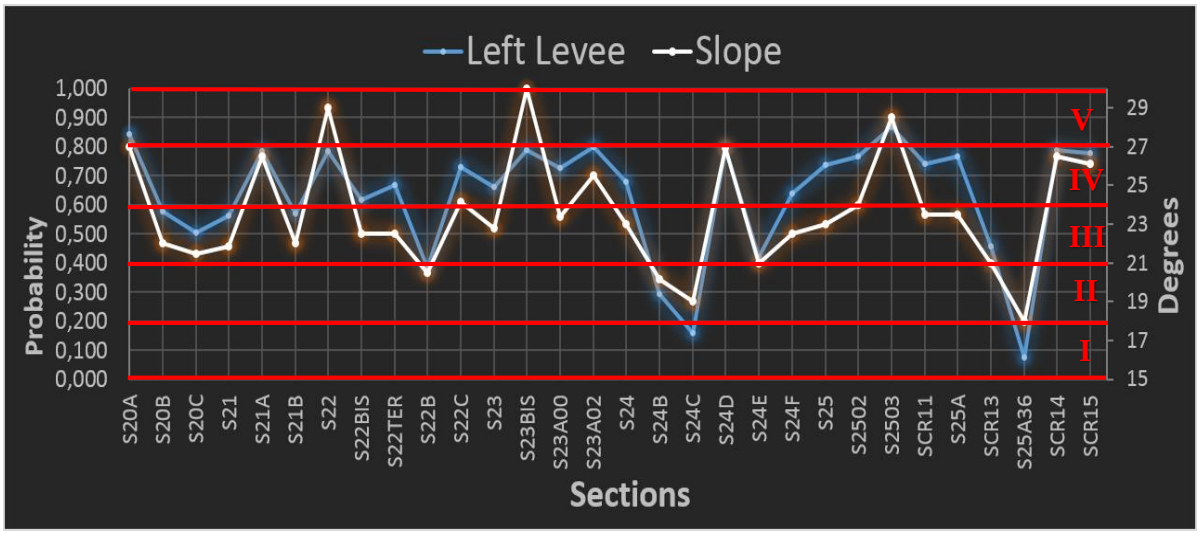

Graph 11: First classification for left levee using the first approach.

Higher classes correspond to higher values of slope angle where, approximately every 3°, they vary in a range of slope of 15°. Using the first approach for the left levee system, the graphs and their corresponding stretches show the majority of the classes fall in a range of probability between 60° and 80°—belonging to the fourth class—with three sections located in the fifth class (S20A, S23A02, S2503).

Even for the second approach, the fourth class is the most prevalent with a few sections located in the fifth class between S2502 and SCR11, before the confluence of the main stem of the Po and the navigation channel after Serafini Island. The fourth class also prevails for right side stretches of the levee system with small classes corresponding to the stretch downstream of the Serafini Dam in front of the artificial channel from SCR4 and SCR8.

The fifth class is associated with areas near confluences of secondary rivers as well as prior to the Serafini Dam (S23A03 and SCR1) corresponding to the confluence of the main stem of the Po and the navigation channel (from SCR4 to SCR8).

The following classifications for the other levees system side (and approaches) are introduced:

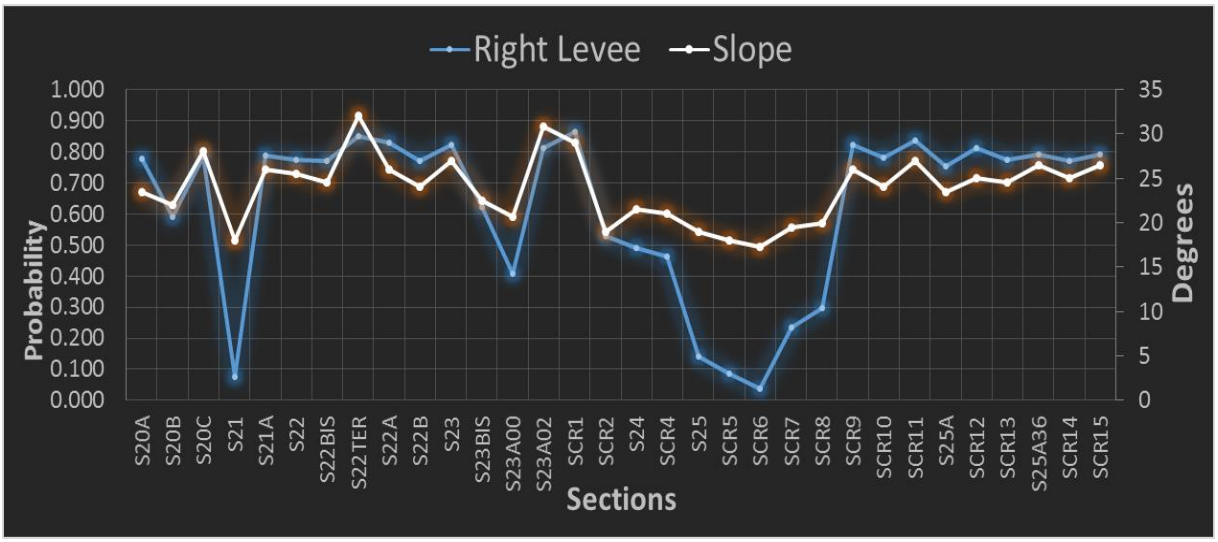

Graph 12: First classification for right levee using the first approach

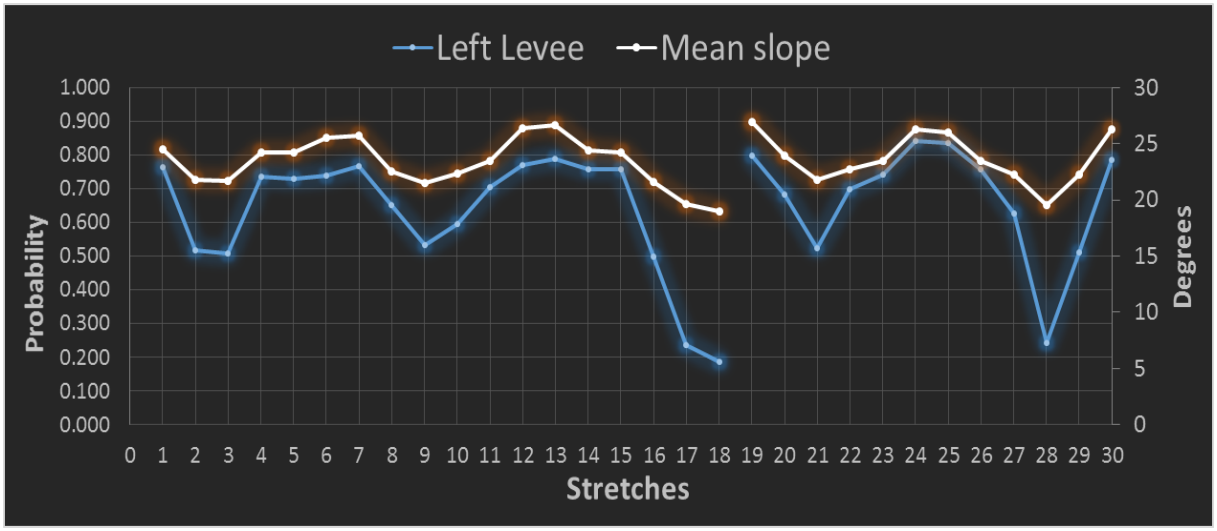

Graph 12: First classification for left levee using the second approach

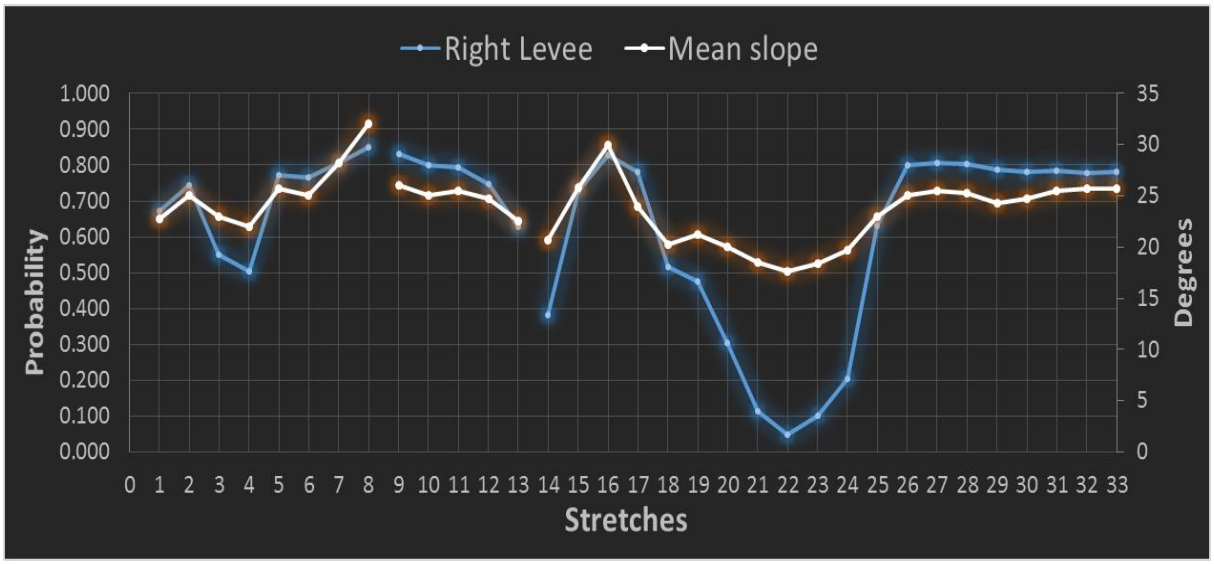

Graph 13: First classification for right levee using the second approach

The *Performance Classification* is presented as a 5-class chart where the unreliable classes stay in the corner and the reliable classes are located on the borders. The values that define the range of indexes are located on the axes (X-axis: the minimum load condition from 0.02 to 0.12 with steps of 0.02; Y-axis: surface width from 0.15 to over 0.25 with steps of 0.25). Each point on the graphic represents an analyzed section or stretch. Graph 14 shows the cloud of points that is spread between the third and the fifth class (0.02 - 0.08 of ΔH_{min} and 0.15-0.225 of surface width).

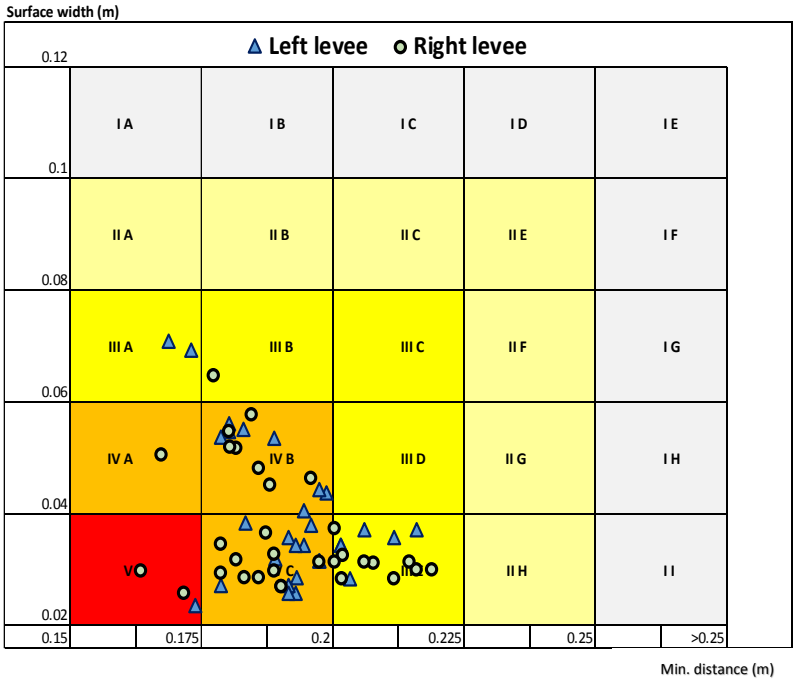

Graph 14: Performance classification for first approach

The graphs of both approaches show more point density in the lower part (0.02-004 of surface width) spread along the axis of the ΔH_{min}.

Comparing the classes obtained by the first classification with the ones of the performance classifications, the lower classes are associated to the III_E, the fourth and third classes corresponds to the IV_B, IV_C and sometimes to III_A, and the fifth class corresponds mostly to V, IV_C and rarely IV_A.

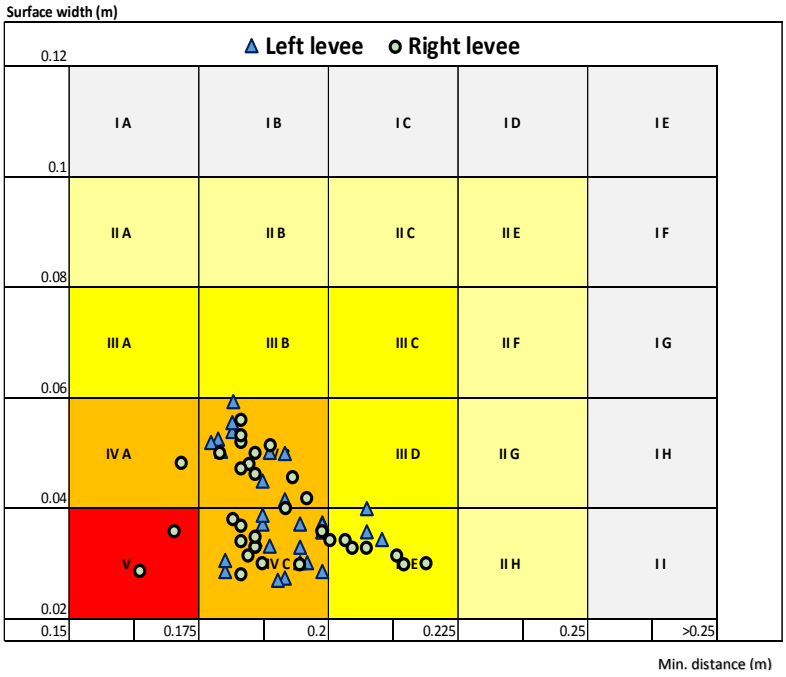

Graph 14: Performance classification for second approach

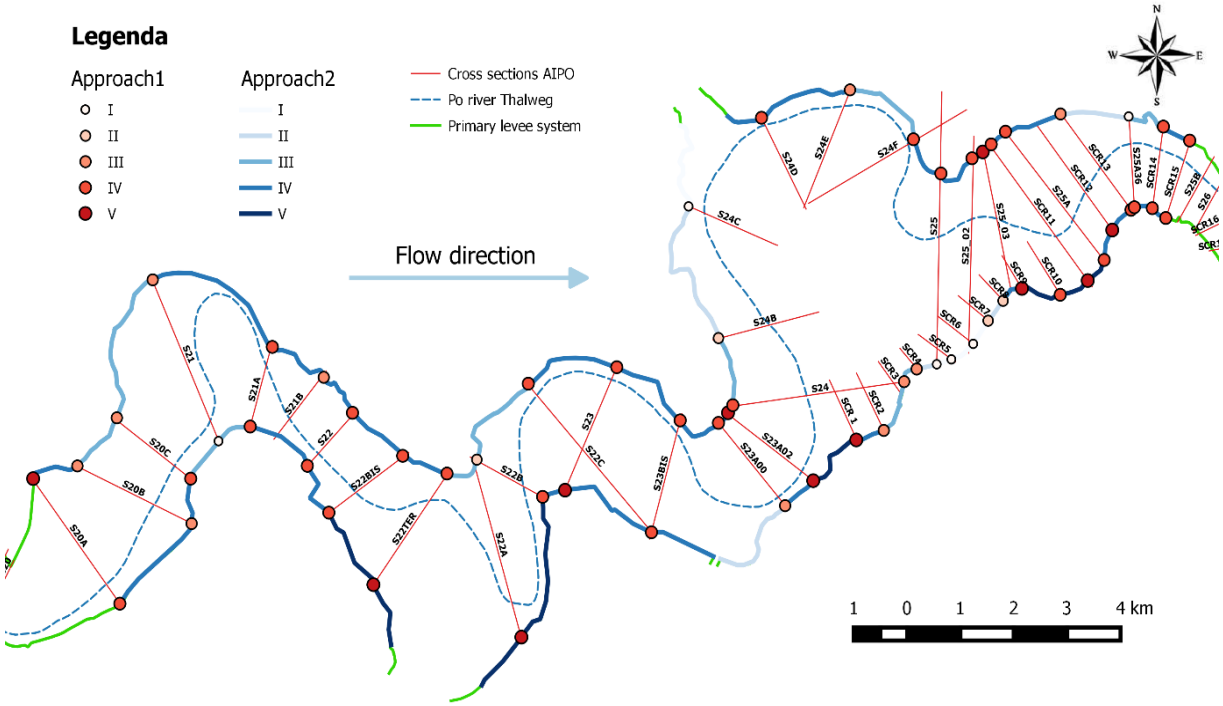

Figure 59: Map of the reliability classes considering overtopping along the levee system from Piacenza to Cremona

The *Piping Classification* is presented as a 5-class graph in the same manner the *Performance Classification* for overtopping is given. The limits of the classes are reported where, on the X-axis, the ratio (Z) between the minimum load condition and the levee crest is discretized every $Z/4$. The same assumption is done for the standard deviation on the Y-axis.

A reliability class for piping is set for values of Z higher than 1 from the moment the water load exceeds the levee crest. This is done based on a failure happening primarily for overtopping rather than piping. Even if one failure occurs, however, it does not imply that the other is neglected.

The result of the classification—for both sides of the levee system as well as both approaches—is that almost all points rest within a reliability class. Since the levee system has been rebuilt in more phases, where the levees base has been enlarged much more than the levee height, the result has been a generous resizing against a triggered threshold for piping failure mechanisms. The few stretches located in a second class, are the ones that present a small increase of the water head due to a higher difference between the outer toe level and the crest level related to a smaller width of the base used in the gradient method.

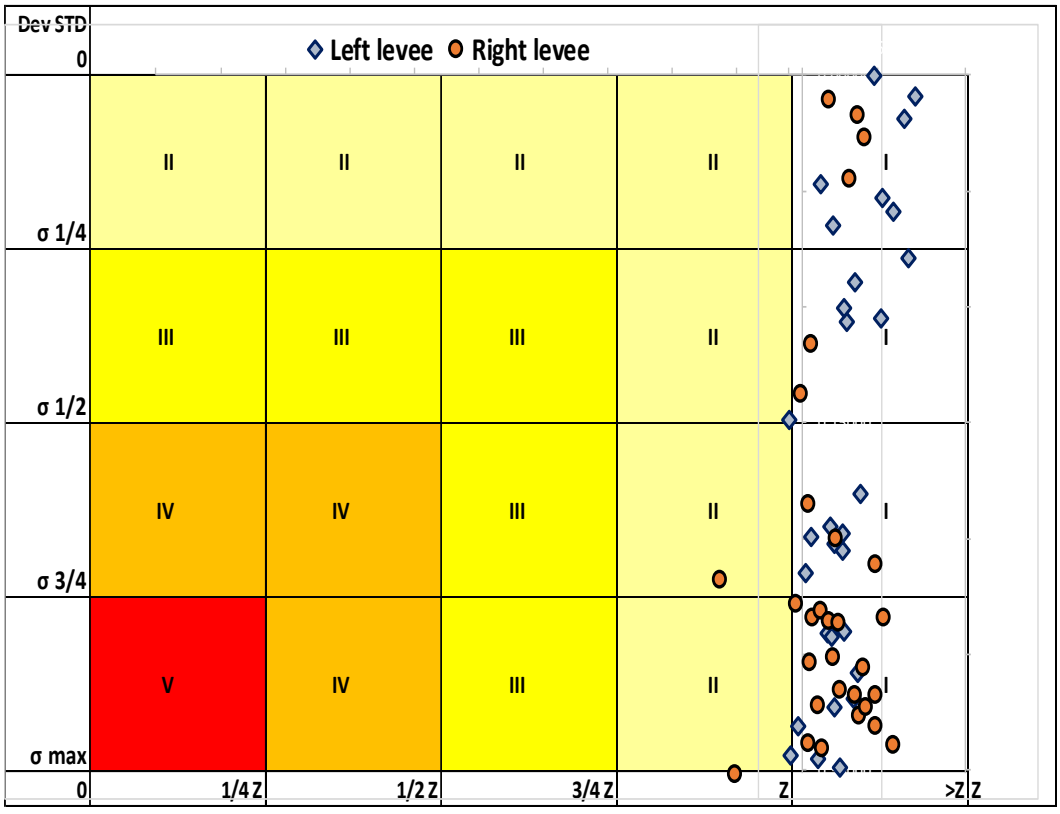

Graph 15: Classification for piping using the first approach

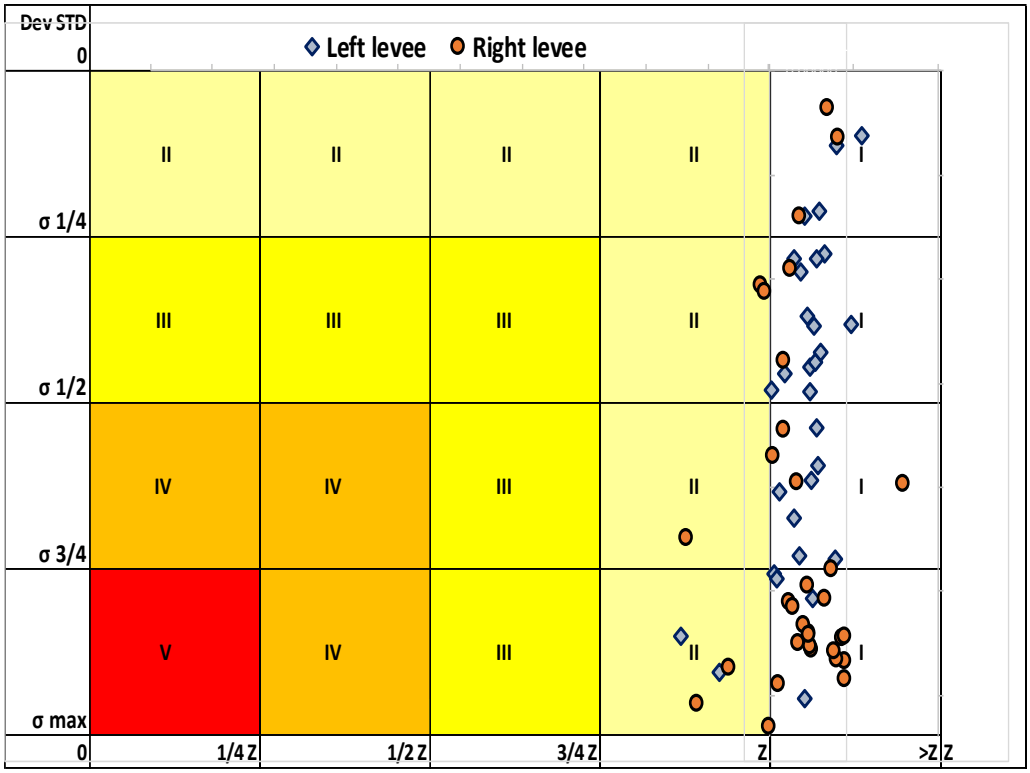

Graph 16: Classification for piping using the second approach

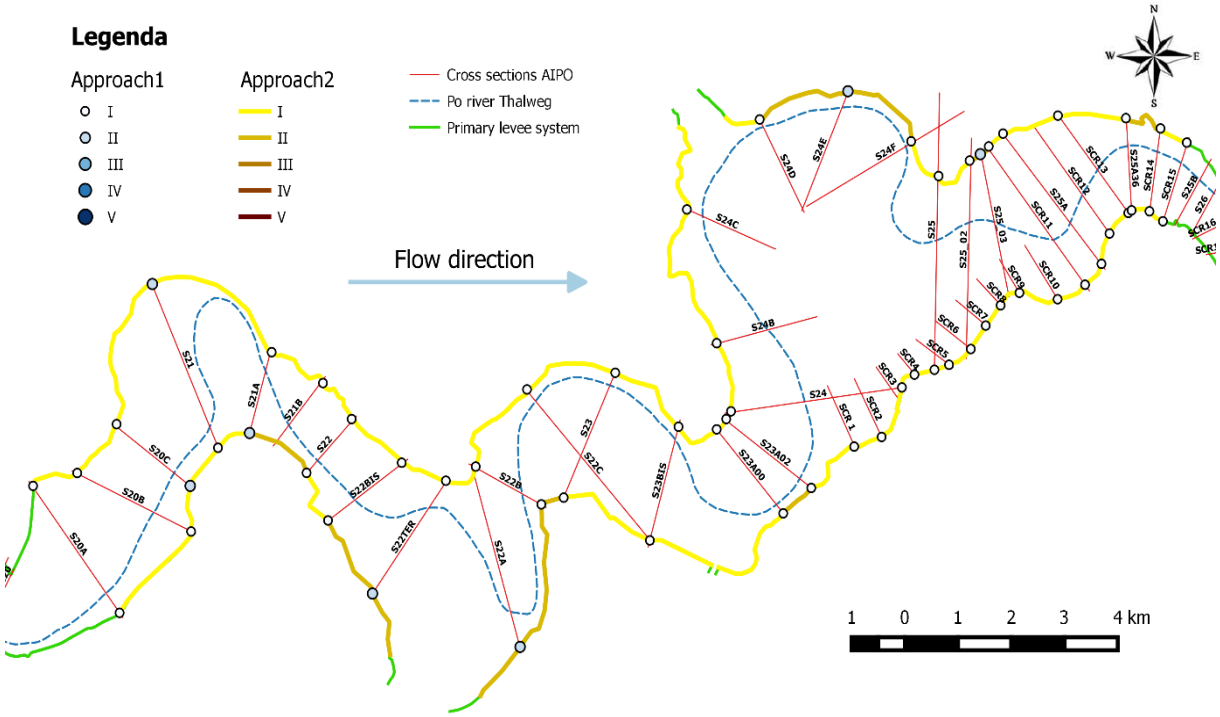

Figure 60: Map of the reliability classes considering piping along the levee system from Piacenza to Cremona

All results of the reliability classifications for both failure mechanisms are reported in the Attachments section.

11. Hydraulic modelling and residual hazard estimation

In this chapter, a practice case is introduced, where an estimation of the hazard is given considering both mechanisms of failure and using the fragility curves previously obtained by the analysis. To do this, it has been decided to simulate, a greater flood profile than the one defined in the Transitional Plan PAI (TR = 200 years); then a flood event with a return period of 500 years is simulated using a 1-D model elaborated with the software HEC-RAS.
To have a complete work, a probabilistic distribution of possible flooding volumes is proposed taking in account rupture and not rupture, due to overtopping, where three scenarios are examined considering a sudden breach formation with three different breach width.

11.1 HEC-RAS 1-D modelling

For the definition of the flood event with a return period of 500 years, the 1-D model has been implemented for the stretch of Po River used for the analysis. The model belongs to the category of quasi-2D model (Castellarin et al., 2011), where the river topography is schematized through several cross sections surveyed in a orthogonal position respect the flow direction and the dike-protected lateral floodplain are reproduced as storage areas. The geometry of the river bed has been reproduced using the measured vertical profiles in correspondence of the Brioschi sections (28 sections).

11.1.1 Calibration

The calibration of the 1-D model for the stretch of Po River between Piacenza and Cremona is done with reference to the flood event that occurred in October 2000. From the moment that a large number of information are available for this event, the calibration has been set varying the roughness coefficient of Manning (n [$sm^{-1/3}$], defined for each cross section) with the purpose to reproduce the flood traces registered at the corresponding sections.
The upstream boundary condition is represent by the flood hydrograph registered at the hydraulic gauge of Piacenza during the event of 2000, while the downstream boundary

condition is in form of a synthetic runoff scale obtained by hydraulic modelling, considering historical events (see Domeneghetti 2012).

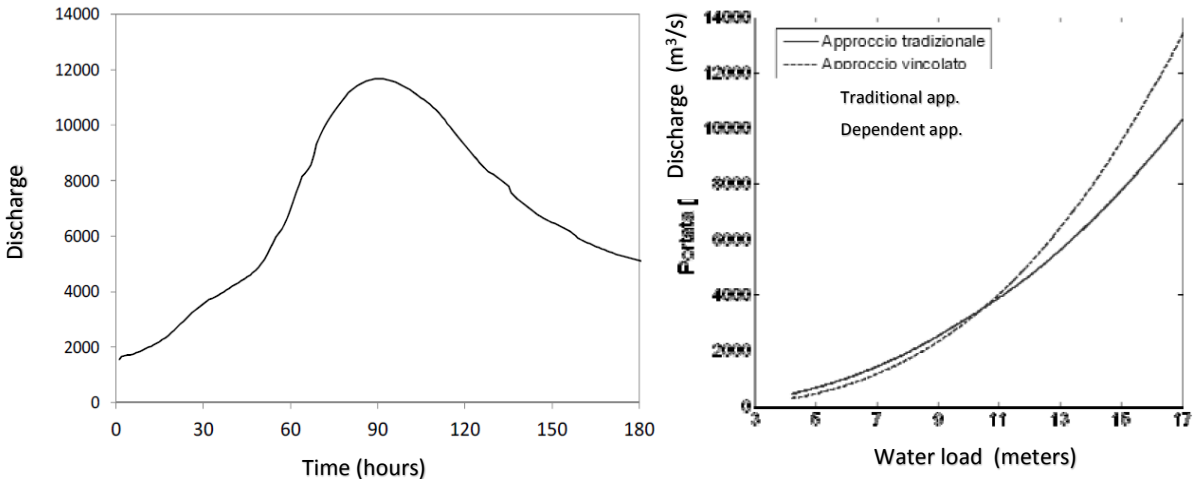

Figure 61: Boundary conditions for 1-D model (upstream on the left, downstream on the right) (A. Domeneghetti 2012)

The definition of synthetic hydrograph for return period of 500 years of the measuring station of Piacenza (DIIAR 2001) is obtained using statistics elaborations, analyzing historical flood events (Castellarin et al., 2011), which data are available from 1951.

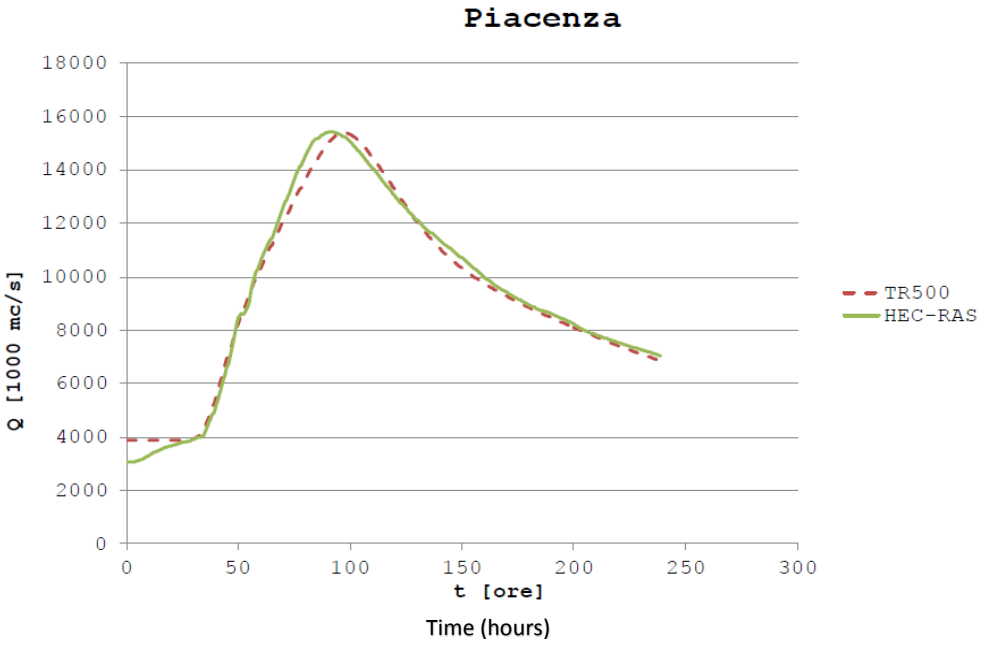

Figure 62: modeled hydrograph for Tr 500 at Piacenza (F. Carisi 2011)

The model permits to consider also the presence of confluence with lateral secondary rivers; in this case only the contribution of the Adda River has been simulated, considering his

contribution (as a maximum discharge observed equals almost 1400 m^3/s during the flood event of 2000) in form of local punctual emission.

The results of the calibration show horizontal profiles of the simulated flood reproduced by the model and assuming the boundary conditions previously reported; they are compared with the traces of the flood observed corresponding to the sections of reference. For each section a hourly hydrograph is given.

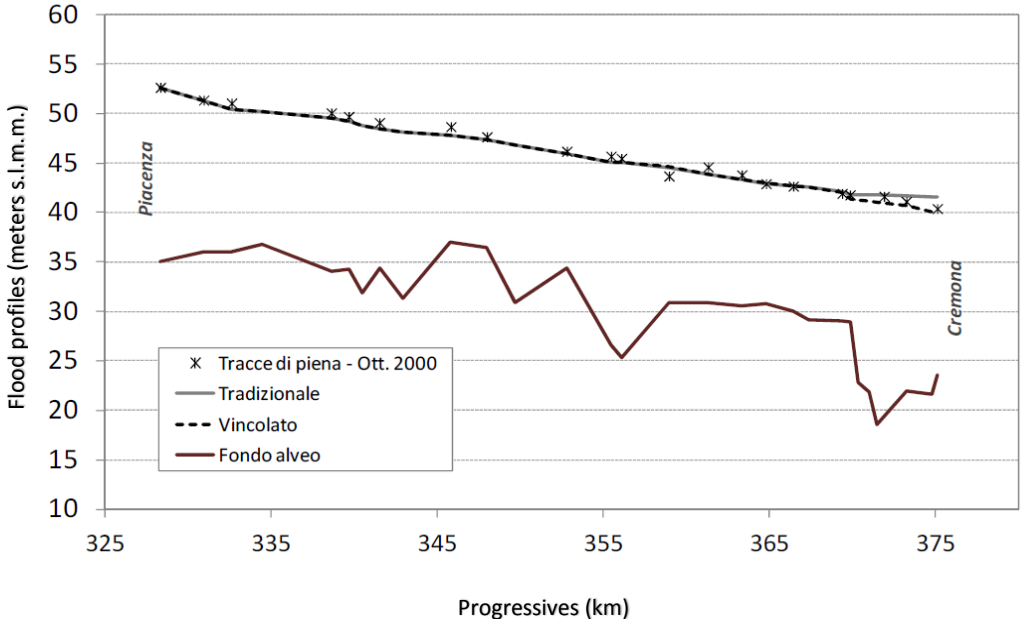

Figure 63: quasi-2D model calibration Piacenza-Cremona: traces of the flood that occurred during October 2000 (black cross), and the flood profiles simulated by the quasi-2D model assuming the traditional and the dependent approach (A. Domeneghetti 2012).

11.1.2 Linear interpolation

From the moment that not all the sections considered in the analysis are used for the hydraulic modelling (as S20C and all the ones SCR corresponding to the navigation channel in front of Serrafini Island), to obtain a complete flood profile of the maximum water level a sort of interpolation between the neglected sections is adopted (Figure 18).

The small distance between each profile permit to assume a linear interpolation, taking in account the real position of all the point to calculate, then to obtain a water head profile as realistic as possible.

Following the graphics of the linear interpolations and the relative equations are introduced.

The value of the water head corresponding to S20C results to be 51.34 meters of elevation, located more or less in the middle of the distance between S20B and S21.

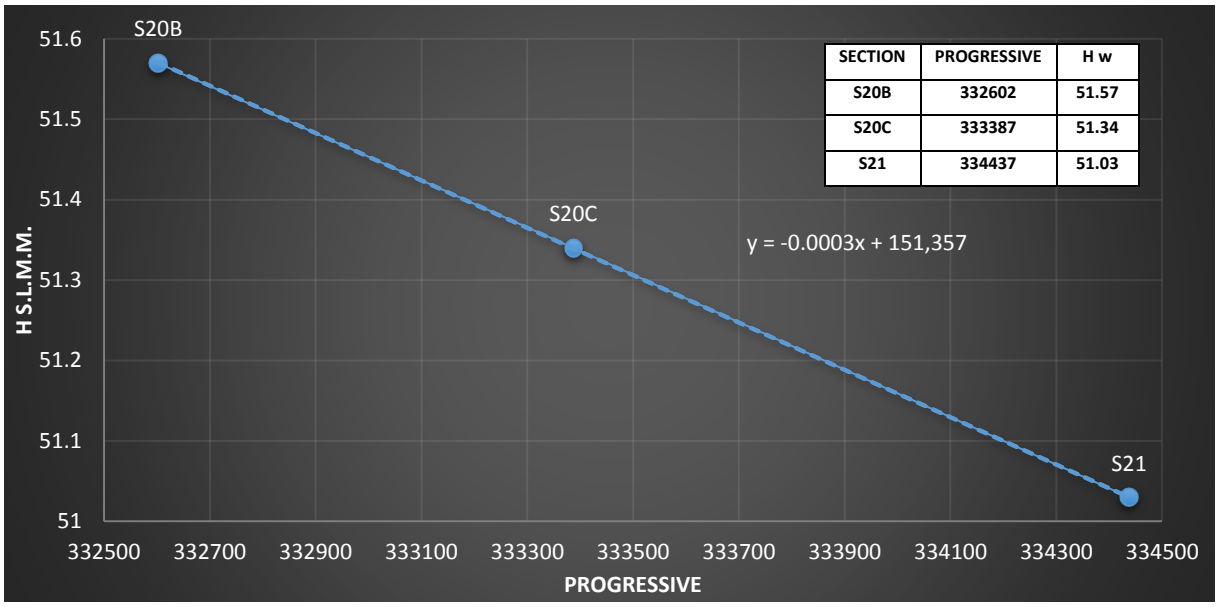

SECTION	PROGRESSIVE	H w
S20B	332602	51.57
S20C	333387	51.34
S21	334437	51.03

Graph 17: linear interpolation between S20B, S20C and S21.

The interpolation of the sections downstream the dam of Serrafini Island has been calculated considering two separated stretches of the channel divided by S25, so two equations are used for the interpolations. From S24 (exactly before the dam) and S25 is possible to notice a decrease of water level higher than 3 meters (from 45.19 to 42.11 meters for a distance of 2.437 km), while after S25 to SCR11 the water level decreases very slowly, staying around a level of 42 meters.

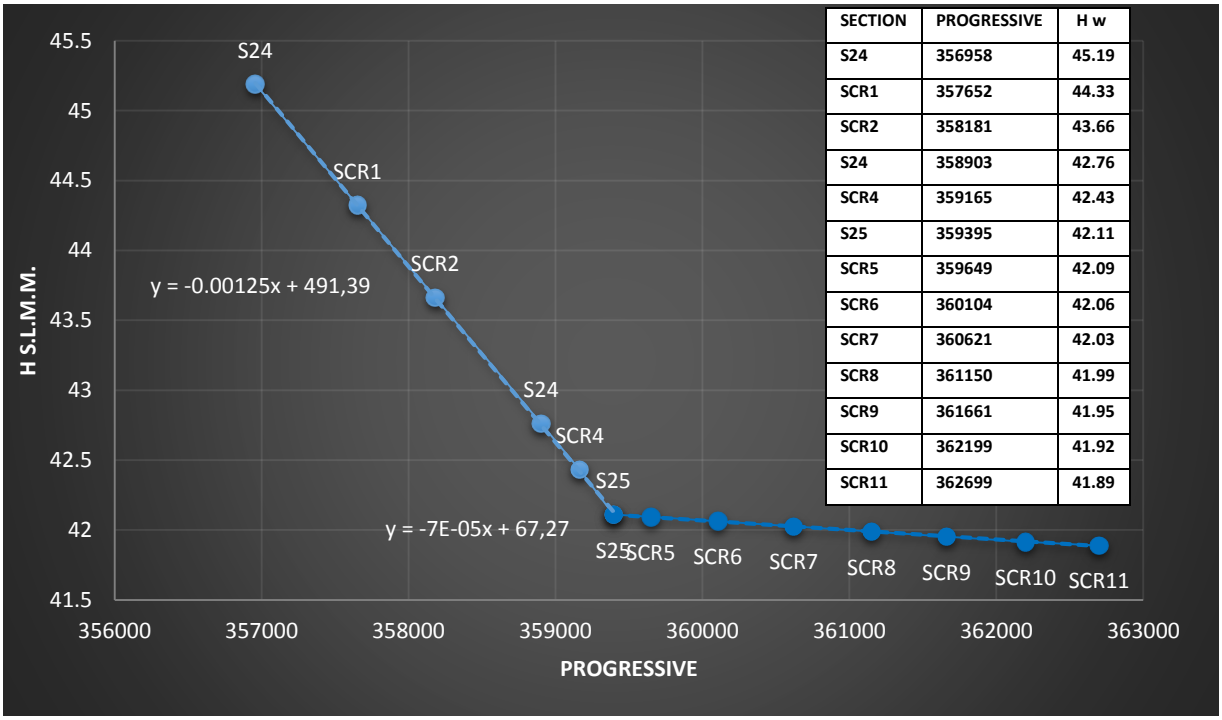

SECTION	PROGRESSIVE	H w
S24	356958	45.19
SCR1	357652	44.33
SCR2	358181	43.66
S24	358903	42.76
SCR4	359165	42.43
S25	359395	42.11
SCR5	359649	42.09
SCR6	360104	42.06
SCR7	360621	42.03
SCR8	361150	41.99
SCR9	361661	41.95
SCR10	362199	41.92
SCR11	362699	41.89

Graph 18: linear interpolation of the stretches S24 – S25 and S25 – SCR11

Once that this step is done, is possible to define a complete profile, for both river side respect the left and right levee system, of the maximum water level obtained by the hydraulic modelling. Following the entire horizontal profile is presented:

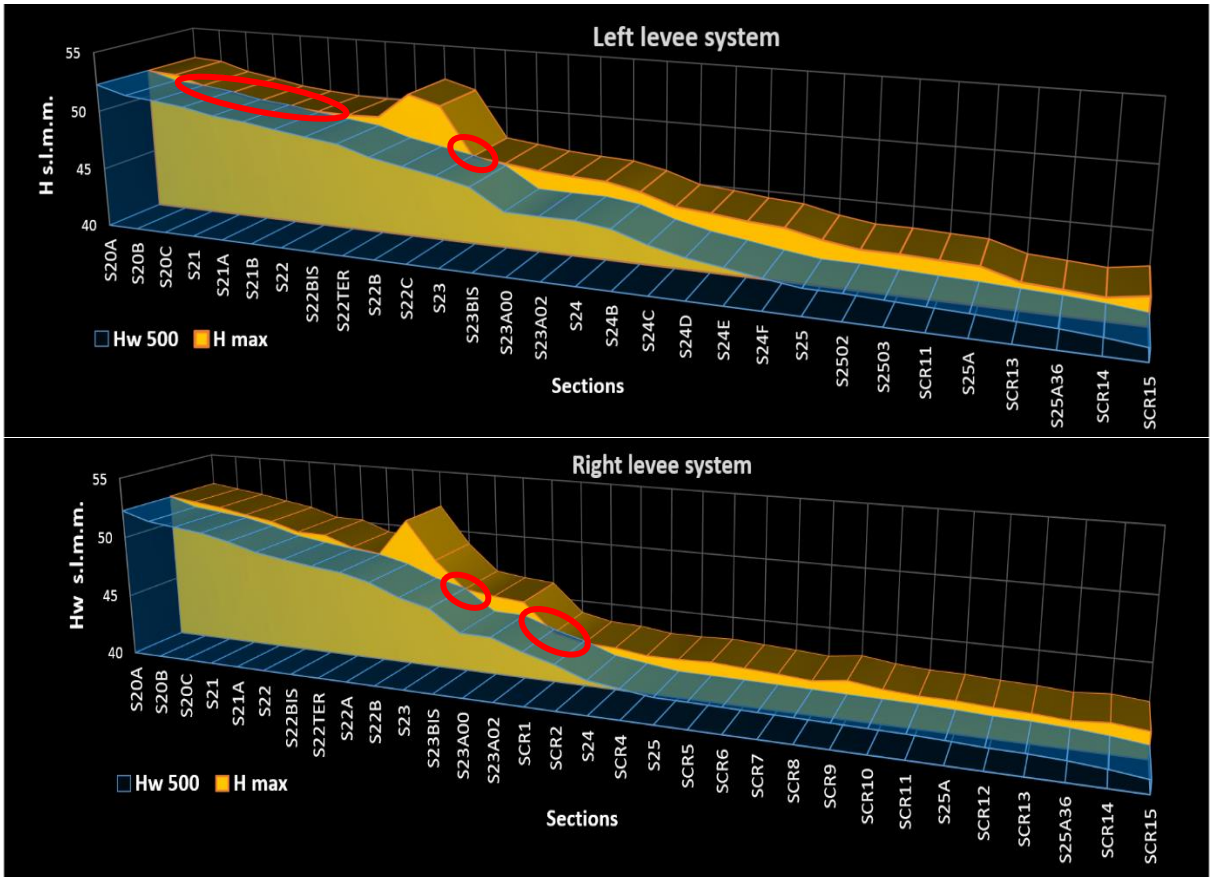

Graphics 19-20: profile of the maximum water level, for a flood event with 500 years of return period, obtained by the hydraulic modelling respect both side of the levee system

In general the profile shows that higher water level is present immediately downstream of Piacenza, very close to the levee top, while after the dam of Serafini Island the difference between the water and the levee crest is greater and quite variable.

Looking to the singular water head value for each section, it has been possible to identify where the simulated flood reach the levee crest and so where an overtopping phenomena takes place (red circle in the previous graphics). Singular point of overtopping are located in correspondence of some sections and also entire stretches of the levee system are involved in overtopping, where for progressive sections the water head results higher than the levee crest.

This aspect is discussed in the next chapter to give an estimation of the hazard.

11.2 Hazard estimation for different approaches

Once defined, the maximum water head profile is used to have an estimation of the residual flood hazard. The value is the product given by the probability of the event to occur for the probability of failure found by the fragility curves, for both mechanisms of failure and approaches, with the corresponding maximum water load (and maximum overflow time) of each stretch analyzed:

Pr. tot = Pr. flood event (Tr) x ***Pr. Levee failure (Hw) = Residual Hazard***

For the first approach, the hazard value is the one obtained by the fragility curves corresponding to each section considered; in the second approach, the hazard is calculated as a mean value of the probability of failure found, on the same fragility curve, by the water load located on the limits of the levee stretch. Where the maximum water level, over the crest, has a value less than 0.1 meters, the probability of failure is given by a subjective graphical extrapolation.

For overtopping, where the water load does not reach the levee crest, the hazard is automatically set as zero; where an overtopping occurs, the maximum water height over the levee crest and the maximum overflow time are considered to give a probability value as in the worst hydraulic load condition. On the left levee system two punctual overtopping take place on the section S20A (0.03 meters *he* and 10 hours *te*), S23 (0.10 meters *he* and 10 hours *te*), and a stretch of overtopping along the levee system includes the sections S21 (0.13 *he*, 5 *te*), S21A (0.12 *he*, 9 *te*) and S21B (0.14 *he*, 6 *te*).

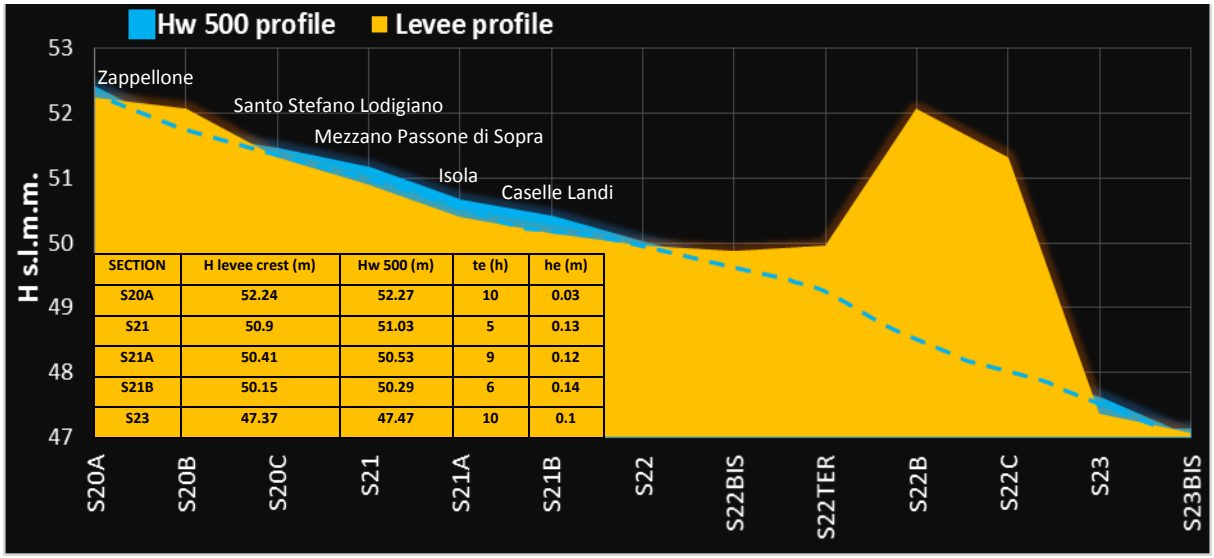

SECTION	H levee crest (m)	Hw 500 (m)	te (h)	he (m)
S20A	52.24	52.27	10	0.03
S21	50.9	51.03	5	0.13
S21A	50.41	50.53	9	0.12
S21B	50.15	50.29	6	0.14
S23	47.37	47.47	10	0.1

Graph 21: scheme of the overtopping phenomena along the left levee system

On the right levee system a punctual overtopping occurs in correspondence of the section S23BIS (0.06 meter *he* and 13 hours *te*) and a linear one includes the section SCR1 (0.30 *he*, 4 *te*) and SCR2 (0.17 *he*, 4 *te*). The overflow time for these last ones is set as the time resulting in the sections that lay before SCR1 and after SCR2.

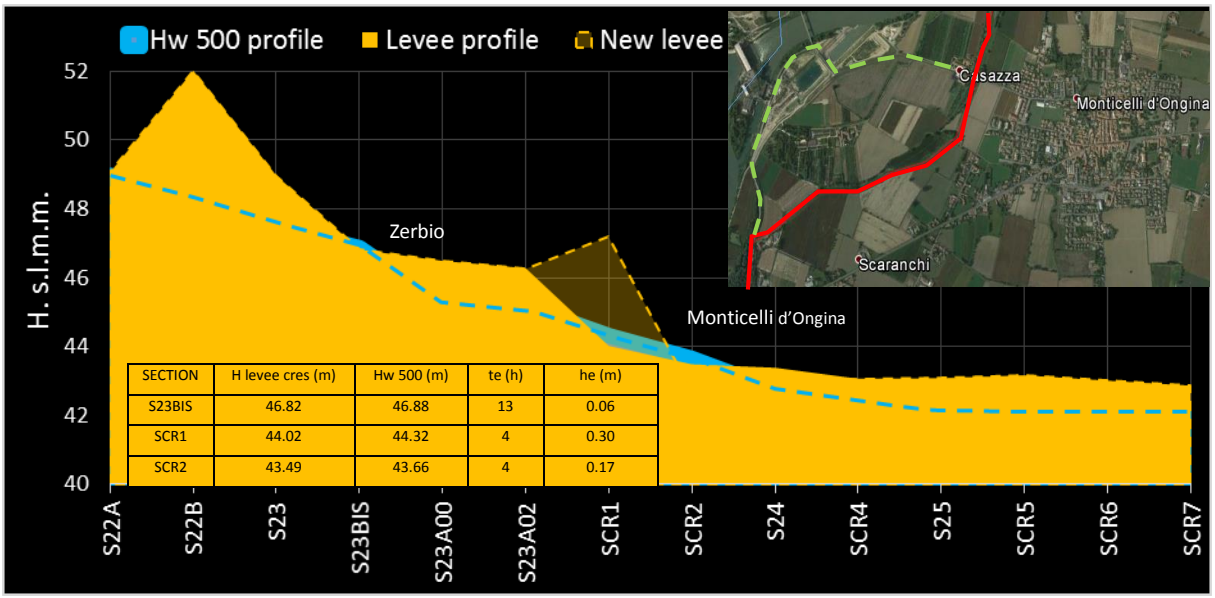

SECTION	H levee cres (m)	Hw 500 (m)	te (h)	he (m)
S23BIS	46.82	46.88	13	0.06
SCR1	44.02	44.32	4	0.30
SCR2	43.49	43.66	4	0.17

Graph 22: scheme of the overtopping phenomena along the left levee system

The presence of a levee located on the riverbank in front of the dam of Isola Serrafini (the dashed line in the previous graphic), with a crest level higher than the main levee system, protects the floodplain area corresponding to the SCR1, leaving unprotected only the area close to the section SCR2. In general during a flood event, the navigation channel is closed while the doors of the dam are completely open, allowing the flooding wave to flow only in the main river bed.

Then to have a water load that gives overtopping downstream the dam is improbable, unless a regurgitation phenomena occurs along the navigation channel and reach the levee system in proximity of the dam.

For piping the water load (from the levee outer toe level) is used to find a hazard value, and the assumptions for the different approaches are the same explained previously for the overtopping. Following the profiles of the maximum water head respect the levee outer toe level are presented:

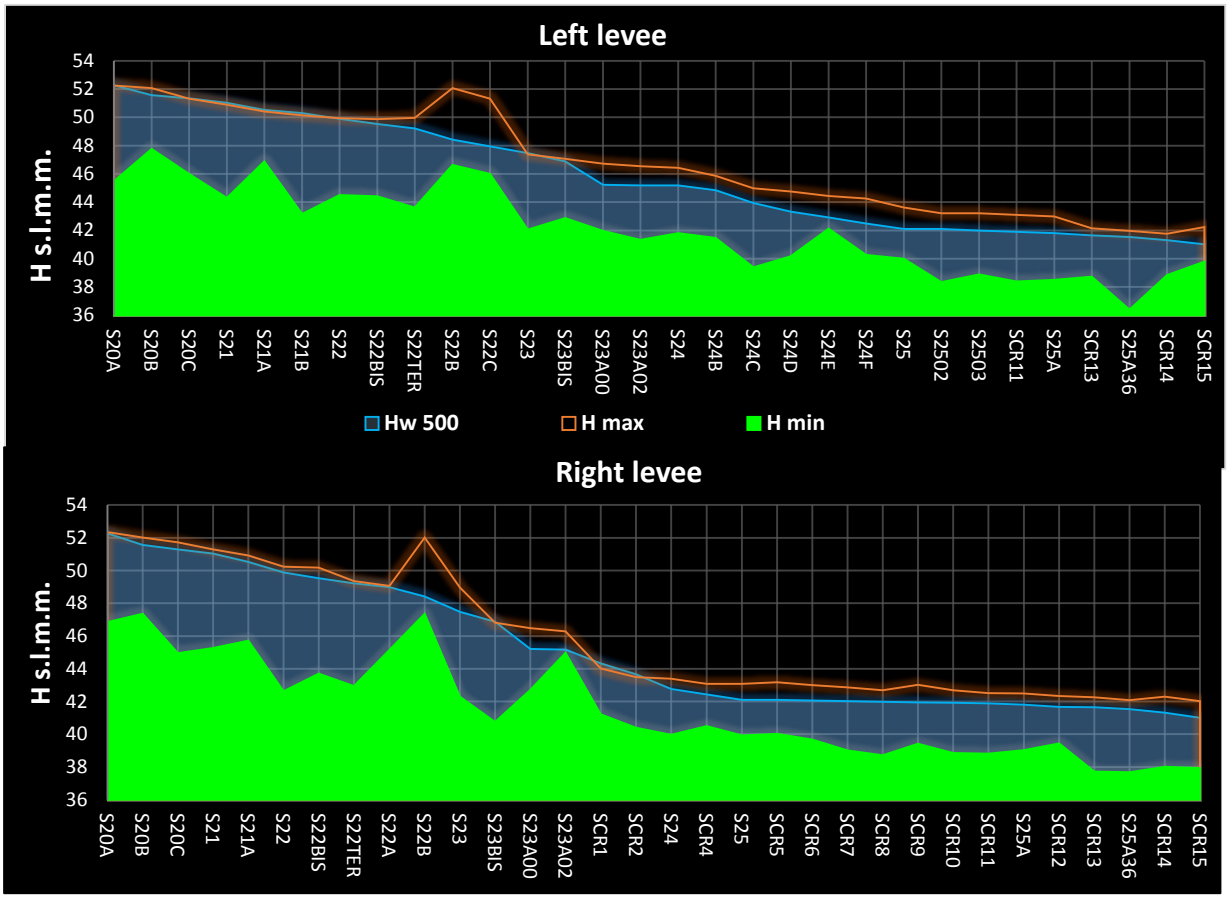

Graphs 23-24: trend of the water load, respect the outer toe level of the levee system, used to define the residual hazard considering piping

The water load trend, respect the land side level, shows a variability along all the rod studied, where higher difference are located downstream Piacenza rather than upstream Cremona, and lower load difference corresponds to the section S22B, S22C, S24E (left side),S22B and S23A02 (right side).

After all this considerations, the residual hazard is assigned to all the stretched of the levee system analyzed from Piacenza to Cremona. Both approaches are used, and the results (reported in tables in the attachments) permit the definition of a “residual hazard map” for the two mechanisms of failure considered in this study.

The following table reports the hazard only for the stretches that present a value higher than zero; for those, the maps representing the residual hazard along the levee system are introduced.

Overtopping residual hazard:

SECTION LF	Failure App 1 (%)	Hazard %	Stretches	Failure (%) App 2	Hazard %
S20A	5.20	1.04	*1*	4.80	0.96
S21	77.98	15.60	*3*	36.17	7.23
S21A	68.76	13.75	*4*	75.63	15.13
S21B	73.08	14.62	*5*	70.80	14.16
S23	65.73	13.15	*6*	36.48	7.30
			11	31.52	6.30
			12	31.45	6.29
SECTION RG	**Failure (%) App 1**	**Hazard %**	**Stretches**	**Failure (%) App 2**	**Hazard %**
S23BIS	35.30	7.06	*12*	14.130	2.826
SCR2	84.47	16.89	*13*	16.120	3.224
			17	47.900	9.580
			18	41.920	8.384

Table 6: Failure probability and the relative hazard value for levee stretches, which present overtopping.

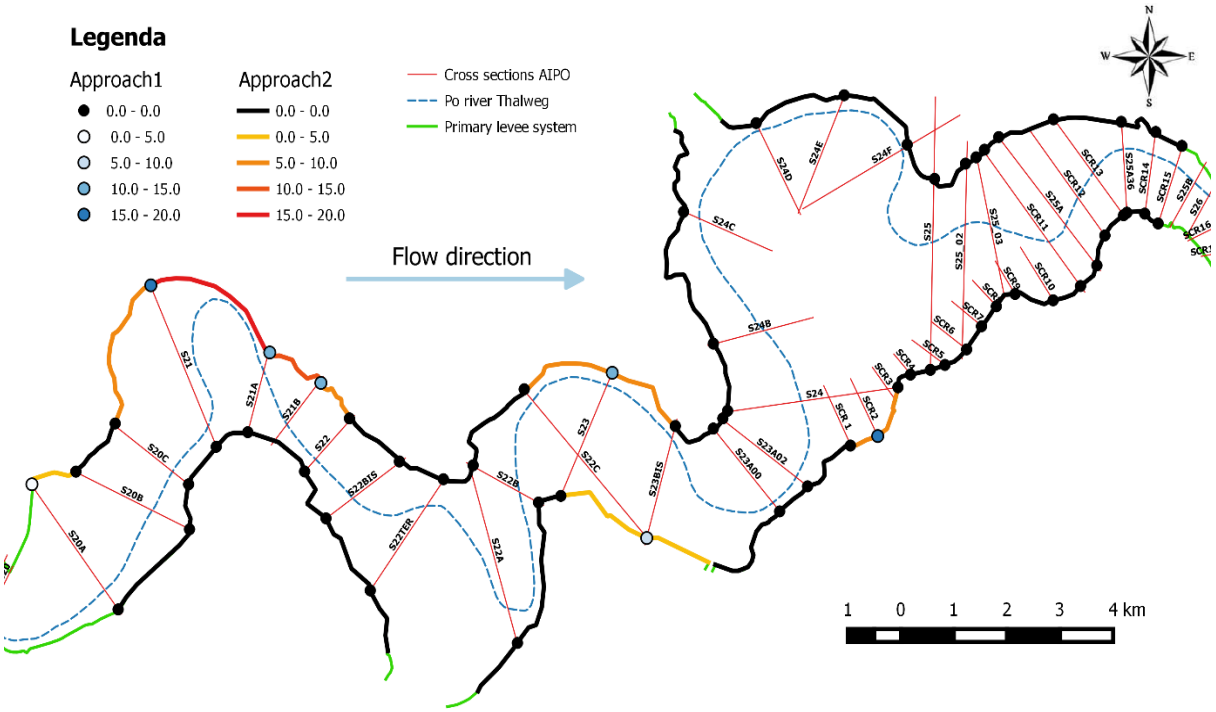

Figure 64: map of the residual hazard (expressed in %) due to overtopping

Piping residual hazard:

Section LF	Failure (%) App 1	Hazard %	Stretches	Failure (%) App 2	Hazard %
S21	1.68	0.34	*1*	1.39	0.28
			4	7.38	1.48
			12	0.47	0.09
			20	1.31	0.26
			29	2.71	0.54
Section RG	**Failure (%) App 1**	**Hazard %**	**Stretches**	**Failure (%) App 2**	**Hazard %**
S22TER	7.75	1.55	*2*	1.00	0.20
S22A	5.38	1.08	*4*	0.24	0.05
			5	2.78	0.56
			7	0.54	0.11
			8	4.42	0.88
			9	3.46	0.69
			10	0.36	0.07
			15	0.50	0.10
			16	0.85	0.17

Table 7: Failure probability and the relative hazard value for levee stretches considering piping.

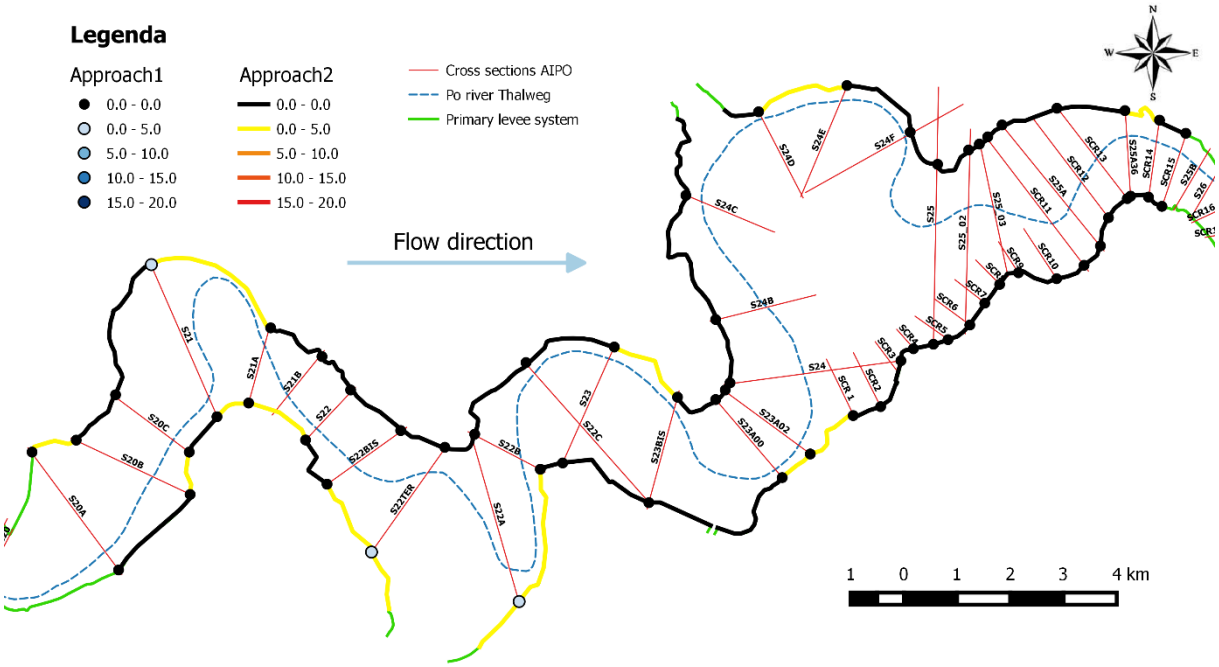

Figure 65: maps of the residual hazard (expressed in %) due to piping

11.3 Flooding water volumes

To complete the hazard analysis, an estimation of the flooding water volumes in time, and their probability distribution, is introduced. It takes in account only the overtopping failure mechanism. As an example, the sections on the left levee system that are involved in a overtopping phenomenon are considered. The water volume that goes over the levee (or through) is calculated in two ways:

- no overtopping failure (so no breaches formation), then the quantity of water that reach the levee crest and passes over it during all the time that the overtopping occurs, where its probability distribution is assumed as a probability of not failure ($1-Pr_{failure}$);

- overtopping failure (breach formation), where the volume of water that flows through the levee, and floods the closest areas, is calculated as the total discharge resulting by the difference between the maximum discharge that the levee can contain, then at the crest level, and the one corresponding to the higher levee toe level, plus the water volume that overflow the levee before the rupture. The probability of failure is defined by the first step of the maximum water height flowing over the levee crest, and then progressively distributed in time.

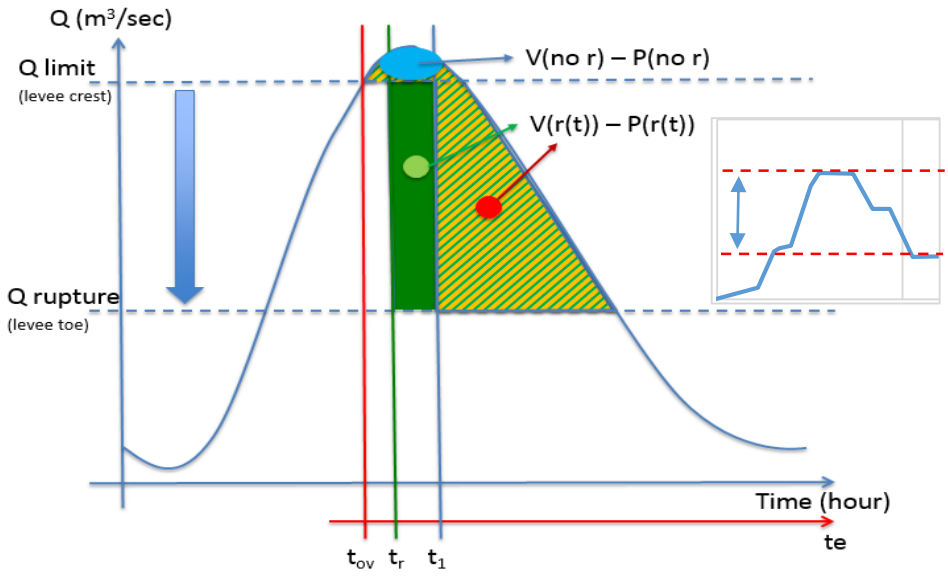

Figure 66: Scheme representing how the flooding water volumes are considered for their estimation: the overtopping volume for no failure (blue), water volume at the moment of the breach formation (green), flooding water volume in a step after the rupture (orange strikes).

The definition of the failure probability distribution in time is done using , for each section considered, the fragility curves obtained with both approaches.

For the first approach, the probability distribution, of a section, is defined by the relative fragility curve. In the second approach, from the moment that the overtopping water height located on a section is used, the probability distribution is set as a avarage of the distributions identified on the fragility curves corresponding to the stretches where the section lays as their limits.

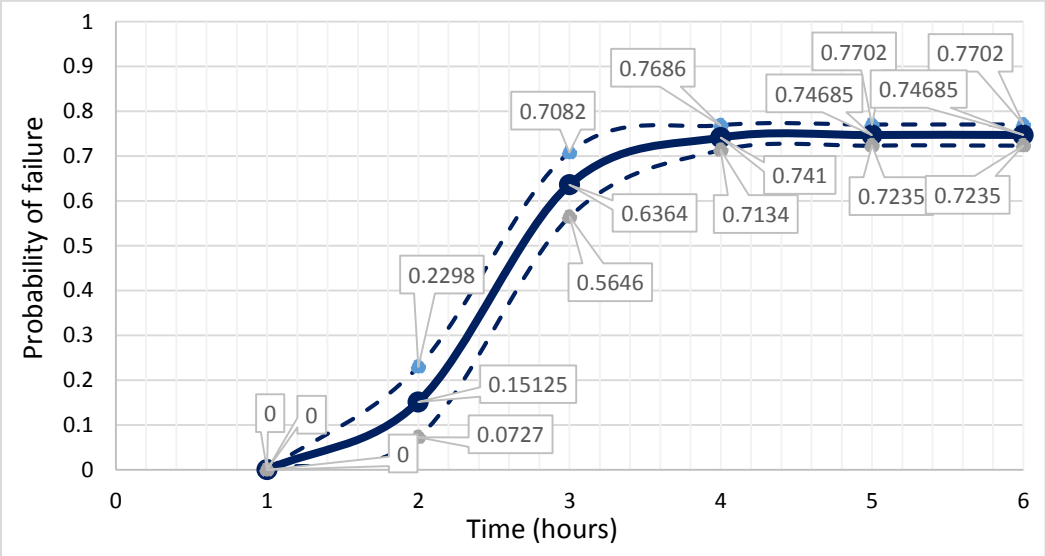

Graph 25: probability of failure distribution for S21 for the second approach, where it is defined as a mean of the distribution found on the fragility curves corresponding to the stretches 3 and 4.

When a rupture takes place, it is assumed that suddenly the levee crest collapses completely until the toe (fig), then a progressive breach formation in time is not considered. To simulate the presence of a breach along the levee system the weir formula is used, where the shape of the breach is taken as a rectangular window. To obtain the total weir discharge the hydrograph is discretized each time step.

$$Qi = 0.385 * (h_i - h_{base}) * b (2g * (h_i - h_{base}))^{1/2}$$

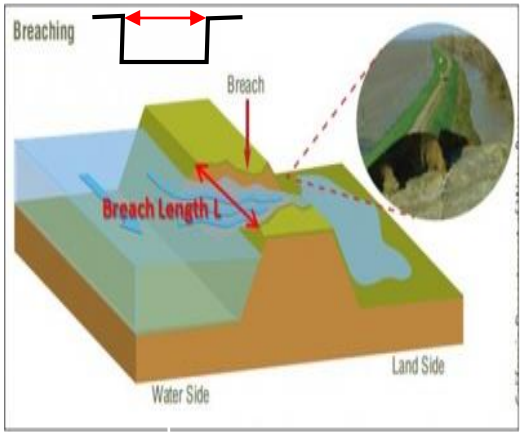

Figure 67: shape of the breach used to estimate the flooding water volumes due to overtopping failure (Dicea Firenze)

11.3.1 Breaches dimension

To understand what value of width has to be assigned to the breach, is possible to resort to the historical rupture. The information available from AdbPo (AdB-Po-IRPI-ST1_1, 2004) permit to select 225 rupture that took place, along the main levee system of Po River, in the period between the event of 1801 e the one of 1951. Of all these, only 84 references about the final dimension of the breaches are reported (A. Domeneghetti 2012).

Their values are summarizing in the following graphic:

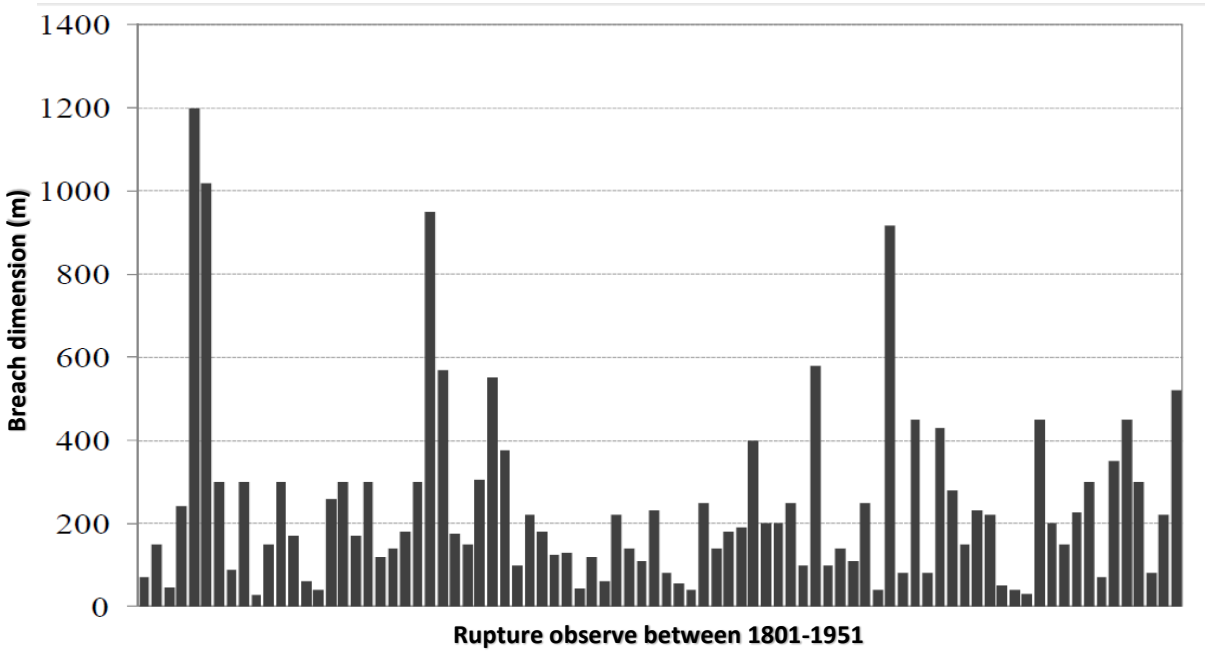

Graph 26: main historical rupture observed along the Po River in the period between 1801-1951 (elaboration from the archive of Coratza, 2005) (A. Domeneghetti 2012)

In the next table are reported the statistical information obtained by the observations:

Total breaches observed	225
Available breaches dimension (b)	84
Minimum (m)	27
Maximum (m)	1200
Mean (m)	240
Median (m)	180

Table 8: statistical information about the historical rupture (elaboration from the archive of Coratza, 2005)

For the calculation of the flooding water volume, due to a levee failure, three scenarios are implemented where the breach dimension is set as the mean, median and minimum values found by the statistical information.

11.3.2 Different scenarios of levee breaches

For the calculation of the flooding water volumes, the section S21, S21A, S21B and S23 are considered with the relative hydrograph. For each of these, discharges corresponding to maximum water load capacity and the one after the levee collapse are associated to the levee crest level (calculated on the topographic profile) and to the higher toe level between the inner and the outer one, respectively. In the next image, an example of the section S23 is reported:

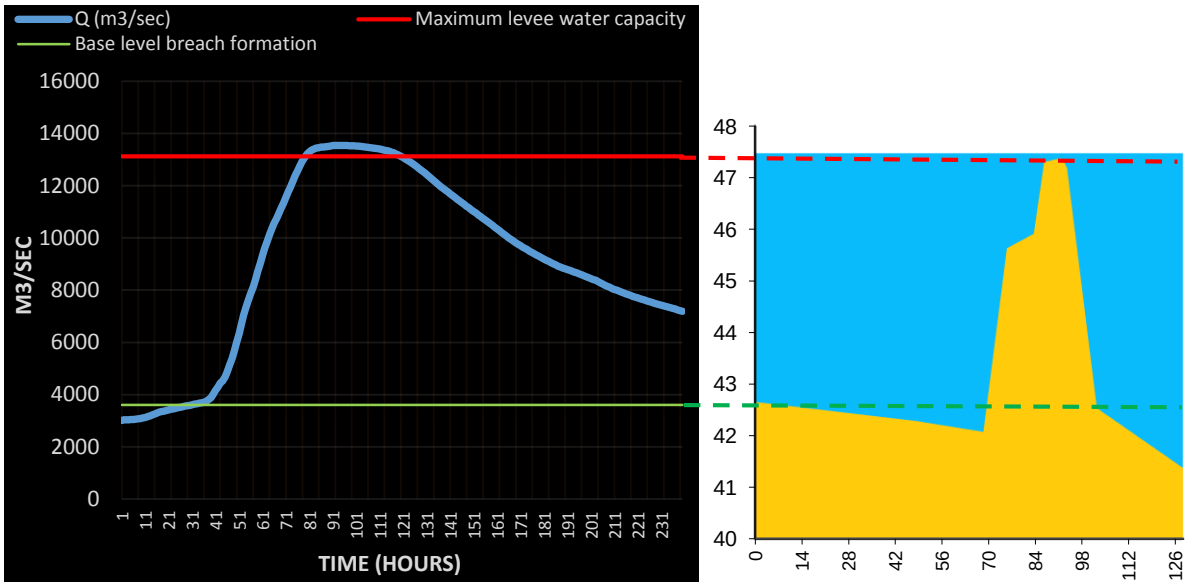

Graph 28: simulated hydrograph, resulting of the hydraulic modelling, of the section S23 and the discharges associated to the levee crest level and the toe level.

The flooding water in case of no failure is calculated from the moment that the overtopping begins until the flood does not reach the levee crest any more. The distribution in time of these volumes are shown in the next graphic, where also the equivalent probability of not failure distribution, for each section, is presented.

The flooding water volume for a levee failure due to overtopping is calculated from the first step of the maximum water load on the levee crest until the overtopping is over. The probability of failure distributions, using both approaches, is given considering only the maximum water load on the crest for all the rest of time that the overtopping takes place.

An example of distribution in time of the volumes corresponding to the section S23, for each breach dimension previously defined, are introduced in the following graphic.

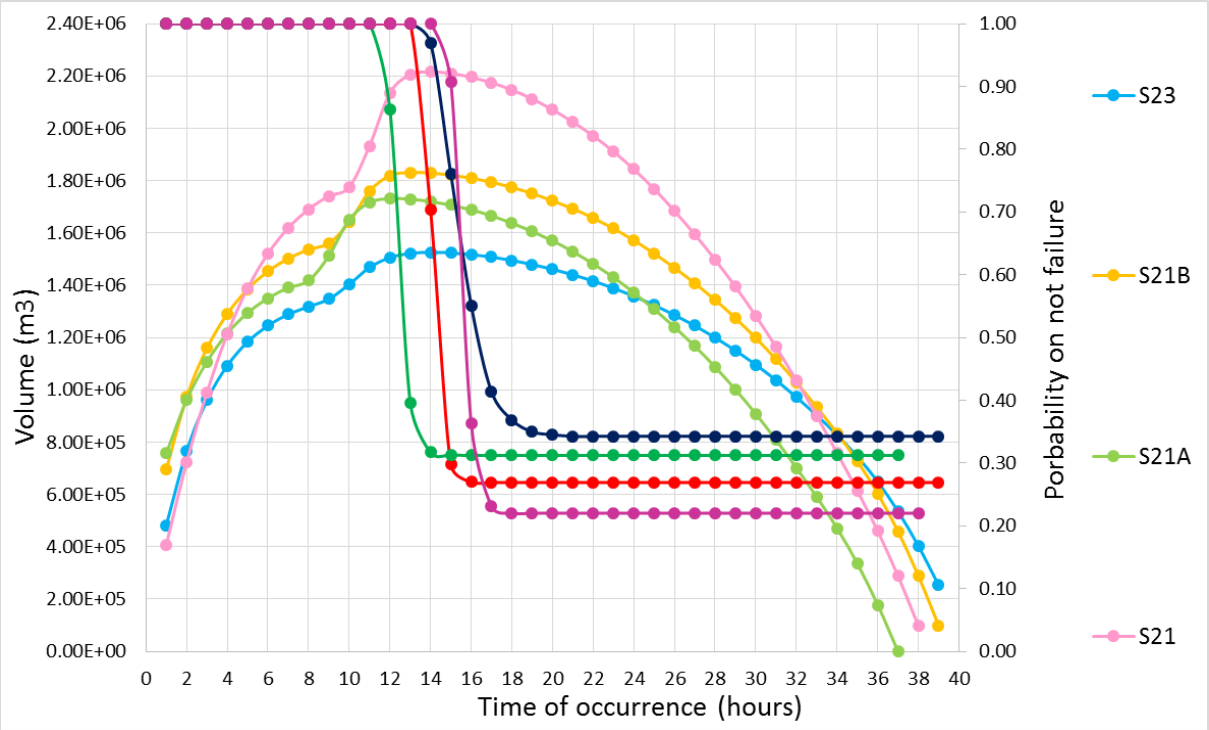

Graph 29: distribution of the flooding volumes at different sections (light tone) and the relative probability of not failure distribution (dark tone) for the first approach

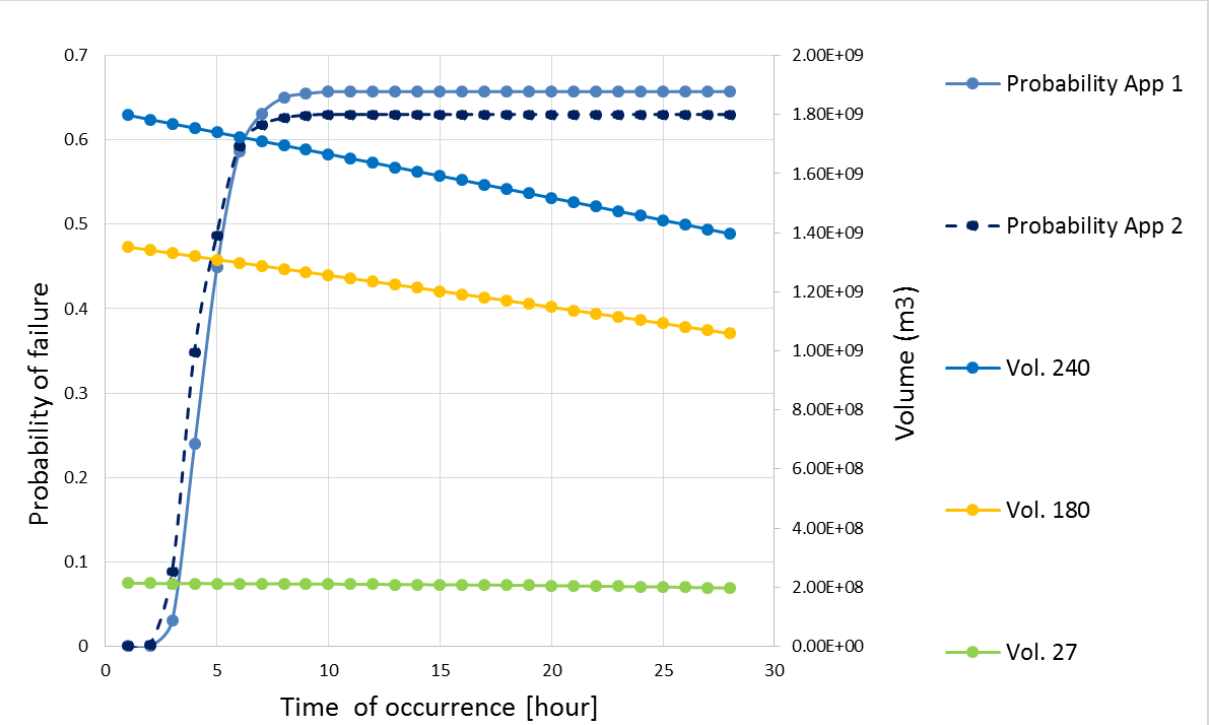

Graph 30: example of distribution of the flooding volumes (vol) for different breach dimensions (240, 180, 27) and the equivalent probability of failure distribution (on S23)

Implementing a convolution (operation between two functions of one variable which consists in integrating the product between the first and the second shifted by a certain value), is possible to obtain a mean value of a variable (the water volume) in function of its covariate.

$$Vmean = \int_0^{tr} V(t)\,\Pr(t)\;dt = \sum_{i=1}^{n} V(ti)\cdot\;\Pr(ti)$$

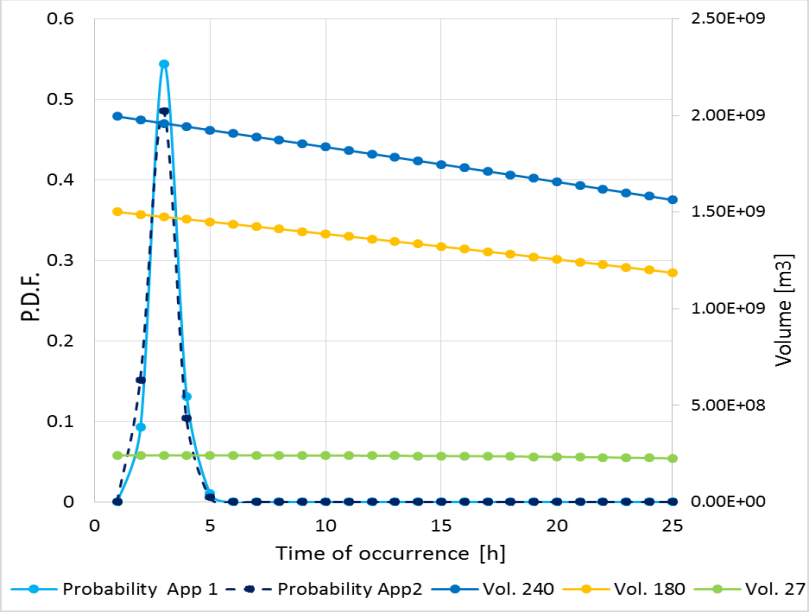

Graph 31: scheme for the operation of convolution in case of breach formation (S21)

For all the other cases previously described, in this way it is possible to estimate an average value of the water volume flooding during the event with a return time of 500 year for each considered river section.

The results are summarized in the next table:

OVERTOPPING				
Volumes (m3)	*S 21*	*S21 A*	*S 21 B*	*S 23*
Apporach 1	1.72E+06	1.19E+06	1.34E+06	9.99E+05
Approach 2	1.65E+06	1.23E+06	1.34E+06	9.58E+05

Table 9: Flooding water volume for not breach formation

BREACH FORMATION						
Approach 1				*Approach 1*		
Volumes (m3)	*Breach 240*	*Breach 180*	*Breach 27*	*Breach 240*	*Breach 180*	*Breach 27*
S 21	1.53E+09	1.15E+09	1.88E+08	1.46E+09	1.10E+09	1.80E+08
S 21 A	1.00E+09	7.56E+08	1.23E+08	1.04E+09	7.81E+08	1.27E+08
S 21 B	1.86E+09	1.40E+09	2.22E+08	1.87E+09	1.40E+09	2.23E+08
S 23	1.14E+09	8.60E+08	1.39E+08	1.10E+09	8.27E+08	1.34E+08

Table 10: Flooding volume for breach formation

About the overtopping only, is interesting to see the flooding volume decreases from S 21 to downstream (with a little rise in correspondence of S 21B) from value that reach over one million of m^3 to one hundred thousand of m^3.

The same effect is not evident considering breach formation. Higher water volume are calculated for S 21B (over 1.8 billion of m^3 for a breach width of 240 meters and tow hundred million of m^3 for a breach width of 27 meters), and lower value for S 21A (one billion m^3 for the larger breach width, and one hundred million m^3 for the smaller one).

12 Results and Discussion

In the following chapter, all the results obtained by the analyses, the classifications and the hazard estimations are examined. First, some considerations about the reliability classes, and the way they are obtained, are discussed followed by the correlations between the indexes and the input data used to define the classifications. These are done to understand how these indexes work to describe a reliability class.
Then a comparison between the classes found and the corresponding value of residual hazard is done to verify if any association is present.

12.1 Reliability Classes

The reliability classes obtained with the proposed, subjective intervals show some slight differences. In general, for both failure mechanisms, the stretches classified with the second approach occasionally result in belonging to a higher class or a lower class with respect to the first approach. This can be explained by the levee reference topography used in the analysis. As previously explained in the first approach, using fixed levee geometry can cause an over, or under, estimation of the failure probability that takes the fragility curve trend. Whereas in the second approach, the levee shape is variable which may represent a more realistic situation. The reliability classifications use indexes that have a physical (or statistical) meaning such as the minimum water load, or the standard deviation of the fragility curves, while the *Performance Classification* uses numerical indexes that describe only the shape of the curve. A good resolution would be to adopt physical indexes as well for this classification such as (on the axis) the hydraulic load corresponding to the minimum distance and the overtopping time to reach higher values of failure probability.

12.1.1 Indexes correlations

For all the classifications created, a series of correlations between the indexes and input information used for the reliability analysis are provided. This allows one to understand how the indexes work and, most of all, their weight as determinate reliability classes. These correlations are done considering both the approaches.

The correlations for the two classifications that describe the levee reliability for overtopping, considering the first approach, are introduced in the next tables:

CORRELATIONS	*LEFT LEVEE SYSTEM*	*RIGHT LEVEE SYSTEM*
PROB. STD./SLOPE	**0.852**	**0.874**
PROB. STD./INNER HEIGHT	**0.068**	**-0.310**
PROB. STD./RIVER BED	**-0.117**	**0.131**
PROB. STD./Δhmin	**-0.894**	**-0.925**
PROB. STD./SURF WIDTH	**0.215**	**0.318**
Δhmin/ SLOPE	**-0.994**	**-0.988**
SURF. WIDTH/ SLOPE	**0.530**	**0.380**
Δhmin/ SURF. WIDTH	**-0.492**	**-0.368**
INNER HEIGHT/Δhmin	**0.000**	**0.329**
RIVER BED /Δhmin	**0.158**	**-0.039**
INNER HEIGHT/SURF. WIDTH	**-0.313**	**-0.200**
RIVER BED /SURF WIDTH	**-0.551**	**-0.381**

Table 11: Correlations between indexes and overtopping input information for analysis using the first approach

The following tables show the correlation considering the second approach:

CORRELATIONS	*LEFT LEVEE SYSTEM*	*RIGHT LEVEE SYSTEM*
PROB. STD./MEAN SLOPE	**0.917**	**0.882**
PROB. STD./INNER HEIGHT	**0.250**	**0.311**
PROB. STD./RIVER BED	**0.224**	**-0.342**
PROB. STD./Δhmin	**-0.914**	**-0.924**
PROB. STD./SURF WIDTH	**0.185**	**0.318**
Δhmin/ MEAN SLOPE	**-0.990**	**-0.976**
SURF. WIDTH/ MEAN SLOPE	**0.457**	**0.270**
Δhmin/ SURF. WIDTH	**-0.469**	**-0.349**
INNER HEIGHT/Δhmin	**-0.181**	**-0.380**
RIVER BED /Δhmin	**0.010**	**0.305**
INNER HEIGHT/SURF. WIDTH	**-0.313**	**-0.078**
RIVER BED /SURF WIDTH	**-0.733**	**-0.781**

Table 12: Correlations between indexes and overtopping input information for analysis using the second approach

It is evident, for both approaches, that the probability value found with the first classification and the outer slope angle have a high positive correlation (as it would be expected).

For the minimum distance, (or minimum load condition), a great negative correlation results between the slope angle and the probability, while for the width of the fragility surface any significant value is noticed.

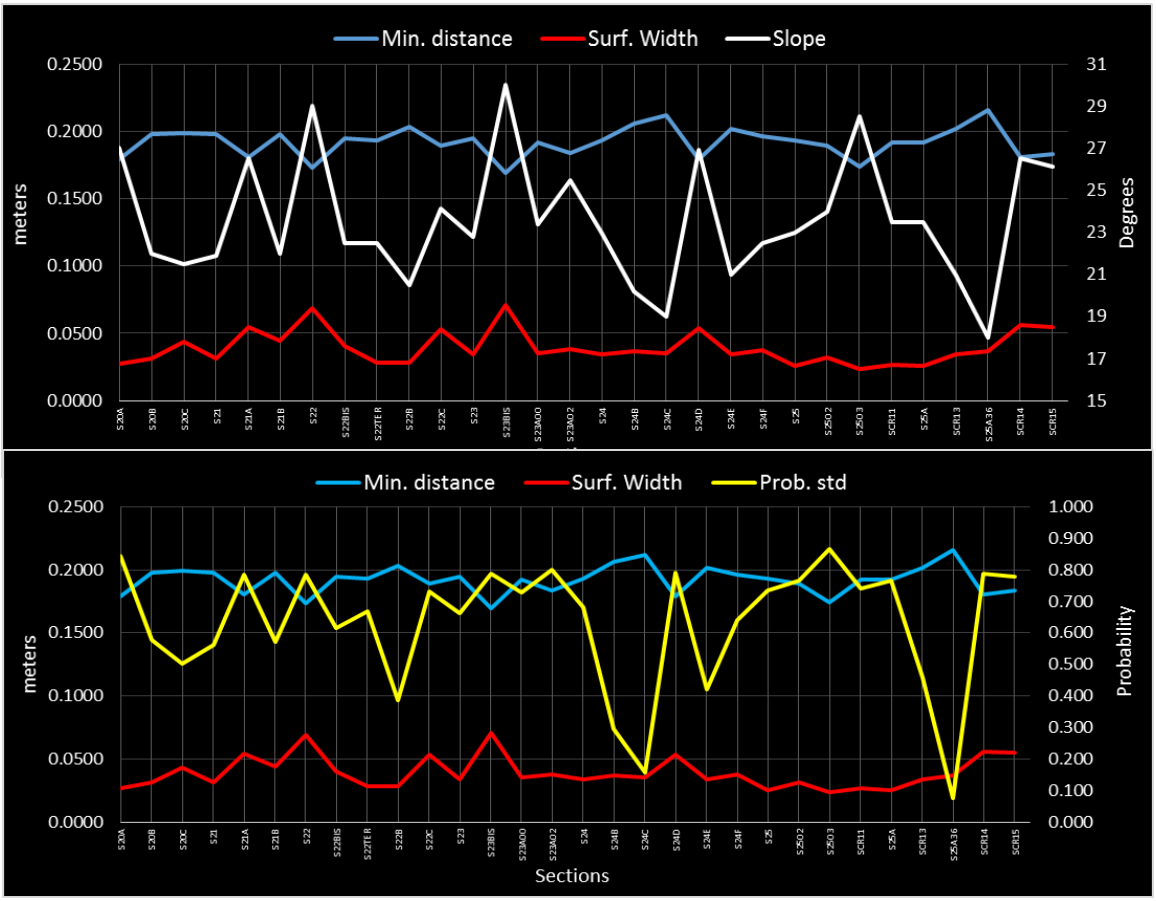

Graph 32: Trends and relations between left levee system indexes using the first approach for overtopping

In observing the results of the first classification, slightly different slope values can drastically change the value of the probability used as a standard to define the classes. It is evidenced in the *Performance Classification* by how the minimum distance has a significant impact when discretizing different classes of levee behavior—or reaction—under hydraulic stress. This is confirmed when looking at the relationship between the two classes of classification, where a V class in the first one corresponds to a IV_A, V and IV_C in the second as one moves along the ΔH_{min} axis.

The correlations for the classifications that describe the levee reliability for piping, with the first approach, are introduced in the following tables:

CORRELATIONS	*LEFT LEVEE SYSTEM*	*RIGHT LEVEE SYSTEM*
Δhmin/ DEV. STD.	**-0.922**	**-0.928**
MEAN HALF WIDTH/ DEV. STD.	**-0.988**	**-0.986**
MEAN HALF WIDTH/ Δhmin	**0.931**	**0.962**
RIVER BED/ Δhmin	**-0.113**	**-0.244**
RIVER BED/ DEV. STD.	**0.236**	**0.283**
INNER HEGHT/ Δhmin	**-0.103**	**0.045**
INNER HEIGHT/ DEV. STD.	**0.120**	**-0.048**

Table 13: Correlations between indexes and piping input information for analysis using the first approach

The correlations for the second approach:

CORRELATION	*LEFT LEVEE SYSTEM*	*RIGHT LEVEE SYSTEM*
Δhmin/ DEV. STD.	**-0.975**	**-0.776**
HALF WIDTH/ DEV. STD.	**-0.971**	**-0.976**
HALF WIDTH/ Δhmin	**0.998**	**0.646**
RIVER BED/ Δhmin	**0.025**	**-0.338**
RIVER BED/ DEV. STD.	**0.041**	**0.256**
INNER HEGHT/ Δhmin	**0.025**	**-0.046**
INNER HEIGHT/ DEV. STD.	**0.041**	**0.066**

Table 14: Correlations between indexes and piping input information for analysis using the second approach

In this case, for both approaches, it appears that the standard deviation of the fragility curve has a significant negative correlation between the levee base width used in the analysis and the minimum water load. However, ΔH_{min} with the base width presents a high, positive correlation.

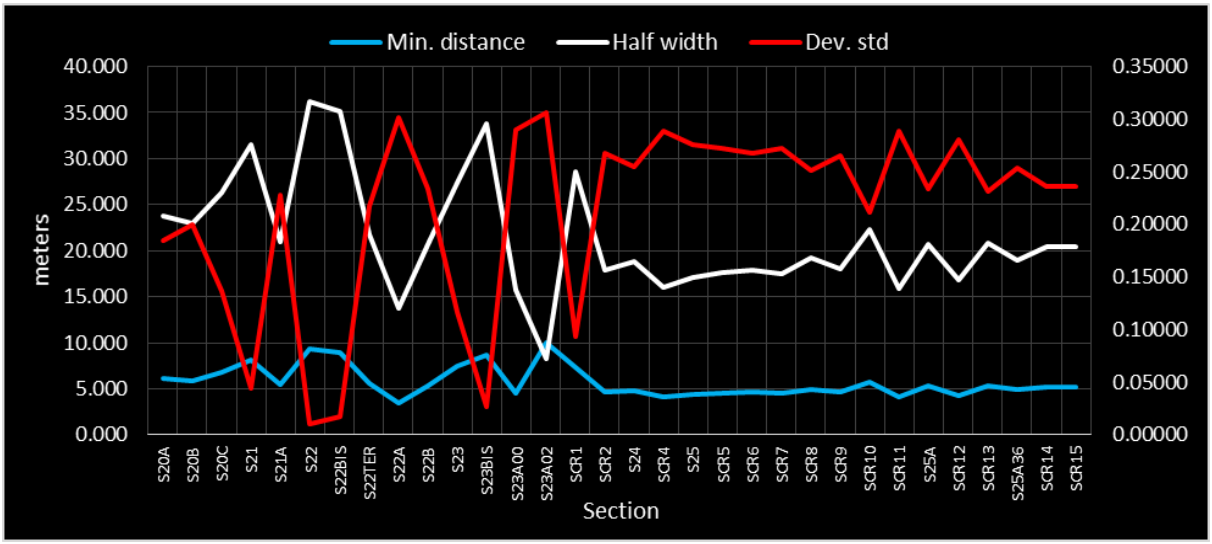

Graph 33: Trends and relationships between right levee system indexes using the first approach for piping

It is plausible to say that, for piping classification, the geometric input is the fundamental characteristic to discretize homogenous levee stretches having similar features since both indexes have the same importance to identify the reliability classes.

12.2 Comparison Between the Classes and the Residual Hazard Value

The reliability classifications and the residual hazard estimations work in different ways whereas the classifications use standard indexes to define homogeneous classes for levee stretches while the hazard is given using a hydraulic model. This model is used to approximately report a real condition of hydraulic stress for a simulated flood event. The comparison between the classes and the residual hazard values allows one to determine if any relation is present and if there are contradictions between the methods.
The following tables summarize the results obtained by the reliability analysis (the reliability classes) and the residual hazard values (higher than zero) for both failure mechanisms and approaches.

Overtopping:

SECTIONS LF	*Failure (%) App1*	*Hazard (%)*	*Classes*	*Performance*	*Stretches*	*Failure (%) App2*	*Hazard (%)*	*Classes*	*Performance*
S20A	5.2	1.04	*V*	*IV C*	1	4.8	0.96	*IV*	*IV C*
S21	77.98	15.596	*III*	*IV C*	3	36.17	7.234	*III*	*IV C*
S21A	68.76	13.752	*IV*	*IV B*	4	75.63	15.126	*IV*	*IV C*
S21B	73.08	14.616	*III*	*IV B*	5	70.8	14.16	*IV*	*IV B*
S23	65.73	13.146	*IV*	*IV C*	6	36.48	7.296	*IV*	*IV B*
					11	31.52	6.304	*IV*	*IV B*
					12	31.45	6.29	*IV*	*IV B*
SECTIONS RG	*Failure (%) App1*	*Hazard (%)*	*Classes*	*Performance*	*Stretches*	*Failure (%) App2*	*Hazard (%)*	*Classes*	*Performance*
S23BIS	35.3	7.06	*IV*	*IV B*	12	14.13	2.826	*IV*	*IV B*
SCR2	84.47	16.894	*III*	*IVC*	13	16.12	3.224	*IV*	*IV B*
					17	47.9	9.58	*IV*	*IV C*
					18	41.92	8.384	*III*	*IV C*

Table 15: Comparison between the reliability classes and the residual hazard value for overtopping failure mechanisms

Piping:

SECTIONS LF	*Failure (%) App1*	*Hazard (%)*	*Classes*	*Stretches*	*Failure (%) App2*	*Hazard (%)*	*Classes*
S21	1.68	0.336	I	1	1.39	0.278	I
				4	7.375	1.475	I
				12	0.47	0.094	I
				20	1.31	0.262	II
				29	2.705	0.541	II
SECTIONS Rg	*Failure (%) App1*	*Hazard (%)*	*Classes*	*Stretches*	*Failure (%) App2*	*Hazard (%)*	*Classes*
S22TER	7.75	1.55	II	2	1.00	0.2	I
S22A	5.38	1.076	II	4	0.24	0.048	I
				5	2.78	0.556	II
				7	0.54	0.107	II
				8	4.42	0.884	II
				9	3.46	0.692	II
				10	0.36	0.072	II
				15	0.50	0.1	II
				16	0.85	0.17	I

Table16: comparison between the reliability classes and the residual hazard value for piping mechanism of failure

What clearly stands out is not all the reliability classes correspond to an equivalent hazard value. For example, a high hazard should be related to an unreliable class and vice versa. This can be explained by the use of the hydraulic information obtained by the modelling, where different combinations of water load—and also overflowing time for overtopping mechanisms—allowing for a completely different hazard value for different hydraulic conditions with respect to what would be expected given the reliability classes.

However, the comparison between the classes for overtopping and hazard estimation, obtained using the first approach, show somewhat of a contradiction. The hazard estimation for sections S21 and S21B (belonging to the third class) shows a high value with respect to the other section (related to the fourth class) even when the hydraulic conditions are not that different. This possible overestimation of the hazard can be related to the numerical code written in MatLab used to obtain fragility curves. An analysis on a large time scale was performed with an overtopping time interval increased from 2 to 15 hours. The steps of discretization have not been increased enough to permit the use of the same sampling step measurement, due to the high computational power needed to perform the analysis. This simplification, together to a smaller number of simulations, could cause an error propagation that would lead to an overestimation of the hazard resulting from the computation.

12.2.1 Flooding volumes estimation

For both approaches, the results of the flooding water computation show approximately similar values. Regarding what has discussed in the previous chapter, it is plausible to assume the second approach may give a more accurate result than the first.

The moment that a failure mechanism occurs does not mean that another should be neglected. On the contrary, this estimation of the flooding volumes can be used simultaneously for other failure mechanisms (such as piping, macro-instability, micro-instability, inner eriosion, etc.), but especially for overtopping together with piping. In addition to being the most common failure mechanisms, piping can be considered a precursor for a overtopping (Viero et al., 2013), where a collapse of part of the foundation soils, then a lowering of the dike itself, may trigger flooding over the crest of the levee.

13 Conclusions

Due to its complexity, this study has highlighted how difficult it is to characterize a levee system and develop a method to establish its reliability.

With this work, a more accurate analysis for levee system is provide, where the results are associated to entire levee stretches, the levee geometry is correct, and the load variables are considered not as uniform, but with a probability distribution that vary in function of the topography variability in the space.

Below are the reported and summarized conclusions of what has been studied.

Literary research provided the perspective of where the levee system of the Po River is situated which allowed the hydrological, hydraulic and territorial contexts to be comprehended. The study of historical and associated levee failure events have provided observations into where the most susceptible areas to flood risk are in the Padana Plain.

The reconstruction of the evolutionary phases of the levee system has shown what the limits are regarding geotechnical data sources of the levee body and its foundation soils as well as issues regarding the availability of this data together with those of land cover.

Therefore, the limited availability of data and the adoption of a simplified stochastic approach already represents an initial form of uncertainty for reliability analysis.

The study for the development of the reliability model has enabled the understanding of the process of the probabilistic method (Monte Carlo), the most recent physical laws used to describe the considered failure mechanisms, and the weight that the input information has on the model.

The physical knowledge used represents more of an ideal condition to the activation of a rupture mechanism. Further, the phenomena themselves are much more complex whereby an interaction between hydraulic conditions and geotechnical characteristics of the foundation and embankments materials describes the erosive processes that leads to the collapse of the levee.

The approaches, thus constructed, allow for the survey to be extended along levee instead of only along the individual sections permitting one to identify which one best approximates the physical reality of the levee system. Although improvements have been applied to the model, the limits are still present nonetheless.

The second approach seems to be better than the first one to perform a reliability analysis (then also a hazard estimation), even if the topography of reference is referred to mean values (this may cause a loss of information); anyway they are representative of a physic reality set as boundary.

Principally among these, the exclusive use of topographic sections does not take into account the presence of obstacles and abrupt changes in the levees' geometry. Additionally, the sections not being equidistant makes it difficult to find an exact correlation between them.

The quantity of the available data is enough to allow an analysis in a probabilistic way using the Monte Carlo method. However, the same distribution of the data is used along all the levee system studied. A good purpose would to discretize also the data distribution in space for levee stretch with different characteristics. A detailed investigation is needed to have a complete knowledge about the geotechnical parameters. To have different value of turf quality using satellite images with very high resolution highlights the vegetation with the infrared elaboration.

The geometric analysis permitted the observation of the morphological and topographical evolution of the levee system and the stretch of river in question. Thus, they allow one to understand how they affect the reliability analysis. In addition, an accurate observation of the cartographic material allows for the identification of the section's actual position compared to the direction of the embankment system development. This permits a correction to obtain the actual geometric data.

The introduction of a probability distribution of the load variables, associated with the topographical spatial variability, of the models showed a certain effect to the delineation of fragility curves. A complete change of the surface was observed for overtopping, while piping showed only a small variation in the failure probability trend. The load variable distributions were assumed and reasoned. In order to obtain more realistic ones, hydraulic modeling would be required. By conducting simulations of flood events with different return times, the possibility to determine the values of variables in space would be possible as well as derive a probability distribution of the more realistic variables.

Classifications and reliability classes, valid for all rivers and dykes, have been defined for a limited stretch of the embankment of the Po River system. In terms of overtopping, the majority of the levee stretches belong to the fourth classes with some peaking at the fifth

and few other stretches in the first class. Almost all the levee system, for piping, resulted in a reliable class with a few stretches belonging to the second class.

Using indexes to discretize the reliability classes with a physical meaning, would allow the correlation of a class to an actual, physical situation.

Analyzing the whole system, from upstream to downstream, would provide the most complete picture possible. A good utilization would be to apply these classifications to an actual flood event that reports levee breaches for the considered mechanisms.

The hazard analysis has verified the usefulness of the fragility curves for hydraulic risk assessment to areas protected by levee systems. In general, with this method and the simplifying assumptions of the model, it can be said that for a 500-year flood event, the catchment area to the left downstream of Piacenza may be subject to hydraulic hazard in terms of overtopping. While for piping, it appears—based on the classification and the hazard values—the levee system has been resized to withstand this type of load.

The comparison between the classes and the hazard value shows how delicate is to give a hazard estimation, especially when the input information (numerical and hydraulic models as well as simplified approaches) represents the first source of uncertainty that gives error propagation in the model run and inaccurate results.

This work can be considered as a foray into what could be a study project to evaluate the reliability of larger levee systems; improving the hydraulic risk assessment for areas protected by hydraulic defense infrastructures where sense of risk is paradoxically less perceived. Undoubtedly, the collaboration between different professionals, such as the geologists, hydrologists and hydraulic engineers mentioned herein, has been instrumental in bringing this work to fruition.

Ringraziamenti

Giunti finalmente alla fine di questo percorso, sono davvero tante le presone da ringraziare.

Primo di tutti ci tengo a ringraziare il Prof. Mario Martina, nonché relatore della mia tesi, per avermi seguito durante la stesura di questo lavoro (che speriamo in futuro di portare avanti), avermi insegnato tanto ma soprattutto avermi dato la possibilità di scrivere una tesi in una materia a me molto a cuore, e aver dimostrato insieme che la collaborazione tra ingegneri e geologi è un gran punto di forza.

Ringrazio il Dott. Alessio Domeneghetti, mio correlatore, che sin dal primo incontro mi ha incoraggiato a portare avanti i miei interessi e mi ha accolto con entusiasmo alla richiesta di lavorare insieme a questa tesi. E grazie per il tempo che mi ha dedicato.

Un grazie va a Maurizio Mazzoleni, che mi ha accolto all'estero per imparare il metodo anglosassone, e mi ha insegnato con pazienza le basi fondamentali di una materia a me sconosciuta.

Ringrazio tutti i miei parenti, che mi hanno sostenuto nei miei studi e mi hanno sempre dato la possibilità di raggiungere i miei obbiettivi.

Grazie a tutti gli amici che ho conosciuto a Bologna (Lorenzo, gli "Scoppaiti, "B.d.s." e gli aspiranti geologi con cui ho condiviso due anni di grandi esperienze durante il corso).

Grazie hai B.G di Trieste, che son sempre stati di grande ispirazione per dare sempre il massimo e mi hanno insegnato a portare a casa dei grandi risultati.

Grazie ai ragazzi del C.I. Casello al Podere, che mi hanno dato il loro aiuto ma soprattutto tanta serenità nei momenti più stressanti.

Grazie a tutto il C.I Monte d'Oro, che considero come la mia seconda casa (o forse anche prima), e ringrazio il gruppo "Mela godo", dei grandi amici che mi sono sempre stati vicini nei miei momenti più bui, e grazie a loro ho imparato a non mollare mai.

Ma il mio più grande GRAZIE va a coloro che, oltre ad essere cari amici, considero i miei veri maestri.

Grazie a Paolo Paronuzzi, che mi ha dato sempre tanta carica ed entusiasmo, mi ha insegnato a pensare con la mia testa, a ragionare con la mente di un ingegnere ed ad osservare con l'occhio di un geologo, ma soprattutto mi ha insegnato che l'esperienza è l'unica vera maestra che ci aiuta a crescere ed ad imparare, e che le cose vanno fatte "pian e ben", ma soprattutto "ben".

Un grazie va a Mario Crevato, che da subito mi ha spronato a dare sempre il meglio di se, a confidare nelle proprie capacità e a cavarsela anche da soli; mi ha fatto capire che la bussola non è solo quella che teniamo in mano ma sta anche dentro la nostra testa, mi ha fatto capire che l'unico modo per affrontare le difficoltà è andando a cercarsele, che una fatica prima è sempre una grande soddisfazione dopo. E aveva ragione!

Farò tesoro di tutti i vostri insegnamenti, grazie di cuore.

14 Bibliography

AdbPo (2001), “Studio dei terreni di fondazione di un tratto campione degli argini maestri del fiume Po attraverso prospezioni geofisiche da eseguirsi mediante metodi sismici ed elettrici”, Dipartimento di Ingegneria Strutturale e Geotecnica del politecnico di Torino, ST1_12.

AdbPO (2005), “Progetto strategico per il miglioramento delle condizioni di sicurezza idraulica dei territori di pianura lungo l’asta medio-inferiore del fiume Po”, Comitato tecnico, Parma, 88 pp.

AIPO (2006) - Caratteristiche del bacino del fiume Po e primo esame dell'impatto ambientale delle attività umane sulle risorse idriche. Autorità di Bacino del fiume Po, Parma.

AdbPO (2014), “Progetto di Piano per la valutazione e la gestione del rischio di alluvioni”, Art. 7 della Direttiva 2007/60/CE e del D.lgs. n. 49 del 23.02.2010, 15 pp.

AdbPO (2014),” Schema di Progetto di Piano per la valutazione e la gestione del rischio di alluvioni”, Art. 7 della Direttiva 2007/60/CE e del D.lgs. n. 49 del 23.02.2010. 49 pp.

Apel, H., Thieken, A. H., Merz, B., and Bl¨oschl, G (2004), “Flood risk assessment and associated uncertainty”, Nat. Hazards Earth Syst. Sci., 4, 295–308.

Apel, H., Thieken, A., Merz, B., and Bl¨oschl, G. (2006), “A probabilistic modelling system for assessing flood risks”, Nat. Hazards, 38, 79– 100, doi:10.1007/s11069-005-8603-7.

Alkema, D., and Middelkoop, H. (2005), “The influence of floodplain compartmentalization on flood risk within the Rhine-Meuse delta.” Nat. Hazards, 36(1–2), 125–145.

Armbruster-Veneti, H. (1999), “U¨ ber das Versagen von Erdda¨mmen”, Wasserwirtschaft, 89, 504–511.

Bligh, W. G. (1912), “The practical design of irrigation works”, 2nd Ed., Constable, London.

Bollrich, G. (2000), “ Technische Hydromechanik, Verlag Bauwesen”, Berlin, Germany.

Burton, C., and Cutter, S. L. (2008), “Levee failures and social vulnerability in the Sacramento–San Joaquin Delta area, California.” Nat. Hazards Rev., 10.1061/(ASCE)1527 6988(2008)9:3(136), 136–149.

Camorani, G., Filippi, F., Cavazzini, A., Lombardo, G., Pappani, G., Forlani, G., (2006), “Il rilievo altimetrico e batimetrico del Fiume Po nel tratto tra confluenza Ticino e l’incile”, Proceedings of X Asita Nat. Conf.

Chapuis, R. P., and Aubertin, M. (2003), “On the use of the Kozeny- Carman equation to predict the hydraulic conductivity of soils.”Can. Geotech. J., 40(3), 616–628.

Carisi F. (2011), “Modello quasi bi-dimensionale per la valutazione del rischio idraulico de esondazione fluviale nella pianura Padana”, tesi di laurea specialistica, DICAM Costruzioni Idrauliche, 209 pp.

Carrier, W. D. (2003), “Goodbye, Hazen; hello, Kozeny-Carman.” J. Geotech. Geoenviron. Eng., 10.1061/(ASCE)1090-0241(2003)129: 11(1054), 1054–1056.

Castellarin, A, Domeneghetti, A, Brath, A. (2001), “Identifying robust large-scale flood risk mitigation strategies: A quasi-2D hydraulic model as a tool for the Po river”. Physics and Chemistry of the Earth, Parts A/B/C 36 (7-8): 299–308 DOI: 10.1016/j.pce.2011.02.008

Cati, L. (1981), “Idrografia e idrologia del Po. Pubblicazione n 19 dell’Ufficio Idrografico del Po”, Istituto Poligrafico e Zecca dello Stato, Roma.

Chapuis, R. P., and Aubertin, M. (2003), “On the use of the Kozeny- Carman equation to predict the hydraulic conductivity of soils.” Can. Geotech. J., 40(3), 616–628.

CIRIA (2013), The international levee handbook, London.

Comune Monticelli (2012), “Relazione Illustrativa”,39 pp.

Coratza, L., (2005), “Aggiornamento del catasto delle arginature maestre di Po”, Autorita di Bacino del fiume Po, Parma.

CUR/TAW (1990), “ Probabilistic design of flood defences”, Report 141, Centre for civil engineering research and codes. Technical advisory committee on water defences, Gouda, The Netherlands, 154 pp.

Dawson, R. J., Hall, J. W., Sayers, P. B., Bates, P. D., and Rosu, C. (2005), “Sampling-based flood risk analysis for fluvial dike systems”, Stoc. Environ. Res. Risk A., 19, 388–402.

de Moel, H., van Alphen, J., and Aerts, J. (2009), “Flood maps in Europe– Methods, availability and use.” Nat. Hazards Earth Syst. Sci., 9(2), 289–301.

Dal Piaz, G.V., Bistacchi, A., Massironi, M. (2003), “Geological outline of the Alps”, *Episodes*, 26/3, 175-180 pp.

DIIAR (200), “Caratterizzazione idrologica dell'asta principale del fiume Po nel tratto che va dalla confluenza della Dora Baltea all'incile del Po di Goro”, Internal report (in Italian).

Di Baldassarre, G., Castellarin, A., Montanari, A., and Brath, A. (2009), “Probability weighted hazard maps for comparing different flood risk management strategies: A case study.” Nat. Hazards, 50(3), 479–496.

Di Baldassarre, G., Montanari, A., Lins, H., Koutsoyiannis, D., Brandimarte, L., and Bloeschl, G. (2010a), “Flood fatalities in Africa: From diagnosis to mitigation.” Geophys. Res. Lett., 37(20), L22402.

Di Baldassarre, G., Schumann, G., Brandimarte, L., and Bates, P. D. (2010b), “Timely low resolution SAR Imagery to support floodplain modelling: A case study review.” Surv. Geophys., 32(3), 255–269.

Di Baldassarre, G., Viglione, A., Carr, G., Kuil, L., Salinas, J. L., and Blöschl, G. (2013), “Socio-hydrology: Conceptualising human-flood interactions.” Hydrol. Earth Syst. Sci., 17(8), 3295–3303.

Bhargava, K., Ghosch, A. K., Agrawal, M. K., Patnaik, R., Ramanujam, S., and Kushwaha, H. S. (2002), “ Evaluation of seismic fragility of structures – a case study”, Nucl. Eng. Des., 212, 253–272.

Domeneghetti, A. (2012), ”Modellistica idraulico-matematica per la definizione di strategie di mitigazione del rischio alluvionale”, tesi di dottorato di ricerca, DICAM Costruzioni Idrauliche, 170 pp.

EU, 2007. Directive 2007/60/EC of the European Parliament and of the Council of 23 October 2007 on the assessment and management of flood risks. Official Journal of the European Union L228, 27–34.

Ferrari, V., Leandri, F, Milesi, C.R. (2008), “Il territorio come ecomuseo, gli argini del Po”, Regione Lombardia, Provincia di Cremona Settore Ambiente, 51 pp.

Gradstein, F.M. & Ogg, J.G. (2004), “Geology time scale-why, how, and where next”, Lethaia, Vol. 37, Oslo. ISNN 0024-1164, 175-181.

Gallizia, P. (1878), “Le piene del Po nel secolo XIX”, in Il Giornale del Genio Civile, 3-32 61-81 125-143.

Hall, J.W., Dawson, R. J., Sayers, P. B., Rosu, C., Chatterton, J. B., and Deakin, R. (2003), “A methodology for national-scale flood risk assessment”, P. I. Civil. Eng.-Water, 156, 235–247,

Giovi,M. & Turitto, O. (2000), “Casistica storica sui processi d’interazione delle correnti di piena del Po con arginature e con elementi morfotopografici del territorio adiacente”, Scienza e vita del momento attuale, V, Istituto Lombardo di scienze e lettere, Milano, 105-160.

Heine, R. A., and Pinter, N. (2012), “Levee effects upon flood levels: An empirical assessment.” Hydrol. Processes, 26(21), 3225–3240.

Hewlett, H. W. M. (1987), “Design of reinforced grass waterways”, Report, (CIRIA) Construction Industry Research and Information Association, London.

ISPRA, “Carta geologica d’Italia”, II edizione, Foglio 60-61.

Khilar, K. C., Fogler, H. S., and Gray, D. H. (1985), “Model for pipingplugging in earthen structures.” J. Geotech. Eng., 10.1061/(ASCE) 0733-9410,111:7(833), 833–846.

Kortenhaus, A. and Oumeraci, H. (2002), “Probabilistische Bemessungsmethoden f¨ur Seedeiche”, (ProDeich), Bericht Nr. 877, Leichtweiss-Institut f¨ur Wasserbau, Braunschweig University of Technology, Germany, 205 pp.

Ludy, J., and Kondolf, G. (2012), “Flood risk perception in lands ‘protected’ by 100-year levees.” Nat. Hazards, 829–842.

Masoero, A., Claps, P., Asselman, E. M., Mosselman, E., and Di Baldassarre, G. (2013), “Reconstruction and analysis of the Po River inundation of 1951.” Hydrol. Processes, 27(9), 1341–1348.

Mazzoleni, M. (2015), “River structure levee system”, UNESCO-IHE MSc. Hydraulic Engineering and River Basin development Module.

Mazzoleni, M., Barontini, S., Ranzi, R., Brandimarte L. (2014), “Innovative Probabilistic Methodology for Evaluating the Reliability of Discrete Levee Reaches Owing to Piping”, American Society of Civil Engineers., ASCEE, J. Hydrol. Eng, 13 pp.

Merz, B. (2006), “Absch¨atzung von Hochwasserrisiken”, Methoden, Grenzen und Mglichkeiten, Habilitationsschrift, E. Schweizerbart’sche Verlagsbuchhandlung (N¨agele und Obermiller), Stuttgart, Germany.

Mignosa, P.(2011), “Le rotte nel tratto Emiliano del fiume Po”, tratto da “Un Po di carte - La dinamica fluviale del Po nell’Ottocento e le tavole della Commissione Brioschi”, a cura di Ireneo Ferrari e Maurizio Pellegrin (ARPA), 204 pp.

Milly, P. C. D.,Wetherald, R. T., Dunne, K. A., and Delworth, T. L. (2002), “Increasing risk of great floods in a changing climate.” Nature, 415(6871), 514–517.

Mostert, E., and Junier, S. (2009), “The European flood risk directive: Challenges for research.” Hydr. Earth Syst. Sci. Discuss., 6(4), 4961–4988. Ohl, C., and Tapsell, S. (2000). “Flooding and human health: The dangers posed are not always obvious.” Brit. Med. J., 321(7270), 1167–1168.

Mozhaev, A. P. (2002), “A porosity distribution in nonuniform homogeneous structures.” Doklady Phys., 47(5), 370–372.

Nigrelli, G. (2013), “Il Po ed il suo bacino”, naturaweb.net, 9 pp.

Ojha, C. S. P., Singh, V. P., and Adrian, D. D. (2001), “Influence of porosity on piping models of levee failure.” J. Geotech. Geoenviron. Eng., 10.1061/(ASCE)1090-0241(2001)127:12(1071), 1071–1074.

Opperman, J., Galloway, G., Fargione, J., Mount, J., Richter, B., and Secchi, S. (2009), “Sustainable floodplains through largescale reconnection to rivers.” Science, 326(5959), 1487–1488.

Ranzi, R., Barontini, B., Mazzoleni, M., Ferri, M., and Bacchi, B. (2012), “Levee breaches and ‘geotechnical uncertainty’ in flood risk mapping.” Proc., Int. Association for Hydro-Environment Engineering and Research (IAHR) Conf., Madrid, Spain.

Sayers, P. B., Hall, J. W., Rosu, C., Chatterton, J. B., and Deakin, R. (2002), “Risk assessment of flood and coastal defences for strategic planning (RASP) – A high level methodology”, in: DEFRA Conference of Coastal and River Engineers, Keel University, UK.

Sellmeijer, J. (1989), “On the mechanism of piping under impervious structures.” Ph.D. thesis, Delft Univ. of Technology, Delft, Netherlands. Singh, V., and Scarlatos, P. (1988). “Analysis of gradual earth-dam failure.” J. Hydraul. Eng., 2(1), 46–69.

Shinozuka, M., Feng, M. Q., Lee, J., and Naganuma, T (2000), “ Statistical analysis of fragility curves”, J. Eng. Mech.-ASCE, 126, 1224–1231.

Steenbergen, H. M. G. M. and Vrouwenvelder, A. C. W. M. (2003), “Theoriehandleidung PC-RING”, Versie 4.0, Deel A: Mechanismenbeschrijvingen, TNO-Report 2003-CI-R0020, TNO Civiele Infrastructuur, Delft, The Netherlands, 2003.

Turitto, O., Cirio, C.G., Nigrelli, G., Bossuto, P., Viale, F. (2010), “Vulnerabilità manifestata dagli argini maestri del fiume Po negli ultimi due secoli”, L’Acqua, 6, 17-34.

USACE (1996), “Risk-based analysis for flood damage reduction studies”, US Army Corps of Engineers, Engineer Manual 1110-2-1619.

USACE (1999), “Risk-based analysis in geotechnical engineering for support of planning studies”, U.S. Army Corps of Engineers Engineer Technical Letter 1110-2-556.

Viero, D.P., D’alpaos, A., Carniello, L., Defina, A (2013), “Mathematical modeling of flooding due to river bank failure”, Advances in Water Resources, Elsevier, 13 pp.

Vorogushyn, S. (2008), “Analysis of flood hazard under consideration of dike breaches”, zur Erlangung des akademischen Grades "doctor rerum naturalium" (Dr. rer. nat.) in der Wissenschaftsdisziplin "Geoökologie" eingereicht an der Mathematisch Naturwissenschaftlichen Fakultät der Universität Potsdam, 165.

Vorogushyn, S., Apel, H., and Merz, B. (2011), “The impact of the uncertaintyof dike breach development time on flood hazard.” Phys. Chem.Earth, 36(7–8), 319–323.

Vorogushyn, S., Merz, B., and Apel, H. (2009), “Development of dike fragility curves for piping and micro-instability breach mechanisms.” Nat. Hazards Earth Syst. Sci., 9(4), 1383–1401.

Vorogushyn, S., Merz, B., Lindenschmidt, K., and Apel, H. (2010), “A new methodology for flood hazard assessment considering dike breaches.” Water Resour. Res., 46(8), W08541.

Vrijling, J. K. and van Gelder, P. H. A. J. M. (2000), “Probabilistic design”, IHE-Delft Lecture notes, Delft University of Technology, The Netherlands.

Vrijling, J. K. (2001),“Probabilistic design of water defence systems in the Netherlands”, Reliab. Eng. Sys. Safe., 74, 337–344.

White, G. F. (1945), Human adjustments to floods, Dept. of Geography Research, Univ. of Chicago, Chicago.

Zanichelli, G, Pavan, S**,** Pecora, S, Ricciardi, G, (2015), **“**Gli eventi di piena del Po del Novembre 2014: un approfondimento”, AdbPO, ARPA.

Attachment 1: topographic input dataset

LEFT LEVEE SYSTEM											
SECTIONS	*ALPHA (°)*	*FALSE SLOPE (°)*	*REAL SLOPE(°)*	*L WIDTH (m)*	*BASE WIDTH (m)*	*REAL WIDTH (m)*	*LAND HEIGHT (m)*	*INNER HEIGHT (m)*	*RIVER BED (m)*	*CREST LEVEL (m)*	THALWEG (m)
S20A	42.12	18.19	27.00	40.82	73.11	49.03	6.76	21.63	2662.50	52.24	30.61
S20B	61.78	19.24	22.00	20.69	32.46	28.60	4.30	19.34	2381.30	52.07	32.73
S20C	77.85	19.91	21.50	31.62	43.99	43.00	5.33	14.30	1738.48	51.33	37.03
S21	90.00	21.86	21.86	26.11	35.34	35.34	6.61	17.34	3105.36	50.90	33.56
S21A	78.96	24.96	26.50	19.35	28.51	27.98	3.53	20.99	1445.49	50.41	29.42
S21B	62.25	19.15	22.00	32.47	49.64	43.93	6.97	18.13	1341.66	50.15	32.02
S22	85.06	28.09	29.00	28.50	46.02	45.85	5.45	21.28	1265.33	49.95	28.67
S22BIS	73.40	20.68	22.50	29.58	60.57	58.05	5.46	17.90	1720.74	49.87	31.97
S22TER	73.38	20.58	22.50	31.26	45.58	43.67	6.34	23.15	2370.45	49.96	26.81
S22B	80.39	19.24	20.50	35.31	51.87	51.14	5.43	19.34	3219.64	52.07	32.73
S22C	90.00	24.14	24.14	32.01	43.99	43.99	5.33	14.30	2420.42	51.33	37.03
S23	90.00	22.77	22.77	23.37	33.21	33.21	5.30	17.80	2330.49	47.37	29.57
S23BIS	56.13	24.81	30.00	20.39	33.11	27.49	4.18	14.88	2018.53	47.06	32.18
S23A00	90.00	23.37	23.37	28.61	36.47	36.47	4.76	20.22	1888.41	46.73	26.51
S23A02	74.25	24.46	25.50	22.50	31.61	30.42	5.20	19.70	1967.36	46.54	26.84
S24	62.99	20.14	23.00	30.28	41.17	36.68	4.60	27.15	1638.87	46.42	19.27
S24B	90.00	20.19	20.19	24.39	34.23	34.23	4.41	18.91	1442.68	45.87	26.96
S24C	74.19	17.35	19.00	28.84	37.09	35.68	5.60	18.07	1614.50	44.98	26.91
S24D	90.00	26.94	26.94	23.45	29.37	29.37	4.56	18.06	1698.11	44.75	26.69
S24E	74.29	20.17	21.00	9.09	19.20	18.48	2.32	17.45	2085.25	44.44	26.99
S24F	78.43	21.69	22.50	20.66	29.43	28.83	3.99	16.40	2203.65	44.25	27.85
S25	44.22	15.86	23.00	18.03	36.74	25.63	3.61	21.34	3315.93	43.62	22.28
S2502	53.35	19.32	24.00	23.69	38.90	31.21	4.87	17.13	3348.92	43.21	26.08
S2503	47.47	21.21	28.50	16.96	37.40	27.56	4.33	27.37	2485.35	43.21	15.84
SCR11	82.39	22.51	23.50	23.27	42.66	42.28	4.69	19.47	2963.05	43.09	23.62
S25A	78.94	22.17	23.50	23.09	41.84	41.07	4.49	21.23	2892.52	42.99	21.76
SCR13	65.63	18.54	21.00	18.27	27.76	25.28	3.41	18.59	2103.02	42.14	23.55
S25A36	71.01	15.81	18.00	37.51	48.03	45.42	5.56	19.05	1552.71	41.96	22.91
SCR14	74.93	25.37	26.50	13.29	17.94	17.33	2.91	21.21	1413.12	41.76	20.55
SCR15	90.00	26.13	26.13	12.42	18.50	18.50	2.44	18.89	1414.06	42.24	23.35

RIGHT LEVEE SYSTEM											
SECTIONS	*ALPHA (°)*	*FALSE SLOPE (°)*	*REAL SLOPE(°)*	*L WIDTH (m)*	*BASE WIDTH (m)*	*REAL WIDTH (m)*	*LAND HEIGHT (m)*	*INNER HEIGHT (m)*	*RIVER BED (m)*	*CREST LEVEL (m)*	THALWEG (m)
S20A	83.05	23.01	23.50	23.82	33.89	33.64	5.48	21.73	2662.50	52.34	30.61
S20B	70.97	20.21	22.00	22.96	41.79	39.50	4.66	19.29	2381.30	52.02	32.73
S20C	71.36	26.27	28.00	26.33	36.56	34.64	6.76	14.69	1738.48	51.72	37.03
S21	65.44	14.58	18.00	31.58	41.97	38.17	6.04	17.74	3105.36	51.30	33.56
S21A	72.49	24.58	26.00	21.02	30.71	29.29	5.20	21.50	1445.49	50.92	29.42
S22	64.59	23.18	25.50	36.26	59.38	53.63	7.60	21.56	1265.33	50.23	28.67
S22BIS	70.59	23.26	24.50	35.10	55.78	52.61	6.48	18.21	1720.74	50.18	31.97
S22TER	42.80	23.09	32.00	21.83	43.91	29.83	6.42	22.55	2369.30	49.36	26.81
S22A	55.71	20.93	26.00	13.69	27.33	22.58	3.91	17.87	3138.06	49.06	31.19
S22B	54.80	20.21	24.00	20.71	41.79	34.15	4.66	19.29	2380.24	52.02	32.73
S23	59.38	23.47	27.00	27.40	65.58	56.44	6.68	19.40	2329.94	48.97	29.57
S23BIS	77.55	22.36	22.50	33.77	40.43	39.48	6.06	14.64	2018.53	46.82	32.18
S23A00	90.00	20.70	20.70	15.74	20.94	20.94	3.78	19.98	1888.41	46.49	26.51
S23A02	90.00	30.82	30.82	8.29	13.62	13.62	1.30	19.44	1967.36	46.28	26.84
SCR1	52.28	22.94	29.00	28.53	45.69	36.14	2.79	25.83	1195.65	44.02	18.19
SCR2	79.77	20.07	21.50	17.84	25.33	24.93	3.08	18.25	2363.00	43.49	25.24
S24	72.66	19.68	21.50	18.84	28.77	27.46	3.42	23.66	1373.99	43.39	19.73
SCR4	54.89	16.87	21.00	15.99	26.76	21.89	2.58	21.13	2071.00	43.07	21.94
S25	77.01	17.56	19.00	17.13	24.16	23.54	3.14	17.37	3315.93	43.08	25.71
SCR5	50.16	13.09	18.00	17.60	33.64	25.83	3.14	18.31	3139.00	43.17	24.86
SCR6	90.00	17.31	17.31	17.93	23.75	23.75	3.34	18.17	3261.00	43.01	24.84
SCR7	79.94	19.34	19.50	17.44	24.78	24.40	3.85	17.97	2910.00	42.87	24.9
SCR8	78.07	18.82	20.00	19.29	27.63	27.03	3.97	18.17	2606.00	42.68	24.51
SCR9	68.39	24.23	26.00	18.08	28.72	26.71	3.61	19.70	2495.00	43.03	23.33
SCR10	69.60	22.39	24.00	22.29	31.43	29.46	3.83	18.54	2884.00	42.68	24.14
SCR11	86.97	26.81	27.00	15.94	26.35	26.32	3.70	18.89	2963.05	42.51	23.62
S25A	59.75	19.54	23.50	20.72	31.41	27.13	3.45	20.73	2892.52	42.49	21.76
SCR12	69.68	23.61	25.00	16.79	25.67	24.07	2.89	20.74	2329.99	42.34	21.6
SCR13	90.00	24.55	24.55	20.80	26.29	26.29	4.53	18.71	2048.48	42.26	23.55
S25A36	54.42	22.28	26.50	19.02	29.67	24.13	4.39	19.17	1564.56	42.08	22.91
SCR14	55.68	20.48	25.00	20.49	35.66	29.46	4.28	21.74	1428.15	42.29	20.55
SCR15	84.72	26.17	26.50	20.37	28.18	28.06	4.10	18.68	1516.51	42.03	23.35

Attachment 2: Classifications and indexes

Overtopping classification: first approach

Sections LF	Prob STD	Δhmin	Surf. Width	Classification	Performance
S20A	0.845	0.1791	0.0271	V	IV C
S20B	0.578	0.1976	0.0313	III	IV C
S20C	0.503	0.1990	0.0435	III	IV B
S21	0.561	0.1976	0.0313	III	IV C
S21A	0.786	0.1806	0.0546	IV	IV B
S21B	0.571	0.1976	0.0442	III	IV B
S22	0.785	0.1734	0.0690	IV	III A
S22BIS	0.616	0.1948	0.0403	IV	IV B
S22TER	0.670	0.1934	0.0284	IV	IV C
S22B	0.385	0.2034	0.0283	II	III E
S22C	0.731	0.1892	0.0533	IV	IV B
S23	0.663	0.1947	0.0341	IV	IV C
S23BIS	0.788	0.1692	0.0707	IV	III A
S23A00	0.728	0.1919	0.0355	IV	IV C
S23A02	0.800	0.1838	0.0382	V	IV C
S24	0.681	0.1933	0.0341	IV	IV C
S24B	0.295	0.2061	0.0370	II	III E
S24C	0.158	0.2118	0.0355	I	III E
S24D	0.792	0.1791	0.0536	IV	IV B
S24E	0.421	0.2018	0.0342	III	III E
S24F	0.640	0.1961	0.0378	IV	IV C
S25	0.736	0.1933	0.0256	IV	IV C
S2502	0.767	0.1893	0.0318	IV	IV C
S2503	0.867	0.1742	0.0234	V	V
SCR11	0.742	0.1919	0.0270	IV	IV C
S25A	0.766	0.1919	0.0256	IV	IV C
SCR13	0.458	0.2018	0.0341	III	III E
S25A36	0.075	0.2160	0.0370	I	III E
SCR14	0.789	0.1806	0.0559	IV	IV B
SCR15	0.779	0.1834	0.0550	IV	IV B

Sections RG	Prob STD	Δhmin	Surf. Width	Classification	Performance
S20A	0.776	0.1905	0.0270	IV	IV C
S20B	0.592	0.1976	0.0313	III	IV C
S20C	0.785	0.1777	0.0646	IV	III B
S21	0.075	0.2160	0.0299	I	III E
S21A	0.787	0.1819	0.0517	IV	IV B
S22	0.773	0.1848	0.0577	IV	IV B
S22BIS	0.771	0.1882	0.0451	IV	IV B
S22TER	0.850	0.1640	0.0297	V	V
S22A	0.829	0.1834	0.0285	V	IV C
S22B	0.770	0.1890	0.0327	IV	IV C
S23	0.822	0.1791	0.0344	V	IV C
S23BIS	0.621	0.1961	0.0463	IV	IV B
S23A00	0.406	0.2021	0.0324	III	III E
S23A02	0.813	0.1678	0.0505	V	IV A
SCR1	0.864	0.1720	0.0257	V	V
SCR2	0.527	0.2004	0.0313	III	IVC
S24	0.490	0.2004	0.0372	III	IVC
SCR4	0.462	0.2018	0.0284	III	III E
S25	0.140	0.2118	0.0284	I	III E
SCR5	0.087	0.2146	0.0313	I	III E
SCR6	0.039	0.2189	0.0299	I	III E
SCR7	0.236	0.2078	0.0310	II	III E
SCR8	0.296	0.2061	0.0313	II	III E
SCR9	0.821	0.1819	0.0317	V	IV C
SCR10	0.782	0.1890	0.0298	IV	IV C
SCR11	0.837	0.1791	0.0294	V	IV C
S25A	0.754	0.1905	0.0270	IV	IV C
SCR12	0.810	0.1862	0.0285	V	IV C
SCR13	0.774	0.1876	0.0365	IV	IV C
S25A36	0.790	0.1808	0.0519	IV	IV B
SCR14	0.772	0.1862	0.0480	IV	IV B
SCR15	0.789	0.1805	0.0547	IV	IV B

Performance classification:

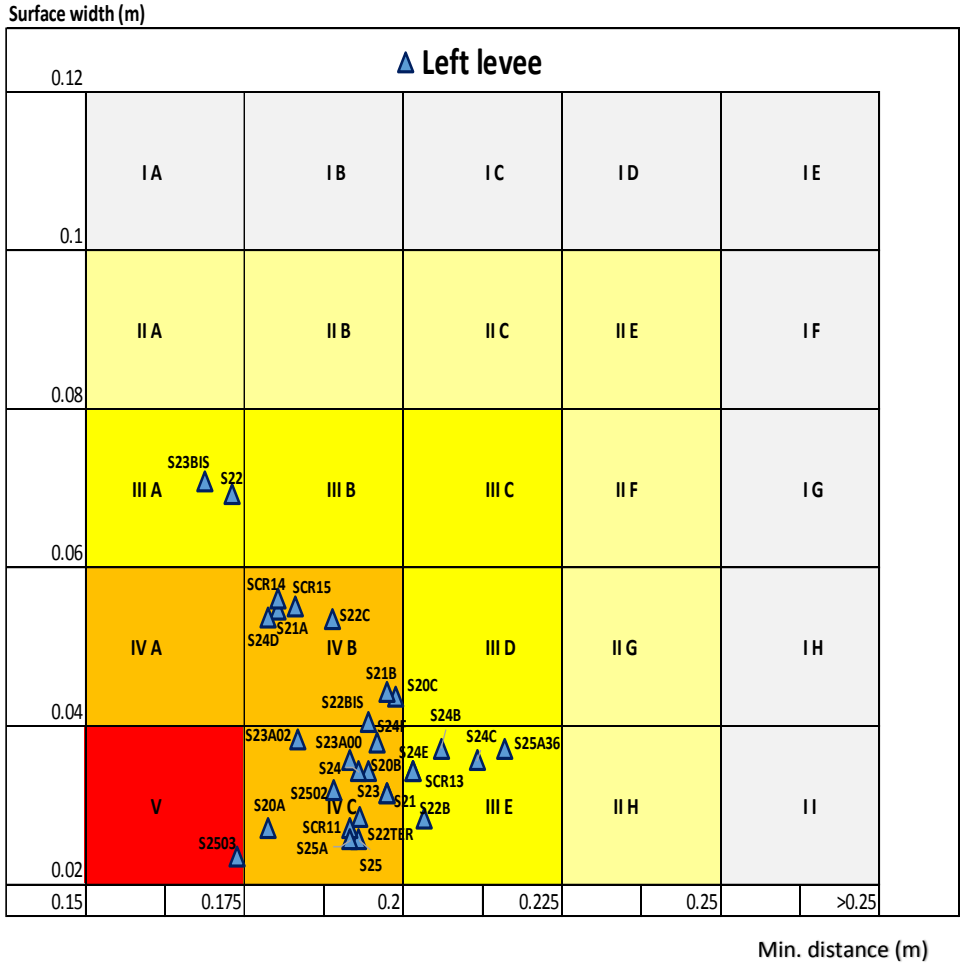

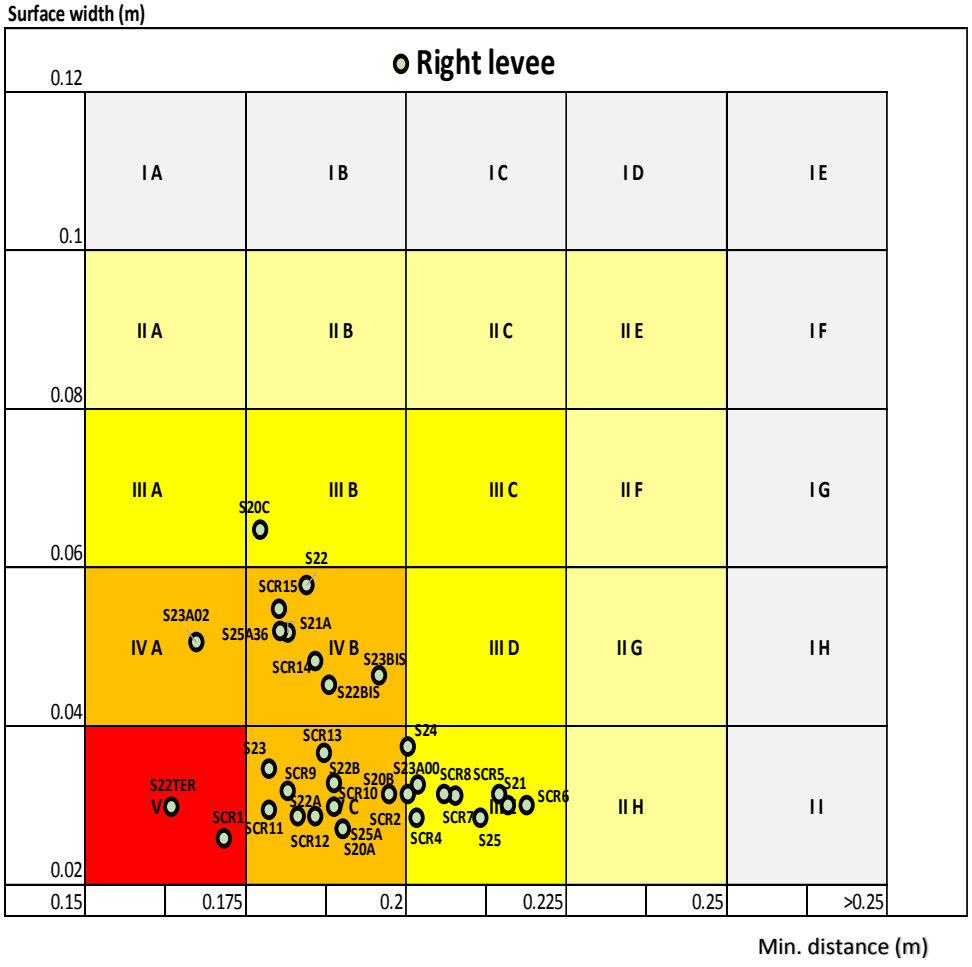

Overtopping: second approach

Sections LF	Stretches	Prob STD	Δhmin	Surf. Width	Classification	Performance
S20A	1	0.763	0.1862	0.0341	IV	IV C
S20B	2	0.516	0.1990	0.0356	III	IV C
S20C	3	0.509	0.1990	0.0371	III	IV C
S21	4	0.735	0.1876	0.0370	IV	IV C
S21A	5	0.728	0.1890	0.0500	IV	IV B
S21B	6	0.737	0.1820	0.0592	IV	IV B
S22	7	0.766	0.1819	0.0538	IV	IV B
S22BIS	8	0.651	0.1961	0.0299	IV	IV C
S22TER	9	0.533	0.1990	0.0284	III	IV C
S22B	10	0.595	0.1947	0.0370	III	IV C
S22C	11	0.705	0.1919	0.0414	IV	IV B
S23	12	0.768	0.1791	0.0523	IV	IV B
S23BIS	13	0.787	0.1777	0.0518	IV	IV B
S23A00	14	0.758	0.1876	0.0385	IV	IV C
S23A02	15	0.757	0.1890	0.0330	IV	IV C
S24	16	0.499	0.1990	0.0355	III	IV C
S24B	17	0.236	0.2076	0.0397	II	III E
S24C	18	0.185	0.2104	0.0341	I	III E
	19	0.797	0.1796	0.0502	IV	IV B
S24D	20	0.683	0.1877	0.0447	IV	IV B
S24E	21	0.524	0.1990	0.0370	III	IV C
S24F	22	0.698	0.1947	0.0299	IV	IV C
S25	23	0.743	0.1919	0.0272	IV	IV C
S2502	24	0.841	0.1805	0.0285	V	IV C
S2503	25	0.835	0.1805	0.0303	V	IV C
SCR11	26	0.758	0.1906	0.0269	IV	IV C
S25A	27	0.627	0.1947	0.0327	IV	IV C
SCR13	28	0.242	0.2075	0.0355	II	III E
S25A36	29	0.510	0.1919	0.0498	III	IV B
SCR14	30	0.785	0.1819	0.0554	IV	IV B
SCR15						

NB: each stretch is included between the section corresponding to the line, and the one in the next line. The empty cells correspond to an affluence.

Sections RG	Stretches	Prob STD	Δhmin	Surf. Width	Classification	Performance
S20A	1	0.671	0.1947	0.0298	IV	IV C
S20B	2	0.745	0.1851	0.0478	IV	IV B
S20C	3	0.552	0.1890	0.0513	III	IV B
S21	4	0.505	0.1933	0.0455	III	IV B
S21A	5	0.773	0.1835	0.0559	IV	IV B
S22	6	0.765	0.1862	0.0499	IV	IV B
S22BIS	7	0.806	0.1720	0.0481	V	IV A
S22TER	8	0.850	0.1642	0.0286	V	V
	9	0.830	0.1834	0.0279	V	IV C
S22A	10	0.800	0.1862	0.0329	V	IV C
S22B	11	0.794	0.1834	0.0367	IV	IV C
S23	12	0.746	0.1862	0.0460	IV	IV B
S23BIS	13	0.627	0.1961	0.0417	IV	IV B
	14	0.382	0.2033	0.0341	II	III E
S23A00	15	0.727	0.1793	0.0499	IV	IV B
S23A02	16	0.828	0.1706	0.0357	V	V
SCR1	17	0.780	0.1819	0.0379	IV	IV C
SCR2	18	0.516	0.1990	0.0356	III	IV C
S24	19	0.475	0.2004	0.0341	III	III E
SCR4	20	0.303	0.2047	0.0327	II	III E
S25	21	0.113	0.2132	0.0313	I	III E
SCR5	22	0.049	0.2189	0.0299	I	III E
SCR6	23	0.101	0.2146	0.0298	I	III E
SCR7	24	0.203	0.2075	0.0327	II	III E
SCR8	25	0.632	0.1919	0.0398	IV	IV C
SCR9	26	0.800	0.1862	0.0329	V	IV C
SCR10	27	0.806	0.1834	0.0339	V	IV C
SCR11	28	0.802	0.1848	0.0313	V	IV C
S25A	29	0.786	0.1876	0.0299	IV	IV C
SCR12	30	0.782	0.1862	0.0346	IV	IV C
SCR13	31	0.784	0.1834	0.0471	IV	IV B
S25A36	32	0.777	0.1834	0.0519	IV	IV B
SCR14	33	0.782	0.1834	0.0530	IV	IV B
SCR15						

Performance classification:

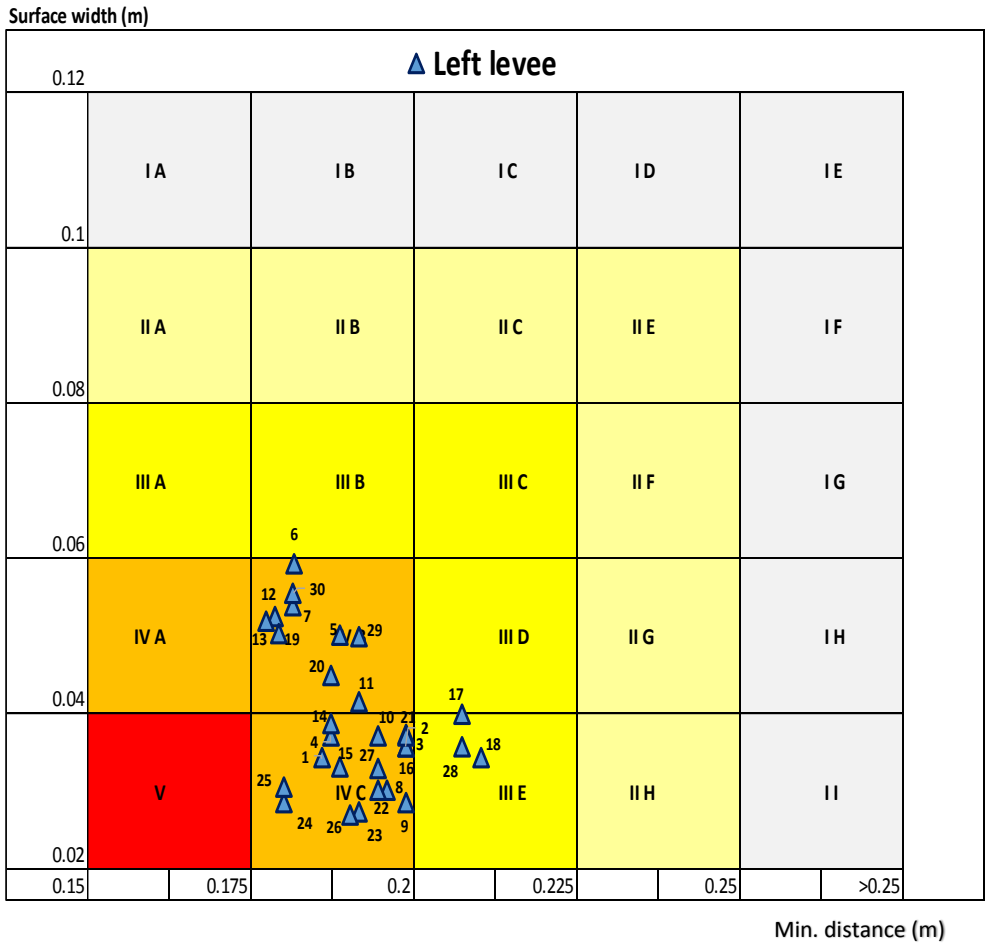

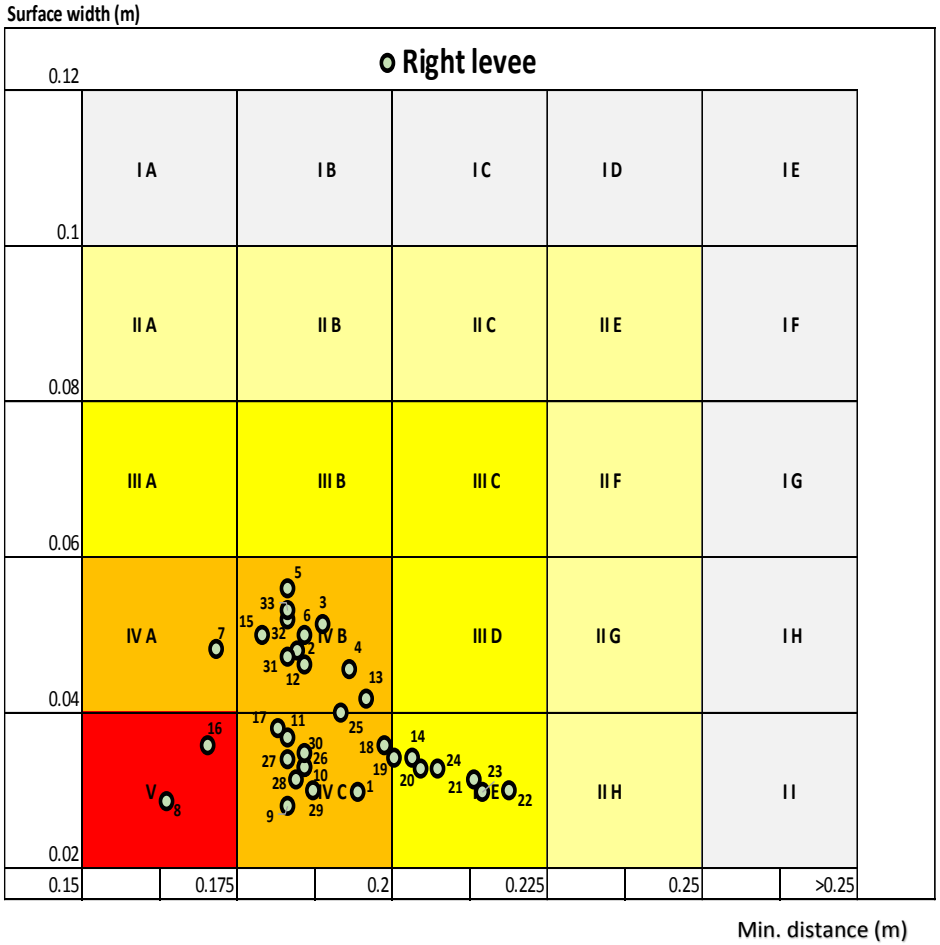

Piping classification: first approach

Section LF	Index1 (Hmin 1% Pr)	H levee	H 1%/ H	Dev. Stand	Classification
S20A	10.000	6.760	1.48	0.00000	I
S20B	5.250	4.300	1.22	0.24053	I
S20C	8.500	5.330	1.59	0.05857	I
S21	6.600	6.620	1.00	0.14855	II
S21A	4.900	3.530	1.39	0.25738	I
S21B	8.250	6.970	1.18	0.04665	I
S22	7.250	5.450	1.33	0.10603	I
S22BIS	7.500	5.460	1.37	0.08950	I
S22TER	7.950	6.340	1.25	0.06460	I
S22B	9.000	5.430	1.66	0.01872	I
S22C	8.150	5.330	1.53	0.05265	I
S23	5.950	5.300	1.12	0.19914	I
S23BIS	5.200	4.180	1.24	0.24237	I
S23A00	7.250	4.760	1.52	0.10487	I
S23A02	5.700	5.200	1.10	0.21457	I
S24	7.700	4.600	1.67	0.07909	I
S24B	6.200	4.410	1.41	0.18040	I
S24C	7.350	5.600	1.31	0.10039	I
S24D	5.950	4.560	1.30	0.19783	I
S24E	2.310	2.330	0.99	0.29311	II
S24F	5.250	3.990	1.32	0.23996	I
S25	4.550	3.610	1.26	0.27282	I
S2502	6.000	4.870	1.23	0.19450	I
S2503	4.300	4.330	0.99	0.28050	II
SCR11	5.900	4.690	1.26	0.20194	I
S25A	5.850	4.490	1.30	0.20513	I
SCR13	4.650	3.410	1.36	0.26863	I
S25A36	9.550	5.560	1.72	0.00924	I
SCR14	3.400	2.910	1.17	0.29487	I
SCR15	3.150	2.440	1.29	0.29822	I

Section RG	Index1 (Hmin 1% Pr)	H levee	H 1%/ H	Dev. Stand	Classification
S20A	6.100	5.480	1.11	0.18485	I
S20B	5.900	4.660	1.27	0.19959	I
S20C	6.730	6.770	0.99	0.13715	II
S21	8.100	6.040	1.34	0.04475	I
S21A	5.250	5.300	0.99	0.22814	II
S22	9.300	7.600	1.22	0.01020	I
S22BIS	9.000	6.480	1.39	0.01703	I
S22TER	5.600	6.420	0.87	0.21765	II
S22A	3.500	3.910	0.90	0.30133	II
S22B	5.300	4.660	1.14	0.23376	I
S23	7.500	6.680	1.12	0.11621	I
S23BIS	8.650	6.060	1.43	0.02667	I
S23A00	4.500	3.780	1.19	0.29035	I
S23A02	10.000	1.300	7.69	0.30589	I
SCR1	7.300	2.790	2.62	0.09305	I
SCR2	4.600	3.080	1.49	0.26729	I
S24	4.850	3.420	1.42	0.25529	I
SCR4	4.100	2.580	1.59	0.28872	I
S25	4.400	3.140	1.40	0.27618	I
SCR5	4.500	3.140	1.43	0.27219	I
SCR6	4.600	3.340	1.38	0.26764	I
SCR7	4.500	3.850	1.17	0.27180	I
SCR8	4.950	3.970	1.25	0.25134	I
SCR9	4.650	3.610	1.29	0.26526	I
SCR10	5.700	3.830	1.49	0.21129	I
SCR11	4.100	3.700	1.11	0.28846	I
S25A	5.300	3.450	1.54	0.23387	I
SCR12	4.300	2.890	1.49	0.28037	I
SCR13	5.350	4.530	1.18	0.23129	I
S25A36	4.900	4.390	1.12	0.25313	I
SCR14	5.250	4.280	1.23	0.23564	I
SCR15	5.250	4.100	1.28	0.23613	I

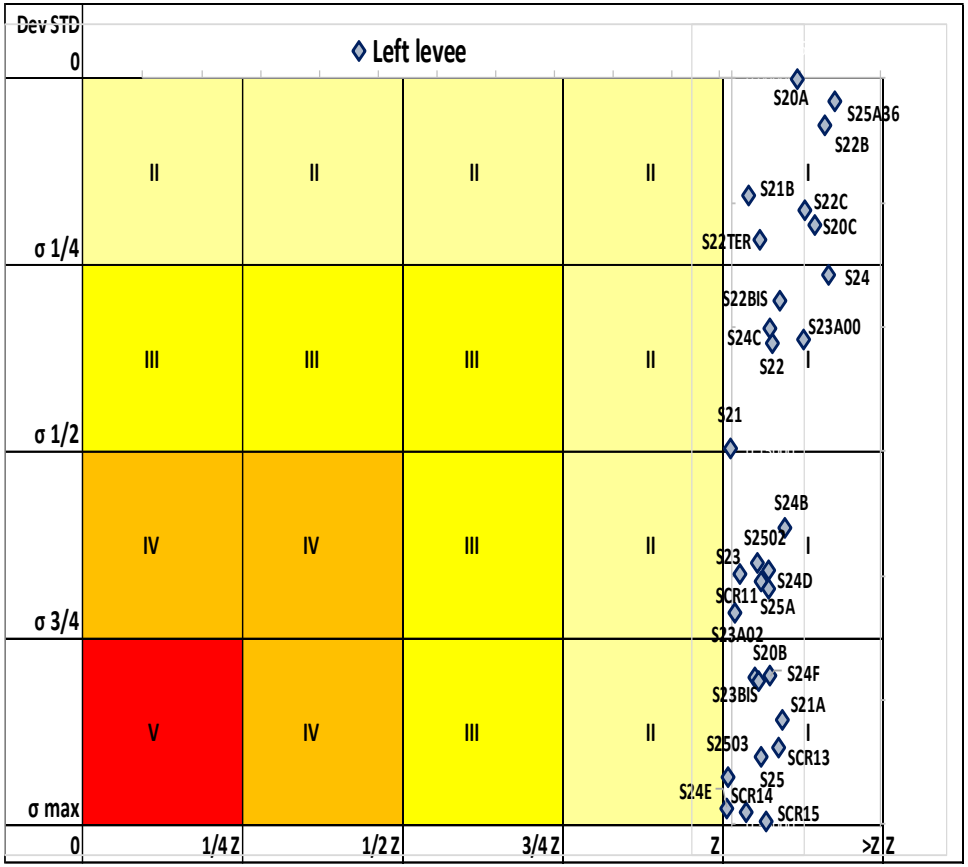
Dev STD
Left levee
0
σ 1/4
σ 1/2
σ 3/4
σ max
0
1/4 Z
1/2 Z
3/4 Z
Z
>Z
Z
II
III
IV
V
I
S20A
S25A36
S22B
S21B
S22C
S20C
S22TER
S24
S22BIS
S24C
S23A00
S22
S21
S24B
S2502
S23
S24D
SCR11
S25A
S23A02
S20B
S24F
S23BIS
S21A
S2503
SCR13
S25
S24E
SCR14
SCR15

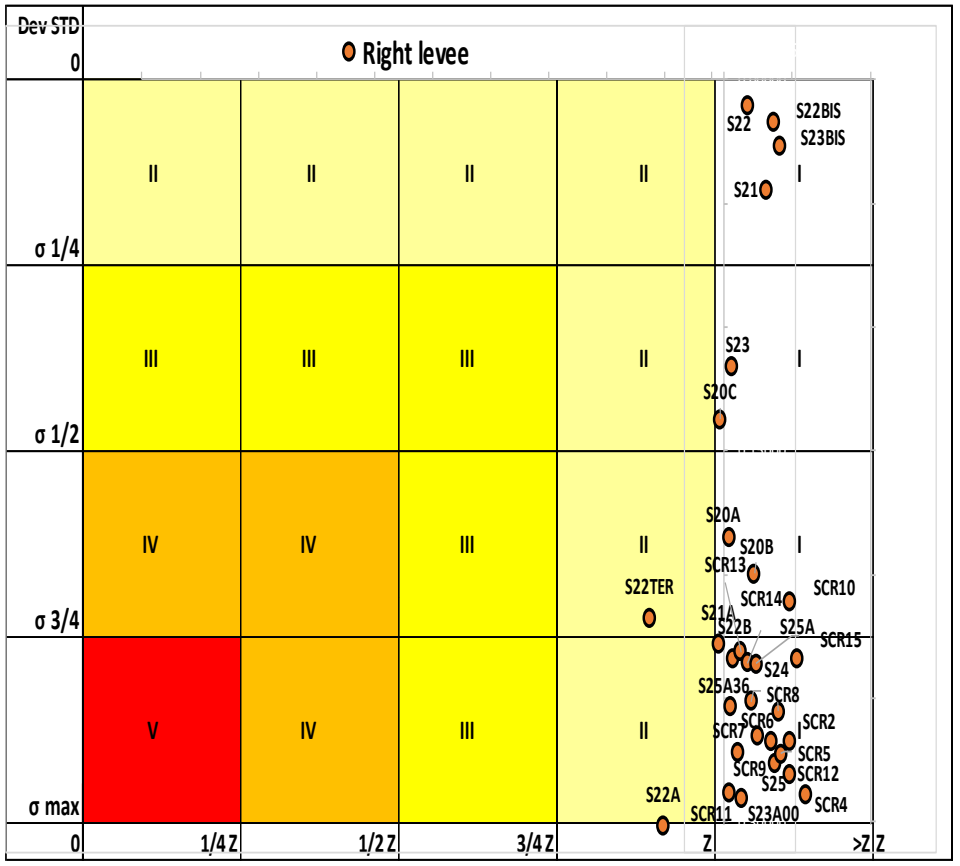
Dev STD
Right levee
0
σ 1/4
σ 1/2
σ 3/4
σ max
0
1/4 Z
1/2 Z
3/4 Z
Z
>Z
Z
II
III
IV
V
I
S22
S22BIS
S23BIS
S21
S23
S20C
S20A
S20B
SCR13
S22TER
SCR14
SCR10
S21A
S22B
S25A
SCR15
S24
S25A36
SCR8
SCR6
SCR2
SCR7
SCR5
SCR9
SCR12
S25
S22A
SCR11
S23A00
SCR4

Piping classification: second approach

Section LF	Stretches	Index1 (Hmin 1% Pr)	Hm levee	H 1%/ H	Dev. Stand	Classification
S20A	1	6.350	5.530	1.15	0.08977	I
S20B	2	6.000	4.815	1.25	0.14198	I
S20C	3	7.100	5.970	1.19	0.09642	I
S21	4	5.400	5.070	1.07	0.20210	I
S21A	5	5.750	5.250	1.10	0.14542	I
S21B	6	7.550	6.210	1.22	0.06964	I
S22	7	7.250	5.455	1.33	0.08795	I
S22BIS	8	7.650	5.900	1.30	0.06704	I
S22TER	9	8.250	5.885	1.40	0.03527	I
S22B	10	8.350	5.380	1.55	0.03108	I
S22C	11	6.550	5.315	1.23	0.11729	I
S23	12	5.450	4.740	1.15	0.21454	I
S23BIS	13	5.750	4.470	1.29	0.17138	I
S23A00	14	6.200	4.980	1.24	0.15367	I
S23A02	15	6.250	4.900	1.28	0.13960	I
S24	16	6.700	4.505	1.49	0.12181	I
S24B	17	6.550	5.005	1.31	0.13458	I
S24C	18	7.200	5.600	1.29	0.09033	I
	19	5.900	4.560	1.29	0.18939	I
S24D	20	2.950	3.440	0.86	0.27148	II
S24E	21	2.900	3.155	0.92	0.28879	II
S24F	22	4.800	3.800	1.26	0.25346	I
S25	23	5.000	4.240	1.18	0.23287	I
S2502	24	4.600	4.650	0.99	0.24121	II
S2503	25	4.500	4.530	0.99	0.24386	II
SCR11	26	5.750	4.590	1.25	0.19668	I
S25A	27	5.500	3.950	1.39	0.23408	I
SCR13	28	5.700	4.485	1.27	0.12237	I
S25A36	29	4.200	4.235	0.99	0.15346	II
SCR14	30	3.250	2.675	1.21	0.30147	I
SCR15						

NB: each stretch is included between the section corresponding to the line, and the one in the next line. The empty cells correspond to an affluence.

Section RG	Stretches	Index1 (Hmin 1% Pr)	H levee	H 1%/ H	Dev. Stand	Classification
S20A	1	5.900	5.070	1.16	0.19727	I
S20B	2	6.200	5.710	1.09	0.17237	I
S20C	3	7.200	6.400	1.13	0.09469	I
S21	4	6.100	5.620	1.09	0.13906	I
S21A	5	6.300	6.400	0.98	0.10247	II
S22	6	9.500	7.040	1.35	0.01733	I
S22BIS	7	6.400	6.450	0.99	0.10541	II
S22TER	8	5.550	6.420	0.86	0.22402	II
	9	3.450	3.910	0.88	0.30341	II
S22A	10	4.000	4.285	0.93	0.28629	II
S22B	11	5.600	5.670	0.99	0.18469	II
S23	12	7.550	6.370	1.19	0.06937	I
S23BIS	13	8.550	6.060	1.41	0.03154	I
	14	4.000	3.780	1.06	0.29425	I
S23A00	15	2.520	2.540	0.99	0.31446	II
S23A02	16	2.800	2.045	1.37	0.23900	I
SCR1	17	5.250	2.935	1.79	0.19793	I
SCR2	18	4.650	3.250	1.43	0.27191	I
S24	19	4.350	3.000	1.45	0.28328	I
SCR4	20	4.150	2.860	1.45	0.29156	I
S25	21	4.400	3.140	1.40	0.28225	I
SCR5	22	4.500	3.240	1.39	0.27853	I
SCR6	23	4.500	3.595	1.25	0.27797	I
SCR7	24	4.600	3.910	1.18	0.27411	I
SCR8	25	4.700	3.790	1.24	0.26987	I
SCR9	26	4.950	3.720	1.33	0.25345	I
SCR10	27	4.550	3.765	1.21	0.26615	I
SCR11	28	4.450	3.575	1.24	0.27604	I
S25A	29	4.600	3.170	1.45	0.27129	I
SCR12	30	4.600	3.710	1.24	0.27073	I
SCR13	31	5.000	4.460	1.12	0.25464	I
S25A36	32	4.950	4.335	1.14	0.25700	I
SCR14	33	5.150	4.190	1.23	0.24649	I
SCR15						

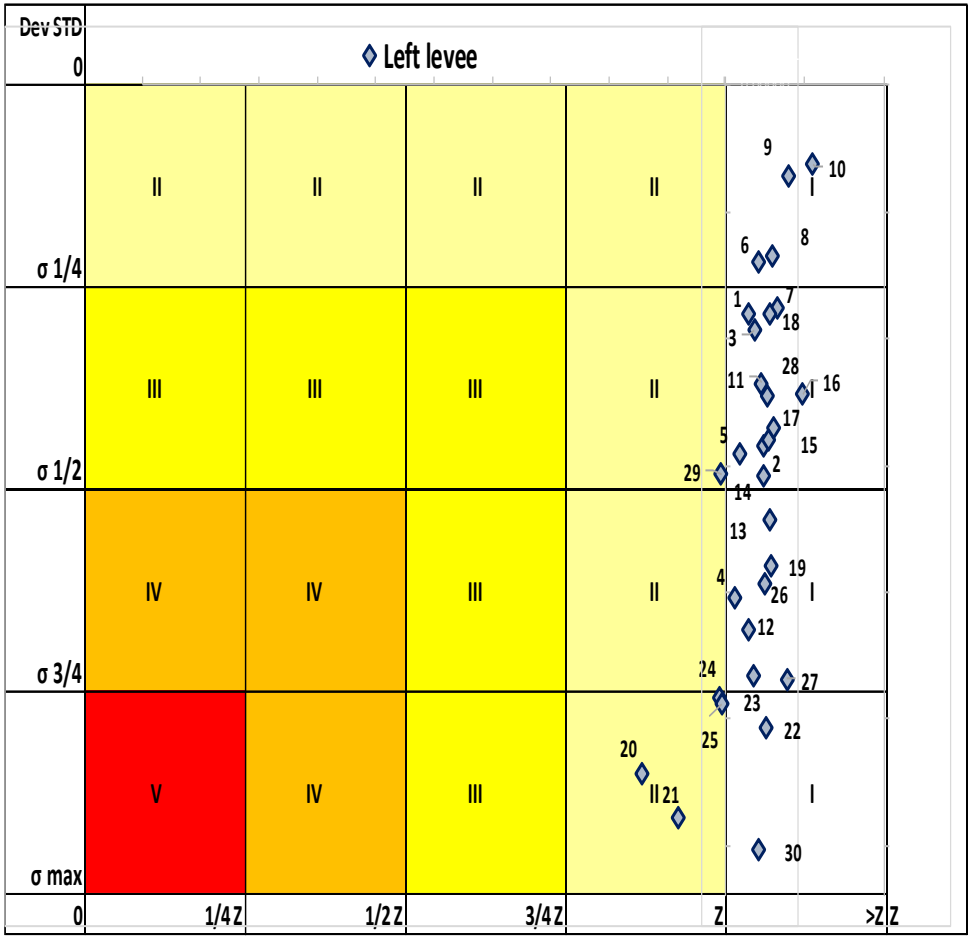
Dev STD
0
Left levee
σ 1/4
σ 1/2
σ 3/4
σ max
0
1/4Z
1/2Z
3/4Z
Z
>Z
Z
II
III
IV
V
I

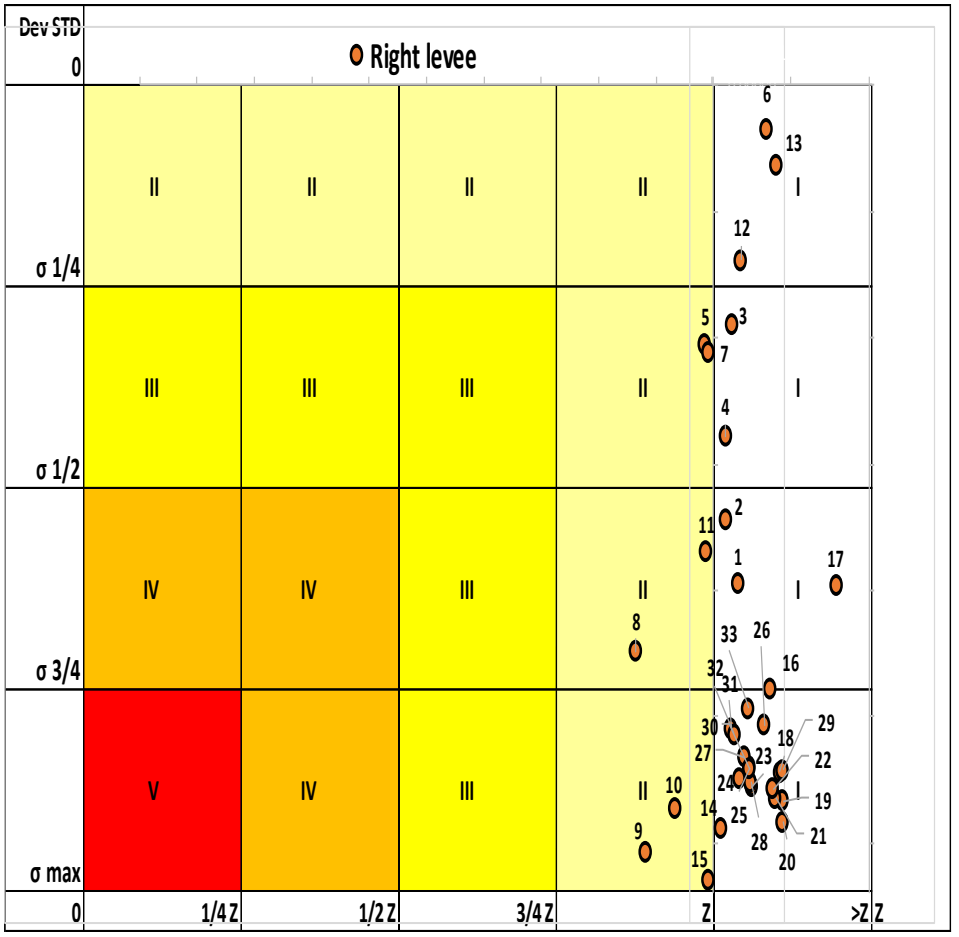
Dev STD
0
Right levee
σ 1/4
σ 1/2
σ 3/4
σ max
0
1/4Z
1/2Z
3/4Z
Z
>Z
Z
II
III
IV
V
I

Attachment 3: Indexes maps

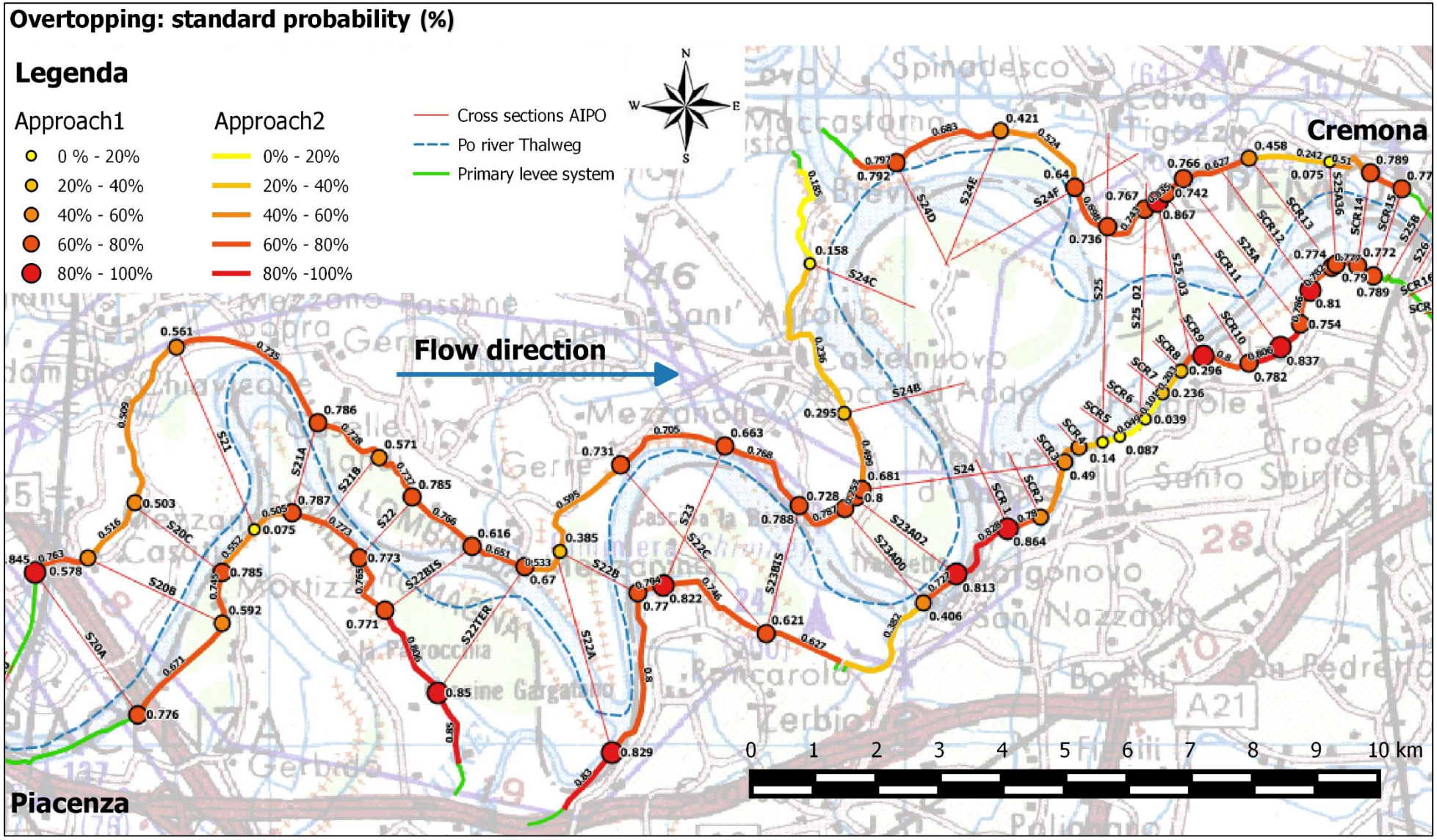

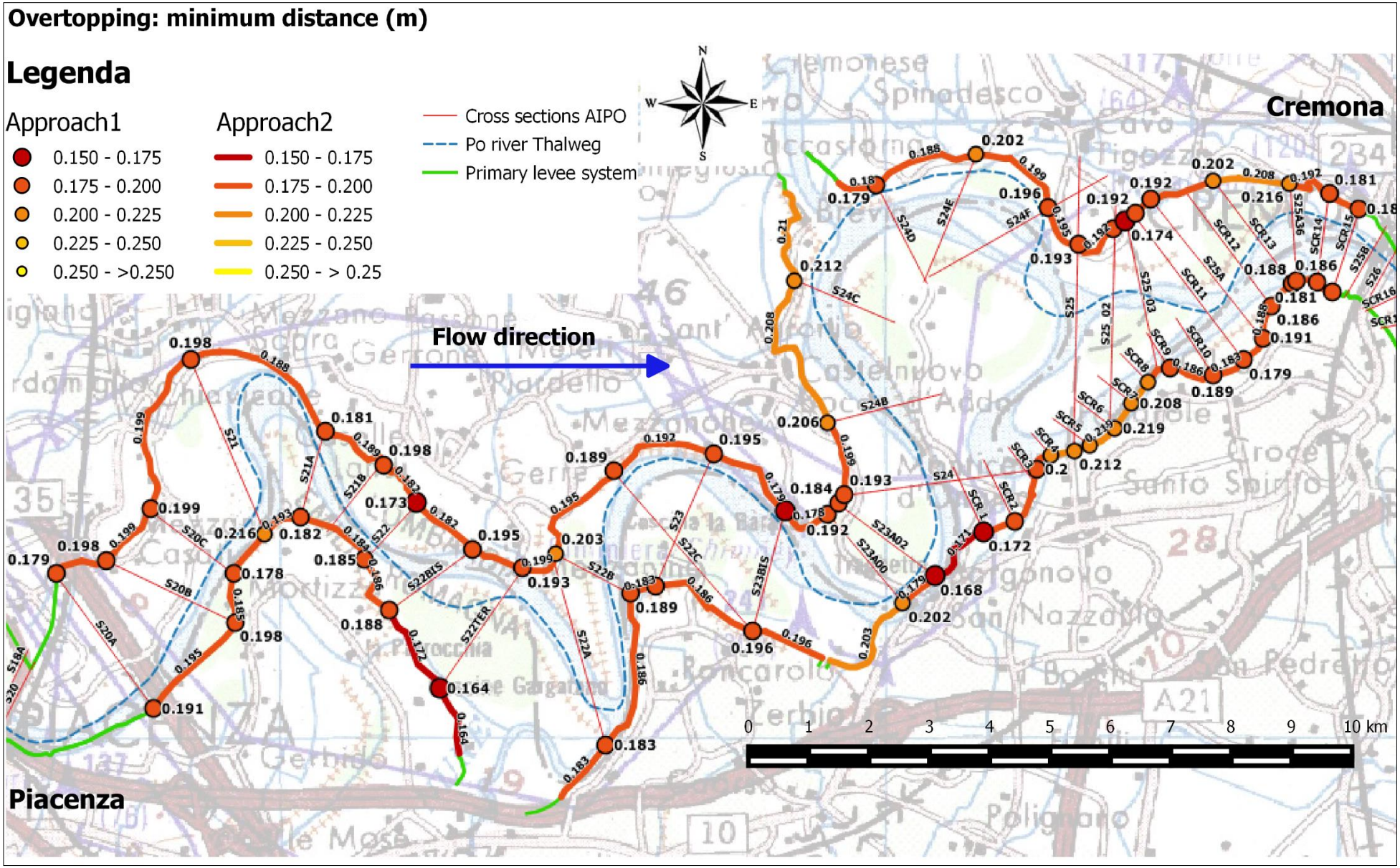
Overtopping: minimum distance (m)
Legenda
Approach1
0.150 - 0.175
0.175 - 0.200
0.200 - 0.225
0.225 - 0.250
0.250 - >0.250
Approach2
0.150 - 0.175
0.175 - 0.200
0.200 - 0.225
0.225 - 0.250
0.250 - > 0.25
Cross sections AIPO
Po river Thalweg
Primary levee system
N
W
E
S
Flow direction
Cremona
Piacenza
0 1 2 3 4 5 6 7 8 9 10 km

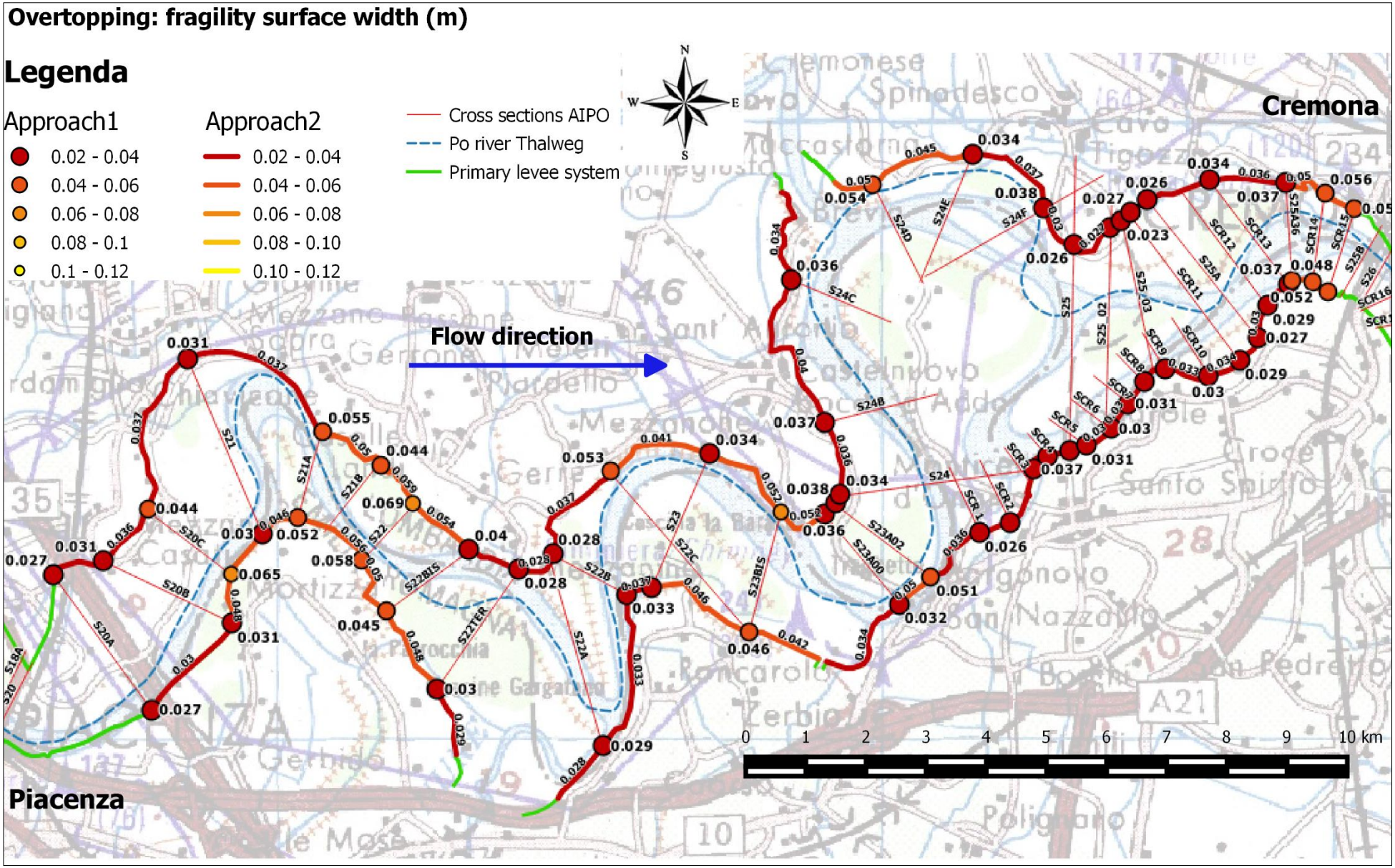
Overtopping: fragility surface width (m)
Legenda
Approach1
0.02 - 0.04
0.04 - 0.06
0.06 - 0.08
0.08 - 0.1
0.1 - 0.12
Approach2
0.02 - 0.04
0.04 - 0.06
0.06 - 0.08
0.08 - 0.10
0.10 - 0.12
Cross sections AIPO
Po river Thalweg
Primary levee system
N
W
E
S
Flow direction
Cremona
Piacenza
0 1 2 3 4 5 6 7 8 9 10 km

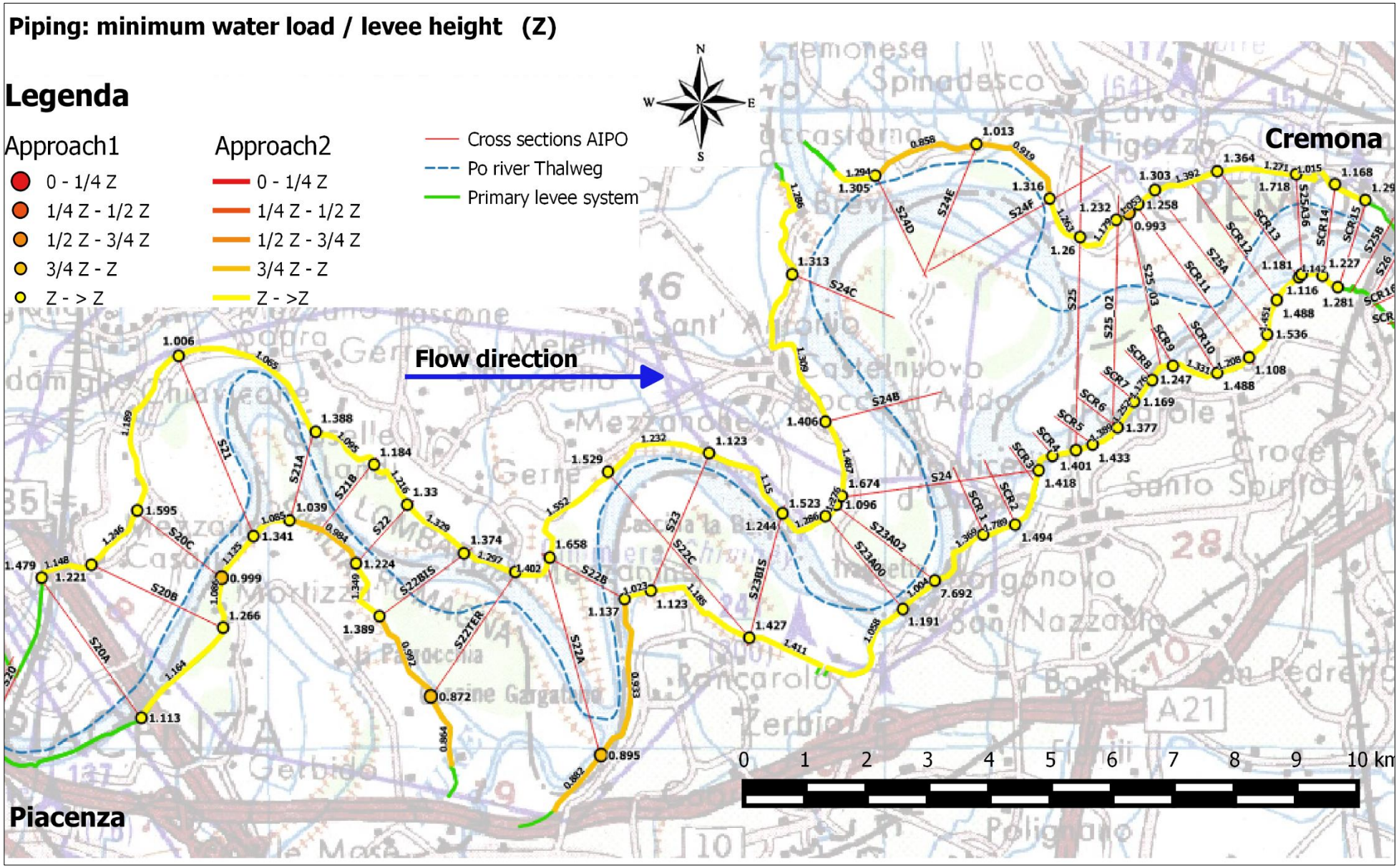
Piping: minimum water load / levee height (Z)
Legenda
Approach1
0 - 1/4 Z
1/4 Z - 1/2 Z
1/2 Z - 3/4 Z
3/4 Z - Z
Z - > Z
Approach2
0 - 1/4 Z
1/4 Z - 1/2 Z
1/2 Z - 3/4 Z
3/4 Z - Z
Z - >Z
Cross sections AIPO
Po river Thalweg
Primary levee system
N
W
E
S
Flow direction
Cremona
Piacenza
0 1 2 3 4 5 6 7 8 9 10 km

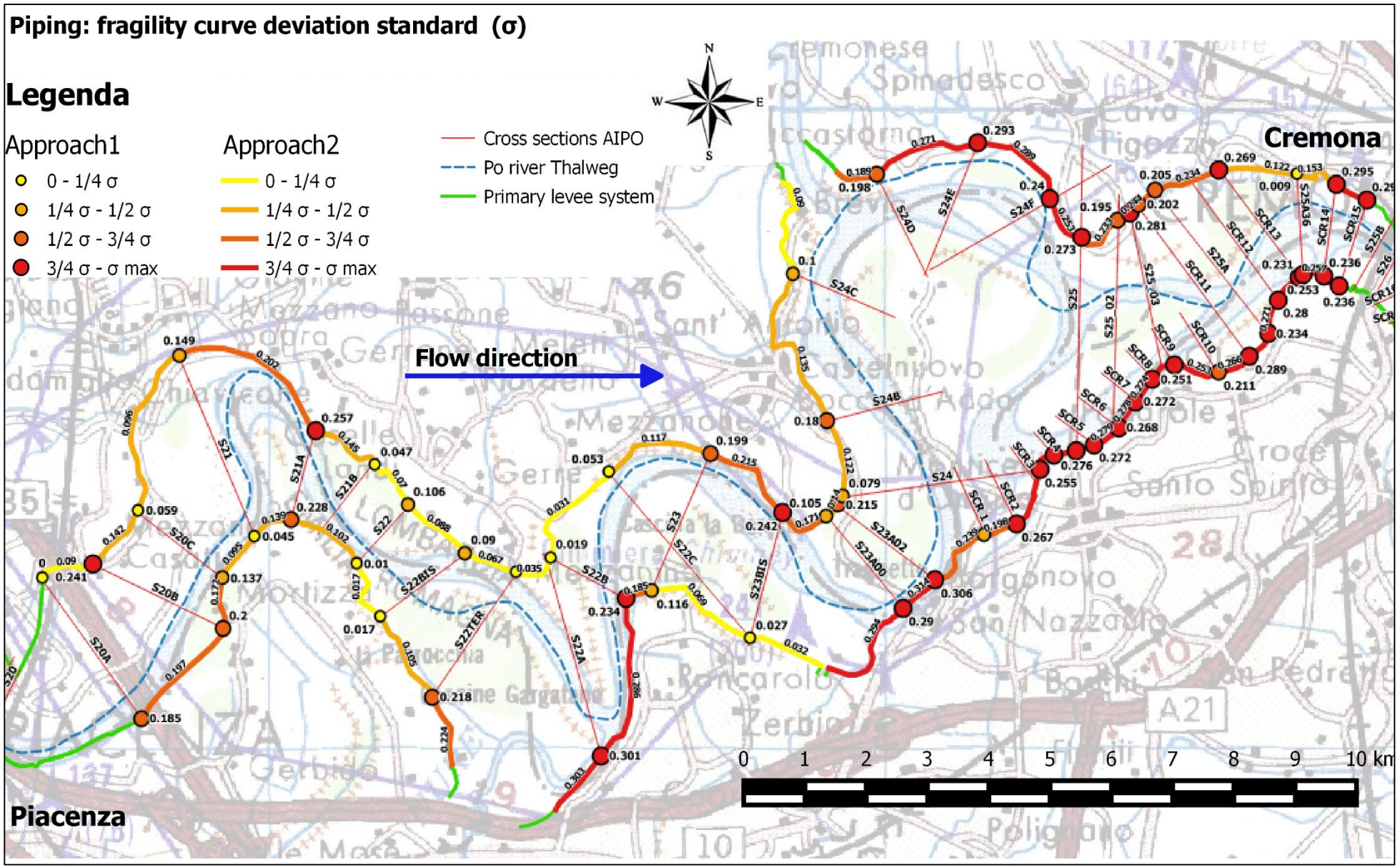
Piping: fragility curve deviation standard (σ)
Legenda
Approach1
0 - 1/4 σ
1/4 σ - 1/2 σ
1/2 σ - 3/4 σ
3/4 σ - σ max
Approach2
0 - 1/4 σ
1/4 σ - 1/2 σ
1/2 σ - 3/4 σ
3/4 σ - σ max
Cross sections AIPO
Po river Thalweg
Primary levee system
N
W
E
S
Flow direction
Cremona
Piacenza
0 1 2 3 4 5 6 7 8 9 10 km

Attachment 4: Classification maps

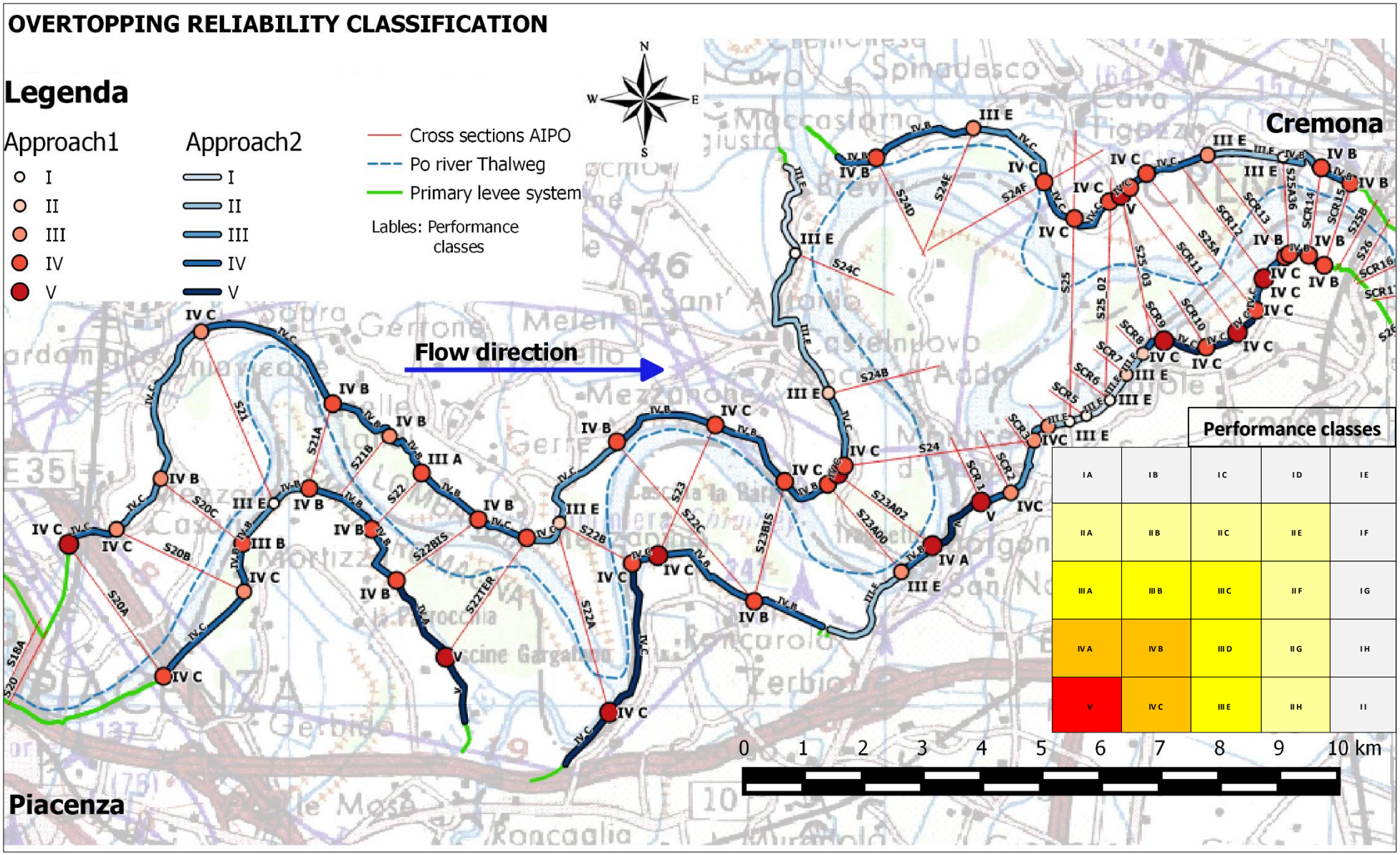

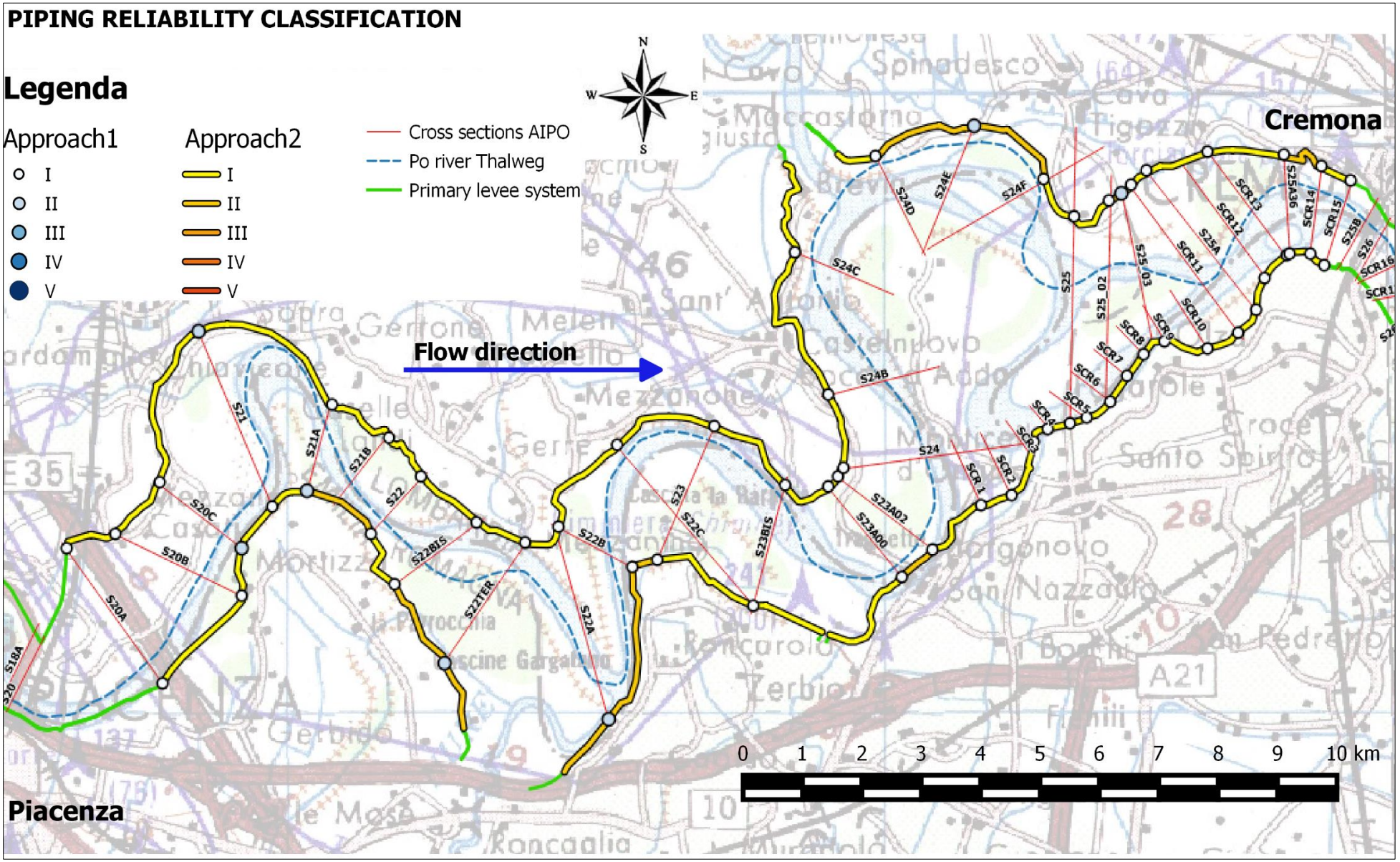
PIPING RELIABILITY CLASSIFICATION
Legenda
Approach1
I
II
III
IV
V
Approach2
I
II
III
IV
V
Cross sections AIPO
Po river Thalweg
Primary levee system
N
W
E
S
Flow direction
Cremona
Piacenza
0 1 2 3 4 5 6 7 8 9 10 km

Attachment 5: Residual Hazard maps

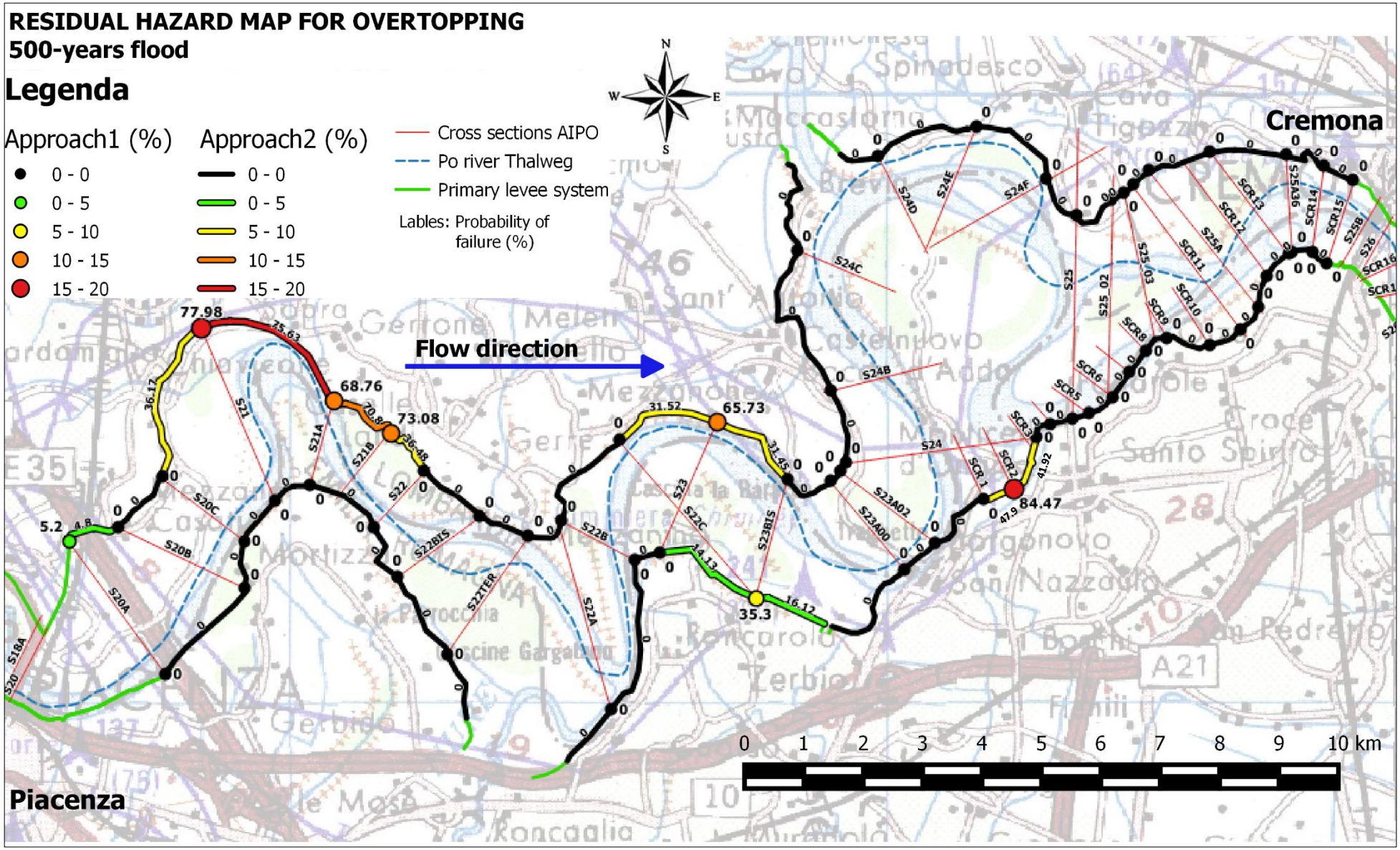

RESIDUAL HAZARD MAP FOR PIPING
500-years flood

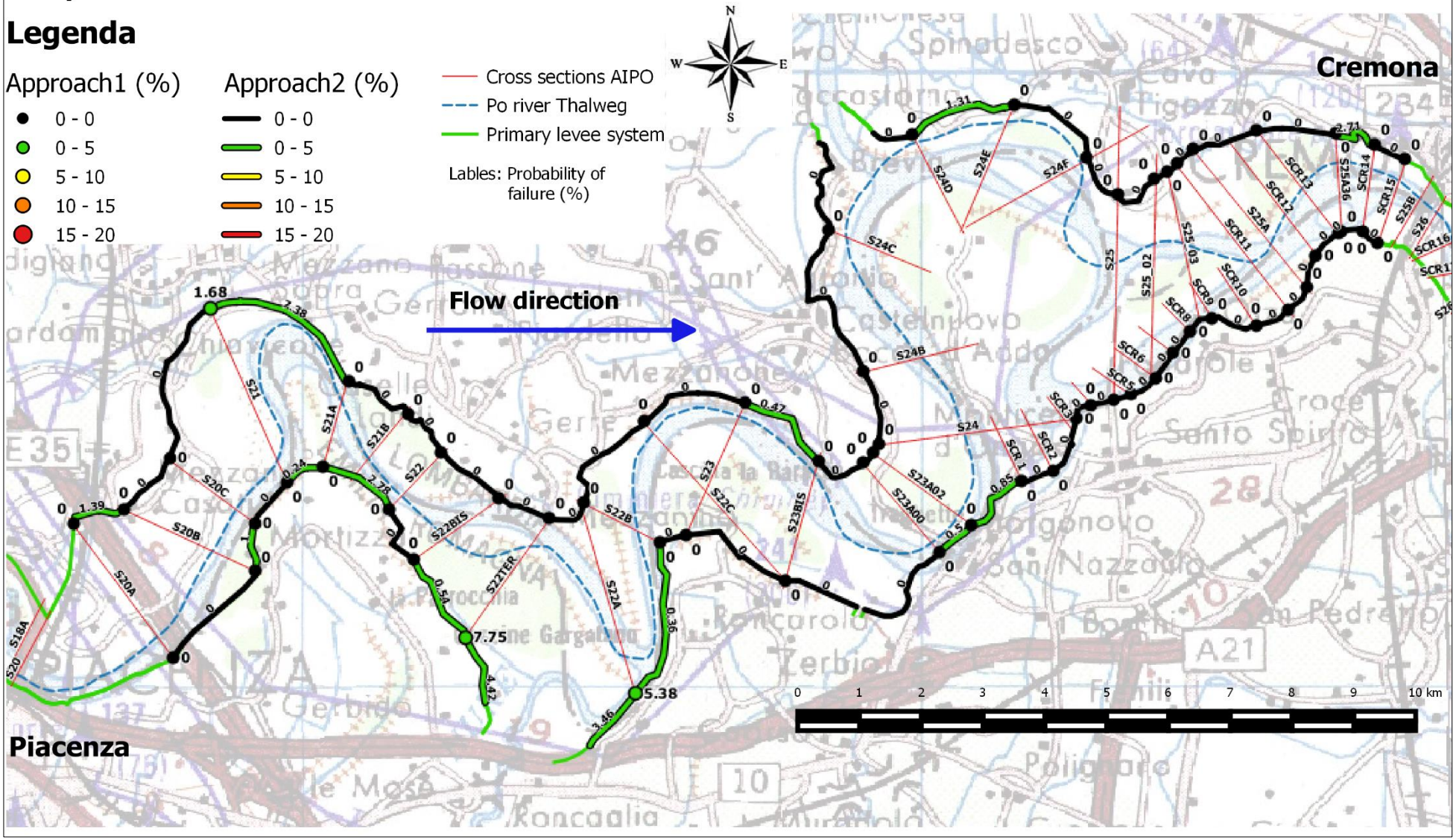

Attachment 6: Summary sheet of flooding water volumes for breach formation due to overtopping

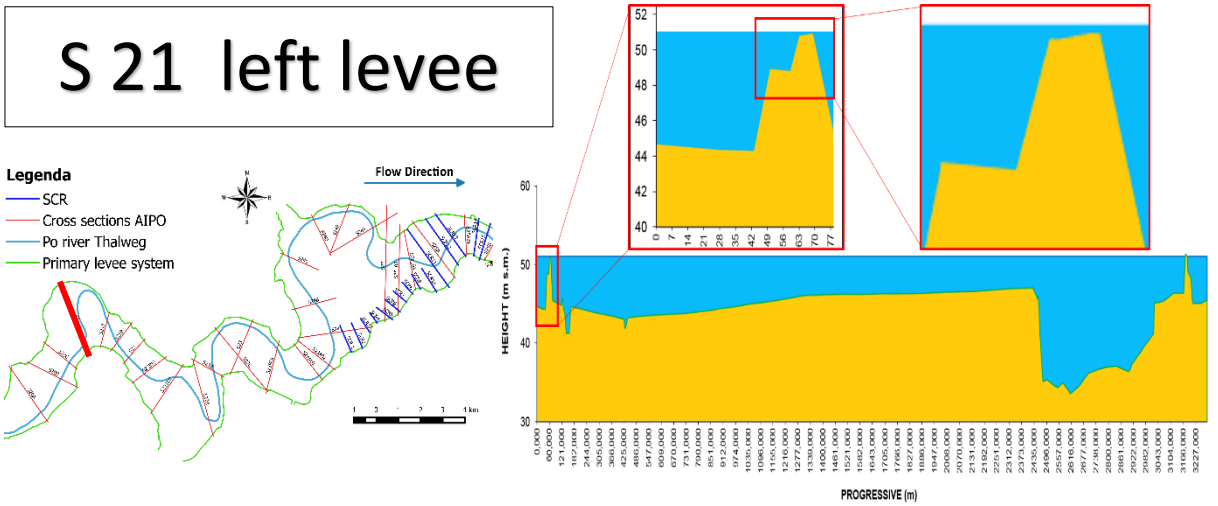

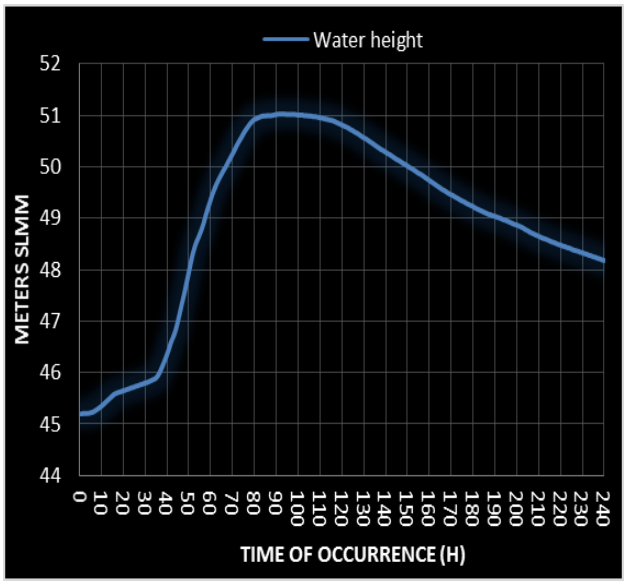

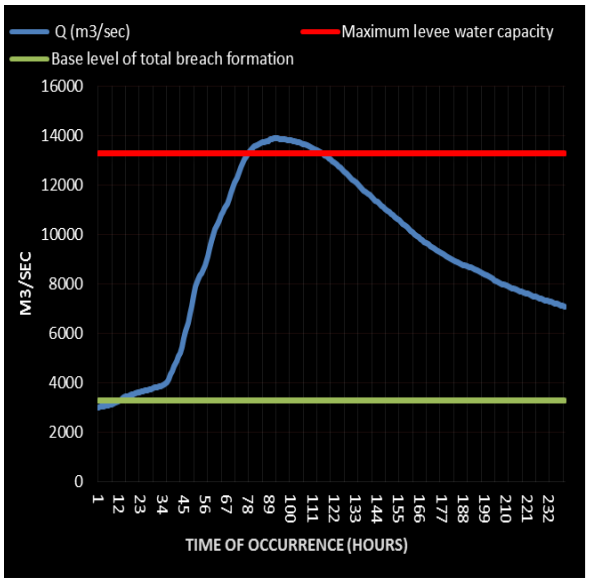

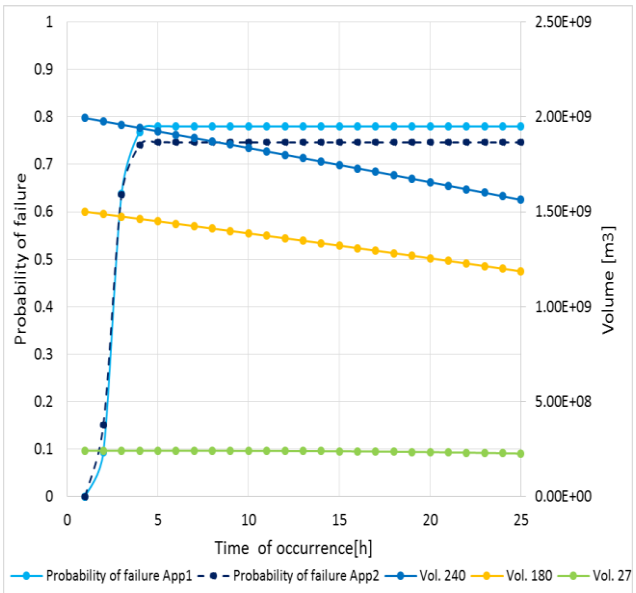

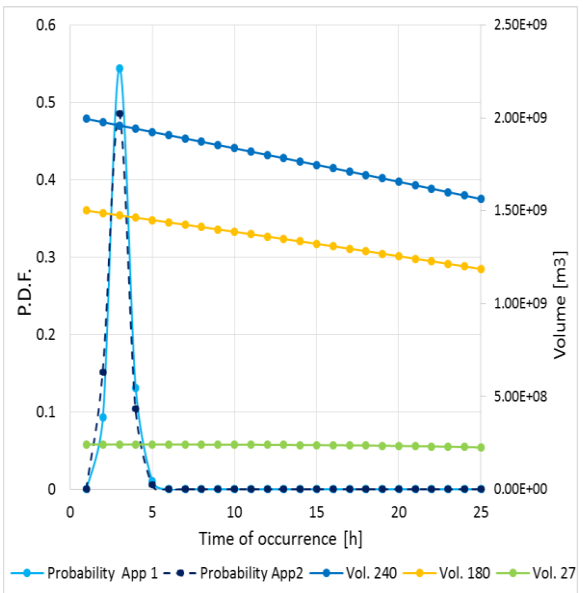

S 21A left levee

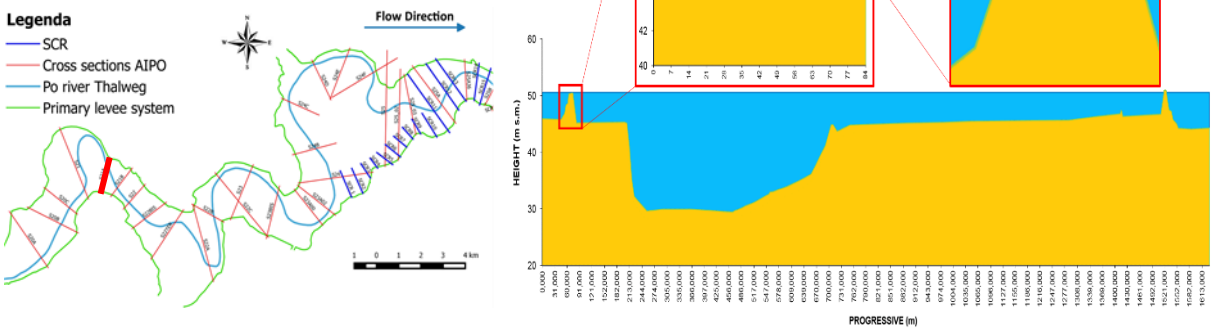

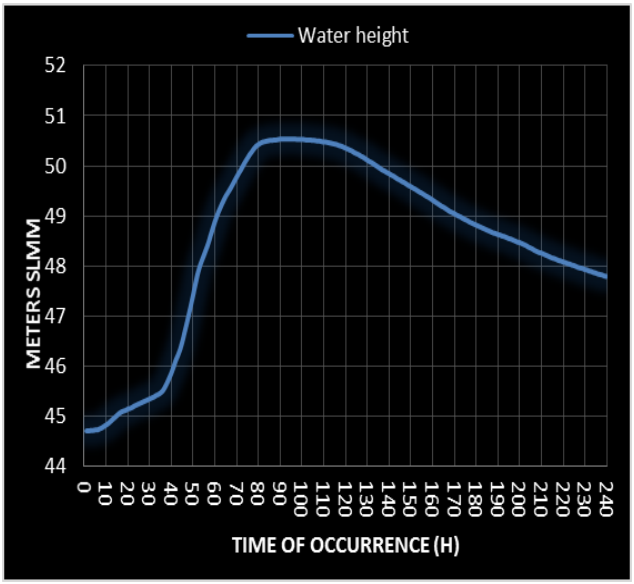

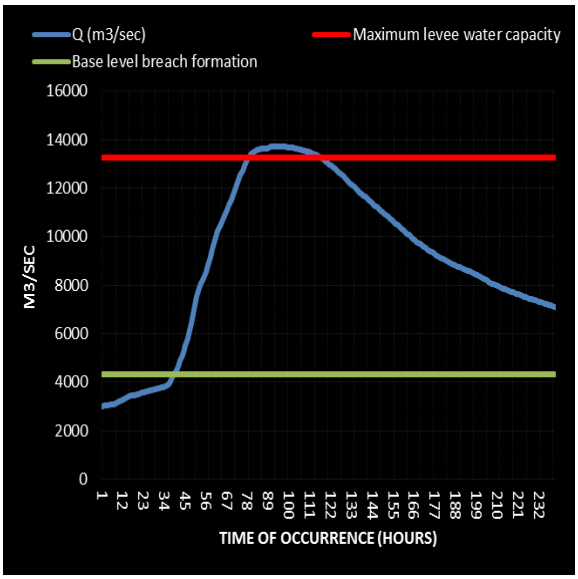

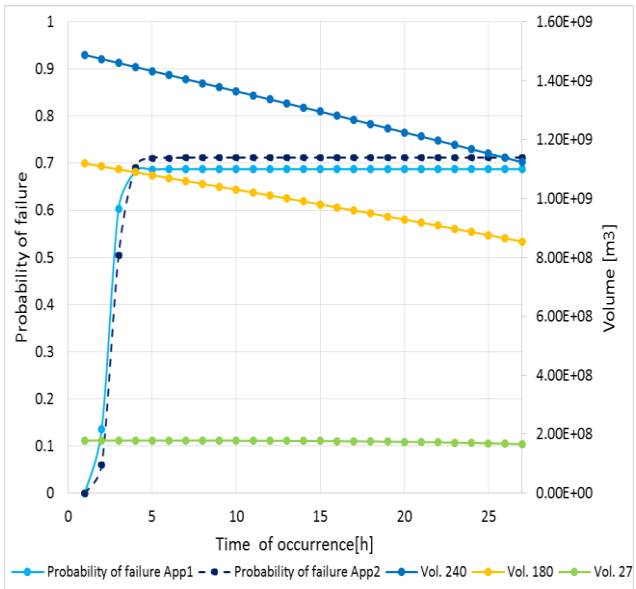

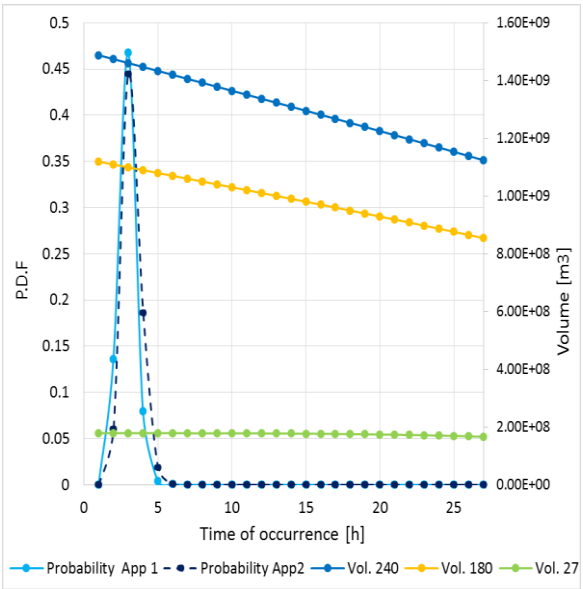

S 21B left levee

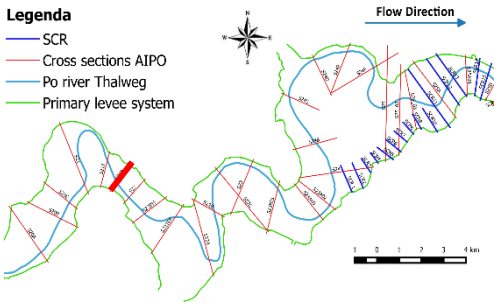

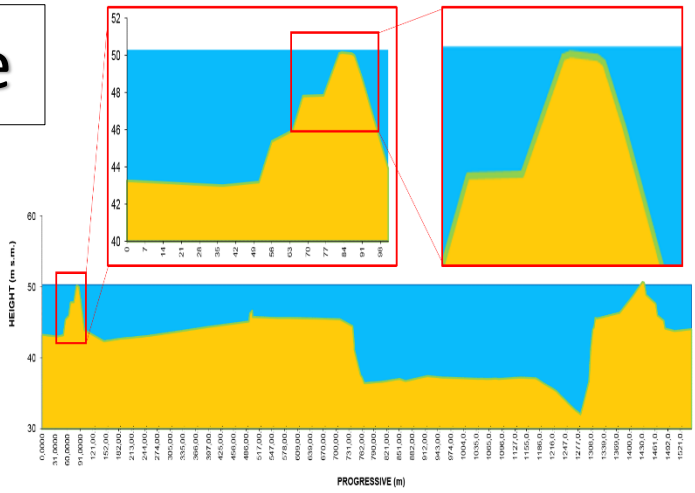

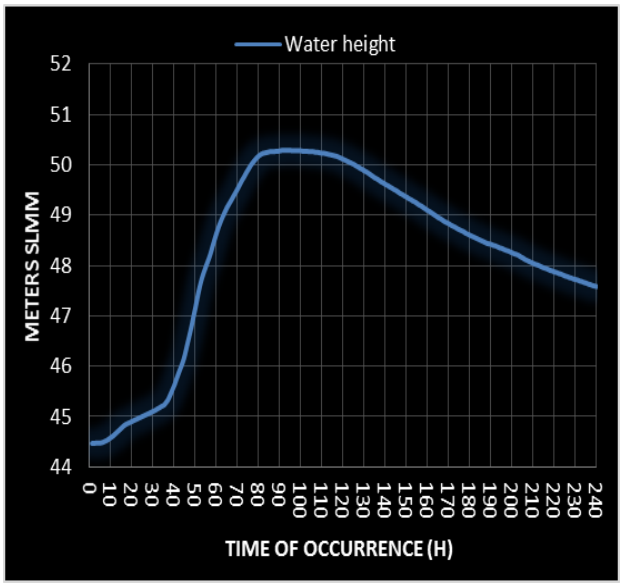

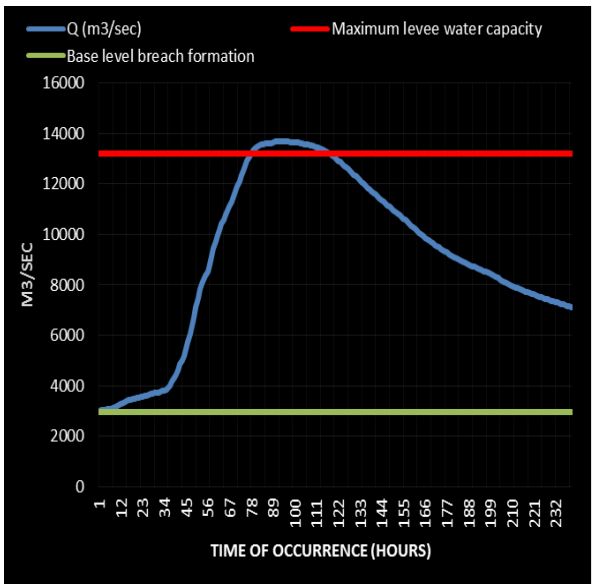

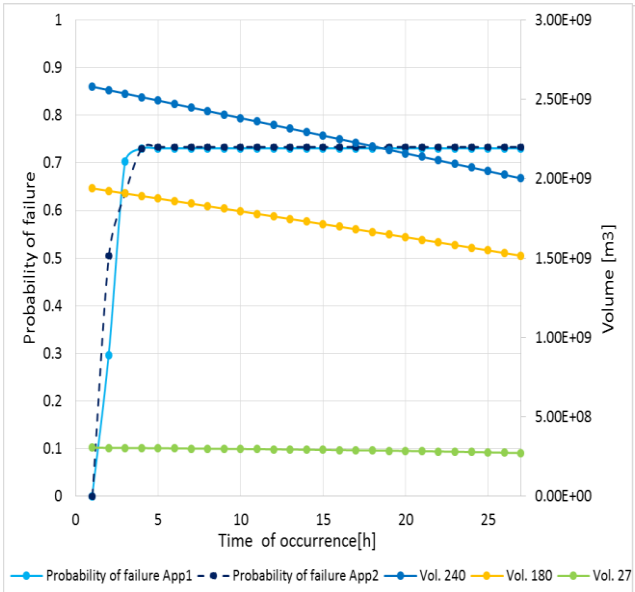

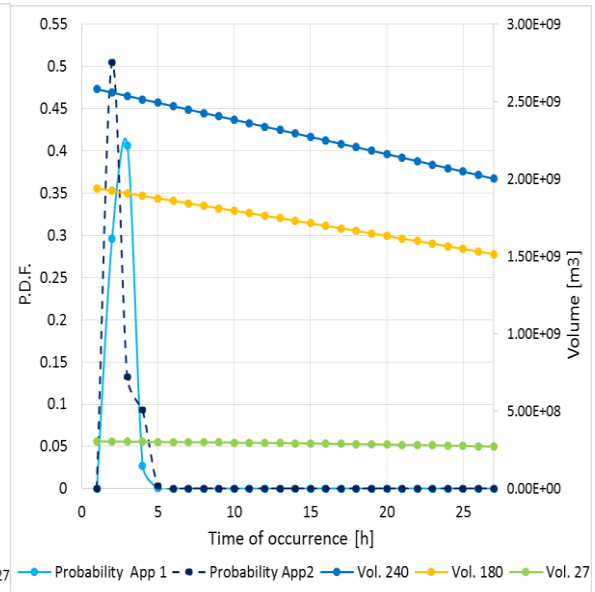

S 23 left levee